SIGNAL TRANSDUCTION MECHANISMS OF CRYPTOCHROME

Carrie L. Partch

A dissertation submitted to the faculty of the University of North Carolina at Chapel Hill in partial fulfillment of the requirements for the degree of Doctor of Philosophy in the Department of Biochemistry and Biophysics.

Chapel Hill
2006

Approved by
Advisor: Aziz Sancar
Reader: Beverly Errede
Reader: Andrew Lee
Reader: Charles Perou
Reader: Ellen Weiss

ABSTRACT

Carrie L. Partch: Signal Transduction Mechanisms of Cryptochrome

(Under the direction of Dr. Aziz Sancar)

Photolyase and cryptochrome flavoproteins help living organisms manage the deleterious and beneficial effects of sunlight. Photolyase maintains genome integrity by reversing UV-induced DNA damage with near-UV/blue-light, and cryptochromes act as blue-light photosensory receptors to regulate growth in plants and entrainment of circadian rhythms in both plants and animals. Although photolyase and cryptochrome are highly structurally homologous and the photocycle of photolyase is known in great detail, we do not currently understand how cryptochromes signal in response to light. It is hypothesized that cryptochrome, like photolyase, employs light-driven electron transfer to initiate signaling, although the photocycle and other downstream signaling events remain to be described in detail. The studies described here were designed to take advantage of differences and similarities in the known functions of photolyases and cryptochromes in order to characterize the signaling mechanisms of cryptochromes. An examination of the structural and biochemical properties of plant and animal cryptochromes demonstrates that although they evolved independently from functionally distinct photolyase progenitors, they possess several unexpected similarities, demonstrating convergence in the evolution of cryptochromes. The implications of these results for the cryptochrome photocycle are discussed.

Metazoan cryptochromes additionally have a critical, light-independent function in the molecular clock that engenders circadian rhythms. Other studies have shown that

cryptochromes act as transcriptional repressors in the major transcription/translation feedback loop of the clock. I studied the interaction of mammalian cryptochromes with protein phosphatase 5 (PP5) and show that inhibition of PP5 by cryptochrome modulates the activity of the major clock kinase, casein kinase I epsilon. PP5 is required for proper cycling of the clock; therefore, these data provide the first demonstration of the role of a phosphatase in the mammalian circadian clock. Furthermore, they suggest that cryptochromes regulate the molecular clock by both transcriptional and posttranslational mechanisms.

For Karin Viktoria Stromberg

ACKNOWLEDGEMENTS

Foremost, I would like to thank Aziz for his training, support and the many opportunities that he provided for me during the course of my time here. I am also grateful for his unending support of my decision to take on another large challenge in addition to my graduate work, motherhood.

I was fortunate to collaborate with several outstanding colleagues in the department who taught me a great deal. In particular, I would like to thank Michael “Sparky” Clarkson for his patience, advice, and hard work. Many current and former lab mates deserve huge thanks for their contribution to my scientific development and personal wellbeing, in particular Müge, Carol, Nikki, Michele, Kezi, Laura, and Mark. I would like to especially acknowledge Carol Thompson and Kezi Ünsal-Kaçmaz for fruitful discussions, and Nikki Worthington, with whom I worked closely in my final months. I was also privileged to work with an excellent undergraduate student who made significant contributions to the circadian clock project, Katie Shields.

I am indebted to many members of my family who encouraged me to follow my dreams. In particular, I want to thank my parents Patty and Kurt Stromberg, who raised me to believe that anything is possible with hard work and perseverance, and Steve and Barb Stentz, who encouraged me to follow a career in the sciences. My aunt, Karin Stromberg, was tremendously supportive and served as a wonderful role model for the dedication, hard work, and sacrifice that it takes to balance a career and family.

Finally, none of this would have been possible without the support and encouragement of my husband, James.

TABLE OF CONTENTS

LIST OF TABLES

LIST OF FIGURES

LIST OF ABBREVIATIONS AND SYMBOLS

$\{^{1}H\}$-^{15}N NOE	heteronuclear nuclear Overhauser effect
Å	Angstrom
bHLH	basic helix-loop-helix
bZIP	basic leucine zipper
BLAST	basic local alignment search tool
BMAL1	brain and muscle ARNT-like 1 protein
CD	circular dichroism
CK2	casein kinase 2 protein
CKI	casein kinase 1 protein
CLOCK	circadian locomotor output cycles kaput protein
CRY	cryptochrome protein
CT	carboxy-terminal domain
Δ	deleted
DMEM	Dulbecco's modified Eagle's medium
E.coli	*Escherichia coli*
E3	ubiquitin ligase enzyme
ECL	enhanced chemiluminescence
EST	expressed sequence tag
ET	evolutionary trace
FAD	flavin adenine dinucleotide
FTIR	Fourier transform infrared spectroscopy
GST	glutathione-s-transferase
HA	hemagglutinin epitope tag
His	6x histidine epitope tag
HRP	horseradish peroxidase
HSQC	heteronuclear single quantum coherence
IB	immunoblot/western blot
IP	immunoprecipitate
J	joule
kDa	kilodaltons
L	liter
LB	Luria broth

ml	milliliter
mM	millimolar
M	molar
MTHF	methenyltetrahydrofolate
NMR	nuclear magnetic resonance
NP-40	Nonidet P40
PAS	PER-ARNT-SIM domain
PBS	phosphate buffered saline
PCR	polymerase chain reaction
PDB	Protein Databank
PER	period protein
PHR	photolyase homology region
PLR	pupillary light response
PP	protein phosphatase
ps	picosecond
RMS	root mean square
RNAi	RNA interference
RT	reverse transcriptase
SDS-PAGE	sodium dodecyl sulfate polyacrylamide gel electrophoresis
SEM	standard error of the mean
Sf21	*Spodoptera frugiperde* ovarian insect cells
shRNA	short hairpin RNA
siRNA	short interfering RNA
UV	ultraviolet
ZT	zeitgeber time

CHAPTER 1

INTRODUCTION

Photolyase/cryptochrome blue-light photoreceptors comprise a class of structurally related flavoproteins found in all kingdoms of life. Photolyases repair UV-induced photoproducts in DNA and cryptochromes use energy from blue light to mediate a variety of growth and adaptive responses in organisms ranging from prokaryotes to humans. This chapter will review the current body of knowledge regarding cryptochromes and their mechanism of action. Given the difficulties in working with recombinant proteins of this family due to cofactor oxidation and/or loss during purification, most of our understanding of cryptochrome function is based on genetic data. This *in vivo* evidence for cryptochrome function will be addressed first, followed by recapitulation of recent advances in our understanding of cryptochrome phototransduction from cell-based and *in vitro* studies.

Cryptochrome genetics and *in vivo* studies

Plant cryptochromes

Cryptochromes were identified first in *Arabidopsis thaliana* in 1993 through the isolation of the HY4 gene (Ahmad and Cashmore, 1993). *Arabidopsis* seedlings grown under light display a variety of photomorphogenic responses with respect to dark-grown seedlings, such as inhibition of stem elongation and stimulation of leaf expansion. In particular, seedlings grown in light have significantly shorter stems (hypocotyl) than seedlings grown in darkness; this response is mediated by blue (400-490 nm), red (600-700 nm) and far-red (700-750 nm) light. A screen for hypocotyl mutants, carried out by Koornneef and coworkers in 1980, identified several mutants (*hy*) that lost the ability to respond to one or more of these monochromatic light conditions (Koornneef et al., 1980). The *hy4* mutant lost responsiveness selectively to blue light, indicating that a blue-light photoreceptor or a component of the blue-light signaling pathway had been disrupted. Molecular cloning of the HY4 gene revealed significant sequence homology to *E.coli* photolyase that was sequenced by Sancar and colleagues (Ahmad and Cashmore, 1993; Sancar et al., 1984). However, even though the recombinant protein co-purified with flavin,

it lacked detectable DNA repair activity (Lin et al., 1995; Malhotra et al., 1995). This led to its definition as the first member in a novel class of blue-light photoreceptors called cryptochromes (CRY), which retain high sequence homology to photolyase yet do not repair DNA.

While the loss of *Cry1* (*hy4*) has a marked effect on photomorphogenic responses under high fluence rates of blue light, the loss of a second cryptochrome gene, cloned in 1996 and named CRY2, has an effect detectable only under low fluence rates (1 μmol $m^{-2}s^{-1}$ or less) (Hoffman et al., 1996; Lin et al., 1998). Since the *Cry1*/*Cry2* double mutant has an even more pronounced phenotype than the loss of either cryptochrome, it was concluded that cryptochromes act redundantly to regulate photomorphogenic responses, with CRY1 primarily operating under bright light and CRY2 operating under dim light conditions. The differential responsiveness of CRY1 and CRY2 to lighting conditions has been explained by the rapid light-dependent degradation of CRY2 protein under moderate to high fluence rates of blue light (Lin et al., 1998). The effect of fluence rate on CRY2 protein levels is rather striking; no change in CRY2 protein levels is seen after treatment with 1 μmol $m^{-2}s^{-1}$ of blue light for up to one hour; however, treatment with 5 μmol $m^{-2}s^{-1}$ blue light for only 15 minutes results in degradation of 90% of protein present in dark-grown seedlings (Ahmad et al., 1998a; Lin et al., 1998).

Arabidopsis cryptochromes likely exert their largest effect on photomorphogenic responses through regulation of gene expression. Expression of approximately one third of all *Arabidopsis* genes was found to change more than two-fold after exposure to white light; 73% of genes differentially expressed under white light were also affected under monochromatic blue light (Ma et al., 2001). Most of the genes that were affected by blue light in wild-type plants were not differentially expressed in the *Cry1*/*Cry2* mutant under the same lighting conditions, indicating that cryptochromes are the major blue-light photoreceptors mediating this response, which occurs on a timescale of minutes to days

(Folta et al., 2003; Ma et al., 2001). However, light-dependent regulation of gene expression in *Arabidopsis* is controlled by a broad spectrum of wavelengths; many of the genes regulated by cryptochromes are also regulated to some extent by the phytochrome family of red-light photopigments, which also absorb blue light (Litts et al., 1983).

Regulation of gene expression by cryptochrome may be mediated entirely by its direct interaction with the E3 ubiquitin ligase COP1. COP1 is a zinc-finger and WD40-repeat protein that is responsible for the degradation of bZIP transcription factors such as HY5, STO, STH, and HFR in the dark (Ang et al., 1998; Duek et al., 2004; Osterlund et al., 2000). The ubiquitin ligase activity of COP1 is rapidly inhibited by light (Duek et al., 2004), followed by translocation out of the nucleus (Osterlund and Deng, 1998; Subramanian et al., 2004; von Arnim et al., 1997), allowing accumulation of transcription factors and initiation of the photomorphogenic transcriptional program. Both CRY1 and CRY2 interact directly with COP1 in a light-independent manner through their C-terminal domains (Wang et al., 2001; Yang et al., 2001). Since overexpression of the CRY C-termini (CCT) is sufficient to produce a constitutive “light-on” phenotype, the COP1-inhibitory region of the C-terminal domain must be repressed by the photolyase homology region of cryptochrome in the dark (Wang et al., 2001; Yang et al., 2001). Light-dependent inhibition of COP1 by cryptochromes has been proposed to act through a two-step mechanism: COP1 is 1) rapidly downregulated as a result of a light-dependent conformational change in C-termini of cryptochromes (Duek et al., 2004; Yang et al., 2001), and 2) it is inhibited on a longer timescale because of the light-dependent translocation of COP1 from the nucleus to the cytoplasm by CRY1 (Osterlund and Deng, 1998; Subramanian et al., 2004; von Arnim et al., 1997).

It has now been demonstrated that CRY1 and CRY2, along with phytochromes, mediate photomorphogenic responses such as inhibition of stem elongation, stimulation of leaf expansion, induction of anthocyanin synthesis, control of photoperiodic flowering,

entrainment of the circadian clock, and regulation of gene expression required for photomorphogenic responses (reviewed in (Batschauer, 2005; Lin and Shalitin, 2003)).

DASH cryptochromes

A new class of proteins in the photolyase/cryptochrome was recently identified, first in the cyanobacterium *Synechocystis* sp. PCC 6803 (Hitomi et al., 2000; Ng and Pakrasi, 2001), and then in plants (Kleine et al., 2003), other prokaryotes (Worthington et al., 2003), and aquatic vertebrates and fungi (Daiyasu et al., 2004). This class was named DASH since the *Synechocystis* protein was more homologous to cryptochromes in higher organisms (*Drosophila*, *Arabidopsis*, and Humans) than prokaryotic photolyases (Brudler et al., 2003). Initial characterization of this class demonstrated that they did not contribute significantly to photoreactivation *in vivo*, which led to their classification as cryptochromes (Hitomi et al., 2000; Worthington et al., 2003). However, there are currently not enough data to propose a physiological function for these proteins.

Animal cryptochromes and the circadian clock

Based on exhaustive biochemical data, it was concluded that humans and other placental mammals do not possess photolyase activity (Li et al., 1993). Therefore, the report of a photolyase ortholog as an expressed sequence tag in the human genome database was unexpected (Adams et al., 1995). Subsequent examination of this and a second photolyase ortholog discovered by our group established that both co-purified with flavin but lacked photolyase activity, and were therefore classified as cryptochromes and proposed to act as novel blue-light photoreceptors for regulating the circadian clock (Hsu et al., 1996). Shortly thereafter, cryptochrome homologs were identified in many other animals, including insects, amphibians, fish, birds, and other mammals (Van Gelder and Sancar, 2003). Currently, the *Drosophila* cryptochrome is the most well characterized animal cryptochrome and therefore *in vivo* evidence for its function will be presented first.

Drosophila *cryptochrome*

Shortly after the implication of mammalian cryptochromes in circadian regulation (Miyamoto and Sancar, 1998; Thresher et al., 1998), *Drosophila* cryptochrome was discovered in 1998 through a genetic screen for circadian rhythm mutants (Stanewsky et al., 1998). Flies, like nearly all other metazoans, have an internal timekeeping mechanism that coordinates physiological and biochemical processes such as development and locomotor activity with the 24-hour solar day. These intrinsic circadian rhythms (circa = about, dies = a day) are created by a molecular clock that functions in complete darkness to generate rhythms with a periodicity of approximately 24 hours. Since the clock does not keep exact 24-hour time, it must be synchronized, or entrained, daily with its surroundings; this occurs predominantly through cues from external light-dark cycles. The vitamin A-based visual opsins are the major contributors to this process since genetically eyeless (Yang et al., 1998), opsin-depleted (Ohata et al., 1998), or blind *Drosophila* (Wheeler et al., 1993) have lower sensitivities in circadian entrainment than wild type flies. However, several studies involving dietary depletion of vitamin A suggested a role of a non-opsin photopigment in circadian photoreception (Ohata et al., 1998; Zimmerman and Goldsmith, 1971). Furthermore, the maximal sensitivity for circadian entrainment in *Drosophila* occurs in blue light (Frank and Zimmerman, 1969; Klemm and Ninneman, 1976; Ohata et al., 1998), well below wavelengths at which *Drosophila*'s rhodopsin maximally absorbs (Zuker, 1996).

The loss of function cryptochrome mutant, named cry^{baby} (cry^{b}), is caused by a destabilizing Asp→Asn substitution at amino acid 410 in the flavin binding domain, with mutant protein expressed at significantly reduced levels relative to wild-type protein. The molecular clock of cry^{b} mutants appears to function normally but is not sensitive to short, phase-shifting light pulses given in the dark, suggesting loss of photoreceptive input to the clock (Stanewsky et al., 1998). In addition, cry^{b} mutant flies take more time to adjust to a shifted light/dark cycle and maintain normal, rhythmic activity under constant light, a condition that causes arrhythmicity in wild-type flies (Emery et al., 2000a; Stanewsky et al.,

1998). Lastly, directed expression of wild-type CRY in the pacemaker neurons of cry^b flies rescues the majority of the light sensitivity of behavioral rhythms, suggesting that CRY is a cell autonomous photoreceptor sufficient for most aspects of circadian light sensitivity (Emery et al., 2000b). Indeed, an important property of the *Drosophila* circadian system is that virtually every single cell in this organism, including the brain, Malphigian tubules, abdomen and wing cells are directly light sensitive and peripheral clocks in these tissues can be reset directly by light exposure (Giebultowicz et al., 2000; Ivanchenko et al., 2001). However, cry^b mutant flies retain partial responses to light/dark cycles, suggesting functional redundancy between cryptochrome and opsins in circadian entrainment; generation of mutant flies eliminating all known opsin-containing photoreceptive organs ($glass^{60j}$) and cryptochrome (cry^b) results in flies that can no longer entrain their circadian rhythms to external light-dark cycles (Helfrich-Forster et al., 2001).

Cryptochrome entrains the molecular clock in *Drosophila* through its light-dependent interaction with the integral clock protein Timeless (TIM). In yeast two-hybrid studies, the interaction of CRY with TIM was found to occur only in the light (Ceriani et al., 1999; Rosato et al., 2001). Since yeast does not have photosensory capability, heterologously expressed CRY must form a photopigment in yeast, capable of undergoing the photochemical reaction required to mediate the TIM interaction. Deletion of the C-terminal 20 amino acids of CRY by truncation (Dissel et al., 2004; Rosato et al., 2001) or random mutagenesis (Busza et al., 2004) leads to CRY-TIM interaction in a light-independent manner. This has been interpreted to mean that the C-terminal domain specifically occludes binding of TIM to CRY in the dark. Synchronization of the molecular clock with the light cycle most likely occurs as cryptochrome induces the rapid, ubiquitin-mediated degradation of TIM (Hunter-Ensor et al., 1996; Lin et al., 2001; Naidoo et al., 1999), which destabilizes the transcriptional repressor PER and allows transcription by the CYCLE/CLOCK heterodimer to occur (Lee et al., 1999). Furthermore, the light-dependent degradation of TIM is absent in larval lateral neurons and

adult Malphigian tubules of *cry*^{b} flies, indicating the absolute requirement of cryptochrome for TIM degradation (Ivanchenko et al., 2001). Cryptochrome may also contribute to entrainment by regulating the subcellular localization of a presumably inactive CRY/PER/TIM complex; irradiation of *Drosophila* S2 cells with light has been reported to result in a significant increase in nuclear GFP-CRY in the presence of PER and TIM relative to dark-grown cells (Ceriani et al., 1999).

Although *cry* mRNA is rhythmically expressed with a peak in the early morning, CRY protein cycles only under light/dark conditions because of its rapid, light-dependent degradation, and accumulates under constant darkness (Emery et al., 2000b; Lin et al., 2001). The light-dependent degradation of CRY is regulated by the 20 amino acid C-terminal domain; loss of the C-terminus (CRYΔC) results in constitutive degradation of the protein. A mutant CRY lacking the C-terminal 20 amino acids (CRYΔC) is undetectable by western blotting (Busza et al., 2004), and overexpression by the UAS promoter in transgenic flies (Dissel et al., 2004) results in barely detectable protein levels that appear to be degraded by the proteosome irrespective of lighting conditions. The absence of the C-terminal domain results in CRY protein that interacts constitutively with TIM (Rosato et al., 2001). Despite this, CRYΔC transgenic flies exhibit oscillations in PER and TIM protein and respond to pulses of light that shift the circadian phase of behavior, although with reduced amplitudes relative to wild-type flies (Busza et al., 2004; Dissel et al., 2004). These data indicate that the light dependence of TIM degradation by cryptochromes is mediated by two separate events: first, light is required to release the repressive C-terminal domain in full length CRY to allow for TIM binding, which is necessary but not sufficient for phototransduction; second, TIM is modified for proteosomal targeting by a cryptochrome-dependent signal that requires light, which can occur in the absence of the C-terminal domain since the photolyase homology region is sufficient for the photoreceptive function of cryptochrome (Busza et al., 2004).

This mechanism of action shares both similarities with and clear differences from the proposed mechanism of action of plant cryptochromes (see below). In the case of both plant and animal cryptochromes, light irradiation appears to result in de-repression of a signal transduction domain, presumably through conformational rearrangement. Light-dependent initiation of signaling by all cryptochromes absolutely requires the photolyase homology region; however, signaling by plant cryptochromes appears to be mediated entirely by the C-terminal domain, since overexpression of this domain is sufficient to generate a constitutive photomorphogenic response (Wang et al., 2001; Yang et al., 2001). In contrast, the photolyase homology region of *Drosophila* cryptochrome appears to require light for two distinct steps in its signal transduction: 1) light-dependent release of the C-terminal domain with concomitant binding of TIM and 2) light-dependent proteosomal targeting of the TIM protein (Busza et al., 2004; Dissel et al., 2004). In summary, cryptochrome functions in the *Drosophila* circadian clock by acting as a cell autonomous photopigment, conveying light information directly to core clock components through protein-protein interactions and light-regulated protein degradation.

Mammalian cryptochromes

The entrainment of circadian rhythms in mammals is fundamentally different from *Drosophila*, since all photoreception in mammals occurs through the retina (Van Gelder and Sancar, 2003) and is communicated to the master circadian clock in the suprachiasmatic nuclei (SCN) of the hypothalamus via the retinohypothalamic tract (Johnson et al., 1988b). As in *Drosophila*, early studies mammalian circadian photoreception identified the apparent role of a non-visual photopigment in the entrainment of mice, since mice with degeneration of the outer retina (*rd/rd*), thus lacking the classical visual photoreceptors, still entrain their rhythms normally (Ebihara and Tsuji, 1980). After the discovery and characterization of mammalian cryptochromes in 1996, it was proposed that they might be the elusive non-visual photopigment (Hsu et al., 1996) and histochemical studies have revealed that both

cryptochromes are highly expressed in the ganglion cells of the inner retina of mice (Miyamoto and Sancar, 1998; Miyamoto and Sancar, 1999) and humans (Thompson et al., 2003).

The potential role of mammalian cryptochromes in circadian photoreception has been studied primarily through the use of mouse genetics. Interestingly, although cryptochromes were introduced into the field of circadian biology as putative blue-light photopigments, current evidence puts them squarely in the core of the circadian clock machinery (Sancar, 2004). The free-running circadian periods of both *Cry1*$^{-/-}$ and *Cry2*$^{-/-}$ mice are shorter and longer, respectively, than wild-type mice, revealing a role for cryptochromes in the molecular clock independent of any presumptive photoreceptive function (Thresher et al., 1998; van der Horst et al., 1999). Furthermore, *Cry1*$^{-/-}$*Cry2*$^{-/-}$ mice are arrhythmic under constant darkness, underscoring the fact that cryptochromes are required for the molecular clock to function in mammals (van der Horst et al., 1999; Vitaterna et al., 1999). These animals do respond behaviorally to light/dark cycles; however, this is due to “masking”, a direct repressive effect of light on locomotor behavior independent of the clock (Mrosovsky, 1999). Cryptochromes were later characterized as essential transcriptional repressors in the feedback loop that generates the mammalian molecular clock (Griffin et al., 1999; Kume et al., 1999).

The mammalian molecular clock consists of an oscillator generated by two interconnected transcription/translation feedback loops (Figure 1.1) (Shearman et al., 2000). The positive arm of the major feedback loop is driven by bHLH/PAS domain-containing transcription factors CLOCK and BMAL1 (Bunger et al., 2000; Gekakis et al., 1998). The CLOCK/BMAL1 heterodimer activates the transcription of core clock genes *Cryptochrome* (*Cry1* and *Cry2*), *Period* (*Per1* and *Per2*), and *Rev-Erb*α. PER and CRY proteins form multimeric complexes that translocate to the nucleus, where they interact with CLOCK/BMAL1 to downregulate transcription, generating the negative arm of the major

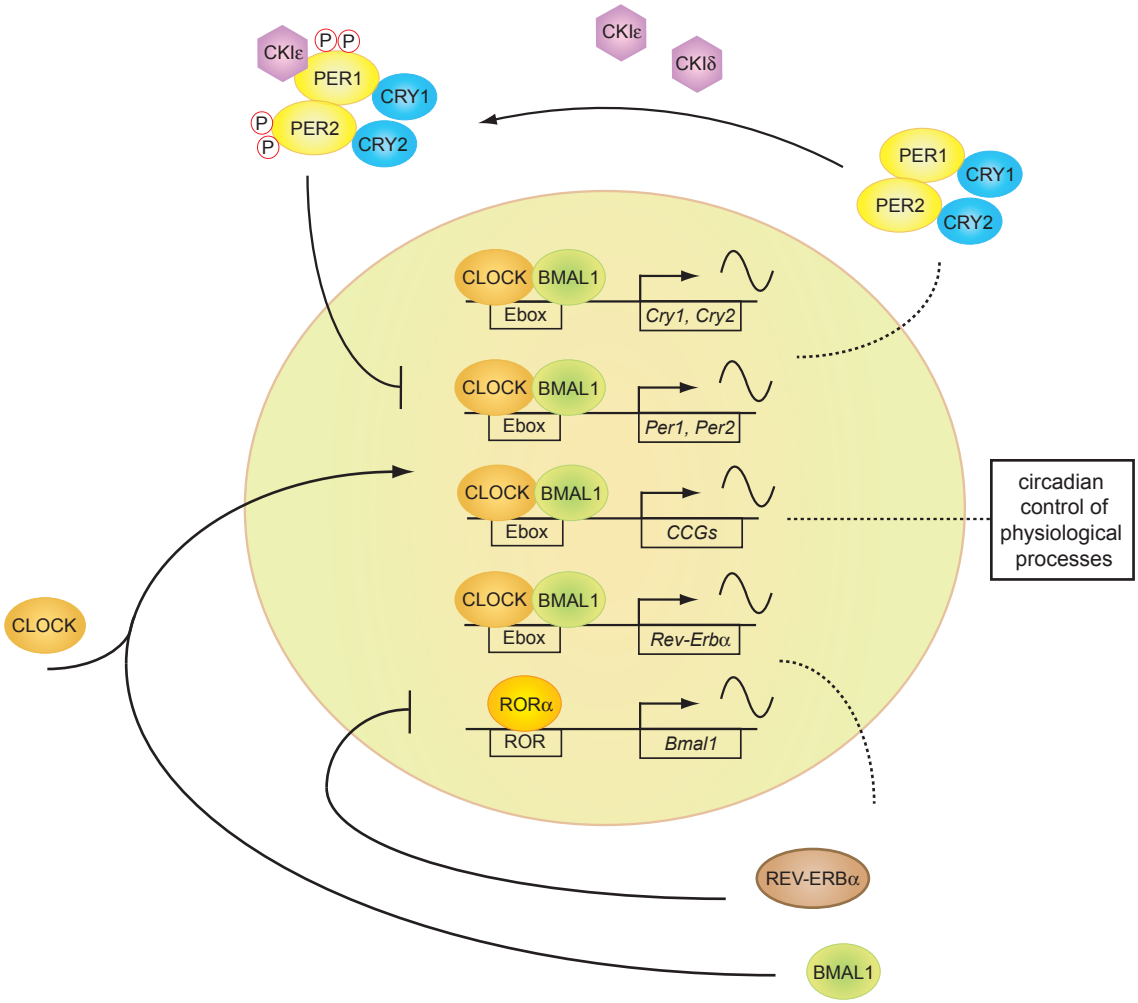

Figure 1.1 Molecular oscillator of the mammalian circadian clock
The oscillator is generated by two interconnected transciption/translation feedback loops consisting of a set of integral clock proteins: CLOCK, BMAL1, PERIOD, CRYPTOCHROME, REV-ERBα, and CKIε/δ. Most clock proteins are rhythmically expressed and but some are not (CLOCK, CKIε/δ). CLOCK/BMAL1 drive the positive arm of the major loop by stimulating transcription at E boxes; PER/CRY heterodimers inhibit CLOCK/BMAL1, constituting the negative arm of the major loop. Rhythmic transcription of REV-ERBα translates into the rhythmic inhibition of RORα to regulate BMAL1 transcription, generating the second, interconnected feedback loop. Clock control of physiological processes arises from the transcriptional regulation of clock-controlled genes (CCGs) by CLOCK/BMAL1.

feedback loop (Griffin et al., 1999; Kume et al., 1999; van der Horst et al., 1999; Vitaterna et al., 1999). In a separate feedback loop, *Bmal1* RNA levels oscillate as a result of the regulated balance between a transcriptional activator, RORα, and inhibitor, REV-ERBα (Sato et al., 2004). This stable and precise molecular oscillator derives its near 24-hour periodicity from the posttranslational regulation of clock proteins, which determines their subcellular localization, intermolecular interactions, and stability. Mutations affecting posttranslational modifications of clock proteins have drastic effects on oscillators from fungi to humans, resulting in changes in period length (Lowrey et al., 2000; Toh et al., 2001) or complete disruption of cycling (Yang et al., 2002).

Since mutations in cryptochromes affect locomotor activity independently of light, behavior does not provide an accurate readout of photoresponse in these mice. The most quantitative demonstration of the effect of cryptochromes on photoreceptive input to the clock is measured through light-dependent gene induction in the SCN. Light given in the middle of the night induces rapid and robust induction of *Period* clock gene mRNA (Shearman et al., 1997), as well as the immediate-early gene *c-fos* (Aronin et al., 1990; Kornhauser et al., 1990). Since the loss of cryptochrome affects steady-state levels of *Per* mRNA due to its role in the clock, the contribution of cryptochrome to circadian phototransduction is most accurately measured through induction of *c-fos* in the SCN.

To determine if cryptochromes mediate circadian photoreception in the absence of visual photoreceptors, photoinduction of *c-fos* was examined in the *rd/rd* background. While *rd/rd* mice exhibit normal levels of *c-fos* induction by light (Guido et al., 1999; Selby et al., 2000; Wollnik et al., 1995), light induction of *c-fos* in *rd/rdCry1*$^{-/-}$*Cry2*$^{-/-}$ mice is reduced approximately 3,000-fold under limiting light (Selby et al., 2000; Thompson et al., 2004a). Even in the presence of all other photoreceptors, the loss of cryptochromes significantly reduces circadian photosensitivity. Mice lacking *Cry2*, the cryptochrome expressed most predominantly in the mouse retina, have a 2-fold decrease in photoinduction of *c-fos*

(Thresher et al., 1998), and mice lacking both cryptochromes exhibit a 10-20-fold reduction in sensitivity (Selby et al., 2000). Reduced responses in cryptochromeless mice are not likely due to secondary or non-specific changes in expression of signaling intermediates on the immediate-early gene induction pathway, since the magnitude and timecourse of *c-fos* induction by serum or forskolin in dermal fibroblast cell lines derived from *Cry1*$^{-/-}$*Cry2*$^{-/-}$ and wild-type mice are similar (Thompson et al., 2004a). In addition, the pupillary light response of *rd/rdCry1*$^{-/-}$*Cry2*$^{-/-}$ mice is reduced 20-fold with respect to *rd/rd* mice, implicating cryptochromes in this non-visual photoresponse as well (Van Gelder et al., 2003). However, the presence of residual photoresponses in *rd/rdCry1*$^{-/-}$*Cry2*$^{-/-}$ mice, both in gene induction and pupillary response, led to the conclusion that yet another non-visual photoreceptor must exist in the inner retina that remains intact in *rd/rd* mice (Selby et al., 2000; Van Gelder et al., 2003). Indeed, in an independent approach, Provencio and colleagues discovered a novel opsin, called melanopsin, which is expressed exclusively in the retinal ganglion cells of the retina that are implicated in non-visual phototransduction, such as circadian photoreception and the pupillary light response (Provencio et al., 2000). Following up on this pioneering discovery, later work showed that these ganglion cells were intrinsically photosensitive and were named intrinsically photosensitive retinal ganglion cells (ipRGCs) (Berson et al., 2002; Hattar et al., 2002). While genetic deletion of this invertebrate-like opsin alone has only minor effects on non-visual photoresponses (Lucas et al., 2003; Ruby et al., 2002), the elimination of visual photoreceptors and melanopsin results in mice that lose all non-visual photoresponses (Hattar et al., 2003; Panda et al., 2003).

These findings raised serious doubts about a photoreceptive role for cryptochrome in mammalian non-visual photoresponses and forced a re-evaluation of the experiments indicative of such a role in mammals. Another genetic approach was taken to address this issue using mice lacking retinol binding protein (RBP). Elimination of dietary vitamin A in the *RBP*$^{-/-}$ genetic background depletes ocular retinaldehyde, the required cofactor of all opsin

photopigments, to undetectable levels by 10 months of age (Quadro et al., 1999). Surprisingly, *RBP*$^{-/-}$ mice raised on a vitamin A-free diet are blind (Quadro et al., 1999) yet retain essentially normal retinohypothalamic photoreception/phototransduction as measured by gene induction in the SCN (Thompson et al., 2001; Thompson et al., 2004b). Importantly, *RBP*$^{-/-}$*Cry1*$^{-/-}$*Cry2*$^{-/-}$ mice raised on the vitamin A-free diet fail to induce *c-fos* in the SCN by light, indicating that inactivation of opsins in combination with the loss of cryptochromes is sufficient to eliminate phototransduction to the SCN (Thompson et al., 2004b). It is unclear why genetic ablation of opsin function (*rd/rdOpn4*$^{-/-}$ (Panda et al., 2003) or *Gnat1*$^{-/-}$*Cnga*$^{-/-}$ *Opn4*$^{-/-}$ (Hattar et al., 2003)) and inactivation of opsins via cofactor depletion (*RBP-/-* mice raised on a vitamin A-free diet (Thompson et al., 2001)), which leaves the opsin apoproteins intact, produce different phenotypes in circadian photoreception. Conceivably, opsin apoproteins, which are clearly required to generate an action potential through the retinohypothalamic tract, could act as G-protein coupled receptors to transmit a signal generated by cryptochrome.

In summary, the available data on the role of mammalian cryptochromes as circadian photopigments indicate that they are neither necessary nor sufficient for generating an action potential through the retinohypothalamic tract to the SCN. However, in their absence, circadian phototransduction to the SCN is significantly compromised, indicating that cryptochromes may generate a signal that is converted to an action potential by melanopsin, or they may amplify or prolong the signal generated by opsins. Given that the phototransduction cascade of melanopsin is highly unusual in mammals, resembling that of invertebrate opsins (Melyan et al., 2005; Panda et al., 2005; Qiu et al., 2005), we can only postulate how cryptochromes might regulate this phototransduction pathway. Using genetic approaches, it is not possible to determine whether cryptochromes act as photopigments or light-independent signal transducers in this pathway. It is clear that expression of mammalian cryptochromes is not necessarily sufficient to confer photoresponsiveness in a

tissue, since the SCN expresses high levels of cryptochromes, yet does not respond directly to light (Herzog and Huckfeldt, 2003). Whether cryptochromes act as photopigments or light-independent signal transducers in a given tissue is likely dependent on the cellular context in which they are expressed. This is a common property of receptors, which can manifest their effector function only when the cell expresses the appropriate adapters/transducers as well (Panda et al., 2005).

Other vertebrate cryptochromes

Unlike mammalian organisms, which rely strictly on communication between ocular photoreceptors and the brain to detect light, a number of other vertebrate animals employ extraocular or cell autonomous photoreception, thereby providing more tractable systems in which to investigate cryptochrome photoreception at a molecular level. In particular, it has been found that peripheral organs in zebrafish, such as the heart and kidney, are directly photosensitive and have light-entrainable circadian clocks (Whitmore et al., 2000). Embryonic cell lines derived from zebrafish possess circadian clocks that are responsive to light/dark cycles (Pando et al., 2001; Whitmore et al., 2000). Action spectrum analysis of the Z3 cell line revealed that light in the near UV/blue range (λ_{max} ~380 nm) is most effective for light-dependent clock gene induction; these data, and the apparent lack of detectable retinal in the cell line, are consistent with photoreception by cryptochromes (Cermakian et al., 2002). While the cell line expresses all six of the zebrafish cryptochromes, a more detailed analysis will be required to make the absolute determination of the identity of the blue light photoreceptor mediating this response (Cermakian et al., 2002). The use of RNAi and small molecule inhibitors of signaling pathways in cell culture provides a promising system for the investigation of cryptochrome photoreception in zebrafish.

The investigation of cryptochrome function in vertebrates has also been advanced significantly in studies of cell autonomous photoreception in isolated tissue samples. In contrast to the mammalian iris and adult chicken iris, the embryonic chick iris is directly

photosensitive to light, and the pupil constricts as it does in the whole animal when the iris is exposed to light *ex vivo*. While melanopsin and both cryptochromes 1 and 2 are expressed in the iris, destruction of the opsin cofactor retinaldehyde by bright light had no effect on the pupillary light response (PLR), indicating that cryptochromes may mediate this response (Tu et al., 2004). Partial downregulation of melanopsin by treating the isolated iris with siRNA had no effect on PLR photosensitivity, but downregulation of either cryptochrome by 50% decreased PLR photosensitivity by a comparable amount (Tu et al., 2004). Action spectrum analysis of the PLR in the isolated iris does not fit the absorption spectrum of any known opsin; instead, it most closely resembled the absorption spectrum of recombinant cryptochromes, with a peak at 420 nm and higher sensitivity at shorter wavelengths (Hsu et al., 1996; Özgür and Sancar, 2003; Tu et al., 2004). These findings strongly suggest that cryptochrome is the photopigment responsible for the PLR in the embryonic chick iris, providing the most compelling evidence to date that cryptochromes function as photosensory pigments in vertebrate animals.

Photolyase/cryptochrome structure, photochemistry, and *in vitro* studies

Structure of the photolyase/cryptochrome family

Photolyases repair UV-induced photoproducts in DNA; however, UV irradiation induces two predominant DNA photoproducts in adjacent pyrimidines, the cyclobutane pyrimidine dimer (CPD) and the (6-4) pyrimidine-pyrimidone photoproduct, and different photolyases are required to repair each type of damage. The three major groups of enzymes in this family, CPD photolyase, (6-4) photolyase, and cryptochromes, are 50-70 kDa proteins that contain two noncovalently bound chromophore/cofactors. One is always flavin adenine dinucleotide (FAD), the catalytic chromophore, and the other serves as a photoantenna and is most commonly methenyltetrahydrofolate (MTHF), or 8-hydroxy-5-deazaflavin (8-HDF) in rare organisms that synthesize this chromophore (Sancar, 2003). Although cryptochromes and photolyases are only moderately related by sequence,

retaining 27-32% sequence identity on average, they are highly structurally homologous. Crystal structures of several photolyases (Komori et al., 2001; Park et al., 1995; Tamada et al., 1997) and the photolyase homology region of two cryptochromes (Brautigam et al., 2004; Brudler et al., 2003) reveal that their Cα backbones are nearly superimposable with RMS deviations of less than 2 Å. The structures are characterized by two modular domains: an N-terminal α/β-domain and a C-terminal α-helical domain, connected by a long, interdomain loop (Figure 1.2). The catalytic FAD chromophore is bound within the α-helical domain in an unusual U-shaped conformation, with the isoalloxazine ring held in the close proximity to the adenine ring, and the second chromophore is bound in a cleft located in between the two domains close to the surface of the protein. A hole of approximately 10 Å in diameter, located in the middle of the α-helical domain, allows access of solvent and oxygen to the FAD molecule and is of the right dimensions and polarity to allow entry of a pyrimidine dimer to within van der Waal's contact distance of the isoalloxazine ring of FAD (Park et al., 1995).

Photolyase photocycle

A photolyase reaction scheme in terms of classic Michaelis-Menton enzymology can be written as:

$$E + S \underset{k_2}{\overset{k_1}{\rightleftharpoons}} ES \xrightarrow[h\upsilon]{k_3 = k_p I} E + P$$

where k_p is the photolytic constant and I is light intensity [reviewed in (Sancar, 2003)]. Reaction mechanisms of CPD and (6-4) photolyases are believed to be very similar, with the exception that (6-4) photolyases must first thermally convert the open form of the (6-4) photoproduct to an oxetane intermediate before repair. A mechanistic description of the *E.coli* CPD photolyase is in accord with the structural features of the enzyme and may be summarized as follows (Figure 1.3). Photolyase contains a positively charged DNA binding groove on one face of the protein, with the active site hole located in the middle of the

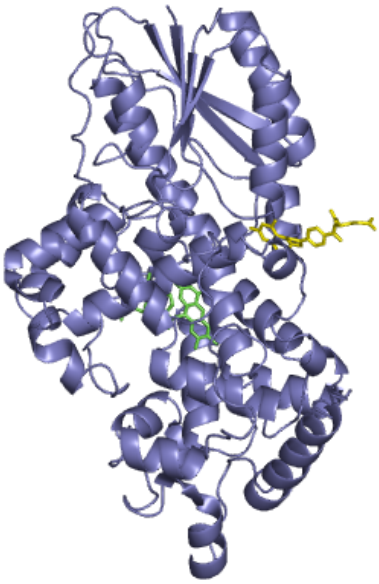

E.coli CPD Photolyase

A.thaliana CRY1-PHR

Figure 1.2 Structures of photolyase and cryptochrome
Ribbon diagram representations of *E.coli* photolyase (PDB: 1DNP4) and the photolyase homology region (PHR) of *A.thaliana* CRY1 (PDB: 1U3C). Note that the crystal structure of photolyase contains both FAD (green) and folate (yellow), whereas that of AtCRY1-PHR contains only FAD.

groove. Photolyase binds the DNA around the cyclobutane dimer in a light-independent reaction and flips the dimer out into the active site cavity to make contact with the flavin (Mees et al., 2004; Park et al., 1995), producing a stable enzyme-substrate complex. Exposure of this complex to light initiates catalysis; the MTHF photoantenna absorbs a photon and transfers the excitation energy to the deprotonated two-electron reduced flavin by Förster dipole-dipole resonance energy transfer. The excited flavin [$^1(FADH^-)^*$] then transfers an electron to the pyrimidine dimer, generating a pyrimidine dimer radical, which undergoes bond rearrangement to yield repaired pyrimidine bases. The flavin neutral radical generated during the reaction is restored to the catalytically active form by back electron transfer from the repaired DNA, and the enzyme and product dissociate. Therefore, photolyase repairs DNA photoproducts using a mechanism of light-induced electron transfer that does not result in a net change of the redox state of the enzyme.

Cryptochrome may utilize a similar photocycle to initiate signal transduction, although there are currently no data to support this hypothesis. In addition, there are only limited studies on the biochemical properties of cryptochromes due to difficulties in the purification of native cryptochromes in preparative quantities or recombinant protein containing chromophore in the quantities required for biochemical analysis. The following sections summarize the current body of work on the biochemical properties of cryptochromes, from bacteria to humans.

Interchromophore energy transfer

In contrast to most other cryptochromes, purification of recombinant *Vibrio cholerae* CRY1 (VcCRY1, DASH class) from *E.coli* yields large quantities of protein containing near stoichiometric amounts of both the $FADH^-$ and MTHF chromophores, making it highly suitable for photochemical studies (Worthington et al., 2003). The dynamics of resonance energy transfer from the photoantenna MTHF to the $FADH^-$ cofactor have recently been studied in VcCRY1 with femtosecond resolution (Saxena et al., 2005). The resonance

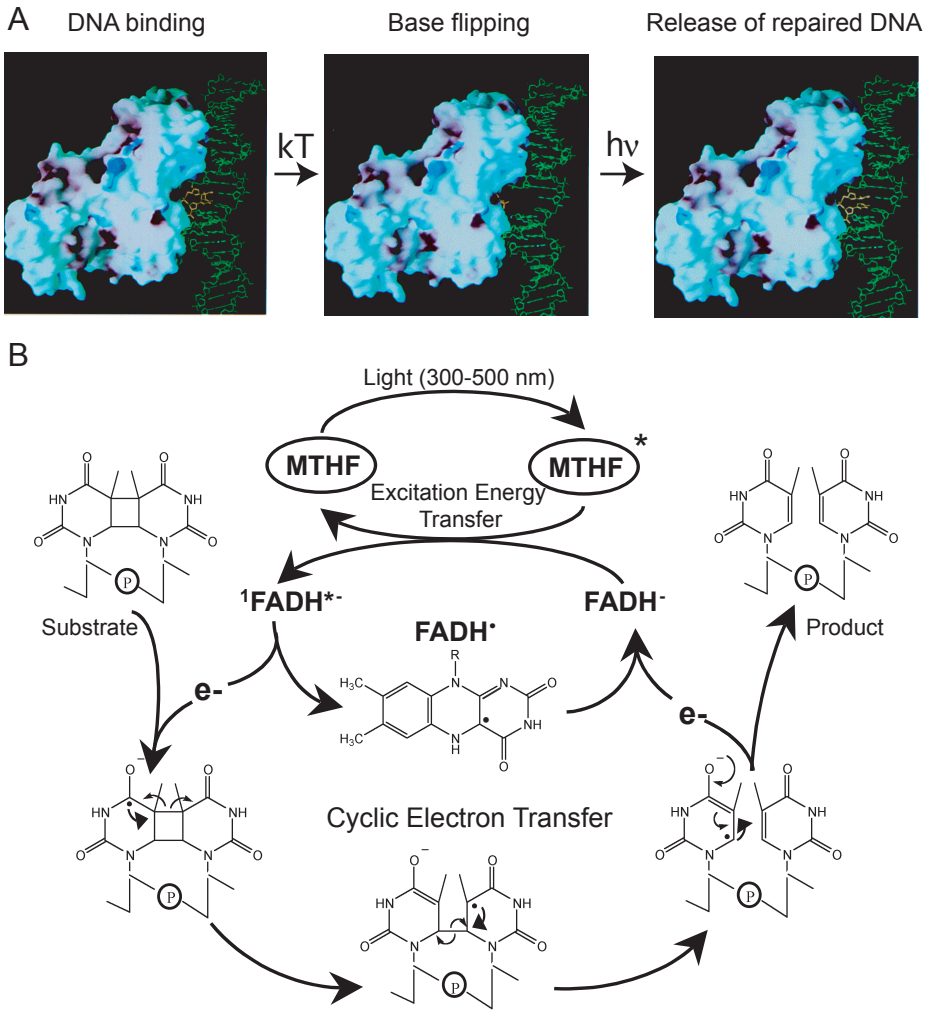

Figure 1.3 Reaction mechanism of CPD photolyase
A. Overall scheme. Photolyase binds DNA in the dark and flips the pyrimidine dimer out of the DNA helix into the active site cavity thermally (kT); after photochemical (h*v*) repair, the dinucleotide leaves the cavity and the E-S complex dissociates. **B.** Catalysis. MTHF absorbs a photon and transfers excitation energy by FRET to $FADH^{\circ -}$, which transfers an electron to the pyrimidine dimer. The dimer undergoes [2+2] cycloreversion to generate a dinucleotide; back electron transfer restores $FADH^{-}$ to the reduced form and converts the dimer to canonical bases.

energy transfer process from MTHF* to $FADH^-$ occurs with a lifetime of 60 ps, approximately five times faster than in *E.coli* photolyase. Furthermore, the fluorescence lifetime of MTHF* is 845 ps, more than twice as long as that in *E.coli* photolyase (Saxena et al., 2004; Saxena et al., 2005). While there are mechanistic similarities of ultrafast resonance energy transfer between *E.coli* photolyase and *V.cholerae* cryptochrome, interchromophore energy transfer appears to be more efficient in cryptochrome than in photolyase, suggesting a shorter interchromophore distance or a more favorable orientation of the two chromophores. Since the two crystal structures of cryptochromes solved to date lack the MTHF chromophore, further studies will be required to understand the structural basis of the different photophysical properties of VcCRY1 and *E.coli* photolyase.

Photoinduced intraprotein electron transfer

It has been found that in many flavoproteins, such as glucose oxidase or cholesterol oxidase, flavin fluorescence is partly quenched by electron transfer from neighboring Trp and Tyr residues to the flavin excited singlet state, which has a high oxidizing potential (Zhong and Zewail, 1999). Thus, flavoproteins are convenient systems for investigation of the kinetics and mechanisms of intraprotein electron transfer though these reactions have no relevance to the biological functions of the particular proteins. As previously mentioned, the catalytically active form of flavin in photolyase is always two-electron reduced and deprotonated flavin adenine dinucleotide ($FADH^-$). Purification of photolyase yields protein containing either the semireduced flavin radical ($FADH^\circ$) or the fully oxidized flavin (FAD_{ox}), which must be reduced *in vitro* by photoexcitation of the protein in the presence of reducing agents (Li et al., 1991; Saxena et al., 2004). Photoreduction in *E.coli* photolyase occurs in part through intraprotein electron transfer along a chain of three tryptophan residues, W382-W359-W306, and in part through W306 and α-helix 15 (Li et al., 1991; Park et al., 1995; Saxena et al., 2004; Saxena et al., 2005; Weber, 2005). However, this photoreduction through intraprotein electron transfer has little or no physiological significance for the activity

of photolyase, since mutations abolishing electron transfer have no effect on the enzymatic activity of photolyase *in vivo* (Kavakli, 2004; Li et al., 1991).

Since the tryptophans of the 'Trp triad' are conserved in cryptochromes from plants to animals, it has been speculated that intraprotein electron transfer may play a role in the cryptochrome photocycle. Several studies investigating the role of tryptophans corresponding to the Trp triad have implicated these residues in regulation of both light dependent and independent reactions mediated by animal cryptochromes (Froy et al., 2002; Zhu and Green, 2001). Mutation of two tryptophans in the Trp triad of *Drosophila* cryptochrome (W342 and W397, corresponding to W306 and W359, respectively, in *E.coli* photolyase) to alanine results in a loss of light stimulation in the regulation of CRY protein stability and repression of PER/TIM-mediated transcriptional inhibition (Froy et al., 2002). However, substitution of these tryptophans with either tyrosine (redox-active) or phenylalanine (redox-inactive) has no effect on these activities. Since phenylalanine is incapable of initiating electron transfer to excited state flavin, it appears that the effect, or lack thereof, of Trp triad mutations in *Drosophila* CRY is due to the effect of the mutations on protein folding rather than the involvement of these residues in cryptochrome photochemistry. Indeed, in this study it was found that overall protein stability in the alanine mutants was significantly reduced, indicating that substitution of tryptophan with a structurally dissimilar amino acid results in loss of protein stability and therefore, signaling capability. In line with this interpretation, mutations of the Trp triad also affect the light-independent transcriptional regulatory activity of mouse and *Xenopus* cryptochromes. Since tryptophan cannot carry out a redox reaction with ground state flavin, these studies again suggest that the Trp triad has a role in maintaining the structural integrity necessary for function, rather than participating in the photocycle, of animal cryptochromes (Froy et al., 2002; Zhu and Green, 2001).

The intraprotein electron transfer pathway has also been implicated in the photoreduction of plant cryptochromes. Irradiation of recombinant AtCRY1 containing fully oxidized flavin in the presence of β-mercaptoethanol results in transient absorption spectra consistent with the formation of a semireduced radical (FADH°) and concomitant production of a neutral tryptophan radical, which presumably abstracts an electron from one of four nearby tyrosine residues (Giovani et al., 2003). Therefore, the FAD cofactor can be photoreduced in a plant cryptochrome, just as in photolyase or cholesterol oxidase, in a process involving tryptophan radicals. Even though it has been shown that the intraprotein electron transfer from Trp to flavin is not part of the photolyase photocycle because the enzyme contains two-electron reduced flavin before and after the photoenzymatic repair reaction (Kavakli, 2004; Sancar, 2003), the same cannot be said for cryptochromes because the redox state of the flavin in cryptochromes *in vivo* is not known. Purified cryptochromes usually contain two-electron oxidized flavin and several recent studies (Giovani et al., 2003; Zeugner et al., 2005) suggest that photoreduction of FAD_{ox} by intraprotein transfer is the primary photochemical step in the cryptochrome photocycle in plants.

One study addressed the role of photoinduced electron transfer through the Trp triad as part of the CRY photocycle by examining the effect of tryptophan mutations on the light-stimulated kinase activity of AtCRY1 (see below). It was found that mutation of either W400 or W324, analogous to W382 and W306 in *E.coli*, to redox-inactive phenylalanine results in a loss of photoreduction of the oxidized mutant protein, consistent with interruption of an electron transfer pathway (Zeugner et al., 2005). Significantly, both the W400F and W324F mutations abolish the light stimulation of kinase activity seen in wild-type protein and plants expressing the mutant cryptochromes appear to lack cryptochrome activity (Zeugner et al., 2005). However, mutations disrupting the intraprotein electron transfer pathway should theoretically affect only the light-stimulated activity; instead, both W400F and W324F have drastic effects on the basal (light-independent) kinase activity of AtCRY1, indicating that

structural perturbations caused by these mutations (as in the case of mouse, *Xenopus* and *Drosophila* cryptochromes) may be responsible for disrupting the light-independent and light-dependent kinase activity of cryptochrome, thus casting doubt about the relevance of 'Trp triad' photochemistry in the photoreceptive function of *Arabidopsis* cryptochromes. The identification of the *in vivo* oxidation state of native cryptochromes will help resolve the questions regarding a putative role of redox active amino acids in the cryptochrome photocycle.

Light-stimulated kinase activity

Phosphorylation is a key regulatory mechanism for nearly all photopigments (Briggs et al., 2001; Kim et al., 2004; Maeda et al., 2003). The C-termini of both plant cryptochromes are phosphorylated *in vivo* in response to light; AtCRY1 is phosphorlyated by phytochrome A in a red light-dependent manner (Ahmad et al., 1998b) and AtCRY2 is phosphorylated by an as-yet unidentified kinase in a blue light-dependent manner (Shalitin et al., 2002). In addition, an ATP-binding and autophosphorylation activity was recently described for AtCRY1 (Bouly et al., 2003; Brautigam et al., 2004; Shalitin et al., 2003). ATP binding by AtCRY1 occurs with a 1:1 stoichiometry (Bouly et al., 2003; Brautigam et al., 2004) and autophosphorylation occurs primarily on serine residues (Bouly et al., 2003). The kinase activity was reported to be dependent on the presence of flavin and a reducing agent, and stimulated 2-3-fold or more *in vitro* in the presence of white light (Bouly et al., 2003; Shalitin et al., 2003). Treatment of recombinant AtCRY1 with flavin antagonists such as potassium iodide (shown to inhibit redox reactions mediated by other flavoproteins), or an oxidizing agent, H_2O_2, abolishes the light stimulation, indicating that AtCRY1 autophosphorylation is regulated by both redox state and light status (Bouly et al., 2003). Blue light-dependent autophosphorlyation of AtCRY1 may represent a significant means of regulation, since the magnitude of blue light-dependent phosphorylation *in vivo* far exceeds

that seen in response to red light and is rapidly reversed, virtually absent after only 15 minutes in the dark (Shalitin et al., 2003).

It is not currently known on which residue(s) the autophosphorylation occurs, but it was reported that the photolyase homology region of AtCRY1 is sufficient to autophosphorylate (Bouly et al., 2003). Furthermore, the crystal structure of the photolyase homology region of AtCRY1 reveals a single molecule of ATP bound in the cavity that corresponds to the active site in photolyase (Brautigam et al., 2004). Unexpectedly, however, the absence of serine residues within 11 Å of the cavity and lack of homology to canonical kinase domains raise questions as to whether the ATP bound in the flavin cavity participates in the kinase reaction (Brautigam et al., 2004). ATP binding and autophosphorylation under light conditions were also demonstrated for human CRY1 but the flavin requirement and light dependence of this reaction were not analyzed (Bouly et al., 2003). Light stimulation of hCRY1 kinase activity *in vitro* is highly unlikely given that recombinant preparations of this protein typically contain little or no chromophore (Hsu et al., 1996; Özgür and Sancar, 2003).

In fact, a recent study of kinase activity in both plant and animal cryptochromes raises some reservations about earlier conclusions regarding the requirement of flavin for kinase activity (Özgür, 2005). The *in vitro* kinase activity of AtCRY1, human CRY1 and CRY2 was not stimulated significantly by white light and did not correlate with flavin content. AtCRY1 and AtCRY2 produced in the baculovirus/insect cell system both contain stoichiometric flavin, and yet AtCRY1 has kinase activity and AtCRY2 does not. Moreover, there was little or no light stimulation of AtCRY1 kinase activity. In addition, human CRY1 and CRY2 produced in this system contain no flavin but have kinase activity similar to that of AtCRY1 (Özgür, 2005). Several questions regarding the kinase activity of cryptochromes emerge: What is the determining factor for kinase activity in cryptochromes in the absence of a canonical kinase domain or apparent dependence on flavin? Why do AtCRY1 and the

human cryptochromes possess the ability to autophosphorylate, but AtCRY2 does not? It is conceivable that the autophosphorylation of cryptochrome, as in the case of phytochromes, may have only minor significance to the photocycle (Matsushita et al., 2003). Clearly, the potential role of autophosphorylation in the cryptochrome photocycle is intriguing and will require more in depth study.

Dimerization

AtCRY1 and AtCRY2 form constitutive homo- and heterodimers in plants, mediated by the N-terminal photolyase homology region (Sang et al., 2005). Dimerization of the protein appears to be required for full activation by light; the constitutive photomorphogenic (COP) phenotype reported after overexpression of GUS-CCT (Cry C-terminal) fusion proteins (Yang et al., 2001) may have been promoted by multimerization of the GUS fusion protein, since overexpression of CCTs fused to monomeric proteins does not cause a COP phenotype (Sang et al., 2005). Dimerization of CRY may simply stabilize the interaction with its dimeric effector, COP1 (Torii et al., 1998), or a unique C-terminal conformation conducive to COP1 binding may be created as a result of domain-swapped cryptochrome dimers.

Cryptochrome and magnetoreception

Recently, photoexcited cryptochrome has also been implicated in magnetoreception in birds and insects. Migratory animals utilize the earth's magnetic field to orient themselves while migrating or homing over vast distances (Lohmann and Johnsen, 2000). The physicochemical mechanism enabling birds to sense the reference direction given by the earth's magnetic field is not known, although it is known that the eye is required (Semm and Demaine, 1986) and that magnetoreception is dependent on light in the blue-green range (Wiltschko and Wiltschko, 1995). Two forms of information can be derived from the geomagnetic field (Lohmann and Johnsen, 2000): 1) a directional, or 'compass', sense allows an animal to orient its movements with respect to the geomagnetic field, and 2) a positional, or 'map', sense provides information on where an animal is with respect to its

destination by analyzing the intensity and inclination of magnetic field lines, which vary across the earth's surface and can be used to estimate position. There is evidence that both mechanisms are employed by animals, some relying on one or both senses (Wiltschko et al., 2004). Furthermore, these two guidance systems rely on separate magnetoreceptors with different mechanisms, based on either 1) biogenic magnetite ("physical model") existing as either single-domain particles (Kirschvink and Gould, 1981), fixed super-paramagnetic particles (Kirschvink et al., 1985), or as a liquid crystal (Edmonds, 1996); or 2) a magnetically sensitive radical-pair reaction ("chemical model") (Ritz et al., 2000; Ritz et al., 2004; Schulten, 1982) Current data suggest a role for magnetite-based magnetoreception in generation of the 'map sense' (Beason et al., 1995) and the radical-pair mechanism in generation of the 'compass sense' (Irwin and Lohmann, 2005; Ritz et al., 2004).

Cryptochromes have been suggested as candidate receptors mediating the radical-pair mechanism (Moller et al., 2004; Mouritsen et al., 2004; Ritz et al., 2000). In this mechanism, the magnetoreceptor must possess an excited state in which photon absorption generates singlet-excited states and subsequent radical pairs (Ritz et al., 2000). Singlet pairs may be converted to triplet pairs, with varying yield depending on the alignment of the receptor in the geomagnetic field. By analyzing the triplet yield over the fixed surface of the retina, animals could obtain directional information from the magnetic field (Moller et al., 2004). The strongest evidence to date for this mechanism in the compass sense of birds was demonstrated by using oscillating magnetic fields to perturb the magnetic orientation behavior of European robins (Ritz et al., 2004). A weak oscillating field that is in resonance with the splitting between the radical-pair states could perturb the signaling mechanism by directly driving singlet-triplet transitions, but is not predicted to affect a magnetite-based receptor since the cellular environment would prevent magnetite particles from tracking weak radio-frequency magnetic fields (Ritz et al., 2004).

In order for a candidate receptor to participate in the radical-pair mechanism, several important criteria must be met. First, the receptor must be expressed in the retina, specifically in neurons that signal geomagnetic information to the brain. Secondly, the receptor should be localized in an ordered lattice with fixed orientation. The receptor must create a radical-pair as a result of photon absorption, and have a long enough lifetime (~100 nanoseconds) to allow the ambient magnetic field to alter the spin correlation, but not slow enough to allow stochastic fluctuations in spin states to dominate the signaling species. Based on evidence presented to date, cryptochromes satisfy several of these criteria, suggesting that they may act as magnetoreceptors for directional sense in animals. Cryptochrome expression in magnetically orienting garden warblers was identified in the subset of retinal ganglion cells that project to the nucleus of the basal optic root (Mouritsen et al., 2004), where magnetically sensitive neurons have been reported (Semm and Demaine, 1986) and the visual flow-fields arising from self motion are processed (Wylie et al., 1998). Moreover, CRY1-expressing ganglion cells in these birds show high levels of neuronal activity at night during magnetic orientation (Mouritsen et al., 2004). Retinal CRY1 expression is predominantly cytoplasmic and is therefore more likely to be maintained in a specific orientation via structural proteins than nuclear protein. Striking differences in the expression of CRY in migratory and nonmigratory birds also supports a unique role for cryptochromes in magnetoreception (Mouritsen et al., 2004). This model depends on the formation of a cryptochrome radical state *in vivo*; although the physiological relevance of such a state is not known, a plant cryptochrome has been shown to generate a radical pair upon photon absorption *in vitro* (Giovani et al., 2003). These studies therefore provide a correlative link between cryptochromes and magnetoreception in animals.

Cryptochromes have also been implicated in the generation of a time-compensated sun compass in monarch butterflies (Sauman et al., 2005). Cryptochrome expression was found in fibers connecting the clock neurons of the dorsolateral region to the optic medulla,

where the dorsal rim photoreceptors (sensitive to polarized light from the sun) terminate (Sauman et al., 2005). This pathway may provide a link between the circadian clock and sun compass input into the brain by providing photoperiodic information used to regulate migratory behavior (Goehring and Oberhauser, 2002).

Towards a model of cryptochrome phototransduction

Photolyase model of cryptochrome function

There are several important points to keep in mind when considering the photolyase reaction mechanism as a potential model for cryptochrome function. First, the catalytically active form of flavin in photolyase is always two-electron reduced and deprotonated flavin adenine dinucleotide ($FADH^-$). This cofactor is readily oxidized *in vitro* to either the one-electron reduced flavin blue neutral radical ($FADH^\circ$) or the fully oxidized form (FAD_{ox}), both of which are catalytically inert (Payne et al., 1987). Photoreduction, resulting from exposure of *E.coli* photolyase containing $FADH^\circ$ to light in the presence of a reducing agent, can convert the flavin to the active $FADH^-$ form, increasing its quantum yield for repair (Heelis and Sancar, 1986; Sancar et al., 1987). However, the photochemical reactions responsible for this conversion are only of marginal physiological significance for photolyase since point mutations blocking the photoinduced electron transfer do not affect enzymatic activity *in vivo* (Kavakli, 2004; Li et al., 1991). It is not known if the photoreduction observed in purified cryptochromes is an integral component of its photochemical pathway, or if it is mechanistically irrelevant, as in photolyases. Further complicating study of the photolyase/cryptochrome family, purification of recombinant proteins from this family rarely yields stoichiometric amounts of both chromophores (Johnson et al., 1988a; Özgür and Sancar, 2003; Todo et al., 1996; Yasui et al., 1994; Zhao et al., 1997). Therefore, the lack of chromophore or the presence of a particular oxidation state of flavin in heterologously expressed, recombinant proteins of this family is not sufficient to make specific models regarding the *in vivo* status of the photoreceptor. Lastly, and perhaps most importantly, a

photon must be absorbed by photolyase while the protein is in the enzyme-substrate complex for catalysis to occur; a photon absorbed by the free enzyme generates an excited state that decays within 1-2 nanoseconds, with no lasting effect on the binding to or activity of photolyase on its substrates (Sancar, 2003). An understanding of the cryptochrome photocycle may therefore depend on the identification of a dark-bound substrate.

Given the high degree of structural homology with photolyase, it is unclear how cryptochromes have lost the ability to repair DNA and what features of cryptochromes explain their unique functions. The goal of my work in Dr. Sancar's laboratory has been to study the light-dependent and light-independent signaling properties of cryptochromes. I have approached this problem mainly from computational and biochemical approaches, using cell and structural biology techniques to complement the studies.

Chapter 2 describes my efforts to clarify evolutionary relationships in the photolyase/cryptochrome family and identify functionally important residues. As part of a larger effort in the Sancar lab to characterize all members of this family, this study provides insights into the structural and sequence differences that define photolyases and cryptochromes.

Chapter 3 presents data from the paper, "Role of Structural Plasticity in Signal Transduction by the Cryptochrome Blue-light Photoreceptor". I have also added some material that extends the findings of the original study. This study examined the biochemical properties of the C-terminal domains that are unique to cryptochromes, and provides the first demonstration of a light-dependent conformational change in cryptochromes.

Chapter 4 describes my study of the light-independent role of cryptochrome in the molecular circadian clock. This study was initiated as part of my rotation project in Dr. Sancar's laboratory, and was based on a protein-protein interaction between cryptochromes and the protein phosphatase 5, identified by a former postdoctoral researcher, Dr. Shaying

Zhao. This study provides the first evidence of a phosphatase in the mammalian circadian clock and accounts for *in vivo* data demonstrating the cryptochromes regulate the clock not only transcriptionally, but through posttranslational mechanisms as well.

Acknowledgements

A large part of this chapter was published as: Partch, C.L. and Sancar, A. (2005). Photochemistry and photobiology of cryptochrome blue-light photopigments: the search for a photocycle. Photochemistry and Photobiology *81*, 1291-1304.

CHAPTER 2

ANCIENT ORIGIN OF CRYPTOCHROME PHOTORECEPTION: REPEATED EVOLUTION AND STRUCTURAL CONVERGENCE OF PLANT AND ANIMAL CRYPTOCHROMES

Summary

Cryptochrome blue-light photoreceptors mediate growth and adaptive processes in organisms ranging from plants to humans, and are homologous to the light-dependent DNA repair enzyme photolyase, found predominantly in prokaryotes. Although it is presumed that plant and animal cryptochromes evolved from photolyase progenitors, the recent discovery of bacterial cryptochromes necessitates a reevaluation of the evolutionary and functional relationships within the photolyase/cryptochrome family. Using a bioinformatics approach, I analyzed the molecular phylogeny of this family and identified eight distinct classes, including a novel class of photolyases. The phylogenetic data provide evidence for the independent evolution of plant and animal cryptochromes from different photolyase progenitors, and trace the origin of both cryptochrome lineages back to the early eukaryotes, over one billion years ago. Evolutionary trace analysis of the photolyase/cryptochrome family identified class-specific residues that likely play a role in the different functions of photolyases and cryptochromes. These studies suggest structural convergence in the evolution of plant and animal cryptochromes, which is supported by biochemical data that, like plants, animal cryptochromes dimerize and interact with the ubiquitin E3 ligase, COP1. These data suggest that signaling mechanisms by eukaryotic cryptochromes may be more similar than previously believed.

Background

The inherent sensitivity of biomolecules to ultraviolet radiation has played a critical role in the formation and evolution of life on Earth. Solar ultraviolet radiation may have helped form the first polynucleotides (Mulkidjanian et al., 2003) and the sensitivity of biopolymers to short wavelength light likely influenced formation and evolution of cellular organisms in the absence of an ozone layer on primordial Earth (Oro et al., 1990). Over the last five billion years, the daily solar cycle has therefore provided one of the most consistent and pervasive adaptive stimuli on Earth. Sunlight has both destructive and beneficial effects on living organisms; although ultraviolet components of sunlight damage DNA and are mutagenic, some organisms have adapted to harness the abundant energy in sunlight through photosynthesis, and most have evolved molecular clocks to coordinate complex physiological processes and behaviors into circadian cycles that are synchronized, or entrained, with the solar cycle. Of the many classes of photosensors that are responsible for the interplay between sunlight and life on Earth, the photolyase/cryptochrome family of blue-light photoreceptors has uniquely evolved to respond to the diverse consequences of sunlight, mediating both its positive and negative effects.

Photolyase is responsible for photoreactivation, the process by which UV-induced DNA damage is reversed with near-UV/blue-light (reviewed in (Sancar, 2003)). Photolyase binds UV-damaged DNA independently of light and photoreactivates after absorption of a photon, which initiates a mechanism of cyclic electron transfer that repairs DNA damage and restores the catalytic competency of the FAD chromophore. Different photolyases are required to repair the main UV-induced DNA photoproducts, cyclobutane pyrimidine dimer (CPD), which constitutes ~80% of UV-induced DNA damage, and (6-4) pyrimidine-pyrimidone photoproduct, which constitutes 10-20% of UV-induced DNA damage. While the mechanism of these photolyases is essentially the same, they share only 28-29% identity at

the amino acid level, providing little indication of residues that contribute to their ability to repair photoproducts or distinguish their substrate specificities.

By definition, a cryptochrome is a photolyase homolog that does not repair DNA; instead, cryptochromes use blue-light to regulate growth and development in plants and entrain the circadian clocks of plants and animals (Partch and Sancar, 2005). In addition, cryptochromes participate in the molecular circadian clock of vertebrates independently of light. Although cryptochromes were discovered over a decade ago, their photocycle is not understood in any detail. It is thought that its photocycle will have significant similarities to photolyase, characterized by light-driven electron transfer; however, in the absence of a defined cryptochrome substrate in any organism, it has been difficult to hypothesize how cryptochromes transduce light into a signaling cascade.

A comparison of photolyase and cryptochrome tertiary structures was expected to highlight functional differences. Photolyase is globular protein composed of an N-terminal α/β domain and a C-terminal α-helical domain with the FAD bound deep within the α-helical domain and the photoantenna in a cleft between the two domains on the surface of the protein (Park et al., 1995; Sancar, 2003). A large opening on the surface of the protein allows direct access of the damaged DNA substrate to the FAD, and a positively charged groove runs along the same face of the protein, contributing to DNA binding. The structure of photolyase therefore corroborates its function as a DNA repair enzyme. The crystal structures of two cryptochromes were recently solved (Brautigam et al., 2004; Brudler et al., 2003) and despite sharing less than 30% identity with photolyase, the structures are nearly superimposable with the DNA repair enzyme, demanding the question: what of photolyase contributes to DNA repair and what makes cryptochrome incapable of repairing DNA?

Expression of photolyases is widespread among prokaryotes and more limited in eukaryotes, with a notable absence in placental mammals. Until recently, cryptochromes had only been identified in plants and animals, and it was commonly accepted that

cryptochromes evolved from a photolyase progenitor. A lack of homology between plant and animal cryptochromes led to several hypotheses that plant and animal cryptochromes evolved independently, with animal cryptochromes closely related to (6-4) photolyase and plant cryptochromes more similar to CPD photolyases (Cashmore et al., 1999). However, the discovery of a class of so-called DASH cryptochromes, found in diverse species from bacteria to vertebrates, has reopened the debate regarding the origin of cryptochromes and questioned their very definition. Although genetic deletion of DASH cryptochromes has no appreciable impact on survival of an organism after UV exposure (Hitomi et al., 2000; Worthington et al., 2003), these cryptochromes possess an intrinsic, although extraordinarily low, degree of photoreactivation on CPDs *in vitro* (Daiyasu et al., 2004). Is this repair function an evolutionary relic carried over from a photolyase progenitor, or does repair somehow constitute an integral component of DASH cryptochrome function? In order to discover and understand functional differences and similarities between members of this family, we must examine how cryptochromes and photolyases are evolutionarily related.

The goal of this study was to identify class-specific motifs that might describe the functional differences between photolyase and cryptochrome, and between different classes of cryptochromes. This was achieved by exhaustive phylogenetic analysis of over 200 members of the photolyase/cryptochrome family from Archaea to humans, including data from a large number of partially sequenced genomes representing more 'ancient' eukaryotes. Evolutionary trace analysis of the photolyase/cryptochrome phylogenetic tree identifies residues that are unique to each functional class, likely to be involved in protein function, and structural mapping of these motifs shows distinct clustering of motifs among photolyases and cryptochrome lineages that potentially highlights their functional differences.

By mapping conserved motifs onto known structures, I made several important discoveries that may help to describe differences between cryptochromes and photolyases.

First, conserved motifs in photolyases are restricted to the active site cavity and surrounding surfaces, while motifs in plant and animal cryptochromes are localized both to the front face of the protein and to a cluster on the rear face of the protein. Secondly, DASH cryptochromes more closely resemble photolyases than cryptochromes. DASH cryptochromes possess the signature motifs of CPD photolyases and lack the CRY-specific distribution of motifs on the rear face of the protein. Lastly, several motifs are structurally conserved in divergent plant and animal cryptochromes, indicative of molecular convergence in cryptochrome evolution. Based on these data, I found that animal cryptochromes unexpectedly share several biochemical properties with plant cryptochromes: the ability to form stable homo- and heterodimeric complexes and the ability to interact with the mammalian homolog of the plant cryptochrome effector, COP1. These data suggest that plant and animal cryptochromes may share more signaling properties than previously thought.

As a result of the comprehensive nature of the phylogenetic analyses, I discovered a new class that segregates independently from all other known classes and is evolutionarily related to plant cryptochromes. A representative gene significantly photoreactivates *in vivo*, demonstrating that these genes represent a new class of photolyases. Furthermore, by identifying the progenitor class of plant cryptochromes, these data provide unambiguous support for the independent and repeated evolution of plant and animal cryptochromes. In addition, I present evidence of ancient cryptochrome sequences that date the origin of both plant and animal cryptochrome lineages back to the appearance of early eukaryotes, approximately one billion years ago.

Experimental Procedures

Sequence retrieval, alignment and phylogenetic analysis

Annotated full-length photolyase and cryptochrome sequences were retrieved from Swiss-Prot/TrEMBL (us.expasy.org/sprot), Ensembl (www.ensembl.org) and Genbank (www.ncbi.nlm.nih.gov) databases using default query parameters. In addition, each database (non-redundant and genomic data sets) was searched by BLAST using full-length coding sequences from representative members of known classes: plant cryptochrome, *A. thaliana* Cry1; vertebrate cryptochrome, human Cry1; insect cryptochrome, *D.melanogaster* Cry; DASH cryptochrome, *V.cholera* Cry1; (6-4) photolyase, *D.melanogaster* (6-4) Phr; Class I CPD photolyase, *E.coli* Phr; and Class II CPD photolyase, *A.thaliana* Phr.

Sequences from incomplete genome records were retrieved from the non-annotated GenBank Trace Archives by discontiguous cross-species Mega BLAST, designed specifically for comparison of divergent sequences from different organisms, using the same set of representative genes as above. TBLASTX alignments (six-frame translation of the nucleotide query sequence against the six-frame translation of the nucleotide sequence match) were examined for protein homology and where possible, consecutive coding regions were combined to generate longer sequence reads.

Protein alignments were performed on the ClustalW server at EBI (www.ebi.ac.uk/clustalw), viewed with ESPript (us.expasy.org) and imported into MEGA 3.0 (www.megasoftware.net) for phylogenetic analysis. Phylogeny was tested by neighbor joining and maximum parsimony methods using 1000 bootstrap replicates to test the reliability of the inferred tree and nodes with less than 50% bootstrap support were condensed. The neighbor joining phylogenetic trees are displayed: a limited tree in Figure 2.1 and a complete tree in Appendix 1. A complete table of sequences used in this study, along with family classification, is included in Appendix 2.

Evolutionary trace analysis and structural mapping

Photolyase/cryptochrome classes identified in the phylogeny were analyzed by a modified evolutionary trace method to identify class-specific residues. Evolutionary trace analysis (Yao et al., 2003) was performed both on the freely available server (mammoth.bcm.tmc.edu/traceview) and by visual inspection of multiple sequence alignments of the superfamily. Residues were considered class-specific if conserved ≥ 80% and unique to the clade; this was particularly important when analyzing animal cryptochromes and (6-4) photolyases, since they share significant homology. Most class-specific residues occurred in clusters of > 8 amino acids; few were found as isolated residues (data not shown). Class II CPD photolyases are highly divergent from all other members of the photolyase/cryptochrome family and are not included in this analysis since they appear to represent an ancient and distinct evolutionary lineage. Drosophiloid 'Insect' cryptochromes could not be analyzed in detail by the ET method due the paucity of full-length sequence data. However, several conserved and unique motifs could be identified by eye in the multiple sequence alignments and are discussed in Figure 2.7.

Class-specific motifs are represented by sequence logos (weblogo.berkeley.edu), a graphical representation of the protein multiple sequence alignment. A logo consists of stacks of one-letter residue symbols, with one stack for each position in the motif. The overall height of the stack indicates the sequence conservation at that position and is a function of the number of sequences analyzed, while the height of symbols within the stack indicates the relative frequency of each amino acid at that position.

Motifs were mapped onto the known tertiary structures of representative family members. Class I CPD photolyase motifs were mapped onto *E.coli* photolyase (PDB code: 1DNP), DASH cryptochrome motifs were mapped onto the *Synechocystis* cryptochrome (1NP7), and plant cryptochrome motifs were mapped onto the structure of the photolyase homology region of *Arabidopsis* CRY1 (1U3C). In the absence of an experimentally determined structure, bilateral cryptochrome motifs were mapped onto a published

homology model of the photolyase homology region of human CRY2 (Özgür and Sancar, 2003). Figures were generated with MacPymol (www.pymol.org).

Plasmids

Caulobacter crescentus gene AAK23409, encoding a representative Class III sequence, was amplified by PCR directly from colonies of the wild-type *C.crescentus* strain CB15 grown on LB agar. The PCR product was cloned into the pMalC2 MBP-fusion vector (New England Biolabs). Full-length FLAG-tagged hCry1 and hCry2 in the pcDNA4B/myc-His vector were generated as described (Özgür and Sancar, 2003). A FLAG-hCry2 plasmid lacking the His tag, used in the pulldown assay, was generated by site directed mutagenesis (Stratagene) according to the manufacturer's protocol. C-terminally truncated hCry2Δ103 was amplified by PCR from the full-length clone with an N-terminal HA epitope tag and C-terminal stop codon and subcloned into the pcDNA4B/myc-His vector. Zebrafish Cry3 and Cry4 coding sequences were amplified by RT-PCR from total RNA isolated from the zebrafish embryonic Z3 cell line (Cermakian et al., 2002). C-terminally truncated zCry3 (encoding amino acids 1-533) and full-length zCry4 were subcloned into the pcDNA4B/myc-His vector with an additional C-terminal FLAG epitope tag. All DNA constructs were verified by sequencing.

In vivo *photoreactivation assay*

Assays were performed in the photolyase-deficient *E.coli* strain UNC523 (phr::kan uvrA::Tn10) and UNC523 complemented with pMalC2 CcPhr or empty vector alone. Cell lines were UV-irradiated and either treated with photoreactivating light (365 nm) or left in the dark to assess UV killing, and survival was quantified by colony formation assay as described before (Worthington et al., 2003). Briefly, cell lines were grown in parallel in LB at 37^{o}C overnight to stationary phase (16-18 hr). The cells were centrifuged at 4,500 rpm for 10 min and resuspended in PBS at a 10^{-1} dilution. 2 ml suspensions were irradiated with 254 nm light at 25°C at a fluence rate of 0.1 J $m^{-2}s^{-1}$ for a dose response of 0, 5, and 10 J/m^2.

0.5 ml of cells were taken at each dose and placed in separate wells of a plastic 6-well plate. For photoreactivation, plates were covered with the plastic cover and two layers of window glass to filter out radiation below 300 nm, and dark controls were wrapped in foil. Photoreactivation was carried out for 2 hr at 25°C using 365 nm light at a fluence rate of 1.5 J $m^{-2}s^{-1}$. All experiments were performed under dim yellow light to prevent uncontrolled photorepair. After photoreactivation, serial dilutions were made in PBS, plated on LB agar in triplicate representing UV or UV + photoreactivation treatments, and incubated in darkness at 37°C for 16 hr. Colonies were counted and survival of photoreactivated samples relative to dark controls was calculated. Minor photoreactivation was seen in UNC523 cells alone and has been previously published (Husain and Sancar, 1987). No difference in survival was seen between UNC523 alone and UNC523 complemented with empty pMalC2 vector, so survival data were combined in the analysis. Data represent results from 3 independent experiments (± SEM).

Expression, purification and spectroscopic analysis of recombinant proteins

MBP-tagged CcPhr protein was purified from *E.coli* UNC523 cells as previously described (Worthington et al., 2003). The presence of non-covalently associated chromophores was assessed by spectroscopic analysis of purified, native MBP-CcPhr or after heat denaturation. To determine the flavin concentration, holoprotein was heated at 95 °C for 5 min in buffer containing 50 mM Tris, pH 7.5, 50 mM NaCl, 5 mM EDTA, 1 mM DTT, and precipitated protein was removed by centrifugation. The absorption spectrum in the 300-700 nm range was recorded, and FAD concentration calculated from 440 nm absorbance using a molar extinction coefficient of 11,300 $M^{-1}cm^{-1}$. When MTHF is released from the enzyme, the 5-10 methenyl bridge responsible for the 380 nm absorption band is broken at neutral pH to generate 10-formyltetrahydrofolate, which does not absorb at > 300 nm and hence does not contribute to the near-UV spectrum of the cofactors (Johnson et al., 1988a).

Expression and purification of His-hCRY2 from baculovirus-infected Sf21 cells was described previously (Partch et al., 2005).

Cell culture, transfection and immunoprecipitation

HEK293T cells were purchased from ATCC and cultured in DMEM with 10% FBS under standard culture conditions. 293T cells were transfected with plasmid DNA using FuGENE 6 (Roche) reagent according to manufacturer's protocol.

For co-transfection/immunoprecipitation experiments, 4 x 10^5 293T cells were seeded into 6 well plates 24 hrs prior to transfection. Cells were transfected with 2-4 μg plasmid DNA (empty vector was used to normalize DNA concentrations) and harvested 48 hrs later, by lysis in NP-40 lysis buffer (50 mM Tris pH 7.5, 150 mM NaCl, 1 mM EDTA, 0.5% NP-40) with a protease inhibitor cocktail (Roche), and clarification at 4°C by centrifugation for 10 min at 14,000 rpm. Soluble extracts were incubated with immunoaffinity resins overnight at 4°C as indicated: HA affinity matrix (Roche) or FLAG M2 agarose (Sigma). Resin was washed three times with NP-40 wash buffer (50 mM Tris pH 7.5, 150 mM NaCl, 1 mM EDTA, 0.05% NP-40) and proteins were eluted with reducing SDS-PAGE sample buffer. For western blot analysis, proteins were separated by SDS-PAGE, transferred to HyBond ECL (Amersham) nitrocellulose membrane and blocked with TBST (50 mM Tris p% 7.5, 135 mM NaCl, 0.1% Tween-20) plus 5% nonfat milk.

Blots were incubated with primary antibodies as follows: mouse monoclonal FLAG (M2) (Sigma), His (Abgent); or rabbit polyclonal HA (H-15) (Santa Cruz), CRY2B (Thompson et al., 2003), COP1 (Biomol). Proteins were detected using the appropriate HRP-conjugated secondary antibody and ECL reagent (Amersham). To analyze multiple proteins from a single blot, membranes were stripped between westerns by incubating for 30 min at 55°C in 60 mM Tris pH 6.8, 2% SDS and 100 mM β-mercaptoethanol, washed four times in TBST and reblocked prior to incubation with new primary antibody.

In vitro *pulldown assays*

FLAG-hCRY2 (lacking His tag) and a vector control were purified from transiently transfected 293T cells by FLAG immunoaffinity purification as described above, except that resin was washed twice with NP-40 wash buffer containing 1M NaCl to remove proteins non-covalently associated with FLAG-hCRY2. The purity and concentration of resin-bound protein was assessed by silver stain. *In vitro* pulldowns were performed by incubating equal volumes of FLAG-hCRY2 or vector control resin with purified His-hCRY2 overnight in a total of 0.5 ml NP-40 wash buffer, rotating at 4°C. Resin was washed three times with the same buffer, bound proteins were eluted with reducing SDS-PAGE sample buffer, and proteins were resolved by SDS-PAGE. *In vitro* protein complexes were identified by western blotting with FLAG or His antibodies.

Primary sequence prediction of coiled-coil domains

Representative sequences from each class (listed in Appendix 3) were individually analyzed for the propensity to form coiled-coil domains using the COILS predictor (www.ch.embnet.org). COILS compares input sequences to a database of known two-stranded coiled-coils and derives a similarity score, from which it calculates a probability that the sequence will adopt a coiled-coil conformation (Lupas et al., 1991). Mean coiled-coil propensities and SEM were calculated for each class; SEM was small for all class mean values and is not included in Figure 2.8.

Results

Evolutionary relationships in the photolyase/cryptochrome family

Phylogeny is, by definition, an expression of the evolutionary development of a molecule. In order to assess evolution of the photolyase/cryptochrome family, I performed an exhaustive search of annotated sequence databases, retrieving over 250 sequences of photolyases and cryptochromes from all kingdoms of life. Phylogenetic analyses by neighbor joining and maximum parsimony methods grouped these sequences into eight major classes. A reduced tree with gene names is shown in Figure 2.1 (a complete tree is shown in Appendix 1; genes and accession numbers used in this study are listed in Appendix 2) (Partch and Sancar, 2005). Seven of these classes have been previously described and functionally characterized to varying degrees: Class I and II CPD photolyases, (6-4) photolyase, DASH cryptochrome, plant cryptochrome, insect cryptochrome, and vertebrate cryptochrome (Sancar, 2003). However, two unexpected findings were made: first, a group of novel, independently segregating bacterial sequences was identified, comprising a new class (Class III); and second, vertebrate-like cryptochrome sequences were discovered in non-Drosophiloid insects.

Discovery of a new prokaryotic class related to plant cryptochromes

Identification of more than 20 bacterial sequences that segregate independently in the phylogenetic analyses reveals discovery of a new class of photolyase or cryptochrome. The new class, Class III, is a sister taxon to plant cryptochromes (Fig. 2.1), indicating a close evolutionary relationship, and the restriction of this class to prokaryotic organisms suggests that it is the likely progenitor of plant cryptochromes. A more comprehensive phylogeny demonstrates clearly that plant cryptochromes evolved from Class III genes (Appendix 1). Before completion of this study, it was not possible to determine functional classification by primary sequence alone; therefore, it was unclear whether these genes were cryptochromes or photolyases. However, a survey of the literature indicated that at

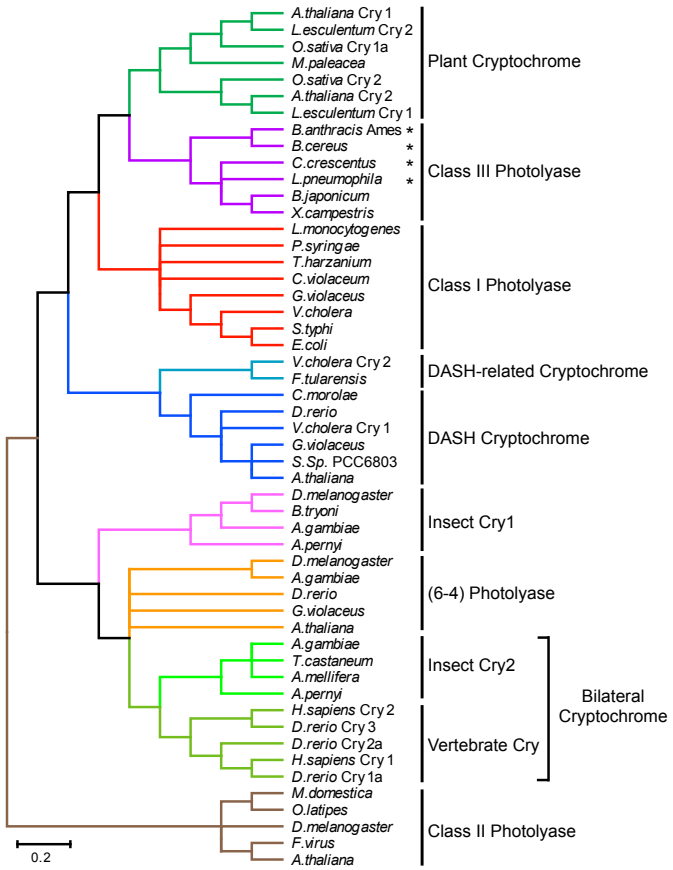

Figure 2.1 Evolutionary relationships in the photolyase/cryptochrome family
Unrooted phylogenetic tree generated using neighbor joining methods. Eight major classes are identified, including a novel group, Class III (purple), from which plant cryptochromes (green) evolved. Asterisks indicate organisms that possess this single gene and a literature report of photoreactivation. Scale bar represents residue substitutions per site.

least four of these bacteria possess the ability to photoreactivate, and a search of their sequenced genomes finds only the Class III gene, indicating that they are likely photolyases (Bender, 1984; Knudson, 1985; Knudson, 1986). These data suggest that plant cryptochromes evolved not from a bacterial cryptochrome as has been suggested (Hitomi et al., 2000; Todo, 1999), but from a novel class of photolyases.

Discovery of vertebrate-like cryptochromes in non-Drosophiloid insects

The absence of vertebrate-like cryptochromes genes in model invertebrates such as *D.melanogaster* and *C.elegans* suggested that the vertebrate gene, and its light-independent clock function, was a chordate innovation (Griffin et al., 1999). However, in the course of these analyses, I identified partial and full-length sequences in several non-Drosophiloid insect species such as mosquito, honeybee, and silkmoth that are highly homologous to vertebrate cryptochromes (Fig. 2.1). These data demonstrate that the origin of vertebrate cryptochrome predates the last common ancestor shared by insects and vertebrates, the Urbilateria (De Robertis and Sasai, 1996). Hence, I propose re-naming this class of vertebrate-like cryptochromes as bilateral cryptochromes, since they are present in at least two branches of the Bilateria, animals defined by bilateral symmetry.

Identification of class-specific signature sequences by evolutionary trace

In order to examine how functional differences between photolyase and cryptochrome arise from differences in primary sequence, I identified and characterized class-specific residues by a modified evolutionary trace analysis. Evolutionary trace (ET) ranks the importance of residues in a protein family by correlating their variation with evolutionary divergence (Lichtarge et al., 1996). The trace rank of a residue is the number of branches into which a phylogeny must be divided for that residue to be invariant within each branch. Therefore, a residue with a low trace rank is highly conserved within a protein family, and residues with a high trace rank are specific to classes. Ordinarily, ET is used to identify active sites in enzymes with a similar function by examining residues with low trace

rank (Shenoy et al., 2006; Sowa et al., 2001); however, in order to identify class-specific residues, I sought residues with the highest trace ranks. In theory, these class-specific residues do not contribute to protein folding or stability, as these residues usually occur with low trace rank. Instead, high-trace rank residues usually contribute to the unique, class-specific differences in function found in a protein family and are usually surface-exposed (Lichtarge et al., 1996; Sowa et al., 2000).

Signature sequences of Class I CPD photolyase localize to the active site

Class I CPD photolyases are the most ancient and divergent class in the photolyase/cryptochrome family (Appendix 1). Because of the divergence of this class, very few sequences were highly conserved; however, the few motifs that were identified were conserved at nearly 100% in all members of this class (Figure 2.2A). The high degree of conservation, particularly in this divergent class, indicates a strong evolutionary pressure to maintain the motifs, supporting a critical role for them in photolyase function. In line with this theory, the motifs mapped exclusively to the active site (Figure 2.2C-D). The motifs surround the surface opening that defines the FAD binding cavity, continue into the cavity, and extend along the charged DNA binding groove on the front face of the protein.

Functional studies of *E.coli* photolyase have shown that arginines 226 and 342 are important for contacting phosphates in the DNA backbone around the dimer (Husain et al., 1987). These key residues are found in Motif 1 and 2, in addition to other residues in all three motifs that make direct hydrogen bonds to FAD (Thr^{234}, Ser^{235}, Asn^{341}, Arg^{344}, and Asn^{378}) in the *E.coli* crystal structure (Park et al., 1995). The third motif consists of a consensus sequence, A·X·N·3X·**W**·Q·**W**·X·A·S·T·G·X·D, where side chains from conserved tryptophans (in bold) play an important role in recognition of the thymine dimer. Localization of residues found in all three motifs to the rim of the FAD binding cavity helps form the asymmetric polarity that is critical for binding and repair of the thymine dimer (hydrophobic on one side for binding the cyclobutane ring, and charged on the other for binding thymine

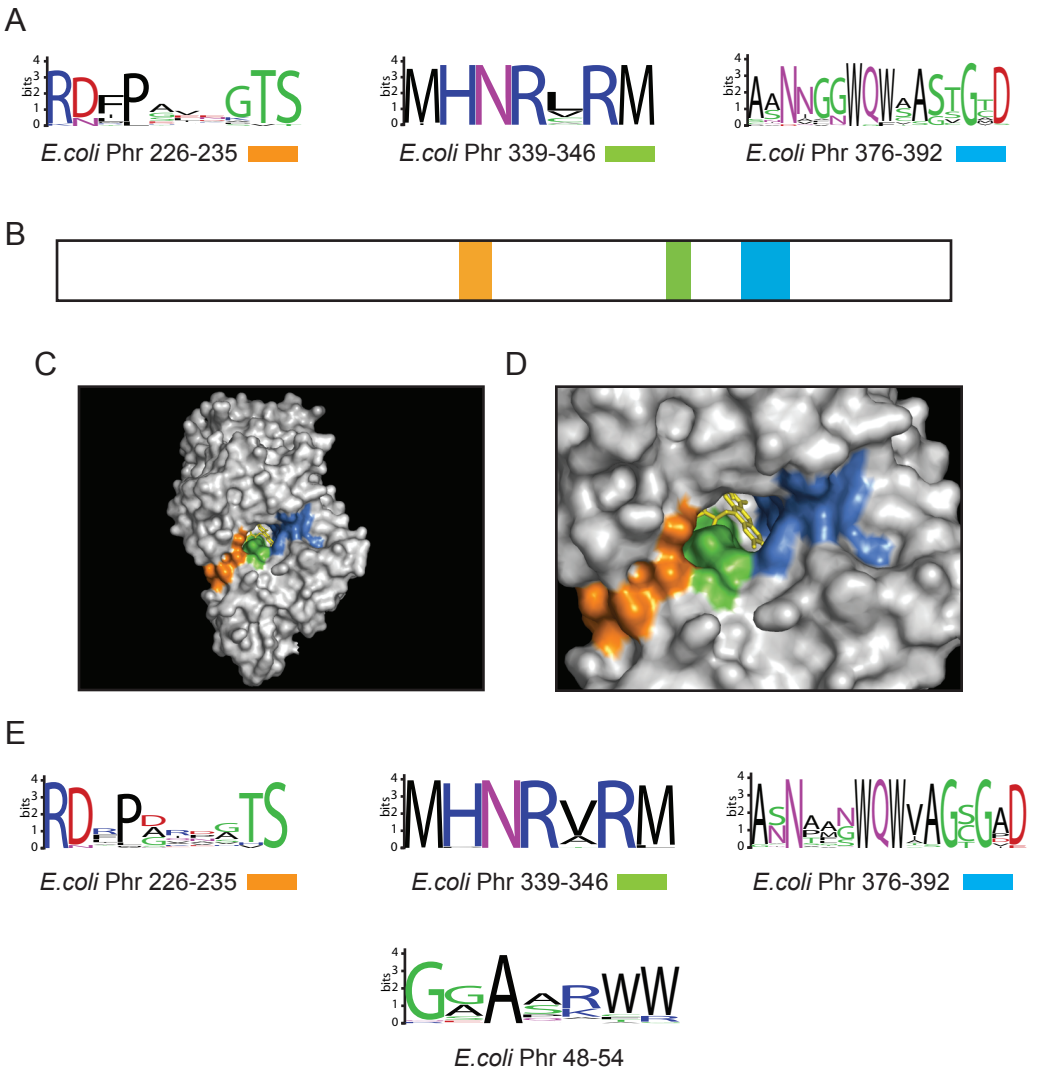

Figure 2.2 Signature sequence motifs of Class I and III photolyases
A. Highly conserved motifs in Class I photolyases. Motifs are shown in sequence logo format, where each residue in the motif is represented by a stack of single letter residue identifiers that constitute the sequence divergence at that site, and the height of each letter represents the degree of conservation. Location of motifs (*E.coli* Phr) is shown below. **B.** Schematic representation of motifs in *E.coli* photolyase. **C.** Structural mapping of Class I motifs on *E.coli* Phr crystal structure. Motifs are mapped by colors indicated in A, FAD shown in yellow. **D.** Enlargement of active site cavity. All three motifs extend into FAD binding site. **E.** Highly conserved motifs in Class III photolyases. Three out of four motifs are similar to Class I motifs.

bases) (Park et al., 1995). Therefore, the three motifs identified by evolutionary trace have proven roles in dimer recognition, chromophore binding, and repair, demonstrating that this approach defines functionally important residues.

Class III signature sequences are similar to Class I CPD photolyase motifs

Reports of photoreactivation in organisms that possess Class III genes exclusively suggest that these proteins possess repair activity. This activity is likely directed towards cyclobutane pyrimidine dimers, since CPDs are the predominant photoproduct formed after UV and therefore contribute most to the reversion in UV-induced killing by photoreactivation (Sancar, 2003). ET analysis of the novel Class III sequences revealed that their most highly conserved sequences resemble Class I photolyases in many aspects (Figure 2.2E). First, Class III proteins possess only a few, highly conserved motifs. Second, the majority of Class III motifs are nearly identical to those found in Class I photolyases. Lastly, all residues that are important in repair of CPDs by Class I photolyases are conserved in Class III genes, providing further support for the hypothesis that these proteins function as CPD photolyases. The sole Class III-specific motif (G·X·A·X·R·W·W) is predicted to map on the surface of the rear face of the protein, with unknown functional significance.

Characterization of a Class III protein

In order to investigate the function of Class III proteins, a representative sequence from the bacterium *C.crescentus* was cloned. *C.crescentus* photoreactivates (Bender, 1984) and possesses only the single Class III gene, therefore making it the candidate photolyase. *C.crescentus* Class III Phr was overexpressed and purified as an MBP-fusion protein (Figure 2.3A) in order to test its repair activity *in vitro*. However, spectroscopic analysis of the purified protein (Figure 2.3 B-C) demonstrated that while the protein retained the MTHF chromophore, it lost the catalytic FAD chromophore during purification. Loss of chromophore binding during purification is common with this family of proteins (Sancar, 2003).

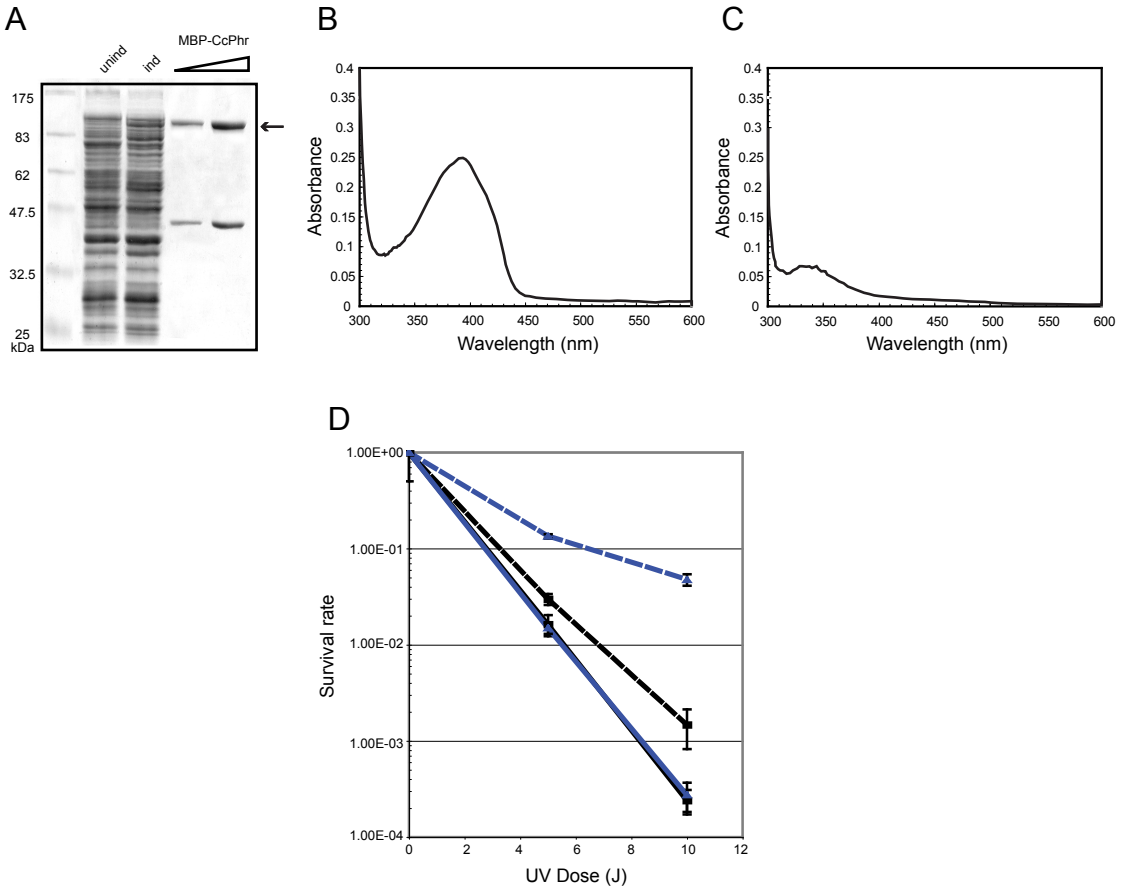

Figure 2.3 Characterization of *C.crescentus* Class III photolyase
A. Purification of MBP-CcPhr. Overexpressed protein was purified by affinity chromatography on amylose resin. Lane 1, uninduced cells; lane 2, induced cells; lanes 3-4, increasing amounts of purified MBP-CcPhr. **B.** Absorbance spectrum of MBP-CcPhr. Peak at 380 nm is indicative of MTHF and possibly FADH°. **C.** Absorption spectrum of chromophores released from MBP-CcPhr by heat denaturation. Protein was heat-denatured at neutral pH and removed by centrifugation. Upon release from the protein, MTHF is converted to 10-formyltetrahydrofolate, which no longer absorbs at $\lambda > 300$ nm; spectrum arises from flavin absorbance, with a predicted peak at 440 nm. **D.** *In vivo* photoreactivation by MBP-CcPhr. Photolyase-deficient *E.coli* UNC523 cells were complemented with MBP-CcPhr (blue) or empty vector (black) and irradiated with 254 nm UV light at different doses. Cells were either photoreactivated with 365 nm light (dashed lines) or maintained in darkness (solid lines) to assess UV killing. Data are representative of three independent experiments (± SEM).

Unfortunately, photolyase is not active in the absence of FAD, thereby preventing an *in vitro* assessment of Class III function using the *C.crescentus* protein at this time.

To test class III function, we assayed for photoreactivation *in vivo* by complementation of a photolyase-deficient E.coli strain, an approach that has worked well to characterize other photolyases (Kihara et al., 2004). The UNC523 *E.coli* strain was transformed with pMalC2-CcPhr or empty vector alone and irradiated with increasing doses of 254 nm UV light to induce photoproduct formation. Cells were either treated with photoreactivating light (365 nm) or kept in darkness to assess total killing by UV, and relative survival was assessed by colony formation assay. Under these conditions, MBP-CcPhr significantly photoreactivated, increasing survival by 15-fold over *E.coli* transformed with vector alone (Figure 2.3D). Therefore, in combination with previously published *in vivo* data from *C.crescentus*, we can state with confidence that Class III proteins are CPD photolyases.

Signature sequences of DASH cryptochromes resemble those of CPD photolyases

A new class of cryptochromes was identified several years ago, comprised of bacterial genes as well as genes in plants, fungus and aquatic vertebrates. The class, named DASH because its bacterial members were more similar to cryptochromes found in eukaryotes (*Drosophila*, *Arabidopsis, Synechocystis* and Human) than bacterial photolyases, was suggested to be the progenitor of eukaryotic cryptochromes (Daiyasu et al., 2004). Our lab and another showed that members of this class did not contribute significantly to photoreactivation *in vivo*, satisfying the definition of a cryptochrome (Hitomi et al., 2000; Worthington et al., 2003); however, one recent study showed that they possess intrinsic, albeit low, CPD repair activity *in vitro* (Daiyasu et al., 2004). Analysis of the DASH class by evolutionary trace indicates, surprisingly, that DASH cryptochromes are highly similar to CPD photolyases in two aspects (Figure 2.4). First, two of four motifs exhibited significant homology to Class I signature sequences (Figure 2.4B), and map to the FAD

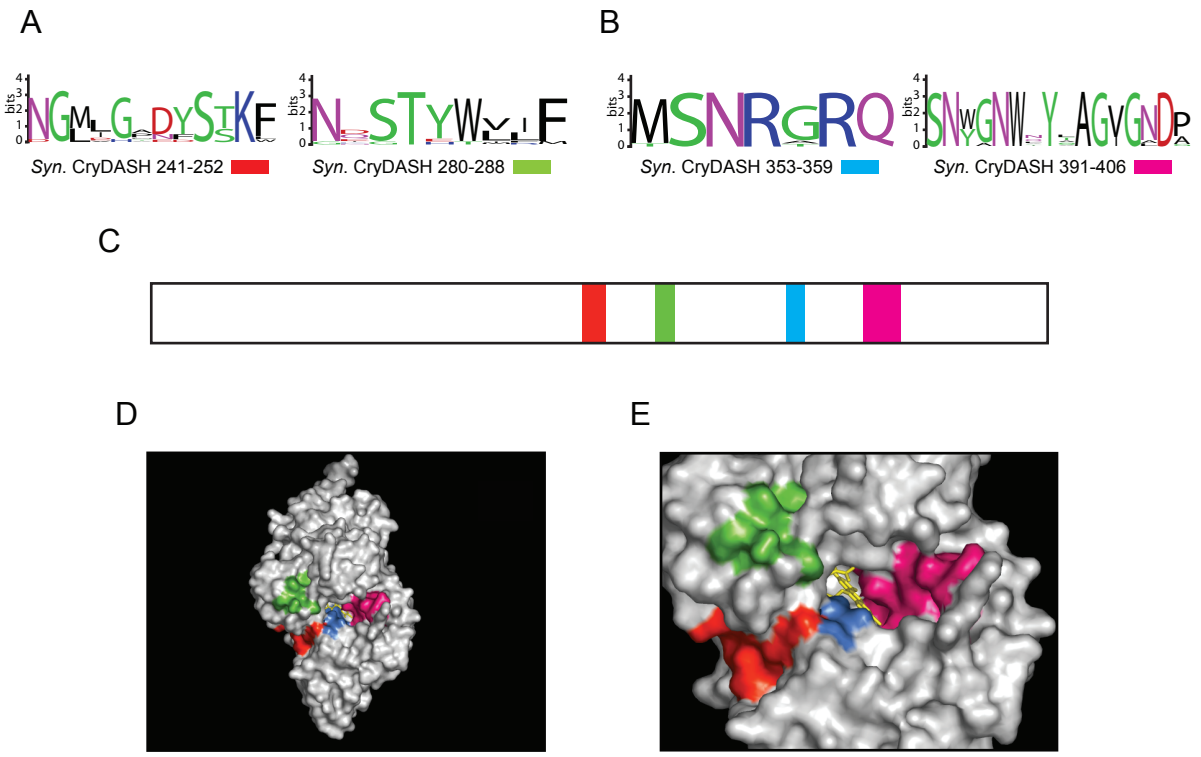

Figure 2.4 Signature sequence motifs of DASH cryptochromes
A. Highly conserved motifs unique to DASH cryptochromes. Location of motifs on *Synechocystis* CRY DASH is shown below. **B.** Highly conserved DASH motifs similar to Class I/III photolyase motifs. **C.** Schematic representation of motifs in *Syn.* CRY DASH. **D.** Structural mapping of DASH motifs on *Syn.* CRY DASH crystal structure. Motifs are mapped by color indicated in A-B, FAD shown in yellow. **E.** Enlargement of FAD binding cavity.

binding cavity on the *Synechocystis* CRY DASH crystal structure (Figure 2.4D-E) (Brudler et al., 2003). The two DASH-specific motifs (Figure 2.4A) also localized to the front face of the protein near the FAD binding cavity, suggesting that they may also play a role in DNA binding or catalytic activity (Brudler et al., 2003).

Plant cryptochrome signature sequences differ significantly from CPD photolyases

All classes examined thus far have only a few motifs that are localized exclusively to the FAD binding cavity and surrounding areas, highlighting the importance of this area for photolyase function. Evolutionary trace analysis of plant cryptochromes yielded considerably different results. In particular, motifs in plant cryptochromes were more abundant in number and longer, averaging twice the length of photolyase motifs (Figure 2.5A). A section of one motif, ranging from residues 49-62, displays homology to a Class III-specific motif (Fig. 2.2E), highlighting their common evolutionary origin. Several motifs were punctuated by differences between plant CRY paralogs (conserved sequences differ in CRY1 vs. CRY2, Fig. 2.5A yellow and orange motifs). Localization of motifs on the AtCRY1 PHR crystal structure was markedly distinct from Class I/III photolyases and the DASH class, because the majority of plant motifs do not map to the FAD binding site (Figure 2.5C, E). Furthermore, several motifs that were not adjacent in primary sequence formed a contiguous strip on the rear face of the protein (Figure 2.5D), suggesting that plant cryptochromes may utilize a different protein interface from photolyases to mediate their light-dependent effects.

Signature sequences of bilateral cryptochromes exhibit similarity to plants in location, but not sequence

Bilateral cryptochromes evolved from (6-4) photolyases, an evolutionarily distinct progenitor from that of plant cryptochromes. Despite this, evolutionary trace analysis of bilateral cryptochromes identified motifs that are similar both in number and structural location to plant cryptochromes (Figure 2.6). Signature sequences of bilateral

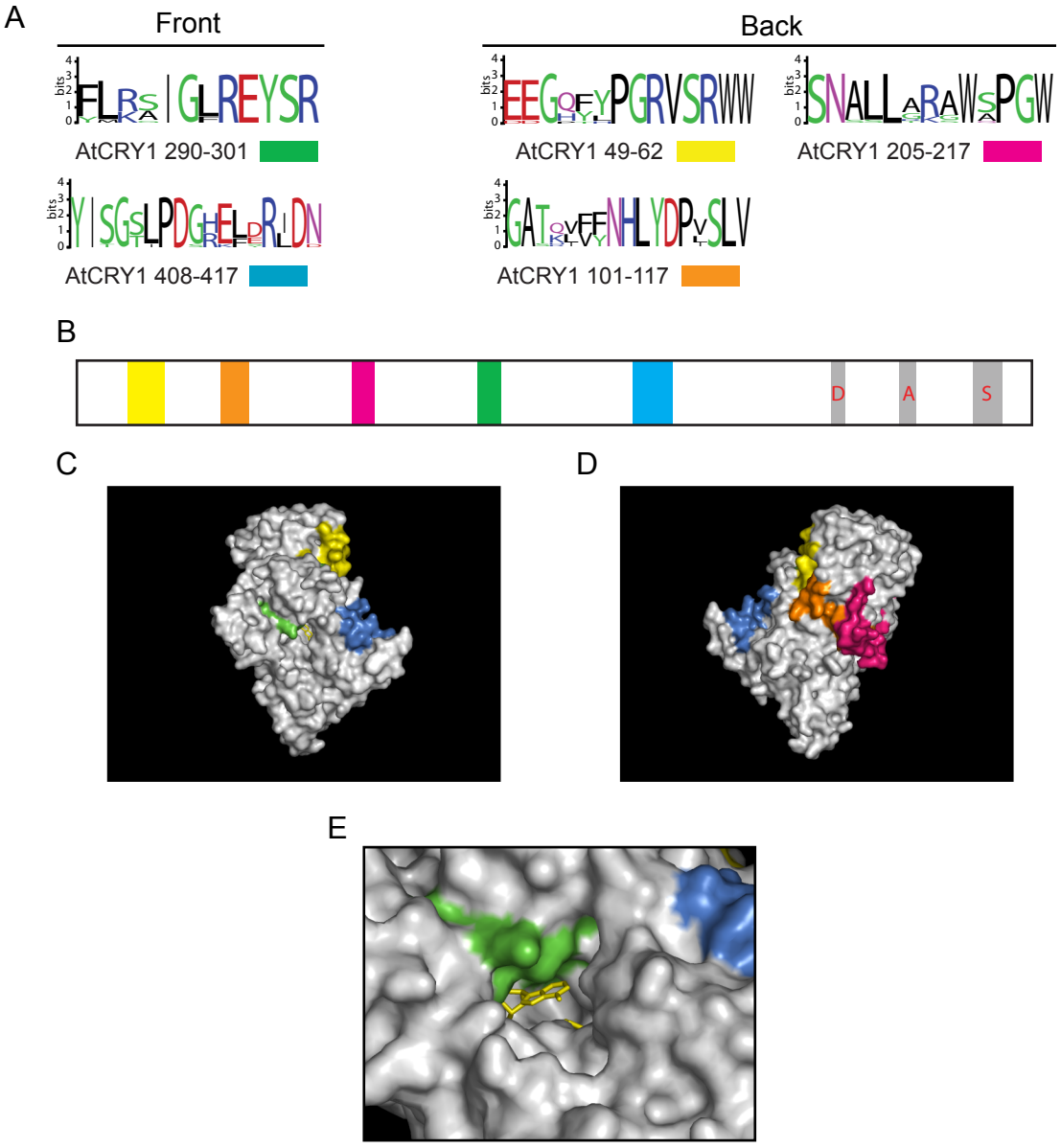

Figure 2.5 Signature sequence motifs of plant cryptochromes
A. Highly conserved motifs in plant cryptochromes. Motifs that map onto the front or back face of the protein are indicated, as well as location of motifs in AtCRY1. **B.** Schematic representation of motifs in *A.thaliana* CRY1. The conserved C-terminal DAS motif is shown in gray. **C.** Structural mapping of plant cryptochrome motifs on the front face of the AtCRY1 PHR crystal structure. Motifs are mapped by colors indicated in A, FAD shown in yellow. **D.** Structural mapping of motifs on the back face of AtCRY1 PHR. **E.** Enlargement of FAD binding cavity. The motif consisting of residues 290-301 (green) extends into the cavity.

cryptochromes do not map inside the FAD binding cavity; however, the most highly conserved bilateral motif is localized to a loop region just underneath the binding cavity (Figure 2.6C, blue). Strikingly, two motifs that are distant in primary sequence form a contiguous patch on the rear face of the protein, in the same location as the strip on plant cryptochromes (Figure 2.6D), although there is no sequence conservation between the plant and animal motifs. An additional bilateral-specific motif (residues 343-354, green) has similarities to a Walker A/P-loop nucleotide-binding motif, and could play a role in the ability of bilateral cryptochromes to autophosphorylate in the absence of a recognizable kinase domain (Bouly et al., 2003; Özgür, 2005).

Bilateral cryptochrome signature sequences are distinct from sequences required for repression of CLOCK/BMAL1

The most well studied function of bilateral cryptochromes in vertebrates is the light-independent repression of CLOCK/BMAL1 transactivation in the molecular circadian clock (Kume et al., 1999; van der Horst et al., 1999; Vitaterna et al., 1999). The sequences responsible for CLOCK/BMAL1 repression have been loosely mapped and are identified in Figure 2.6B. Inhibition by CRY requires either repression domain-1 (RD-1) or two discontinuous sequences, RD-2a and RD-2b (Hirayama et al., 2003). The regions identified in the previous study are too large to be entirely conserved on a class-specific level; however, I detected no overlap of these regions with any of the class-specific motifs at the primary sequence level. Furthermore, the RD motifs cluster on the hCRY2 structure on the top, front face of the protein, completely separate from the class-specific motifs (Figure 2.6E-F). These data suggest that bilateral-specific motifs play a role in some other function of bilateral cryptochromes, and that repression of CLOCK/BMAL1 by bilateral cryptochromes is not driven by short, highly conserved sequence elements.

Structural convergence of plant and bilateral cryptochromes

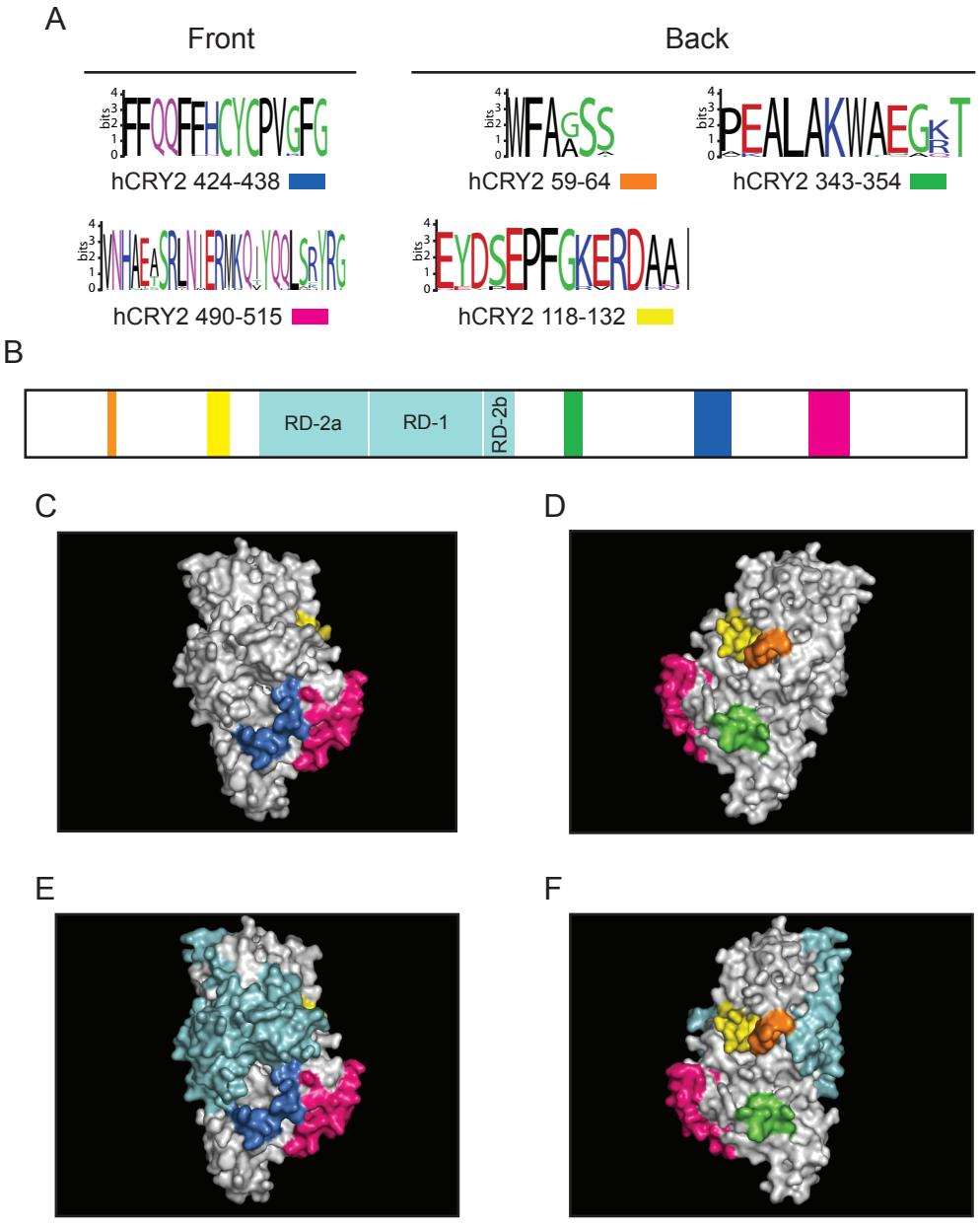

Figure 2.6 Signature sequence motifs of bilateral cryptochromes
A. Highly conserved motifs in bilateral cryptochromes. Motifs that map onto the front or back face of the protein are indicated, as well as location of motifs in hCRY2. **B.** Schematic representation of motifs in hCRY2. Sequences required for repression of CLOCK/BMAL1 transactivation are indicated in cyan. **C.** Structural mapping of bilateral cryptochrome motifs on the front face of the hCRY2 PHR homology model. Motifs are mapped by same colors as in B. **D.** Structural mapping of motifs on the back face of hCRY2 PHR. **E.** Sequences required for transcriptional repression of CLOCK/BMAL1 are mapped (cyan) onto the front and rear (**F**) face of hCRY PHR.

Molecular convergence is defined as the occurrence of a similar evolutionary event in two distinct evolutionary lineages; this differs from parallel evolution, where similar changes occur in proteins evolving independently from the same ancestor (Doolittle, 1994). Three criteria must therefore be satisfied in order to properly identify molecular convergence: first, the two molecules in question must have independent evolutionary origins; second, analogous sequences or structures must be present in the independent lineages; and third, the convergent features must not be present in ancestral sequences, indicating positive selective pressure in the gain of new sequence or structural features.

Plant and bilateral evolutionary origins are clearly distinct, as demonstrated by a comprehensive molecular phylogeny of the photolyase/cryptochrome family (Fig. 2.1, Appendix 1). To determine if molecular convergence occurred in plant and animal cryptochromes, I examined the localization of motifs in the N-termini of human, *Drosophila*, and *Arabidopsis* cryptochromes. As shown in Figure 2.7A, location of class-specific motifs significantly overlaps in all three classes although there is minimal conservation of the physicochemical properties of conserved residues, even between the more closely related insect and human cryptochromes. In order to establish the specific acquisition of these traits in plant and animal cryptochrome lineages, I analyzed the degree of conservation in motif regions in cryptochromes and their ancestral classes (Figure 2.7B). While residues in plant and bilateral cryptochromes were >80% conserved throughout the majority of the motif (a defining characteristic of the motifs), sequences in either Class III or (6-4) photolyases were not conserved to any appreciable degree. These data strongly suggest that conservation of these regions with respect to the rest of plant and bilateral genes was not inherited from their independent progenitors, therefore satisfying the definition of molecular convergence.

Shared biochemical properties of plant and bilateral cryptochromes: dimerization

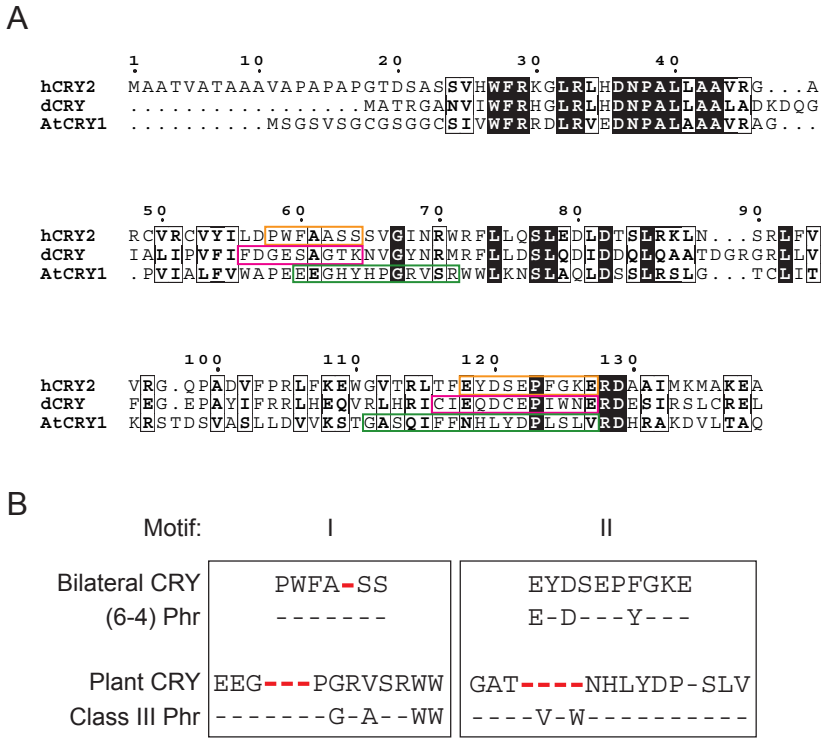

Figure 2.7 Structural convergence of plant and animal cryptochromes
A. Overlap of motif locations in plant and animal cryptochromes. Highly conserved motifs unique to bilateral, insect, and plant cryptochromes are boxed. **B.** Progenitor sequences are not conserved at plant and animal motif locations. Degree of sequence conservation in each class was analyzed; residues are shown if sequence is ≥80% conserved. Black dashes indicate conservation <80% and red dashes indicate paralog conservation ≥80% (residues ≥80% conserved in CRY1 or CRY2).

Since plant and animal cryptochromes appear to share localization of function-defining class-specific residues, I investigated the possibility that they may also share other biochemical properties. Plant cryptochromes have been reported to dimerize through their photolyase homology regions, both in homo- and hetero-complexes that are required for function (Lin and Todo, 2005; Sang et al., 2005). I first investigated the possible dimerization of bilateral cryptochromes by co-transfection/co-immunoprecipitation assay. If dimerization depends on one or more of the bilateral-specific motifs, then bilateral cryptochromes should not interact with cryptochromes that do not possess these class-specific motifs. A few vertebrates possess a gene of unknown function, Cry4, which is equally related to bilateral cryptochromes and (6-4) photolyases, without possessing any of the known activities of either class (Figure 2.8A, in red) (Kobayashi et al., 2000). Zebrafish CRY4 is therefore the most similar family member to bilaterals, but lacks the class-specific motifs of bilateral cryptochromes, allowing the specificity of dimerization to be tested.

I examined homo- and heterodimerization of bilateral cryptochromes by transfecting 293T cells with various full-length FLAG-cryptochromes or empty vector in the presence of HA-hCRY2 Δ103, lacking the C-terminal domain, and immunoprecipitating FLAG proteins (Figure 2.8B). HA-hCRY2 Δ103 precipitated significantly with bilateral cryptochromes hCRY1, hCRY2, and zCRY3, and importantly, interacted only weakly with the closely related zCRY4. These data suggest that bilateral cryptochromes, like plants, can form stable homo- and heterodimers, which do not require cryptochrome C-terminal domains, and may occur through class-specific sequences.

In order to verify that bilateral cryptochromes interact directly, I performed an *in vitro* pulldown assay. Full-length FLAG-hCRY2 or mock-transfected cells were purified at high stringency from 293T cells and left on FLAG resin (Figure 2.8C). Purified His-hCRY2 was incubated with the FLAG resins and binding was assessed by western blotting. As shown in

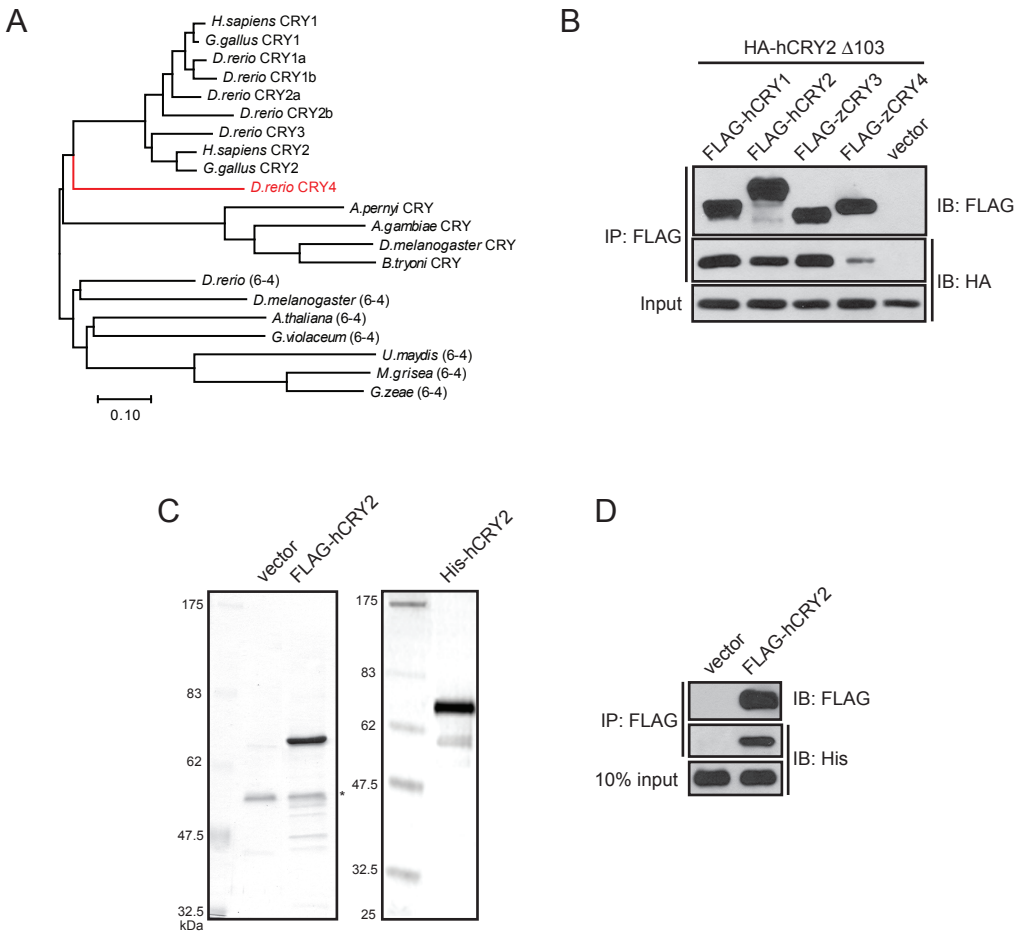

Figure 2.8 Bilateral cryptochromes homo- and heterodimerize
A. Evolutionary relationship of bilateral cryptochromes and zCRY4. All nodes in the unrooted NJ tree had >50% bootstrap support; scale bar represents residue substitutions per site. **B.** Bilateral cryptochromes homo- and heterodimerize. 293T cells were co-transfected with hCRY2 Δ103 and FLAG-constructs as indicated. Extracts were immunoprecipitated with FLAG resin and analyzed by western blotting. **C.** Purification of FLAG- and His-hCRY2 for *in vitro* pulldown. FLAG-hCRY2 (or empty vector control) was purified from 293T cells and left on FLAG resin. Purity was assessed by silver stain of SDS-PAGE; asterisk indicates FLAG antibody heavy chain. **D.** Homodimerization of hCRY2 *in vitro*. Purified His-hCRY2 was incubated with FLAG-hCRY2 or a mock purified resin for *in vitro* pulldown assay. Complexes were detected by western blotting.

Figure 2.8D, hCRY2 formed a stable homodimer in the absence of other proteins, indicating that dimerization is an intrinsic property of bilateral cryptochromes.

Shared biochemical properties of plant and bilateral cryptochromes: interaction with the E3 ubiquitin ligase, COP1

Since dimerization of plant cryptochrome facilitates interaction with its dimeric effector, the E3 ubiquitin ligase, COP1, I investigated the possibility that bilateral cryptochromes might also interact with COP1. The COP1 gene is highly conserved between plants and mammals (Figure 2.9A), targeting homologous proteins for proteosome-mediated degradation (Yi and Deng, 2005). A previous study further demonstrated that structural and functional similarities exist between mammalian and plant COP1, since a partial clone of mouse COP1 could moderately compensate for mutant COP1 in plants; moreover, these data suggested that mammalian COP1 was interacting with plant cryptochromes in light-regulated exclusion of COP1 from the nucleus (Wang et al., 1999). However, a yeast two-hybrid study examined the interaction of mouse cryptochromes with this partial clone of mCOP1 and did not observe an interaction, concluding that the CRY:COP1 interaction was specific to plants (Yang et al., 2001).

In light of the discoveries of the current study, I examined the possible interaction of mammalian cryptochromes and full-length COP1 by co-transfection/co-immunoprecipitation from 293T cells. As shown in Figure 2.9B, FLAG-mCOP1 specifically interacted with mCRY2, as well as mCRY1 (data not shown). Furthermore, I have preliminary data that demonstrate an effect of mammalian cryptochromes on the posttranslational modification of COP1 in U2OS and 293T cells (data not shown), indicating that the interaction of cryptochromes and COP1 has functional consequences in mammalian cells. Collectively, these biochemical data corroborate the results from the sequence analysis, suggesting structural and/or functional convergence, and demonstrate that plant and animal cryptochromes share several important functional properties.

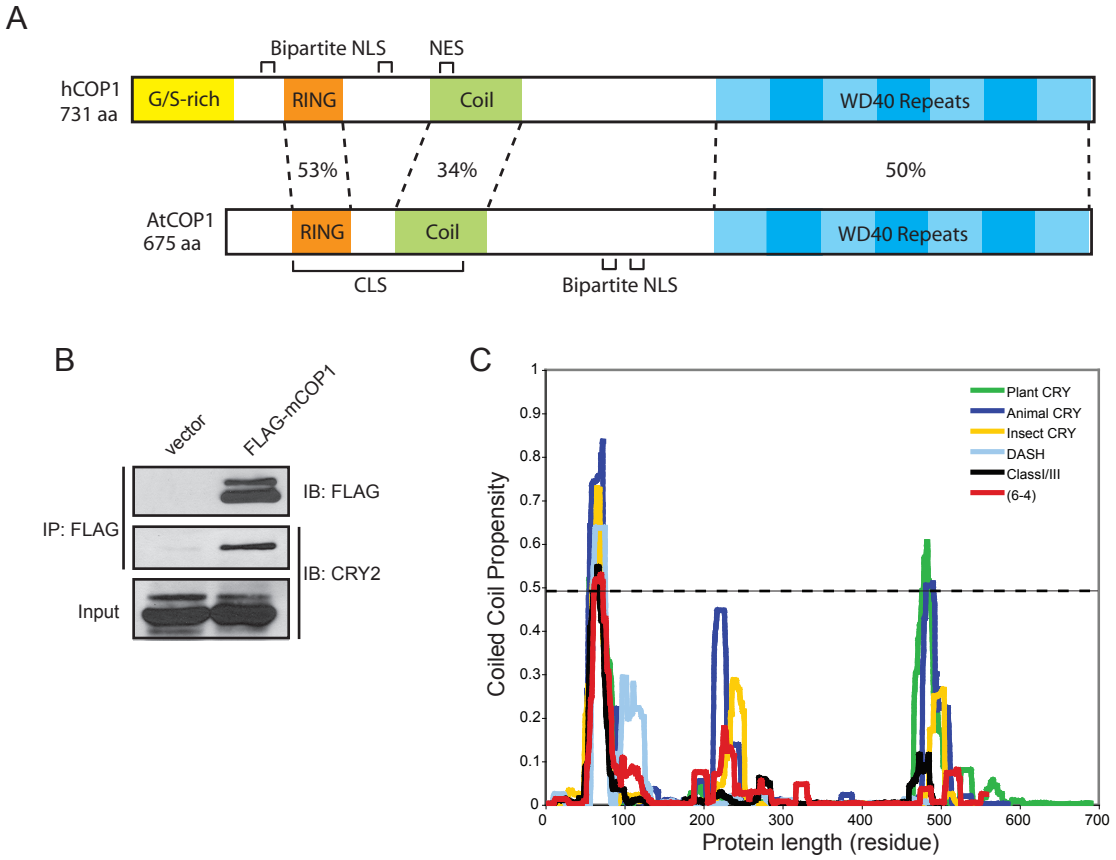

D

Residues:	0-100	101-200	201-300	301-400	401-500	501-600
Class I/III Photolyase	56-78					
DASH	60-78	(98-126)				
Plant CRY	56-88				468-498	
(6-4) Photolyase	59-85					
Bilateral CRY	54-92		(215-230)		479-511	
Insect CRY	52-82		(236-253)		(493-506)	

Figure 2.9 Bilateral cryptochromes interact with the E3 ligase COP1
A. Schematic representation of domain structure and homology between human COP1 and *A.thaliana* COP1. RING, catalytic Ubiquitin ligase domain; Coil, coiled-coil domain; NLS, nuclear localization signal; NES, nuclear export signal; CLS, cytoplasmic localization signal. % identity between indicated domains. **B.** Interaction of mCRY2 and mCOP1. 293T cells were transfected with FLAG-mCOP1 or empty vector and mCRY2. Extracts were immuno-precipitated with FLAG resin and analyzed by western blotting. **C.** Coiled-coil predictions for photolyase/cryptochrome classes. Propensity for coil formation was analyzed for individual sequences; mean values were calculated for each class. Dashed line indicates significance cutoff. **D.** Sequence range of significant predicted coiled-coil domains. Criteria for significance: peak propensity ≥ 0.5, residues with values ≥ 0.2 are included in the range. Values in parentheses are peaks with maximum values ≥ 0.2, below the signficance cutoff.

Identification of potential dimerization interfaces in plant and bilateral cryptochromes

Plant and bilateral cryptochromes may use one or more of their conserved motifs as a dimerization interface, or they may utilize a more common dimerization motif, such as the coiled-coil domain. Coiled-coil domains mediate both homo- and heterodimerization of many proteins, including COP1, through bundles of helical segments (Kohn et al., 1997). The flavin binding domain of the photolyase/cryptochrome family is extensively helical; in order to determine if these proteins have coiled-coil domains, I analyzed sequences from each class for their propensity to form coiled-coils using the COILS predictor (Lupas, 1996). Figure 2.9C displays the mean values of coiled-coil propensity for each class. All members of this family have significant coiled-coil propensity in the N-terminal domain, from residues 55-80; in fact, a previous study determined that this motif in Class I photolyases displays sequence characteristics of a leucine zipper (Patterson and Chu, 1989). Importantly, plant and bilateral cryptochromes are the only other classes that possess an additional prediction of coiled-coil formation, occurring in the photolyase homology domain just before the beginning of their unique C-terminal domains (Fig. 2.9C-D). These coiled-coil domains are therefore potential dimerization interfaces for plant and bilateral cryptochromes. Interestingly, zCRY4, which interacted weakly with bilateral cryptochromes, also has a significant coiled-coil prediction in this region (data not shown); however, since the coiled-coil prediction in bilateral cryptochromes overlaps one of their signature sequences (Fig. 2.6), stable dimerization may require all or part of this conserved sequence that zCRY4 lacks.

Using signature sequences to trace evolution of cryptochromes

My initial finding that vertebrate cryptochromes are not limited to chordates, but in fact are common to the Bilateria (Fig. 2.1), suggested a more ancient origin of this lineage then previously demonstrated (Daiyasu et al., 2004; Lin and Todo, 2005) and one current hypothesis suggests that (6-4) photolyases evolved from animal cryptochromes (Kanai et

al., 1997). In order to understand the evolution of (6-4) photolyases and bilateral cryptochromes, I searched fungi, protist, and cyanobacteria genomes for evidence of class-specific signature sequences. As a class, (6-4) photolyases had only one motif conserved between all members that was unique from the closely related bilateral cryptochromes (Figure 2.10A). This motif corresponded in sequence to the most highly conserved bilateral motif (Figure 2.10B) that maps to a loop region just below the FAD binding cavity (Figure 2.10C, in red).

Genomes of distantly related organisms were searched using full-length coding sequences for human Cry1, *A.thaliana* Cry1, *A.thaliana* (6-4), or *D.melanogaster* (6-4) (since plant and animal (6-4) photolyases form distinct subgroups) by discontinuous Mega BLAST, which is optimized to identify homologs in divergent sequences (Ma et al., 2002). These searches retrieved over 20 significant matches to putative cryptochromes and (6-4) photolyases (Appendix 4). Importantly, although query sequences were full-length, only the most highly conserved region, corresponding to part of the FAD binding domain, and containing the signature sequences shown in Figure 2.10A-B, was identified in most searches. A number of these sequences are aligned in Figure 2.10D, illustrating the minor differentiation of bilateral cryptochromes from (6-4) sequences in this highly conserved region. Most sequences were clearly related to either bilateral cryptochromes or (6-4) photolyase through conservation of the signature motifs; however, a group of fungal sequences (boxed in green) displayed properties of both (6-4) photolyase and cryptochrome, both in the region displayed and in flanking regions (data not shown). Classification of these genes will require further functional studies.

Sequences with high homology to the (6-4) signature motif were found in a wider variety of fungi and protists than bilateral cryptochromes, suggesting that (6-4) photolyase predates bilateral cryptochromes. Perhaps most importantly, I identified a full-length, putative (6-4) gene in the cyanobacteria *Gloeobacter violaceus* that is 50% identical to

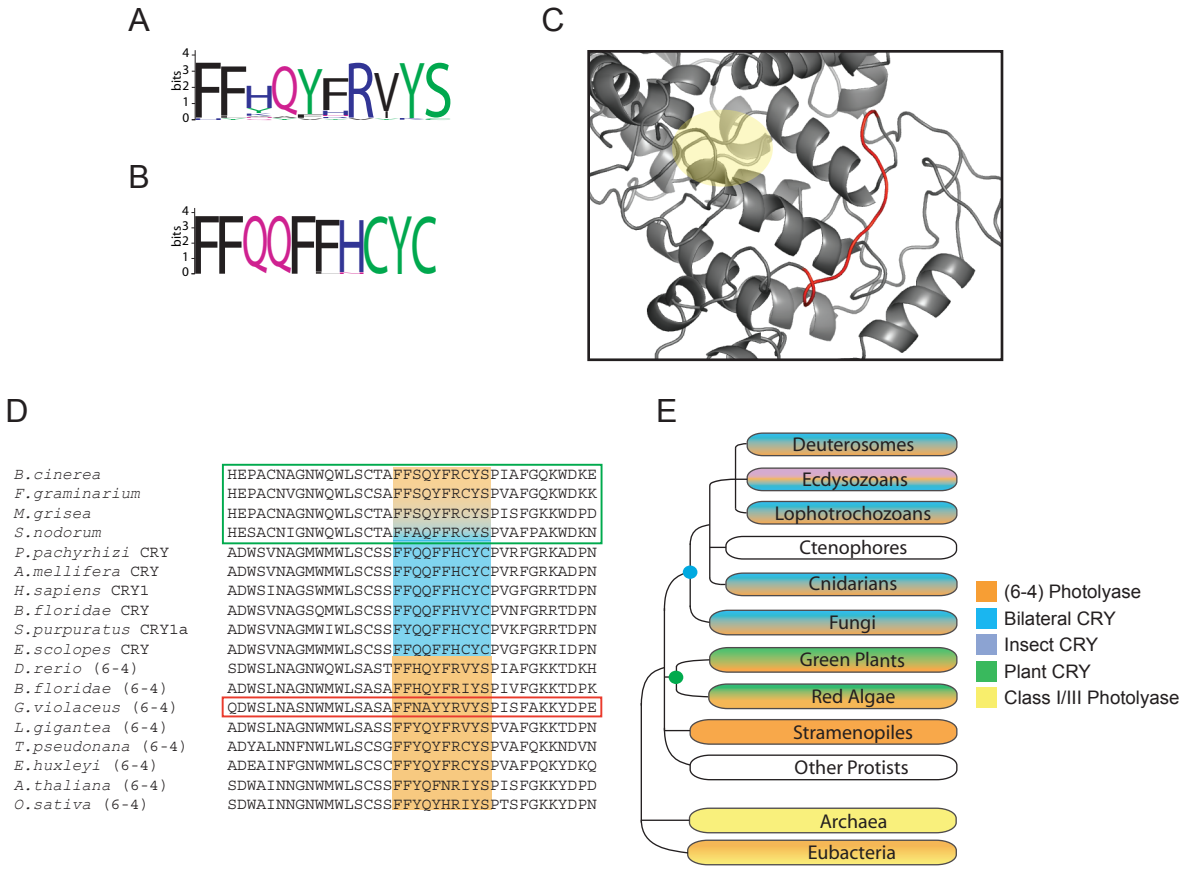

Figure 2.10 Tracing evolution of the photolyase/cryptochrome family with signature sequences

A. Signature sequence motif of (6-4) photolyase. The single, unique and highly conserved motif in the (6-4) photolyase class. **B.** Analogous motif in bilateral cryptochrome. **C.** Mapping motif on the hCRY2 PHR homology model (corresponds to blue motif in Fig. 2.6). Ribbon diagram illustrates location of the motif (red) in a flexible region adjacent to the FAD binding cavity (yellow circle). **D.** Sequence alignment of highly conserved region in the bilateral/(6-4) lineage. Bilateral (blue) and (6-4) (orange) motifs are indicated. The cyanobacterial *G.violaceus* sequence (boxed in red), a putative (6-4) photolyase, is the most ancient sequence retrieved, and putative fungal (6-4) photolyases (boxed in green) were the most divergent from the conserved motif. **E.** Species phylogeny and evolution of the photolyase/ cryptochrome family. Colored key indicates spread of classes throughout kingdoms of life; white indicates a lack of available sequence data. DASH cryptochromes were left out for simplicity, although they are present from eubacteria to deuterosomes. Blue and green filled circles represent nodes at which modern bilateral and plant cryptochrome sequences were present, dating the origin of both lineages to the emergence of eukaryotes.

Drosophila (6-4) photolyase (boxed in red, Figure 2.10D). This is the first record of a (6-4) photolyase in any prokaryote. The genome of *G.violaceus* is fully sequenced, and a search for members of the photolyase/cryptochrome family revealed three genes: a Class I CPD photolyase, a DASH class member, and a (6-4) photolyase. Phylogenetic analyses of multiple molecular and morphogenic characteristics of cyanobacteria strongly suggest that *G.violaceus* is an early branching lineage (Nakamura et al., 2003), indicating that the full photolyase complement (CPD (Class I, II, and III), (6-4), and DASH) was present at the emergence of cyanobacteria at least 2.5 billion years ago (Dvornyk and Knudsen, 2005).

With available sequence data, both plant and animal cryptochrome lineages can be traced back to the emergence of early eukaryotes. Using the *A.thaliana* Cry1 coding sequence to query databases yielded expected matches to other plant cryptochromes, and a single, distant homolog in the red algae *Cyanidioschyzon merolae* (Appendix 4) (Matsuzaki et al., 2004). These data suggest that plant cryptochromes began to evolve from Class III photolyase before the divergence of red and green algae, over 1.5 billion years ago Figure 2.10E, green circle) (Hedges et al., 2004). Similarly, sequences with high homology to bilateral cryptochromes were found the cephalopod *Euprymna scolopes*, the cnidarian *Nematostella ventensis,* and the pathogenic fungus *Phakospira pachyrhizi*. These data demonstrate that bilateral cryptochromes existed with class-specific sequences as long as 1.3 billion years ago, before the divergence of fungi and metazoans (Figure 2.10E, blue circle) (Hedges et al., 2004). As more sequence data from primitive eukaryotic organisms become available, these evolutionary timelines can be refined for a greater understanding of how cryptochromes evolved from photolyases and what evolutionary pressures might have driven changes in function.

Discussion

Photolyase and cryptochromes are flavoproteins that carry out vastly different biological reactions, from repair of UV-induced DNA damage to regulation of growth and the circadian clock. Although the mechanism by which photolyases repair DNA is known in detail, these studies have been of little help thus far in determining how cryptochromes transduce photic information. The identification of cryptochrome signaling mechanisms is currently one of the major questions in the field of photobiology. The goal of this study was to identify functionally important sites and clarify evolutionary relationships in the photolyase/cryptochrome family, and was designed to take advantage of our knowledge of photolyase's mechanism to compare and contrast with cryptochrome findings.

The sequence-based approach used here, based on the evolutionary trace method, is predicated on two hypotheses: first, that a protein family should not only retain its fold but also conserve location of functional sites; and second, that functional sites should have a lower substitution rate, interspersed by mutation at sites that cause a divergence in function. The basis of these hypotheses is that a function retained or evolved from a progenitor should take place at or near the same structural site, since such a site is well defined and because protein backbone variation within a family is minimal (Lichtarge et al., 1996). However, in the case of cryptochrome evolution from photolyases, I found this not to be true. The functional site of photolyase is well characterized, and class-specific motifs identified by evolutionary trace were exclusively localized to this site as predicted; however, the majority of class-specific motifs in both plant and animal cryptochromes were absent from this region, localized instead to the opposite face of the protein. These data suggest that an extensive adaptive process occurred in the evolution of cryptochromes, characterized by more than mutation of a few key residues surrounding the photolyase active site to generate a new function.

As with any sequence-based approach, potential concerns arise both with the method of analysis and with assumptions that must be made in order to carry out the analysis. A major concern in this particular approach is the reliability of the phylogenetic tree used to perform the evolutionary trace analysis. Sufficient sequences must be used to generate a meaningful and reliable tree, and multiple sequence alignments used to generate trees must be verified and manually adjusted, if necessary, to avoid overemphasizing differences between proteins. Regarding the photolyase/cryptochrome family, several prior studies have made these serious errors, resulting in trees that suggested implausible evolutionary scenarios or contained non-photolyase-like sequences (Kanai et al., 1997; Kleine et al., 2003). Multiple sequence alignments used to generate trees in this study were manually examined and edited to determine that proteins were properly aligned. For this reason, the unique C-terminal domains of cryptochromes were not included in these analyses, since none are highly conserved within their own class. The last concern applies to incorrect grouping of proteins from related sister taxa into a single clade, reducing the ability to correctly identify class-specific residues. Fortunately, there are numerous functional data to support the division of photolyases and cryptochromes into classes indicated by the phylogeny.

Reclassification of the DASH class as a probable photolyase

One of the surprising findings of this study was the determination that DASH cryptochromes resemble CPD photolyases more than cryptochromes. This result is supported by data suggesting that at least some members of the DASH class possess weak CPD repair activity *in vivo* and *in vitro* (Daiyasu et al., 2004; Hitomi et al., 2000). The observed weak CPD repair activity by DASH proteins implies that their optimal substrate has not been identified. Indeed, preliminary studies in our lab indicate that DASH proteins repair non-standard substrates such as damaged RNA (McDowell-Buchanan, 2006) and single-stranded DNA (C. Selby and A. Sancar, unpublished data) preferentially as compared to

Class I photolyases. Therefore, results from this study, in combination with functional data, suggest that the DASH class does not satisfy the definition of cryptochrome. Initial *in vivo* studies on the DASH may have missed their potential contribution to photoreactivation as an artifact of the experimental system; photoreactivation assays deliver UV damage in a matter of seconds and the photoreactivating light dose over a timescale of minutes to hours (Worthington et al., 2003). It is possible that substrates repaired by DASH proteins are not generated or repaired significantly on this timescale, or do not contribute to UV-induced cell death. Further studies are ongoing to characterize preferred substrates and the true physiological function of the DASH class.

Repeated evolution and convergence of plant and animal cryptochromes

Another major finding of this study was the identification and initial characterization of a novel class of prokaryotic CPD photolyases, Class III, that are the most likely progenitors of plant cryptochromes. Importantly, many bacteria that possess Class III photolyases interact symbiotically with plants, such as *A.tumefaciens*, *M.loti*, and *B.japonicum*, providing a possible mode of gene transfer. The evolutionary origin of plant cryptochromes has long been elusive, since plant and animal cryptochromes are as similar to *E.coli* photolyase as they are to each other (Partch et al., 2005). This study also resolves the debate on the origin of the (6-4)/bilateral clade; identification of (6-4) photolyases, but not bilateral cryptochromes, in protists and the cyanobacterium *G.violaceus*, strongly suggest that (6-4) photolyase is the progenitor of this lineage. These data provide the first solid evidence for the independent evolution of plant and animal cryptochromes.

Although classes of the photolyase/cryptochrome family likely share a primordial ancestor, such a progenitor, that clearly predates distinction between photolyase subclasses, has not been identified in Eubacteria or Archaea. At issue here is the distinction between parallel and convergent evolution: parallel evolution is defined as the occurrence of similar evolutionary events in lineages evolving independently from the same

ancestor, while convergence is defined as similar changes after evolution from different ancestral sequences (Doolittle, 1994). The shared properties in higher cryptochromes evolved independently from divergent and functionally distinct progenitor classes; therefore, convergence, rather than parallel evolution, is the most parsimonious explanation for the observed similarities.

Conservation of structural elements in plant and animal cryptochrome lineages is compelling evidence for convergence of function. Based on these data, I examined animal cryptochromes for biochemical properties of plant cryptochromes, such as the ability to form stable, light-independent homo- and heterodimeric complexes, and found that they share this functional similarity as well. Dimerization may occur through an interface composed of surface accessible motifs, or it may occur through conserved structural elements such as the C-terminal coiled-coil domain. This coiled-coil domain was recently shown to be critical for the clock function of mammalian cryptochromes (Chaves et al., 2006), although its role in cryptochrome function was not made clear. Furthermore, both animal and plant cryptochromes interact with the dimeric ubiquitin E3 ligase, COP1. Dimerization of cryptochromes likely stabilizes the interaction with COP1 and appears to be required for plant cryptochrome signaling *in vivo* (Sang et al., 2005). At this time, it is unknown whether dimerization of bilateral cryptochromes and interaction with COP1 play a role in their function in the circadian clock. Although my preliminary data suggest that the mammalian CRY:COP1 interaction is physiologically relevant (data not shown), further studies are required to elucidate the role of these interactions *in vivo*.

Convergent properties arise as the result of similar adaptive solutions to environmental pressures. In the case of cryptochromes, convergence may have occurred as the result of a change in substrate, from DNA photoproducts to protein-protein interactions, driven by the need for a light-modulated interaction site that could potentially accommodate more than one effector. The increased importance of protein-protein

interactions in cryptochrome function is supported by the number of conserved, surface accessible motifs in plant and animal cryptochromes with respect to photolyases, including the DASH class. Furthermore, plant and animal cryptochromes possess extended C-terminal domains that are involved in phototransduction *in vivo* (Busza et al., 2004; Dissel et al., 2004; Rosato et al., 2001; Yang et al., 2000). Acquisition of C-termini that are unique to, and unrelated between, plant and animal lineages, may also have played a key role in the convergent evolution of the cryptochrome photoreceptor.

Evolution of the photolyase/cryptochrome family

Collectively, these analyses allow us to piece together the evolution and diversification of the photolyase/cryptochrome family. The full complement of photolyases was present before the emergence of eukaryotes: Class I, II, and III CPD photolyases, (6-4) photolyase, and the DASH class. Sometime before the split between red algae and green plants, over one billion years ago, a Class III photolyase underwent an adaptive change and began evolving into the plant class of cryptochromes. At the same time in a distinct evolutionary event, (6-4) photolyases began evolving into bilateral cryptochromes, such that the bilateral cryptochrome genes as we know them today were present before the split between fungi and metazoans. From the presence of the photolyase/cryptochrome family in modern day animals, their last common ancestors, the Urbilateria, must have possessed a Class II CPD photolyase, a (6-4) photolyase, a DASH class, and a bilateral cryptochrome. Extant lineages have lost one or more of these classes, and a new class of cryptochromes evolved in Ecdysozoans that is limited to certain insect species, including the model invertebrate *D.melanogaster*.

Another group also identified the existence of vertebrate-like cryptochromes in the Ecdysozoan lineage and demonstrated that they retain the ability to regulate clock transcription in insect cells (Zhu et al., 2005). Collectively, our discoveries have tremendous implications for the dual functionality of bilateral cryptochromes, which act as light-

dependent photosensory receptors to modulate non-visual photoresponses, and as light-independent regulators of transcription in the molecular circadian clock. Instead of arising as a vertebrate innovation with an limited, light-independent role in the circadian clock as previously proposed (Griffin et al., 1999), the evolutionary timeline of bilateral cryptochromes suggests that they evolved as photosensory receptors first, and adapted their light-independent function to the origin of the metazoan circadian clock.

The evolution of blue-light photosensory receptors for growth and circadian rhythms from photolyase progenitors is a reasonable consequence of the continuous adaptive stimulus of the daily solar cycle, given the strong selective pressure of solar UV irradiation. Many classes of photosensory receptors exist that are specific for nearly all wavelengths of visible light (van der Horst and Hellingwerf, 2004). However, near-UV/blue-light receptors are conceivably the most likely target for evolutionary pressure since these wavelengths of light penetrate to the greatest depths in aquatic environments (Ragni, 2004), such as those in which life began, and convey the most information about timing of the solar cycle.

Acknowledgements

This study was a collaborative effort with Nikki Worthington, although I originated the project and developed its seminal ideas. Figures 2.1 and 2.7-2.10 are the direct products of my efforts, and Figures 2.2 and 2.4-2.6 resulted from our equal efforts. N.Worthington and C.Selby are responsible for the work in Figure 2.3; C. Selby cloned the *C.crescentus* gene, purified the MBP-CcPhr protein, and did the preliminary in vivo photoreactivation assay, and N.Worthington performed replicate experiments.

CHAPTER 3

ROLE OF STRUCTURAL PLASTICITY IN SIGNAL TRANSDUCTION BY THE CRYPTOCHROME BLUE-LIGHT PHOTORECEPTOR

Summary

Cryptochromes are blue-light photoreceptors that regulate a variety of responses such as growth and circadian rhythms in organisms ranging from bacteria to humans. Although plant and animal cryptochromes share a high degree of structural homology with the light-activated DNA repair enzyme photolyase, they lack DNA repair activity; instead, cryptochromes possess carboxy-terminal extensions of 40-250 amino acids beyond the photolyase homology region that are involved in phototransduction. *In vivo* data support a model of cryptochrome signaling based on light-dependent conformational rearrangement of these C-termini followed by effector binding or regulation. I analyzed the structures of C-terminal domains from an animal and a plant cryptochrome by computational, biophysical, and biochemical methods and found the isolated domains to be intrinsically unstructured. I show that the photolyase homology region and C-terminal domains stably interact, inducing tertiary structure in the C-terminal domain. In addition, I demonstrate a light-dependent conformational change in the C-terminal domain of *Arabidopsis* Cry1, resulting in an order-to-disorder transition after irradiation by white light. Collectively, these findings provide the first biochemical evidence for the proposed conformational rearrangement of cryptochromes upon light exposure.

Background

Upon their discovery, cryptochromes were postulated to be photoreceptors due to the high degree of homology they share with the light-activated DNA repair enzyme photolyase, and the observation that, like photolyase, they possess two chromophores, MTHF and FAD. Despite structural similarities between cryptochromes and photolyases, the photocycle and mechanism of signal transduction of cryptochromes have not been determined. It is hypothesized that cryptochromes utilize a photocycle analogous to that of photolyase, involving light-driven electron transfer, to initiate signaling (Cashmore, 2003; Sancar, 2003). Photolyases catalyze the light-dependent repair of UV-induced DNA photoproducts such as cyclobutane pyrimidine dimers or (6-4) pyrimidine-pyrimidone photoproducts by a well-characterized mechanism. Photolyase binds UV-damaged DNA independently of light; after absorption of a photon by the photoantenna, MTHF, the energy is transferred by Förster resonance energy transfer to the catalytic chromophore, $FADH^-$, which splits the DNA photoproduct by non-reductive electron transfer.

High resolution crystal structures of three photolyases and the structures of two cryptochromes obtained by molecular replacement reveal significant conservation of tertiary structure, consisting of an N-terminal α/β domain and a C-terminal α-helical flavin binding domain that are connected by a long interdomain loop (Brautigam et al., 2004; Brudler et al., 2003; Komori et al., 2001; Park et al., 1995; Tamada et al., 1997). There are no obvious structural explanations for the loss of DNA repair by cryptochromes, since the structures of photolyases and cryptochromes align to within 2 Å over the peptide backbone. Cryptochromes in plants and animals are distinguished from photolyases by the presence of extended C-terminal domains ranging from 40-250 amino acids beyond the photolyase homology region (PHR) of approximately 500 amino acids. Importantly, these C-terminal

domains have been shown *in vivo* to mediate phototransduction by both *Arabidopsis* and *Drosophila* cryptochromes.

In *Arabidopsis*, cryptochromes regulate light-dependent growth and developmental processes, such as initiation of photomorphogenesis and regulation of flowering time by day length, in addition to contributing to circadian photoreception. Regulation of photomorphogenesis by cryptochromes is mechanistically best understood, achieved primarily through light-dependent inhibition of the E3 ubiquitin ligase, COP1 (reviewed in (Lin and Shalitin, 2003)). Studies of the interaction between *Arabidopsis* cryptochromes and COP1 suggest an inhibitory mechanism driven by light-dependent conformational change of the cryptochrome C-termini since the CRY:COP1 interaction is stable and occurs independently of light through the C-terminal domain of cryptochromes, yet inhibition of COP1 by CRYs occurs only after light irradiation (Wang et al., 2001; Yang et al., 2001). Furthermore, transgenic overexpression of the C-terminal domain of either AtCRY1 or AtCRY2 results in a constitutive photomorphogenic phenotype, in which dark-grown transgenic plants display characteristics of light-grown wild-type plants (Yang et al., 2000). Collectively, these data suggest that signaling by *Arabidopsis* cryptochromes is achieved by regulating the accessibility or conformation of part of the C-terminal domain to COP1 in a light-dependent manner.

The single *Drosophila* cryptochrome, dCRY, is a circadian photoreceptor that promotes degradation of the integral circadian clock protein dTIM in response to light (Lin et al., 2001). Although the photolyase homology domain is clearly responsible for light absorption, the C-terminal domain of dCRY is essential for maintaining the light-dependence of the CRY:TIM interaction; in its absence, dCRY interacts with dTIM independently of light and promotes its degradation (Busza et al., 2004; Dissel et al., 2004; Rosato et al., 2001). These data suggest that a light-modulated interaction of the photolyase homology region of

dCRY with its C-terminal domain with is critical for proper regulation of effector binding and phototransduction.

The C-terminal domains of cryptochromes have not been characterized using computational or structural methods. Of the two cryptochromes whose structures have been solved by x-ray crystallography, the *Synechocystis* CRY lacks a C-terminal extension and *Arabidopsis* CRY1 was truncated at the C-terminus prior to crystallization (Brautigam et al., 2004; Brudler et al., 2003). I sought to determine the structures of C-terminal domains from two prototypical cryptochromes, human cryptochrome 2 (hCRY2-CT) and *Arabidopsis* CRY1 (AtCRY1-CT), in order to gain some insight into how cryptochromes function as photoreceptors. I found that both the hCRY2-CT and AtCRY1-CT are intrinsically unstructured in solution, although the two C-termini share no sequence similarities. Furthermore, primary sequence analyses of all known plant and animal cryptochromes indicate a high propensity for disorder in the C-terminal domains. I show here that the C-terminal domains interact directly with their cognate photolyase homology regions (PHR), and that these interactions induce stable, protease-resistant tertiary structure in the C-termini. Finally, I demonstrate a light-dependent conformational change from order-to-disorder that is localized to a short region of the C-terminal domain of *Arabidopsis* Cry1, providing the first biochemical evidence for the proposed conformational rearrangement of cryptochromes in response to light.

Experimental procedures

Primary sequence analyses of disorder

Sequences of all annotated plant and animal cryptochromes, along with several photolyases and bacterial cryptochromes, were obtained from GenBank and Swiss-Prot and analyzed for disorder propensity using PONDR VL-XT (www.pondr.com) and DisEMBL Remark 365 (dis.embl.de) algorithms with default settings. Sequences were aligned with ClustalW to differentiate the photolyase homology region (PHR) from the C-terminal (CT) domains; the PHR was designated as the sequence from the N-terminus to the point at which homology with *E.coli* photolyase ended, and the CT domain as the remaining C-terminal sequence. Mean disorder propensity was calculated for these two domains from PONDR VL-XT predictions (a table of these values is in Appendix 4). Variance in PONDR predictions for all PHRs was tested by ANOVA two-factor with replicates and did not vary from photolyases to cryptochromes ($p>0.9$).

Expression and purification of recombinant proteins

The C-terminal domains of hCRY2 (hCRY2-CT; residues 490-593) and AtCRY1 (AtCRY1-CT; residues 506-681) were subcloned into the pET21b(+) vector (Novagen), eliminating the N-terminal T7-tag and retaining only 11 amino acids of vector sequence including the C-terminal His tag, AAALEHHHHHH. All DNA constructs were verified by sequencing. All proteins were expressed in *E. coli* BL21(DE3)GOLD (Stratagene) and were highly soluble. Proteins were initially purified using Ni-NTA affinity chromatography according to the manufacturer's protocol (QIAGEN), followed by gel filtration chromatography (AcA 34 Ultrogel, Biosepra) on a 2.5 cm by 75 cm column equilibrated with 50 mM sodium phosphate, pH 7.0, 300 mM NaCl, 1 mM β-mercaptoethanol at a flow rate of 0.4 ml/min at 4°C. Both C-terminal constructs were also generated with a single N-terminal His tag introduced by PCR and purified similarly. Protein concentrations were determined by

absorbance at 280 nm using theoretical molar extinction coefficients (ε) of 2680 $M^{-1}cm^{-1}$ and 16,500 $M^{-1}cm^{-1}$ for the hCRY2-CT and AtCRY1-CT, respectively, as obtained by the ProtParam program (www.expasy.ch). GST-fusion CRY-CT constructs of various cryptochromes were made by subcloning the C-termini into pGEX 4T-1 vector (Amersham Biosciences) as follows: hCRY2 residues 483-593; mCRY2 residues 510-592; zCRY3 residues 460-598; and AtCRY1 residues 506-681. The proteins were purified using glutathione sepharose chromatography according to the manufacturer's protocol (Amersham) and protein concentrations were estimated against a known protein standard by Coomassie staining of SDS polyacrylamide gels

All baculoviral expression constructs were made using pFastBac-HTa (His tag) or pFastBac-1 (FLAG tag) vector (Invitrogen). Full-length AtCRY1 and hCRY2 proteins have a single N-terminal His tag and the C-terminally truncated hCRY2 (hCRY2-PHR; amino acids 1-512) has a single N-terminal FLAG tag (DYKDDDYK) added by PCR. Baculoviruses were produced according to the Bac-to-Bac protocol (Invitrogen); all viral stocks had a final titer of approximately 1 x 10^9 pfu/ml. For expression and purification of His-tagged proteins, 500 ml Sf21 cells (at 1 x 10^6 cells/ml) were inoculated with 5 ml viral stock and grown for 48 hours at 27°C. Cells were spun down, washed once with PBS, and the proteins were purified by affinity chromatography according to the manufacturer's protocol. Expression of the FLAG-tagged hCRY2-PHR was performed as above, and the protein was purified as described previously (Özgür and Sancar, 2003). Protein concentrations were estimated against a known protein standard by Coomassie staining of SDS polyacrylamide gels.

Secondary structure prediction and analysis by circular dichroism spectroscopy

Secondary structure was predicted using the PredictProtein service (cubic.bioc.columbia.edu/predictprotein) and confirmed by the JPred algorithm (www.compbio.dundee.ac.uk). Circular dichroism spectra were obtained using an Applied

Biophysics π*-180 spectropolarimeter equipped with a temperature control unit. All spectra were collected at 22°C using a 0.1 cm path-length quartz cuvette in 10 mM sodium phosphate, pH 7.0 with protein concentrations ranging from 0.08 to 0.2 mg/ml. Data were recorded in millidegrees every 0.2 nm between 185 and 260 nm. Spectra shown represent the mean of three scans. Secondary structure features were extracted from the CD data using the CDSSTR algorithm on Dichroweb (www.cryst.bbk.ac.uk/cdweb). The reference signal from the buffer was subtracted from all spectra prior to calculations.

NMR spectroscopy

Isotope-labeled hCRY2-CT and AtCRY1-CT were prepared using M9 minimal medium containing ^{15}N-NH_4Cl (Cambridge Isotopes) as the sole nitrogen source. Uniformly ^{15}N-labeled hCRY2-CT and AtCRY1-CT were concentrated to 1-1.5 mM in Buffer B (40 mM sodium phosphate buffer, 50 mM NaCl, pH 7.0) to which 7% (v/v) D_2O, and 0.02% NaN_3 were added. ^{15}N-^{1}H HSQC and $\{^{1}H\}$-^{15}N NOE (Farrow et al., 1994) data were collected at 20°C using a Varian INOVA 500 spectrometer equipped with a standard gradient-equipped triple resonance probe. Chemical shifts were referenced to 2,2-Dimethyl-2-silapentane-5-sulfonate sodium salt. Proton resonances were saturated with a 120° pulse spaced every 5 milliseconds for 4.5 seconds before the acquisition of the NOE (Nuclear Overhauser Enhancement) portion of the heteronuclear NOE spectrum; proton saturation was omitted from this period in the reference spectrum. Spectra were processed using NMRPipe software (Delaglio et al., 1995) and visualized using NMRView (Johnson, 1994).

Partial proteolysis

Three types partial proteolysis assays were performed on purified cryptochromes: titration of trypsin concentration, timecourse of digestion with constant trypsin, and timecourse of digestion under light and dark conditions. For the trypsin titration, equal masses of His full-length CRY or CT domain were aliquoted into tubes containing PBS for a

constant volume, and reactions were initiated with the addition of a 1:4 serial dilution of sequencing grade trypsin (Promega) at 1:1600, 1:400, 1:100, 1:25 (w/w). Reactions were stopped with 3X SDS buffer (150 mM Tris, pH 6.8, 6 mM EDTA, 6% SDS, 432 mM β-mercaptoethanol, 30% glycerol) after 15 min at 25°C, resolved by 12.5% SDS-PAGE and visualized by Coomassie staining. For trypsin digestion kinetics, equal masses of CRYs were digested in PBS with 1:1600 trypsin (w/w) at 25°C and reactions were stopped at 5, 30, 60 and 90 minutes, resolved by 12.5% SDS-PAGE and analyzed by silver stain or western blotting using an anti-CRY2B antibody (Thompson et al., 2003) or anti-GST to quantify protein remaining after digestion. Data from at least 3 independent experiments are plotted and standard error of the mean (SEM) is shown.

The kinetics of light-dependent partial proteolysis of full-length AtCRY1 was performed as above, except that two reactions were set up: a dark and light reaction that were pre-treated with either 30 minutes of darkness or 13.9 $\mu moles/cm^2/s^{-1}$ of cool white fluorescent light passed through heat-reflecting glass (Precision Glass & Optics). The dark timecourse was carried out under dim yellow light and the light timecourse was carried out under 13.9 $\mu moles/cm^2/s^{-1}$ of cool white fluorescent light. Reaction products were resolved on 8% SDS-PAGE and analyzed by silver stain for total protein or by western blotting using either an anti-AtCRY1 C-terminal antibody (Santa Cruz Biotechnology) to quantify the C-terminal domain, or using an anti-His antibody (Abgent) to quantify the N-terminal domain remaining after digestion. Densitometric quantification of antibody-reactive bands or total protein was performed with ImageQuant 5.0 software (Molecular Dynamics) and expressed relative to undigested controls in each experiment. Data from at least 3 independent experiments are plotted and standard error of the mean (SEM) is shown.

In vitro *pulldown assays*

The hCRY2-PHR used in the binding assays was generated by purification of the protein from Sf21 extracts without elution from FLAG resin. Briefly, a 1 ml cell pellet corresponding to 500 ml culture volume was lysed in 10 ml lysis buffer (50 mM Tris pH 7.5, 150 mM NaCl, 1 mM EDTA, 1% Triton X-100) on ice for 30 minutes and clarified by centrifugation at 14,000 rpm at 4°C for 20 minutes. The soluble extract was incubated with 250 μl of activated FLAG resin (Sigma) overnight at 4°C, washed twice with Tris-buffered saline (TBS; 50 mM Tris pH 7.5, 150 mM NaCl), once with TBS containing 1 M NaCl, and once again with TBS. A negative control, FLAG-hCHK1 resin, was prepared as above from transiently transfected 293T cells. Purity and concentration of both immobilized proteins was determined by silver staining of purification gels. FLAG resin bound to 5 μg of FLAG-hCRY2-PHR or FLAG-hCHK1 was incubated with 5 μg hCRY2-CT (~3-fold molar excess of CT) overnight in PBS at 4°C after removing 5% of the volume for analysis of the input. The beads were washed once with 500 μl PBS, once with 500 μl PBS containing 250 mM NaCl, and once again with 500 μl PBS. Bound proteins were resolved on 12.5% SDS-PAGE and visualized by western blotting with either anti-FLAG (Sigma) or anti-His (Abgent) antibody. Binding assays of cross-species interactions were performed as above, except that 5 μg of hCRY2-CT or AtCRY1-CT was added to 5 μg hCRY2-PHR immobilized on FLAG resin. All binding assays shown are representative of three independent experiments.

Results

Cryptochrome C-terminal domains possess sequence characteristics of disordered proteins

Throughout evolution, cryptochromes have maintained a surprising degree of structural homology to photolyases, which is somewhat unexpected given that they have lost photolyase's ability to repair UV-damaged DNA. Although representative members of the cryptochrome family (dCRY, hCRY2, and AtCRY1) share only 21-27% sequence identity with *E.coli* photolyase at the amino acid level, I determined that more than 90% of the secondary structure of *E.coli* photolyase is conserved with these prototypical cryptochromes within their photolyase homology regions (data not shown). The overall domain architecture and chromophore binding regions of the photolyase/cryptochrome subfamily members are shown in Figure 3.1A. Although C-terminal domains of cryptochromes from insects, vertebrates and plants have no identifiable similarity at the primary sequence level, secondary structure predictions for plant and animal C-terminal domains are similar and predict domains largely devoid of ordered structure (Figure 3.1B).

Proteins that lack ordered structure are enriched in residues that appear frequently in flexible regions such as P, E, D, K, S, and Q, while being poor in rigid, order-promoting amino acids such as W, Y, F, C, V, I, and L, as compared to the average folded protein in the Protein Databank (Romero et al., 2001; Vihinen et al., 1994). Consequently, primary sequence is a strong indicator of the propensity for intrinsic disorder. The PONDR VL-XT and DisEMBL neural network predictors were independently developed and trained to predict disorder in primary sequences based on experimentally determined regions of disorder and high flexibility (Linding et al., 2003; Romero et al., 1999). Both PONDR VL-XT and DisEMBL predicted significant propensity for disorder along the length of the C-terminal domains of both hCRY2 (Figure 3.2A) and AtCRY1 (Figure 3.2B). Accurate predictions of disorder could not be made for the 40 amino acid-long insect cryptochrome C-terminal

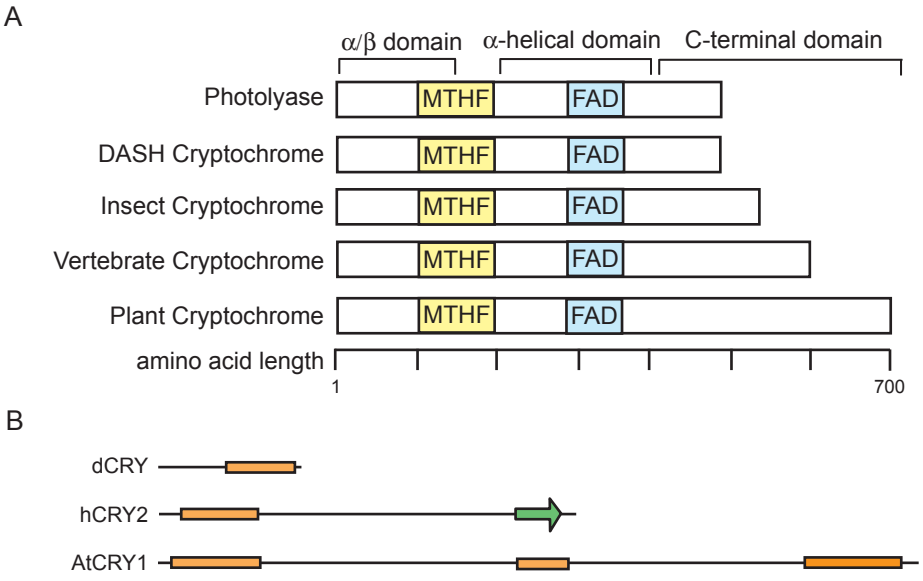

Figure 3.1 Cryptochrome domain organization and secondary structure predictions

A. Domain organization of photolyase/cryptochrome family members. The three domains are indicated with approximate binding sites of the non-covalently bound chromophores, folate (MTHF) and flavin (FAD). **B.** Secondary structure predictions of animal and plant cryptochrome C-terminal domains. Predicted alpha-helices and beta-sheets are indicated by boxes and arrows, respectively.

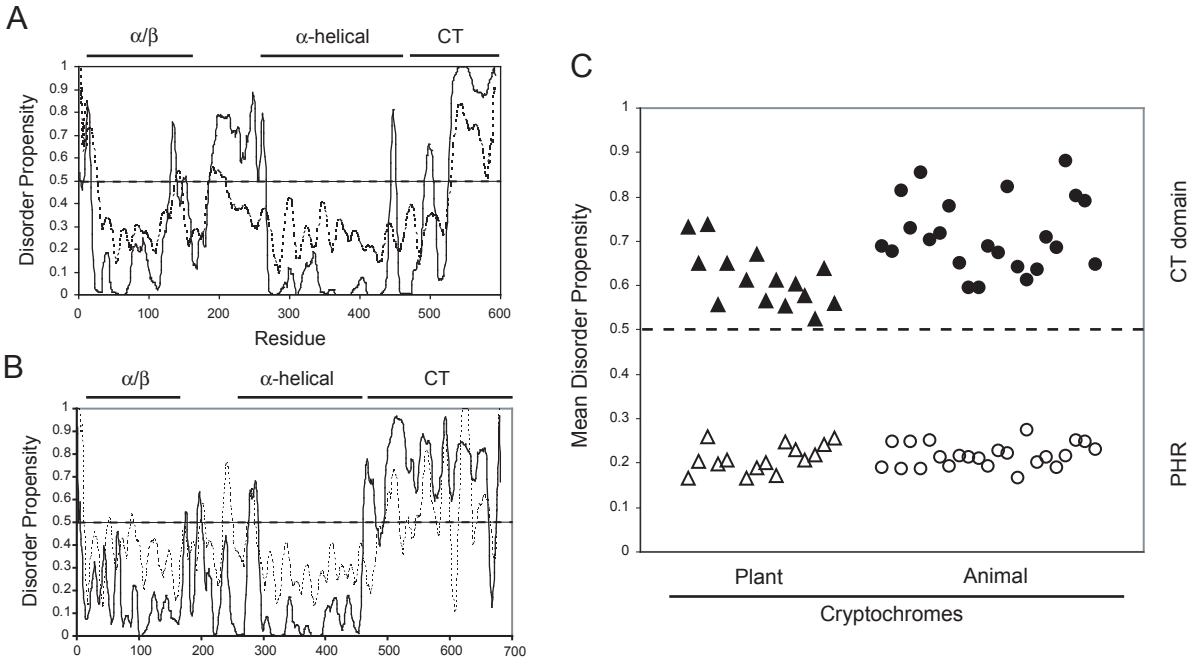

Figure 3.2 Cryptochrome C-termini have a high propensity for intrinsic disorder **A.** Predictions of disorder propensity for hCRY2 using the PONDR VL-XT (solid line) and DisEMBL Remark 465 (dashed line) algorithms. Sequences with disorder propensity >0.5 (horizontal dashed line) for longer than 30 amino acids are considered to be significantly disordered. Note the disordered region between amino acids 200-270, corresponding to the interdomain loop. **B.** Disorder predictions for AtCRY1. **C.** PONDR VL-XT disorder predictions for individual plant and animal PHR or CT domains. Mean disorder propensity was calculated for the PHR (open) and CT (filled) domains for plant (triangle) and animal (circle) cryptochromes.

domains, since the lower limit of accuracy for disorder prediction using PONDR VL-XT is 30-40 amino acids (Dunker et al., 2000).

In order to determine whether this feature is common to all cryptochrome C-terminal domains, we applied the PONDR VL-XT algorithm to 42 cryptochrome sequences and calculated mean disorder propensities for the PHR and C-terminal domains (Appendix 4). The mean disorder propensity of the PHR for all cryptochromes and 15 photolyases was low and did not vary considerably (0.214 ± 0.041). However, the C-terminal domains of all plant and animal cryptochromes had a significant mean propensity for disorder (Figure 3.2C). Interestingly, many C-terminal domains had long stretches of predicted disorder interrupted by short, 'ordered' minima (Fig. 3.2B), which are thought to correspond to regions important for protein-protein interactions (Fuxreiter et al., 2004).

Cryptochrome C-termini lack ordered secondary and tertiary structure in solution

To test whether cryptochrome C-terminal domains are truly intrinsically disordered, I used circular dichroism spectroscopy to examine the secondary structure composition of the C-terminal domains of the two most extensively studied animal and plant cryptochromes, hCRY2 and AtCRY1. The CD spectra (Figure 3.3) of cryptochrome C-termini with either N- or C-terminal His-tags were dominated by large, negative ellipticities at 200 nm, indicative of random coil, and lacked spectral features associated with α-helices and β-sheets (>80% turns/unordered by computational analysis of the CD data). The region around 220 nm, predictive of α-helices, was not affected by high solute concentrations (2.5 M glucose, data not shown) that approximate the density of the cell, which have been demonstrated to induce folding in some disordered proteins (Davis-Searles et al., 2001; Dedmon et al., 2002; Qu et al., 1998), indicating that the *in vivo* structures of the isolated C-terminal domains of the proteins are likely disordered.

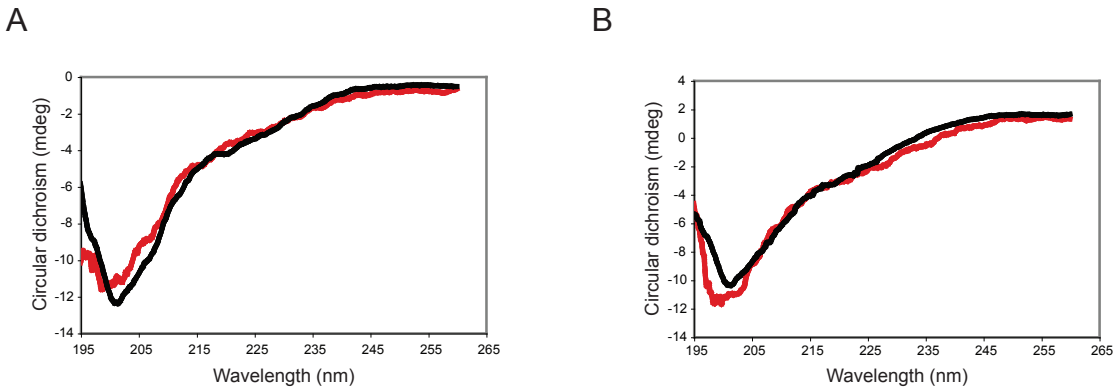

Figure 3.3 Plant and animal cryptochrome C-termini lack secondary structure elements

A. Far-UV circular dichroism spectra of His-hCRY2-CT were taken at 22˚C using 0.15 mg/ml protein in 10 mM sodium phosphate, pH 7.0. Key: N-terminal His-tag (black line), C-terminal His-tag (red line). **B.** Circular dichroism spectra of His-AtCRY1-CT taken as above. Key: N-terminal His-tag (black line), C-terminal His-tag (red line).

We collected ^{1}H-^{15}N heteronuclear single quantum coherence (HSQC) spectra of uniformly ^{15}N-labeled hCRY2-CT and AtCRY1-CT in order to assess the structural complexity of these domains. As shown in Figure 3.4, there was minimal chemical shift dispersion of the amide protons in both hCRY2-CT (Fig. 3.4A) and AtCRY1-CT (Fig. 3.4B), indicative of solvent-exposed backbone and/or conformationally-averaged random coil (Wishart and Sykes, 1994). To obtain further information about the structure and dynamics of these C-terminal domains, we acquired heteronuclear {^{1}H}-^{15}N NOE spectra, which provide quantitative information on mainchain flexibility in polypeptides. In particular, {^{1}H}-^{15}N NOE values are positive in folded, globular proteins and small or negative in unfolded and disordered proteins (Cho et al., 1996; Donne et al., 1997; Farrow et al., 1997). For hCRY2-CT, all but two of the 58 quantifiable NOE peaks were negative, signifying extreme flexibility of the polypeptide with backbone motion on a timescale characteristic of disordered proteins (Fig. 3.5A and Table 1). The AtCRY1-CT was similarly flexible, with 92 of 113 NOE peaks negative (Fig. 3.5B and Table 1). Altogether, the spectroscopic data demonstrate that the hCRY2-CT and AtCRY1-CT domains lack ordered structure and are highly flexible, two primary characteristics of intrinsic disorder.

Probing cryptochrome structure with partial proteolysis

Flexibility of the peptide backbone is the key determinant for susceptibility to attack by proteases, such that disordered regions are preferentially digested over other surface exposed protease-sensitive sites during partial proteolysis (reviewed in (Fontana et al., 2004)). At very low trypsin concentrations (1:1600 (w/w) trypsin:protein), globular proteins are not digested and thus under these conditions, sensitivity to trypsin serves as a reliable indicator of backbone flexibility near potential cleavage sites. As shown in Figure 3.6A, GST-fusion proteins of several plant and animal cryptochrome C-termini were significantly

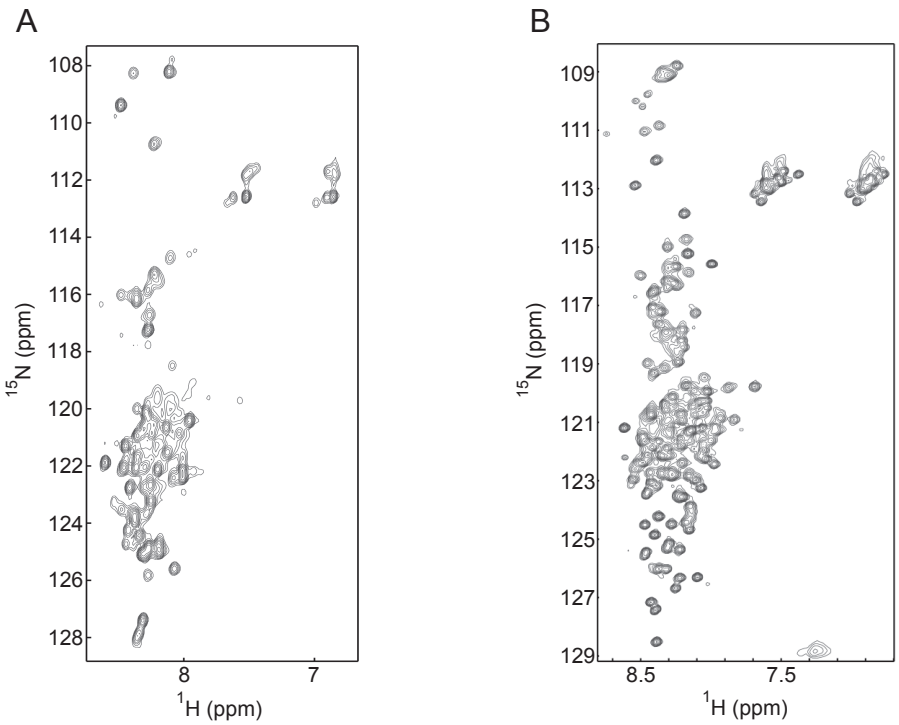

Figure 3.4 Cryptochrome C-termini lack ordered tertiary structure in solution
A. HSQC spectrum of uniformly ^{15}N-labeled hCRY2-CT. Spectrum was acquired with 1.5 mM hCry2-CT at 20˚C in 40 mM sodium phosphate, pH 7.0, 50 mM NaCl. Water was returned to the z-axis before each acquisition. Scale is in parts per million (ppm). **B.** HSQC spectrum of uniformly ^{15}N-labeled AtCRY1-CT, acquired with 1 mM protein as above.

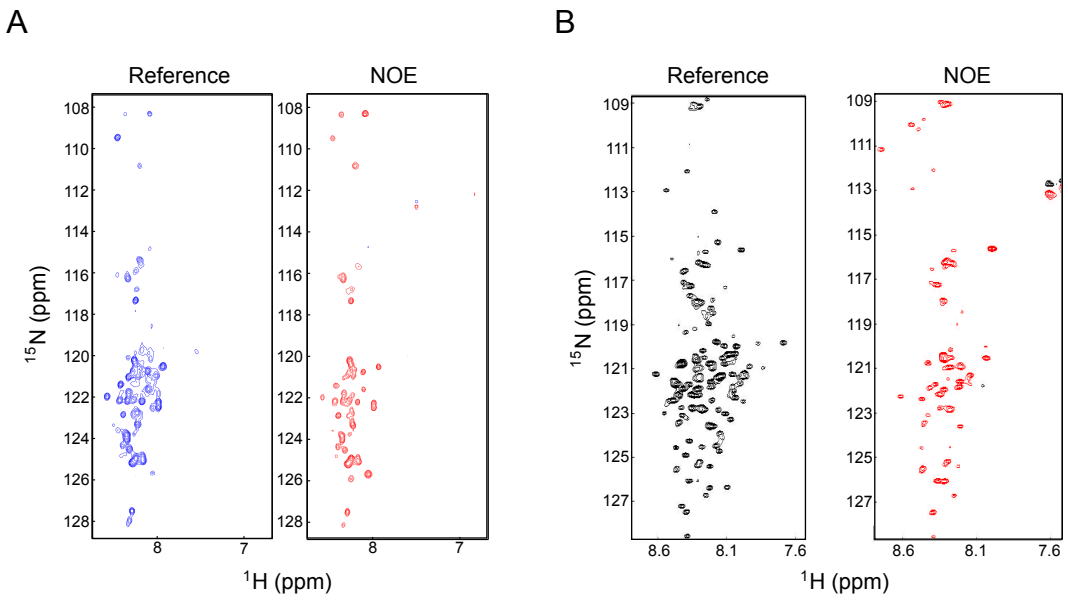

Figure 3.5 Cryptochrome C-termini are highly flexible in solution
A. {^{1}H}-^{15}N heteronuclear NOE spectrum of ^{15}N-hCRY2-CT. Spectra are shown without (Reference) and with (NOE) ^{1}H saturation. Positive peaks are blue, negative peaks are red. **B.** {^{1}H}-^{15}N heteronuclear NOE spectrum of ^{15}N-AtCRY1-CT. Positive peaks are black, negative peaks are red.

Table 1: Statistical analysis of heteronuclear {^{1}H}-^{15}N NOE data from cryptochrome C-termini

	hCRY2-CT	AtCRY1-CT
Peptide length (amino acids)*	114	186
NOE peaks quantified	58	113
Mean peak value	-0.785	-0.254
Standard deviation	±0.748	±0.364
Range of peak values		
High	0.937	0.535
Low	-3.717	-2.191
Median	-0.692	-0.246

* Including 11 amino acids from vector

Steady state heteronuclear {^{1}H}-^{15}N NOE values were obtained from the ratio of peak intensities observed with and without ^{1}H saturation.

degraded during partial proteolysis while the globular protein GST was not appreciably degraded under these conditions.

I then used partial proteolysis to probe for possible conformational changes of the C-terminal domain in the distinct environments of the full-length protein or as an isolated C-terminal domain, using a His-tagged or GST-fusion protein. Although trypsin cleavage sites (lysine or arginine residues not followed by a proline) are evenly distributed throughout the hCRY2 sequence (Fig. 3.6B), the full-length protein was minimally digested at high concentrations of trypsin (Figure 3.6C & D), indicative of a globular fold encompassing the whole protein. Despite accumulation of a slightly digested, C-terminally truncated intermediate, there is no evidence for efficient digestion of the C-terminus in the full-length protein (which would result in a loss of approximately 12 kDa) in contrast to the isolated hCRY2-CT, which was highly susceptible to proteolysis at low trypsin concentrations. I performed a kinetic analysis of digestion using 1:1600 (w/w) trypsin and monitored the integrity of the C-terminal domain after digestion by western with an anti-CRY2 antibody directed against an epitope 25 amino acids from the end of the protein (Figure 3.6B, boxed residues). As shown in Figure 3.6 E & F, digestion of hCRY2-CT past the anti-CRY2 epitope was nearly complete by the end of the 90-minute timecourse, in contrast to the full-length protein. Facile digestion of the isolated hCRY2-CT is a reflection of its disordered nature; the decrease in proteolytic susceptibility of the C-terminal domain in the context of the full-length protein suggests that the C-terminus is interacting with the PHR domain and adopting a stable, tertiary structure, a process common to many disordered proteins upon ligand binding (reviewed in (Dyson and Wright, 2002)).

Intraprotein domain interactions in cryptochrome

To investigate whether the isolated hCRY2-CT and PHR domains form a stable complex, I performed direct pulldown assays. FLAG-hCRY2-PHR or the similarly sized

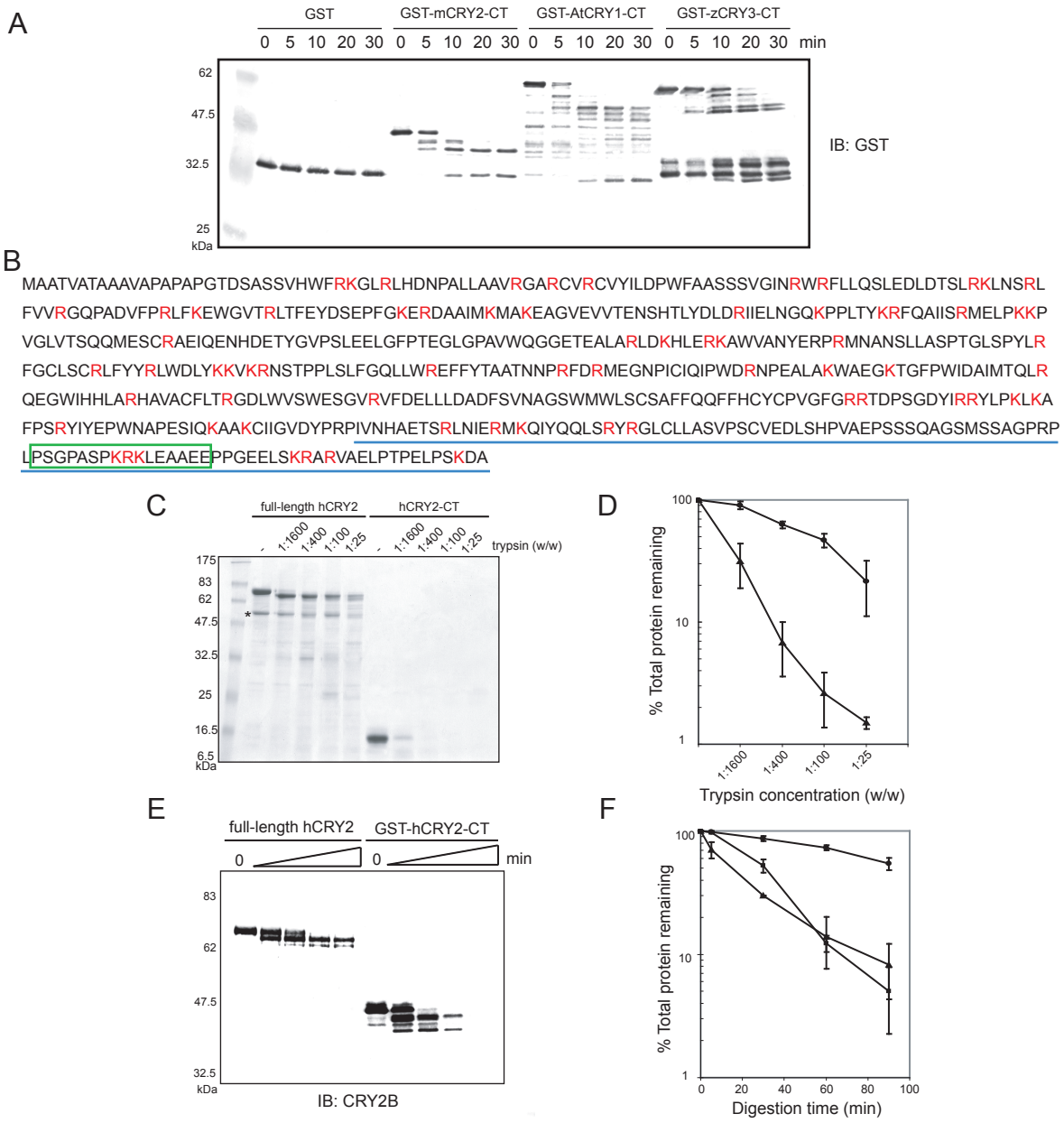

Figure 3.6 Cryptochrome PHR induces ordered structure in the C-terminus
A. Partial proteolysis of purified GST-Cry CT proteins. Cry CT domains are sensitive to digestion with limiting trypsin (1:1600 (w/w)). **B.** Trypsin map of hCRY2. Predicted trypsin cleavage sites are shown in red. The CT domain is underlined and the anti-CRY2B antibody epitope is boxed. **C.** Trypsin titration of hCRY2 FL or CT domain. FL and His-hCRY2-CT were digested with serial dilutions of trypsin and analyzed by Coomassie staining. Asterisk indicates co-purifying contaminant. **D.** Quantitative analysis of trypsin titration by densitometry. Key: FL hCRY2 (circles), hCRY2-CT (triangles). **E.** Kinetics of trypsin digestion of hCRY2 FL or GST-CT domain. FL and GST-hCRY2-CT were digested with trypsin at 1:1600 (w/w) and analyzed by western blot with anti-CRY2B. **F.** Quantitative analysis of digestion kinetics by densitometry. Key: FL hCRY2 (circles), GST-hCRY2-CT (squares) and His-hCRY2-CT (triangles, data not shown). All plots are representative of 3 independent experiments (±SEM).

control protein FLAG-hCHK1 were immobilized on FLAG resin and incubated with hCRY2-CT. The hCRY2-CT bound robustly to hCRY2-PHR, but not to the negative control, hCHK1 (Figure 3.7A). In order to further examine the specificity of the PHR-CT interaction, I performed binding experiments using immobilized hCRY2-PHR, adding either hCRY2-CT or AtCRY1-CT (Figure 3.7B). While the hCRY2-CT stably interacted with hCRY2-PHR, the AtCRY1-CT exhibited only weak binding. These data suggest that binding of the hCRY2 PHR and C-terminal domain involves specific intermolecular interactions. The weak, cross-species binding of the animal PHR and plant C-terminal domain likely results from the high degree of structural similarity observed in all the cryptochrome PHR domains.

Light-dependent conformational changes in the AtCRY1 C-terminal domain

There are currently significant limitations on performing photochemical studies on vertebrate cryptochromes since purification of recombinant proteins yields grossly sub-stoichiometric amounts of the catalytic chromophore FAD (Özgür and Sancar, 2003). Consequently, the previous studies were performed on hCRY2 lacking detectable chromophore, representing the 'dark' state of the molecule. In contrast, AtCRY1 can be purified from insect cells with stoichiometric FAD in the fully oxidized state (Lin et al., 1995). Although FAD is only active in the two electron-reduced form in all photolyases, there is some evidence that AtCRY1 is moderately photochemically active *in vitro* with fully oxidized flavin (Bouly et al., 2003; Kottke et al., 2006; Shalitin et al., 2003).

In order to determine if AtCRY1 changes conformation in response to light, I performed partial proteolysis in the dark and under white light and monitored the susceptibility to digestion, and therefore the conformation, of the C-terminal domain using an antibody directed against the CT domain (~40 amino acids from the end of the protein). Limiting amounts of trypsin easily digest the isolated AtCRY1-CT domain and, as with hCRY2, the C-terminal domain is significantly protected in the context of the full-length

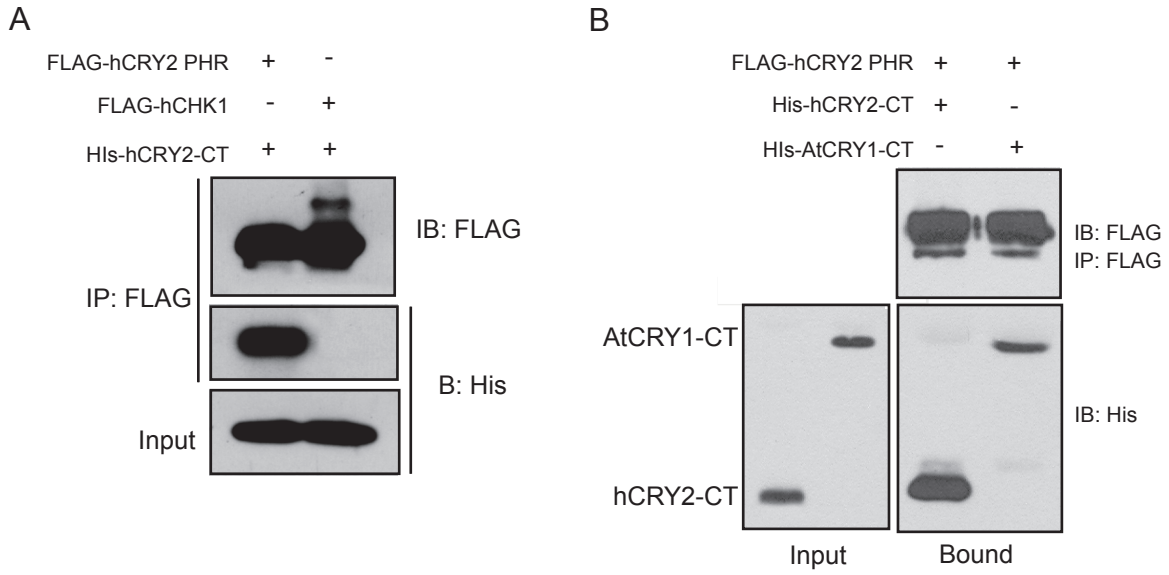

Figure 3.7 Isolated hCRY2 PHR and CT domains interact
A. Isolated hCRY2 PHR and CT domains specifically interact. *In vitro* pulldown of hCRY2 CT domains and hCRY2 PHR or a control, hCHK1. **B.** Cross-species specificity of the PHR-CT domain interaction by pulldown assay. The hCRY2 PHR domain exhibits species specificity for the hCRY2 CT domain over the AtCRY1-CT domain.

protein (data not shown). Irradiation of AtCRY1 with white light resulted in a five to ten-fold increase in the digestion rate of the C-terminal domain in the region of the anti-CT epitope as compared to a reaction carried out in the dark (Figure 3.8A). The full-length protein was initially converted to a slightly C-terminally truncated form, some of which accumulates in insect cells during overexpression and co-purifies with the full-length protein, corresponding to cleavage at the penultimate C-terminal arginine residue. However, cleavage past this point, which eliminates anti-CT antibody reactivity, was enhanced ten-fold in the presence of light (Fig. 3.8B), indicating that this region of the C-terminal domain undergoes an order-to-disorder transition upon light exposure. Further cleavage of the C-terminus occured at relatively equal frequency in dark and light-treated samples, as monitored by silver stain of total protein or western against the N-terminal His tag (Figure 3.8C, data not shown), indicating that the conformation of the rest of the protein is relatively similar in both dark and light-treated samples.

Potential trypsin cleavage sites in the AtCRY1 C-terminus are indicated in Figure 3.9A. The lack of cleavage in the beginning of the C-terminal domain suggests that a stable, compactly folded domain exists in the context of the full-length protein, followed by a semi-stable domain where the majority of the proteolytic cleavages take place. Significantly, we do not detect a large-scale conformational rearrangement of the entire C-terminal domain in response to light; instead, the change in conformation appears to be limited to a relatively small region from amino acids 610-655, which contains the anti-CT epitope and the highly conserved STAESSS region of the DAS motif (DQXVP-Acidic-STAESSS), conserved in all plant cryptochromes (Lin and Shalitin, 2003). Therefore, these studies have identified a light-dependent molecular switch in AtCRY1.

Based on these and other data on the role of cryptochrome C-terminal domains in phototransduction, it is possible to propose a reasonable model for the role of light-

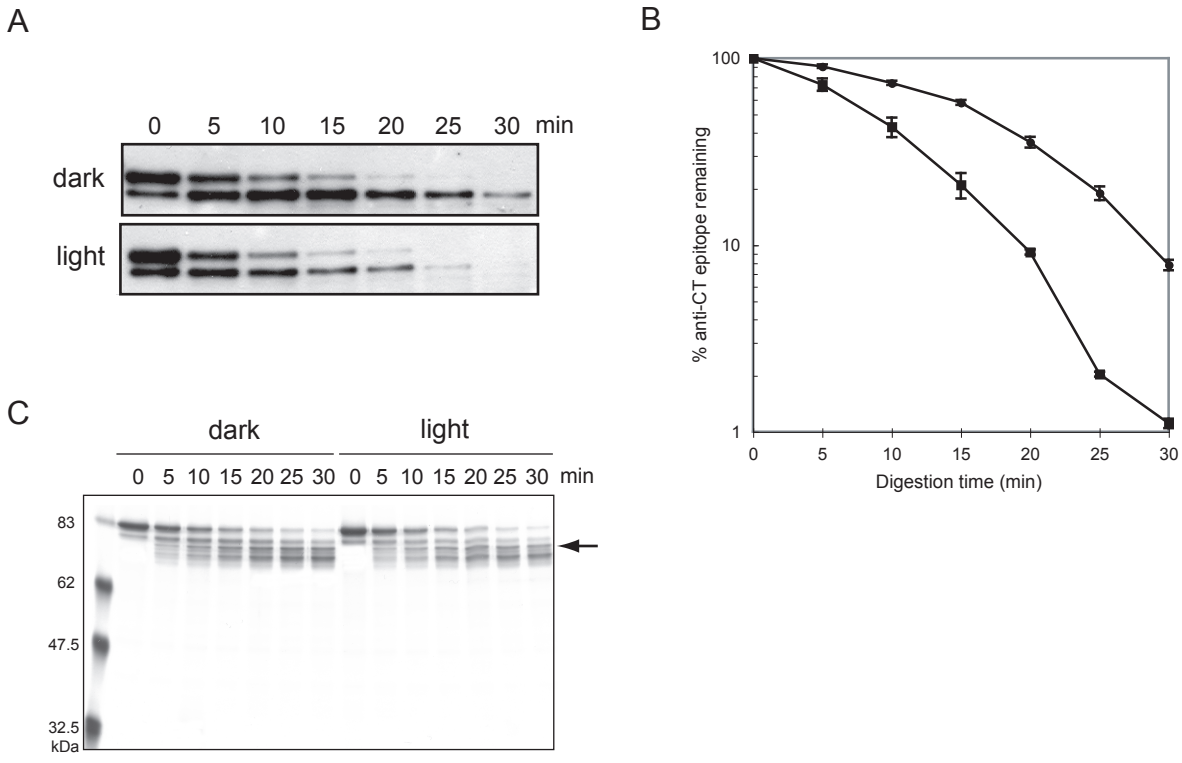

Figure 3.8 Light-dependent increase in proteolytic susceptibility of AtCRY1
A. Irradiation with light increases sensitivity of the C-terminal domain of AtCRY1 to trypsin. Purified AtCRY1 was maintained in darkness or irradiated for 30 minutes with white light before addition of 1:1600 (w/w) trypsin. Samples were maintained in darkness or white light for the duration of the digestion. Digestion was monitored by western blotting with anti-AtCRY1 CT antibody. **B.** Quantitative analysis of the effect of light on proteolytic sensitivity of AtCRY1. Densitometric analysis of anti-AtCRY1 CT reactivity from three independent experiments (±SEM). Key: dark (circles), light (squares). **C.** Light-dependence of AtCRY1 digestion does not affect digestion of the whole C-terminal domain. Representative silver stain of SDS-PAGE analysis of trypsin digestion timecourse; no stable, small molecular weight fragments were detected. Arrow indicates loss of anti-CT reactive band.

dependent conformational change and subsequent inhibition of COP1 activity by AtCRY1. Since randomly generated mutations affecting the interaction of AtCRY1 with COP1 cluster in the beginning of the C-terminal domain where proteolysis is unaffected by light (Fig. 3.9A), this region is likely responsible for the stable, light-independent interaction of plant CRYs and COP1 (Yang et al., 2001). The switch region around the STAESSS motif is therefore most likely responsible for the inhibition of COP1 activity by photoactivated cryptochromes.

While in a stable CRY:COP1 complex, the WD40 domain of COP1 binds to a short, linear motif in its degradation targets, such as the bZIP transcription factor HY5, and promotes their ubiquitination under dark conditions (Holm et al., 2001; Osterlund et al., 2000). In response to light, AtCRY1 rapidly inhibits COP1 activity, possibly by interfering with binding of degradation targets. Analysis of the sequence surrounding the switch region of AtCRY1 revealed two potential WD40 binding motifs: a HY5-like COP1 interaction motif and a WD40 interaction motif for the F-box protein β-TrCP (Figure 3.9B). The linear motif in HY5 is defined minimally as V·P·E/D·ϕ·G (ϕ designates a hydrophobic residue) (Holm et al., 2001), and the β-TrCP motif conforms to the consensus D·pS·X·X·X·pS (pS designates a phosphoserine) (Wu et al., 2003). One or both of these motifs are conserved in all plant cryptochromes, suggesting a role for these motifs in cryptochrome function. According to the light-dependent switch model of AtCRY1 function, COP1 is fully competent to ubiquitinate HY5 in the stable CRY1:COP1 complex that exists in the dark (Figure 3.9C). However, irradiation of the complex by blue light results in release of the AtCRY1 switch region from the PHR, allowing it to compete for HY5 binding to the COP1 WD40 domain, thereby creating a mechanism for the rapid and stable inhibition of COP1 activity by photoactivated cryptochromes.

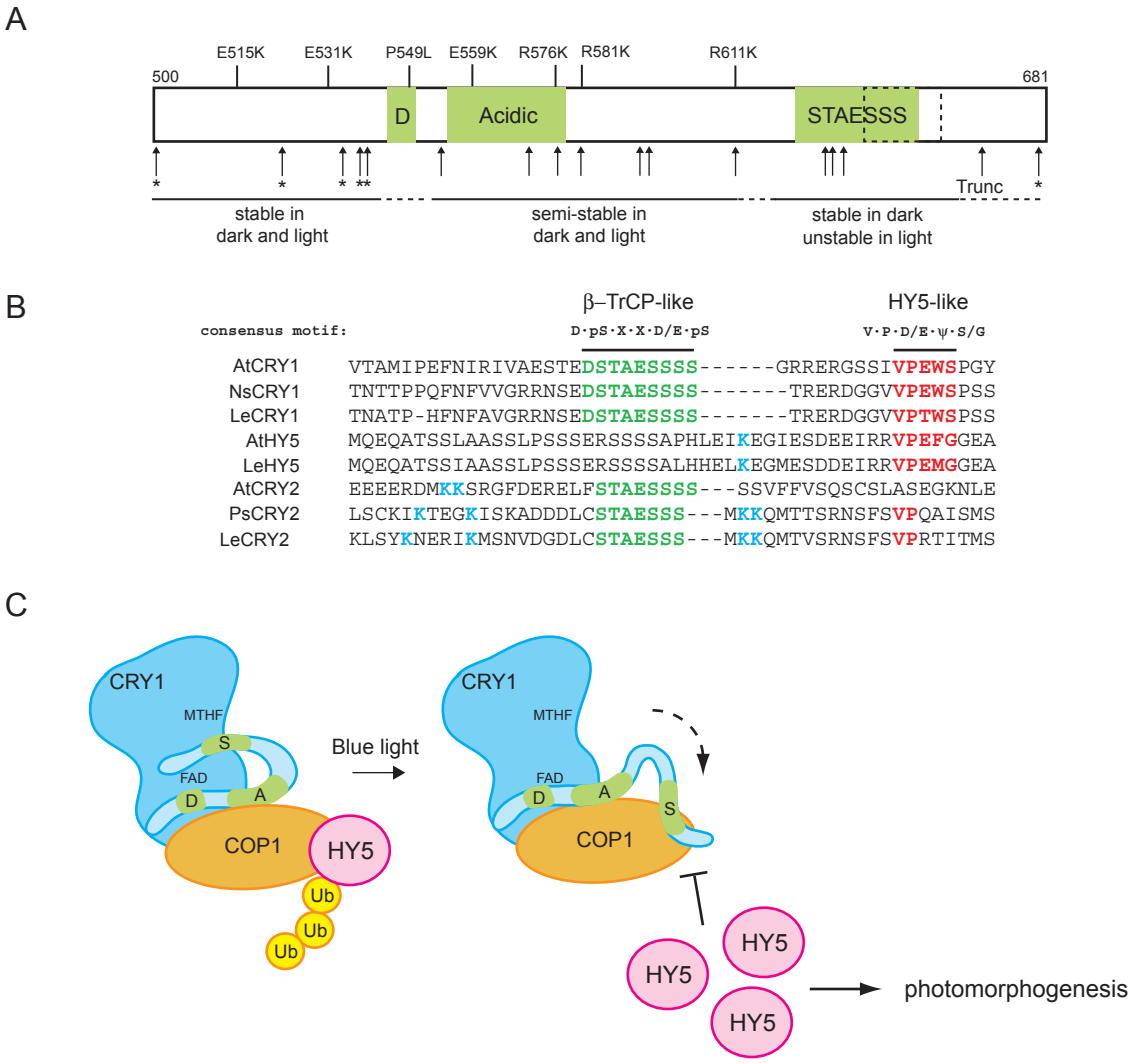

Figure 3.9 Model of light-dependent conformational change in AtCRY and inhibition of COP1 ubiquitin ligase activity

A. Schematic of the AtCRY1 C-terminal domain. Predicted trypsin cleavage sites are indicated by arrows; asterisks denote sites where cleavage was not detected by silver stain analysis of proteolytic fragments. The anti-AtCRY1 CT epitope is boxed. Mutations that disrupt the CRY1:COP1 interaction are shown above the schematic. **B.** Identification of WD40 interaction motifs in plant CRY C-termini. Two WD40 interaction motifs were identified in the CRY switch region: a β-catenin-like β-TrCP binding motif (green) and a HY5-like COP1 binding motif (red). Potential ubiquitin conjugation sites are shown in blue. **C.** Model for the role of structural plasticity in inhibition of COP1 by cryptochrome. Light initiates a photochemical reaction that releases a switch region near the STAESSS motif from a stable interaction with the PHR domain. The switch region competes for binding to the COP1 WD40 domain with targets such as HY5.

Discussion

Cryptochromes are photoreceptors that mediate a wide variety of growth and adaptive responses in diverse organisms. Although a detailed photocycle has yet to be described for any cryptochrome, it is known that C-terminal domains are involved in regulating cryptochrome phototransduction in both *Drosophila* and *Arabidopsis*. In the present study, I have examined the structures of C-terminal domains from plant and animal cryptochromes using biophysical and biochemical methods and shown that these domains lack ordered structure and are highly flexible in solution, two definitive characteristics of intrinsically disordered proteins. Since the isolated C-termini of either AtCRY1 or AtCRY2 are biologically active in *Arabidopsis*, the disordered nature of these domains is functionally relevant (Yang et al., 2001). Indeed, these data suggest that all or some part of the plant CRY C-termini must be disordered in order to interact with their effector, COP1. I have demonstrated here that a stable interaction between the PHR and CT domains induces ordered, protease-resistant structure in the C-terminus, which is reversed in a defined region by irradiation with white light, creating a light-dependent switch. Furthermore, I identify interaction motifs that suggest a reasonable model for the inhibition of COP1 ligase activity.

Disorder is a common characteristic of signal transduction proteins

My finding that cryptochrome C-terminal domains are intrinsically disordered is consistent with their presumed role as signal transduction domains. Disordered regions are more common in signal transduction and regulatory proteins than in metabolic and biosynthetic pathway components (Bell et al., 2002; DiGiammarino et al., 2001; Esteve et al., 2003; Iakoucheva et al., 2002; Matthews et al., 1995). There are many recognized benefits of disorder in a signaling domain. First, inherent structural plasticity may allow for efficient recognition of multiple, diverse interaction partners (Meador et al., 1992; Shoemaker et al., 2000). Second, the energetic cost of binding with induced folding can

allow high specificity interactions to occur with relatively low affinity, ideal for signaling exchanges (Rosenfeld et al., 1995; Schulz, 1979; Spolar and Record, 1994). Finally, disordered proteins may be subject to increased regulation by proteolysis (Prakash et al., 2004; Salghetti et al., 2001). In fact, several cryptochromes are regulated by light-dependent phosphorylation and proteolysis, and evidence from *in vivo* studies indicates that the C-terminal domains play a key role in these regulatory mechanisms (Ahmad et al., 1998a; Busza et al., 2004; Lin et al., 2001; Shalitin et al., 2002). Since disorder has recently been identified as a primary determinant for both phosphorylation and ubiquitin-mediated proteolysis, it seems likely that light-dependent increases in phosphorylation and ubiquitination may result from an increase in C-terminal disorder after light exposure (Iakoucheva et al., 2004; Prakash et al., 2004).

Intraprotein interactions affect the structure of cryptochrome C-termini

Since the size of full-length cryptochromes (60-70 kDa) precludes NMR studies, I took advantage of the proteolytic susceptibility of disordered proteins to probe the larger structural conformations of plant and animal cryptochromes. By doing this, I identified a stable interaction between the PHR and C-terminal domains in both plant and animal cryptochromes that increases the ordered tertiary structure of the C-terminal domains, as measured by a decrease in proteolytic susceptibility. I confirmed this interaction further by direct pulldown assay, demonstrating that the isolated PHR and CT domains stably and specifically interact. Disorder predictors such as PONDR VL-XT predict that the majority of cryptochromes have short, 'ordered' regions within their disordered C-termini. These short, ordered regions are often important for function and/or protein-protein interactions, acting as nucleation sites for induced folding (Dyson and Wright, 2002; Fuxreiter et al., 2004). Further investigation will be required to determine if these sites are involved in mediating the PHR-CT interaction.

Structural plasticity and linear interaction motifs in regulation of CRY function

Previous studies highlighted the likely role of light-dependent conformational change in the C-terminus as the mechanism by which *Arabidopsis* cryptochromes inhibit their effector, the E3 ubiquitin ligase COP1 (Yang et al., 2001; Yang et al., 2000). My data support the previously proposed model and further suggest that only a small region of the C-terminus, localized to the highly conserved STAESSS motif, undergoes structural rearrangement in response to light. The identification of two linear WD40 interaction motifs in this light-dependent switch region suggests that release of this switch allows cryptochrome to compete for COP1 binding with ubiquitination targets. Linear interaction motifs, such as the HY5 COP1-binding motif, play an important role in signaling and protein-protein interactions and are most frequently located in disordered regions (Neduva and Russell, 2005). From a signaling perspective, they permit transient, lower affinity interactions to occur on a timescale that is compatible with the rapid regulation of physiological processes. Finally, since the disordered *Arabidopsis* CRY C-termini efficiently inhibit COP1 *in vivo*, these data suggest that a conserved linear motif somewhere in the CRY C-termini is responsible for the inhibition of COP1, and that this motif is somehow repressed from binding COP1 by the CRY PHR under dark conditions. I propose that one or both of the WD40-binding motifs in the switch region may satisfy these conditions.

The light-dependent switch model may also explain how sequence differences in plant CRY1 and CRY2 C-termini translate into two critical functional differences in the activity and regulation of these photoreceptors. First, while the β-TrCP-like STAESS motif is conserved in all plant cryptochromes, only CRY1 proteins possess the complete HY5-like COP1-specific motif (Figure 3.9B). Fittingly, CRY1 is a much better inhibitor of COP1 *in vivo*, as evidenced by greater defects in photomorphogenic phenotypes in *Cry1* mutant plants versus *Cry2* mutant plants (Lin and Shalitin, 2003). The increased inhibition of COP1

by CRY1 versus CRY2 may therefore reflect the ability of CRY1 to better compete with HY5 in binding to COP1.

Secondly, while CRY1 protein stability is not affected by light, the C-terminal domain of CRY2 is phosphorylated and the protein is rapidly degraded after exposure to blue light (Shalitin et al., 2002). The light-labile nature of CRY2 protein therefore limits efficient CRY2 phototransduction to low light levels and is thought to play a key role in the CRY2-specific modulation of photoperiodic flowering (Mockler et al., 2003). Although this study does not provide evidence for a light-dependent conformational change in *Arabidopsis* CRY2, *in vivo* data suggest that de-repression of the CRY2 C-terminal domain in response to light is followed by ubiquitination by COP1 (Lin and Shalitin, 2003; Yi and Deng, 2005), implicating a light-dependent conformational change similar to that which I propose for CRY1. β-catenin utilizes a motif similar to that found in the STAESS domain of CRYs to interact with the β-TrCP E3 ligase, and ubiquitin conjugation occurs most efficiently on lysine residues located 9-13 amino acids upstream of the WD40 interaction motif (Wu et al., 2003). Significantly, all plant CRY2 proteins possess lysine residues upstream of the β-TrCP-like motif with this optimal spacing (Figure 3.9B), and the stability of CRY1 can be explained by the complete absence of lysine residues in the C-terminus of every plant CRY1 (data not shown). The biochemical studies presented here and identification of these linear motifs therefore provide testable models of cryptochrome phototransduction and how regulation of the two cryptochromes occurs differentially *in vivo*.

Conservation and divergence in cryptochrome signaling mechanisms

While several studies have demonstrated that the C-terminal domains of *Arabidopsis* and *Drosophila* cryptochromes are functionally important, the two C-terminal domains appear to regulate signaling differently. *Arabidopsis* cryptochromes appear to use their long C-terminal domains to directly signal to effector proteins, while *Drosophila* cryptochrome

utilizes its short C-terminal domain to regulate binding of effectors to the PHR domain in a light-dependent manner (Yang et al., 2001; Yang et al., 2000). Although the signaling endpoints for *Arabidopsis* and *Drosophila* cryptochromes are quite different, light-dependent changes in cryptochrome C-terminal domain conformation appear to be a common factor in regulating the ability to signal to downstream effectors. Although recent data suggest that cryptochromes in the chicken iris are capable of photoreception (Tu et al., 2004), there are no biochemical data on light-dependent signaling by vertebrate cryptochromes at this time, and therefore we can only speculate that the observed structural similarities in plant and animal cryptochromes underlie functional similarities. However, the C-terminal domains are not required for the light-independent function of vertebrate cryptochromes (Busza et al., 2004; Hirayama et al., 2003; Zhu et al., 2003), indicating that they may play a functional role in the photoreception.

Acknowledgements

A large part of this work was published as: Partch, C.L., Clarkson, M.W., Özgür, S., Lee, A.L., and Sancar, A. (2005). Role of structural plasticity in signal transduction by the cryptochrome blue-light photoreceptor. Biochemistry *44*, 3795-3805. Permission was granted by the American Chemical Society for publication in this dissertation. Figures 3.1-3.3 and 3.6-3.9 are the direct products of my efforts; M. Clarkson obtained NMR spectra and performed analysis of the data, generating Figures 3.4-3.5 and Table 1, and S. Özgür supplied insect cell-purified hCRY2 and AtCRY1 used in the *in vitro* assays. I thank Johnny M. Massengale for helping to establish purification conditions for the CRY C-termini and Ashutosh Tripathy of the UNC Macromolecular Interactions Facility for helpful discussions.

CHAPTER 4

DYNAMIC REGULATION OF THE MAMMALIAN CIRCADIAN CLOCK BY CRYPTOCHROME AND PROTEIN PHOSPHATASE 5

Summary

Circadian rhythms coordinate a variety of physiological processes with the daily solar cycle, controlling cellular growth and tissue homeostasis in mammals. Although two integrated transcription/translation feedback loops generate the molecular clock, the 24-hour periodicity of this oscillator is established in large part by the posttranslational regulation of clock proteins. Specifically, phosphorylation of the PER proteins by CKIε regulates their subcellular localization and degradation, affecting their role in the negative arm of the major feedback loop of the clock. CKIε activity is strictly regulated by inhibitory autophosphorylation, requiring an unidentified phosphatase for activation *in vivo*. Our lab previously demonstrated that the clock protein cryptochrome interacts with protein phosphatase 5 (PP5) and inhibits its activity. Here I show that PP5 regulates the kinase activity of CKIε and that inhibition of PP5 activity by cryptochrome allows potential crosstalk between CRY and CKIε to regulate PER phosphorylation levels. Expression of a dominant-negative PP5 mutant reduces PER phosphorylation by CKIε *in vivo* and loss of PP5 by stable knockdown results in hypophosphorylation of PER and disrupts circadian cycling in cultured cells. Like CKIε, PP5 mRNA is expressed both in the master circadian clock and in peripheral tissues independently of the clock transcription factors CLOCK/BMAL1. Furthermore, I show that PP5 inhibits CLOCK/BMAL1-mediated transactivation of clock gene transcription in a manner that is mechanistically independent of cryptochrome. These data suggest that PP5 and cryptochrome dynamically regulate both the positive and negative feedback loops of the mammalian circadian clock.

Background

Circadian rhythms organize the systemic synchronization of physiological and behavioral processes of an organism with the daily solar cycle, and contribute to the evolutionary fitness of bacteria, plants, and animals (DeCoursey and Krulas, 1998; DeCoursey et al., 1997; Green et al., 2002; Michael et al., 2003; Ouyang et al., 1998; Woelfle et al., 2004). The master circadian clock in mammals is located in the suprachiasmatic nuclei (SCN) of the anterior hypothalamus, where it operates with an intrinsic periodicity of about 24 hours. The clock is entrained to the 24-hour day by light input from the retina, and synchronizes molecular clocks in peripheral tissues through humoral and neural outputs [reviewed in (Reppert and Weaver, 2002)].

The molecular oscillator that generates the clock consists of two interconnected transcription/translation feedback loops (Shearman et al., 2000). The positive arm of the major feedback loop is driven by bHLH/PAS domain-containing transcription factors CLOCK and BMAL1 (Bunger et al., 2000; Gekakis et al., 1998). The CLOCK/BMAL1 heterodimer activates the transcription of core clock genes *Cryptochrome* (*Cry1* and *Cry2*), *Period* (*Per1* and *Per2*), and *Rev-Erb*α. PER and CRY proteins form multimeric complexes that translocate to the nucleus, where they interact with CLOCK/BMAL1 to downregulate transcription, generating the negative arm of the major feedback loop (Griffin et al., 1999; Kume et al., 1999; van der Horst et al., 1999; Vitaterna et al., 1999). In a separate feedback loop, *Bmal1* RNA levels oscillate due to a balance between a transcriptional activator, RORα, and inhibitor, REV-ERBα (Sato et al., 2004).

Posttranslational regulation of clock proteins determines their subcellular localization, intermolecular interactions, and stability, and establishes the 24-hour periodicity of the clock. CLOCK and BMAL1 are phosphorylated upon heterodimer formation, which correlates with nuclear entry and transactivation of clock gene transcription (Kondratov et al., 2003; Tamaru et al., 2003). While CKIε has been implicated in phosphorylation of BMAL1, the CLOCK

kinase is not known (Eide et al., 2002). Phosphorylation does not affect binding of the heterodimer to DNA; however, it may contribute to CLOCK/BMAL1 stability or interaction with other proteins, since the phosphorylated heterodimer is enriched in multimeric nuclear clock protein complexes (Lee et al., 2001a).

CKIε, and a related kinase CKIδ, also regulate the subcellular localization and stability of PER proteins. Phosphorylation of PER1 by CKIε is required for nuclear entry of the PER/CRY complex, providing a tunable mechanism to time re-entry of the repressor complex, which in turn is critical for setting the period of the molecular oscillator (Lee et al., 2004; Takano et al., 2004). The importance of PER phosphorylation is underscored by mutations in either CKI kinase or in phosphoacceptor sites of PER proteins that result in decreased PER phosphorylation and shortened circadian periods in mammals, including humans, where deviations from normal circadian periods manifest as sleep phase disorders (Lowrey et al., 2000; Toh et al., 2001; Xu et al., 2005). Hyperphosphorylation of PER by CKIε leads to polyubiquitination and degradation by the proteosomge (Akashi et al., 2002; Miyazaki et al., 2004). PER phosphorylation is deregulated in the absence of cryptochromes, leading to constitutive nuclear localization (PER1 and PER2) and degradation (PER2) of PER proteins, suggesting that cryptochromes modulate PER phosphorylation and stability *in vivo* (Shearman et al., 2000; Yagita et al., 2000).

The kinase activities of CKIε and CKIδ are tightly regulated by inhibitory autophosphorylation, requiring dephosphorylation of at least eight sites for activation (Gietzen and Virshup, 1999). Although serine/threonine phosphatases such as PP1, PP2A and PP2B are capable of activating CKIε/δ *in vitro*, specific physiological activators of CKIε have not been identified (Cegielska et al., 1998). Moreover, CKIε/δ do not appear to be constitutively active *in vivo*; the activity of CKIε/δ in certain pathways occurs only in a

stimulus-dependent manner and may rely on different phosphatases depending on the signaling pathway or cellular context (Liu et al., 2002; Swiatek et al., 2004).

The role of phosphatases in the clock is therefore likely to be complex, since they may be involved in stimulating CKIε/δ activity, and/or act in direct opposition to clock kinases by dephosphorylating clock proteins. In *Drosophila*, PP2A opposes the activity of DBT (the CKIε homolog) to stabilize PER (Sathyanarayanan et al., 2004), and a similar role has been proposed for an unidentified, calyculin A-sensitive mammalian phosphatase (Eide et al., 2005). However, the *Neurospora* clock is differentially regulated by two related phosphatases, *Neurospora* homologs of PP1 and PP2A. The phosphorylation state and stability of the clock protein FREQUENCY (FRQ) is distinct in strains containing mutants of these two phosphatases although they both dephosphorylate FRQ *in vitro*, indicating that they target different sites on FRQ or other clock proteins to yield dissimilar phenotypes (Yang et al., 2004). It is therefore conceivable that multiple phosphatases may differentially regulate the mammalian clock.

Our lab previously identified an interaction between CRYs and the protein phosphatase 5 (PP5), and demonstrated that CRYs inhibit PP5 activity *in vitro*; it was suggested that PP5 may play a role downstream of cryptochrome function in mammals (Zhao and Sancar, 1997). In this study, I found that PP5 dynamically regulates both the positive and negative arms of the major feedback loop of the clock through distinct interactions with clock proteins. In addition to cryptochromes, PP5 interacts with both CKIε and the CLOCK/BMAL1 heterodimer in mammalian cells, resulting in changes in clock protein stability and activity. PP5 activates CKIε through dephosphorylation of inhibitory autophosphorylated residues, and cryptochrome regulates CKIε activity as a non-competitive inhibitor of PP5. PP5 expression in the SCN and liver, like that of CKIε, is regulated independently of the clock, although both proteins undergo circadian-dependent

nuclear translocation concurrent with hyperphosphorylated PER. Expression of a dominant-negative PP5 reduces CKIε activity towards PER proteins and downregulation of PP5 by siRNA results in PER hypophosphorylation and disruption of circadian cycling *in vivo*. Finally, I show that PP5 inhibits CLOCK/BMAL1-mediated transactivation of clock gene transcription independently of cryptochromes, which correlates with dephosphorylation of the CLOCK protein. Collectively, these data provide the first functional evidence of a protein phosphatase in the mammalian circadian clock and reveal that PP5 and cryptochrome regulate the clock by dynamic interactions with clock proteins in both the positive and negative arms of the clock.

Experimental procedures

Plasmids

hCKIε in pRSETB vector with N-terminal His tag was a gift from D. Virshup (University of Utah). The coding region of hCKIε was amplified by PCR and cloned into pcDNA4B/myc-his for mammalian expression. Full-length rat PP5 in pET21a vector with N-terminal GST fusion was a gift from S. Rossie (Purdue University). Human PP5 was amplified from 293T RNA by RT-PCR and cloned into pcDNA4B/myc-His, with an additional C-terminal HA epitope tag. The H304N hPP5 mutant was generated from this vector using the QuikChange Kit (Stratagene). The hPP5 TPR domain (amino acids 1-179) was amplified by PCR and cloned into pcDNA4B/myc-His. The mammalian expression construct of hCry2 in pcDNA4/myc-His was previously described (Özgür and Sancar, 2003), and hCry1 was cloned in a similar manner (Hsu et al., 1996). mClock and mBmal1 in pBluescript vector were a gift from J. Takahashi (Northwestern University). The coding regions of mClock and mBmal1 were PCR-amplified and cloned into the pSG5 mammalian expression vector with N-terminal FLAG tags. hPer1 was amplified from 293T RNA by RT-PCR and cloned into pcDNA4/myc-His. hPer2 in the pCS vector with two N-terminal myc tags was a gift from L. Ptácek (University of California, San Francisco). Additional constructs eliminating the His tag in pcDNA4 CKIε, Cry2, and Per1 were generated by mutagenesis with the QuikChange Kit (Stratagene). The pBIND vector (*Renilla* luciferase control) for luciferase assays was used from the Mammalian Two-Hybrid kit (Promega), and pGL3 Basic vector fused to 2.0 kb of the 5' flanking region of *mPer1* (pGL3::*mPer1*) was a gift from C. Weitz (Harvard University). All constructs were verified by DNA sequencing.

Cell lines, cell culture, transfection, and in vivo *phosphorylation*

HEK293T and NIH/3T3 cell lines were purchased from ATCC, the RGC-5 cell line was a gift from N. Agarwal (UNT Health Science Center), and the BJ fibroblast cell lines (stably transfected with pSuper-Retro empty vector, pSR, or with pSR containing a shRNA

against PP5, pSR-PP5 (Zhang et al., 2005)) were a gift from X.-F. Wang (Duke University). 293T, NIH/3T3 and RGC-5 cells were cultured in DMEM with 10% FBS, and BJ cells were cultured in DMEM with 20% FBS, under standard culture conditions. 293T cells were transfected with plasmid DNA using Lipofectamine 2000 (Invitrogen) or FuGENE 6 (Roche) reagent according to manufacturer's protocol. For *in vivo* measurement of PER1 phosphorylation by CKIε, 4 x 10^5 293T cells were transfected with PER1, and/or CKIε and PP5 H304N-expressing plasmids, and treated 48 hrs later with 100 μg/ml cycloheximide. PER phosphorylation was analyzed in equal volumes of total protein extract by western blotting (n=3).

Immunoprecipitation, antibodies and western blotting

For co-transfection/immunoprecipitation experiments, 4 x 10^5 293T cells were seeded into 6 well plates 24 hrs prior to transfection. Cells were transfected with 2-4 μg plasmid DNA (empty vector was used to normalize DNA concentrations) and harvested 48 hrs later, by lysis in NP-40 lysis buffer (50 mM Tris pH 7.5, 150 mM NaCl, 1 mM EDTA, 0.5% NP-40) with a protease inhibitor cocktail (Roche), and clarification at 4°C by centrifugation for 10 min at 14,000 rpm. For precipitation of endogenous proteins, 150 mm dishes of RGC-5 cells at 80% confluence were harvested similarly. Soluble extracts were incubated with immunoaffinity resins overnight at 4°C as indicated: HA affinity matrix (Roche), microcystin sepharose (Upstate), protein A agarose (Invitrogen), FLAG M2 agarose (Sigma), or His affinity agarose (Santa Cruz). Resin was washed three times with NP-40 wash buffer (50 mM Tris pH 7.5, 150 mM NaCl, 1 mM EDTA, 0.05% NP-40) and proteins were eluted with reducing SDS-PAGE sample buffer. For western blot analysis, proteins were separated by SDS-PAGE, transferred to Hybond ECL (Amersham) nitrocellulose membrane and blocked with TBST (50 mM Tris pH 7.5, 135 mM NaCl, 0.1% Tween-20) plus 5% nonfat milk.

Blots were incubated with primary antibodies as follows: mouse monoclonal FLAG (M2) (Sigma), myc (9E10) (Santa Cruz), His (Abgent), PP5 (Transduction Labs); rabbit polyclonal HA (H-15), PP1 (FL-18), CKIε (H-60) (all from Santa Cruz), CRY2B (Thompson et al., 2003); guinea pig polyclonal PER1, PER2, BMAL1 (gift from C. Lee, FSU); or rat monoclonal CRY1 (raised against a rodent-specific C-terminal peptide of CRY1, NSNGNGGLMGYAPGENVPSC and affinity purified against recombinant protein). Proteins were detected using the appropriate HRP-conjugated secondary antibody and ECL reagent (Amersham). To analyze multiple proteins from a single blot, membranes were stripped between westerns by incubating for 30 min at 55°C in 60 mM Tris pH 6.8, 2% SDS and 100 mM β-mercaptoethanol, washed four times in TBST and reblocked prior to incubation with new primary antibody. Western blots were scanned and quantified by densitometry using ImageQuant 5.0 software (Molecular Dynamics). All immunoprecipitation data are representative of at least 3 independent experiments.

Expression and purification of recombinant proteins

Purification of CKIε from *E. coli* was performed as described (Gietzen and Virshup, 1999), using pRSETB-hCKIε to generate full-length hCKIε with an N-terminal His tag. Purification of PP5 from *E. coli* was performed as described (Sinclair et al., 1999), using pET21a-GST-rPP5 to generate full-length rPP5 (94% identical to hPP5) after cleavage of GST by thrombin, leaving four additional residues at the N-terminus, GSGS. Purification of His-hCRY2 from baculovirus-infected Sf21 cells was performed as described (Özgür and Sancar, 2003).

In vitro *kinase and phosphatase assays*

Autophosphorylation reactions were performed in kinase buffer (25 mM Tris pH 7.5, 10 mM $MgCl_2$, 0.1 mM ATP, and 1 μCi/reaction [γ^{32}P]ATP (3000 Ci/mmol, NEN Research Products)) for 30 min at 37°C. To monitor dephosphorylation of CKIε by PP5,

autophosphorylated CKIε (CKIε-P, 500 nM) was added to 100 nM PP5 in kinase buffer (all reactions with PP5 include 10 μM palmitoyl-CoA, 2 mM $MnCl_2$, and 1 mM iodoacetamide). Aliquots were removed at indicated timepoints and quenched in 3X SDS-PAGE sample buffer, resolved by SDS-PAGE, and silver stained to ensure equal protein loading. Signals were obtained on Molecular Dynamics Phosphorimager screens and quantified using ImageQuant 5.0 software (Molecular Dynamics). Stimulation of CKIε activity by PP5 was measured by adding CKIε-P to either PP5 or PP5 storage buffer (20 mM Tris pH 7.6, 1 mM EGTA, 4 mM $MnCl_2$, 0.1% β-mercaptoethanol, 50% glycerol) in the presence of casein (Sigma). To assess the concentration dependence of PP5 inhibition by CRY2, PP5 was preincubated with indicated concentrations of CRY2 for 20 min on ice prior to the reaction with CKIε-P. Kinetic analyses of CRY2 inhibition were performed by varying the CKIε-P concentration from 120 - 1200 nM with 100 nM PP5, in the presence or absence of 200 nM CRY2, for 5 min at 37°C. Timecourse experiments showed the phosphatase assay was linear for up to 15 min (data not shown). The concentration of dephosphorylated CKIε after the reaction was determined by normalizing ^{32}P-signal remaining after phosphatase treatment to the ^{32}P-signal intensity of CKIε-P prior to treatment. Untransformed data were analyzed by nonlinear least squares regression using the kinetic equation [$y=(V_{max}*X)/(K_m+X)$] to calculate V_{max} and K_m, and plotted on a double reciprocal Lineweaver-Burk plot (GraphPad Prism 4.0).

Mouse liver extract preparation

Mice from the C3H/HeJ genetic background (*rd/rd*; Jackson Laboratories) were used to generate wild-type and CRY knockout mice for this study, due to poor mating of *Cry1*$^{-/-}$ *Cry2*$^{-/-}$ mice in the C57BL/6J background, and were genotyped as previously described (Selby et al., 2000). The mean age of *rd/rdCry1*$^{-/-}$*Cry2*$^{-/-}$ and wild-type littermate controls (*rd/rdCry1*$^{+/+}$*Cry2*$^{+/+}$) used was 13 ± 0.8 months. Mice housed under a 12:12 hour light/dark

schedule were sacrificed at indicated Zeitgeber times (n=3; ZT0=lights on). Livers were excised, minced into 2 mm^3 pieces and frozen on powdered dry ice. Tissue was ground in NP-40 lysis buffer with protease inhibitors using 10 strokes of a dounce homogenizer. Extracts were clarified by centrifugation for 20 min at 14,000 rpm at 4°C, and protein concentration was measured by Bradford assay (BioRad) using known standards. Western blots are representative of results from three independent sets of mice sacrificed at the same ZT.

In situ *hybridization*

Mice (C3H/HeJ) housed under 12:12 hour light/dark schedule were sacrificed at ZT8 or ZT20 and whole brains were frozen on powdered dry ice. The antisense *PP5* probe was generated by *in vitro* transcription with T7 RNA polymerase (Promega) in the presence of ^{35}S-UTP from a pBluescript SK+ vector containing nucleotides 846-1481 of *mPP5* and linearized with BamHI. The sense *PP5* probe was transcribed from an EcoRI-linearized plasmid with T3 RNA polymerase (Promega). The *Per2* probe was generated and *in situ* hybridizations were performed as described (Thompson et al., 2001). Briefly, coronal sections (18 μm thick) were fixed with formalin, treated with 10 μg/ml proteinase K (BMB), and acetylated with triethanolamine and acetic acid anhydride. After dehydration with ethanol, brain sections were hybridized overnight in a humidified chamber at 55 ˚C with 6 x 10^5 cpm of riboprobe in 50% formamide/20 mM Tris-HCl pH 8/5 mM EDTA/0.3 M NaCl/10 mM phosphate buffer/1x Denhardt's solution/10% dextransulfate/0.2% sarcosyl/0.2 mg/ml salmon sperm DNA. A high stringency wash was carried out at 65 ˚C for 45 min with 50% formamide/4x SSC/7.7 mg/ml DTT, and the sections were treated with 1 μg/ml RNase A for 30 min before washing again in high stringency wash buffer. The slides were dehydrated with ethanol and subjected to autoradiography. Images were obtained using a Leica M420 macroscope density-calibrated with a Kodak control scale T-14 and an Optronics DE1750 camera. Quantitation was performed with Scion Image 1.62a (Scion Corp. version of NIH

Image). *PP5* expression at ZT8 and ZT20 (n=3 at each ZT) was analyzed by one sample t-test (p=0.5).

Serum-induced circadian cycling and subcellular fractionation of fibroblast cell lines

5 x 10^5 NIH/3T3 or BJ (pSR or pSR-PP5 stable lines) cells were seeded in 6 cm dishes and grown to confluence (~4 days). Circadian synchronization was achieved by serum shock: cells were incubated with DMEM containing 50% horse serum for 2 hrs (time=0 at initiation of serum shock), and maintained in DMEM with 0.5% FBS for the remainder of the timecourse. Circadian-asynchronous controls were maintained in the original growth medium for the course of the experiment. Cells were harvested at indicated times in NP-40 lysis buffer plus protease inhibitors and protein concentrations were determined by Bradford assay. 50-100 μg protein extract was resolved on either 6.5% or a split 5/10% SDS-PAGE in order to visualize the full range of PER phosphorylation.

For subcellular fractionation of extracts, cells were trypsinized 3 min at 25°C, washed once in PBS, divided into two equal volumes, and cells were pelleted by centrifugation for 3 min at 4,000 rpm at 25°C. One pellet was resuspended in NP-40 lysis buffer for total protein, and the other was lysed in an equal volume of Buffer A (10 mM HEPES pH 7.9, 10 mM KCl, 1.5 mM $MgCl_2$, 0.34 M sucrose, 1 mM DTT, 10% glycerol, 0.1% Triton X-100) for 5 min on ice. Nuclei were pelleted at 3,500 rpm for 4 min at 4°C; supernatant (cytosol) was removed, nuclei were washed once in Buffer A lacking Triton X-100, and resuspended in an equal volume of NP-40 lysis buffer. Equal cellular volumes were resolved by SDS-PAGE and clock protein expression analyzed by western blotting. Purity of the cytosolic and nuclear extracts was assessed by proper localization of known cytosolic and nuclear proteins (data not shown).

Luciferase reporter gene assay

2 x 10^5 293T cells were seeded into 12 well plates 24 hrs prior to transfection. Duplicate wells were transfected with 1 μg DNA (250 ng each Clock and Bmal1, 100 ng pBIND (*Renilla* luciferase, Promega), 10 ng pGL3::*mPer1*, and empty vector or indicated constructs to 1 μg total DNA). 48 hrs later, cells were harvested in 200 μl 1X passive lysis buffer (provided in Dual Luciferase Assay Kit from Promega) by rocking at 25°C for 15 min. Luciferase measurements were obtained according to manufacturer's protocol using a Molecular Devices L_{max} 1.1 luminometer. Firefly luciferase activity driven by the *mPer1* promoter was normalized to *Renilla* luciferase activity as a transfection control. Equal volumes of extract were analyzed for protein content by western.

Results

PP5 is expressed in the SCN and liver independently of the clock

Our lab previously identified an interaction between PP5 and the core circadian clock proteins CRY1 and CRY2 by yeast two-hybrid and direct pull-down experiments. Cryptochromes are highly expressed in the master circadian clock located in the SCN (Miyamoto and Sancar, 1998). To determine if PP5 co-localizes with cryptochromes in the suprachiasmatic nuclei, *PP5* mRNA expression was analyzed by *in situ* hybridization. Although previous reports have suggested that *PP5* expression is ubiquitous (Bahl et al., 2001; Xu et al., 1996), we demonstrated that *PP5* mRNA is enriched in the SCN with respect to other subcortical regions of the brain (Figure 4.1A). However, unlike clock genes under the circadian control of CLOCK/BMAL1, such as *Per2*, *PP5* mRNA did not oscillate between day (ZT8) and night (ZT20) (Figure 4.1B-C).

Since PP5 abundance could oscillate posttranscriptionally, I analyzed clock protein expression in mouse liver extracts harvested over a 24-hour period. While the expression level and phosphorylation status of core clock proteins PER1, BMAL1 and CRY1 oscillated with circadian time, expression of both PP5 and CKIε was constant (Figure 4.1D). Moreover, their protein levels were unaffected in the absence of both cryptochromes, which abolishes the molecular oscillator and increases expression of genes controlled by CLOCK/BMAL1 (Figure 4.1D, last two lanes) (Vitaterna et al., 1999). These data demonstrate that PP5 is expressed independently of the molecular clock.

Subcellular localization of PP5 is regulated by the clock

Although CKIε protein levels are static, CKIε undergoes a circadian-dependent nuclear translocation as part of a multimeric clock protein complex (Lee et al., 2001b). To determine if PP5 subcellular localization parallels that of CKIε, I utilized a cell-based assay to study circadian cycling. Individual cultured fibroblast cells possess intrinsic circadian rhythms with periods of approximately 24 hours; however, cells in culture are asynchronous

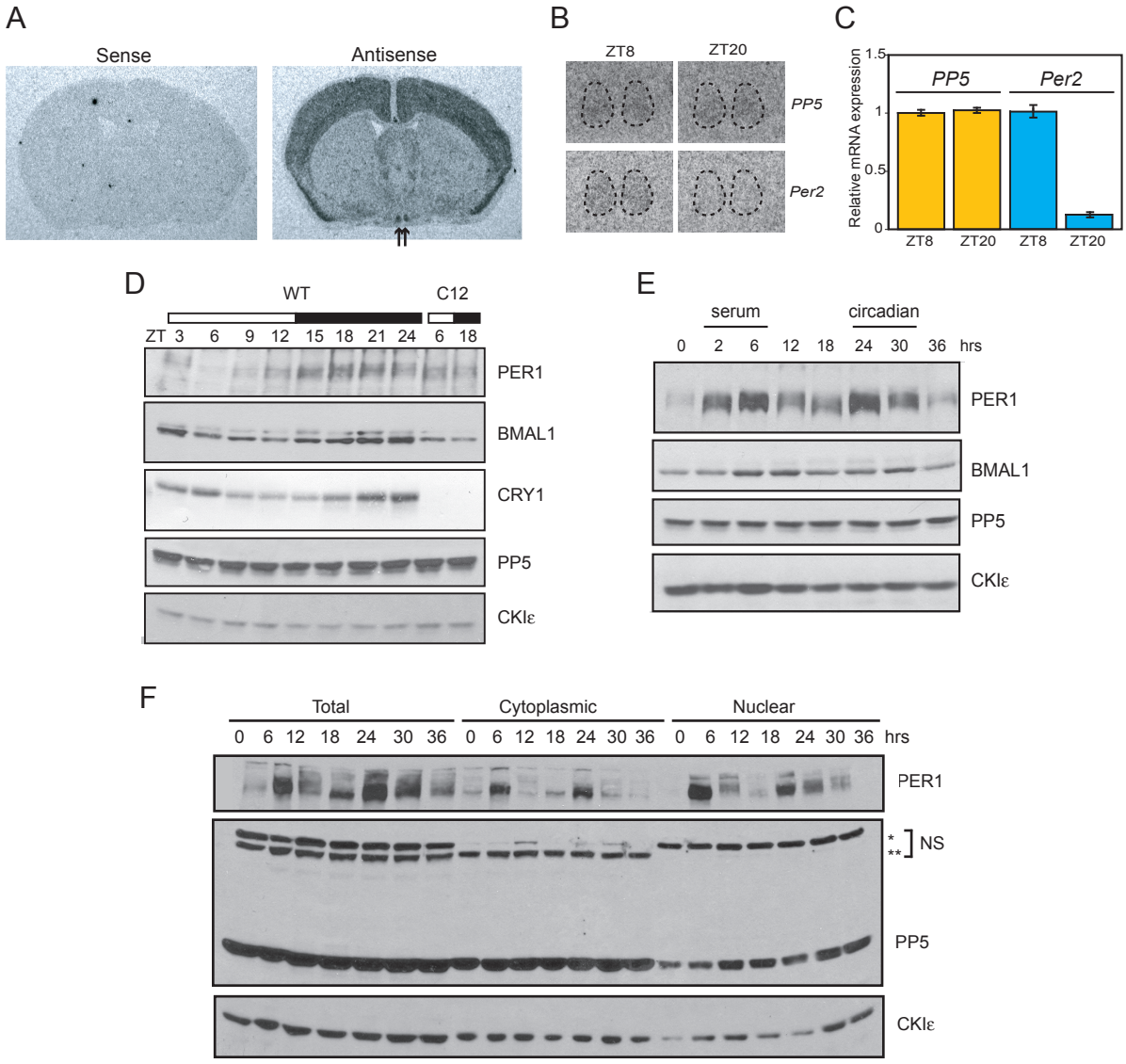

Figure 4.1 PP5 expression in the mouse

A. *PP5* mRNA is expressed in the SCN. *In situ* hybridization was done on coronal sections of mouse brain using sense or antisense ^{35}S-labeled riboprobes for *PP5*. Double arrows indicate SCN. **B.** Magnification of SCN. *PP5* and *Per2* mRNA in the SCN (dotted lines) at ZT8 and ZT20 (ZT0 = lights on at 7 a.m.). Relative *Per2* mRNA levels at ZT8 and ZT20 is representative of clock gene expression. **C.** Quantiative analysis of *PP5* and *Per2* mRNA in the SCN (n=3, ± SEM). **D.** Protein expression over circadian time in liver. Total protein extract from wild-type (WT) and *Cry1*$^{-/-}$*Cry2*$^{-/-}$ (C12) mice sacrificed at ZT times (light schedule indicated above ZT times with white or black bars) was analyzed by western blot. **E.** Clock protein expression in serum-synchronized (SS) NIH/3T3 cells. Hours indicate time after initiation of serum shock. **F.** Subcellular localization of proteins in SS-NIH/3T3 cells. Equal cellular volumes of total, cytoplasmic, and nuclear extracts were analyzed by western blot. NS indicates *nuclear or **cytoplasmic non-specific bands in PP5 western.

due to the lack of a synchronizing stimulus and small differences in periods between individual cells (Nagoshi et al., 2004). Fibroblast molecular clocks can be synchronized by serum shock, which induces robust PER expression through immediate-early gene pathways, and effectively synchronizes the phase of all cells for 3-4 circadian oscillations in culture (Balsalobre et al., 1998). I first synchronized NIH/3T3 cells with a serum shock and analyzed clock protein expression in total cellular extracts (Figure 4.1E). Serum shock induced robust, clock-independent expression of PER1 by 6 hours, with a second peak of PER1 protein at 24 hours as the result of CLOCK/BMAL1-mediated transactivation (Nagoshi et al., 2004). Importantly, expression of PP5 and CKIε was not affected by circadian cycling in this cell-based system.

I then analyzed the circadian regulation of clock protein subcellular distribution by circadian-synchronizing NIH/3T3 cells and fractionating cells for cytoplasmic and nuclear extracts. Synchronization of NIH/3T3 fibroblast clocks by serum shock recapitulated the *in vivo* schedule of PER1 posttranslational modification and a subsequent change in subcellular localization, where phosphorylation is first required for nuclear translocation and retention, and then leads to degradation (Figure 4.1F, (Lee et al., 2001b)). Moreover, serum shock resulted in the appearance of hyperphosphorylated PER1 in nuclear extracts on a circadian timescale (30-36 hours after serum induction), while no nuclear PER1 was detected in circadian-asynchronous controls (data not shown). Significantly, synchronization of fibroblast clocks resulted in an increase in nuclear PP5 and CKIε concomitant with hyperphosphorylated PER1, suggesting that these proteins are part of a multimeric complex. Two non-specific bands from the PP5 antibody (Figure 4.1F, NS) demonstrate integrity of the fractionation since one protein is entirely cytoplasmic and the other is nuclear. Significantly, nuclear extracts are not contaminated by cytoplasm, in which both PP5 and CKIε are predominantly expressed. The non-specific nuclear band also serves as a loading control, demonstrating that the two-fold change in PP5 nuclear

abundance is specific (data from 4 independent experiments were analyzed for circadian oscillation of nuclear PP5 by ANOVA: $p<0.001$, F score 13.94).

Interaction of PP5 with core circadian clock proteins

To investigate the potential role of PP5 in the clock and the mechanism by which its localization is controlled by the clock, I analyzed the interaction of PP5 with each core mammalian clock protein in co-immunoprecipitation assays. Initially, interacting proteins were identified in extracts from 293T cells transfected with HA-PP5 or empty vector and the individual clock proteins, following immunoprecipitation with anti-HA resin (Figure 4.2A). While none of the clock proteins were precipitated in the absence of PP5 (data not shown), both CRY1 and CRY2 were precipitated by PP5. In addition, I detected an interaction between PP5 and the clock kinase CKIε. No interaction was detected between PP5 and either PER1, PER2 or CLOCK and BMAL1 monomers under these conditions.

To verify the interaction of PP5 with clock proteins *in vivo*, endogenous PP5 was precipitated from RGC-5 cell lysate using microcystin agarose, and the presence of endogenous CRY or CKIε was examined by western blotting. Microcystin is a microalgal toxin that binds with picomolar affinity to the active site of the PP5 catalytic domain and has been used to purify PP5 (Meek et al., 1999). Endogenous CRY1 and CRY2 coprecipitated with endogenous PP5 (Figure 4.2B); however, I was not able to detect an interaction between microcystin-precipitated PP5 and CKIε (Figure 4.2B). Since microcystin binding to the active site of PP5 precludes interaction between endogenous PP5 and CKIε, this suggests that PP5 and CKIε may interact through the catalytic domain of PP5.

Regulation of PP5:clock protein interactions by PP5 phosphatase activity

PP5 contains three tetratricopeptide repeat (TPR) domains in its N-terminus, which act as an autoregulatory module to inhibit phosphatase activity (Figure 4.3A) (Sinclair et al., 1999). TPR domains facilitate protein-protein interactions, and in PP5, they mediate

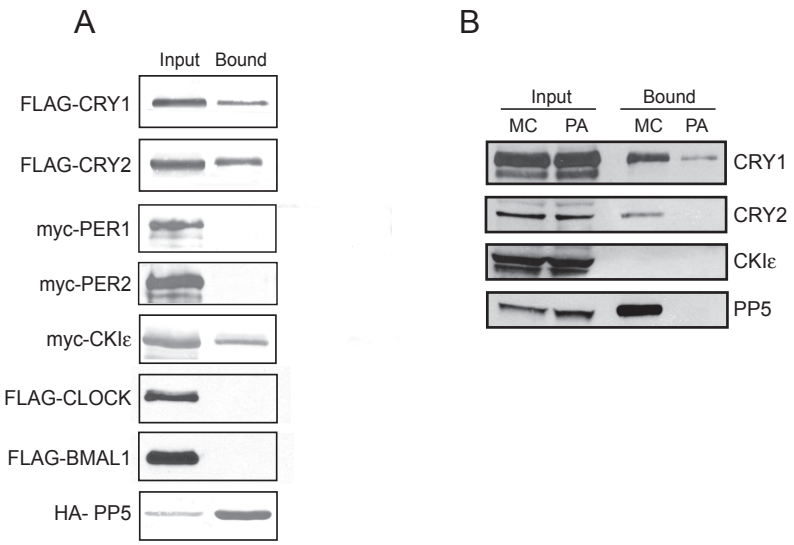

Figure 4.2 PP5 interacts with clock proteins
A. Interaction of PP5 with core clock proteins. 293T cells were co-transfected with HA-PP5 or empty vector (data not shown) and individual FLAG- or myc-tagged clock proteins as indicated. Extracts were immunoprecipitated with anti-HA resin and analyzed by western blotting with anti-FLAG or anti-myc antibodies. **B.** Interaction of PP5 with endogenous proteins. Endogenous PP5 was precipitated from RGC-5 cell extract with microcystin agarose (MC). Protein A (PA) agarose was used as a negative control. The presence of endogenous PP5, CRY1, CRY2 and CKIε was tested by western blotting with antibodies to native proteins.

interaction with modulators of PP5 activity, such as HSP90 and $G\alpha_{12/13}$ (Ramsey and Chinkers, 2002; Yamaguchi et al., 2002). The previous yeast two-hybrid study demonstrated that CRY and PP5 interact through the TPR domain. I confirmed that CRY interacts with the PP5 TPR domain using co-transfection/co-immunoprecipitation experiments. As shown in Figure 4.3B, CRY2, but not CKIε, was precipitated by the PP5 TPR domain.

Since microcystin binding at the active site of PP5 occludes interaction with CKIε, this implies that CKIε requires the PP5 active site for interaction and suggests that it may be a substrate of PP5. Therefore, disruption of PP5 catalytic activity might stabilize the PP5:CKIε interaction. The PP5 (H304N) mutant is catalytically inactive but maintains normal cellular localization (Borthwick et al., 2001). I tested for quantitative differences in protein-protein interactions by reciprocal coimmunoprecipitation of wild type (WT) or H304N mutant PP5 (MT) with CRY2 or CKIε from 293T cells (Figure 4.3C-D). Disruption of PP5 phosphatase activity stabilized the PP5:CKIε interaction by more than 2-fold without having an effect on the PP5:CRY2 interaction (Figure 4.3E). In the case that loss of phosphatase activity might also stabilize a previously undetected PP5:PER complex, I analyzed the interaction of PP5 with both PER proteins and observed no interaction, although both PER proteins could interact with CKIε, indicating that they were properly folded (data not shown).

The interaction of CRY and CKIε with distinct domains of PP5 suggests that both proteins might be able to interact with PP5 concurrently in a ternary complex. CRY does not interact with CKIε directly, although it exists with CKIε in a ternary complex in the presence of PER proteins (Akashi et al., 2002). I tested for formation of a CRY:PP5:CKIε ternary complex by immunoprecipitating FLAG-CRY2 with CKIε in the presence and absence of PP5 (Figure 4.3F). Significantly, CKIε was detected in CRY2 immunoprecipitates only in the

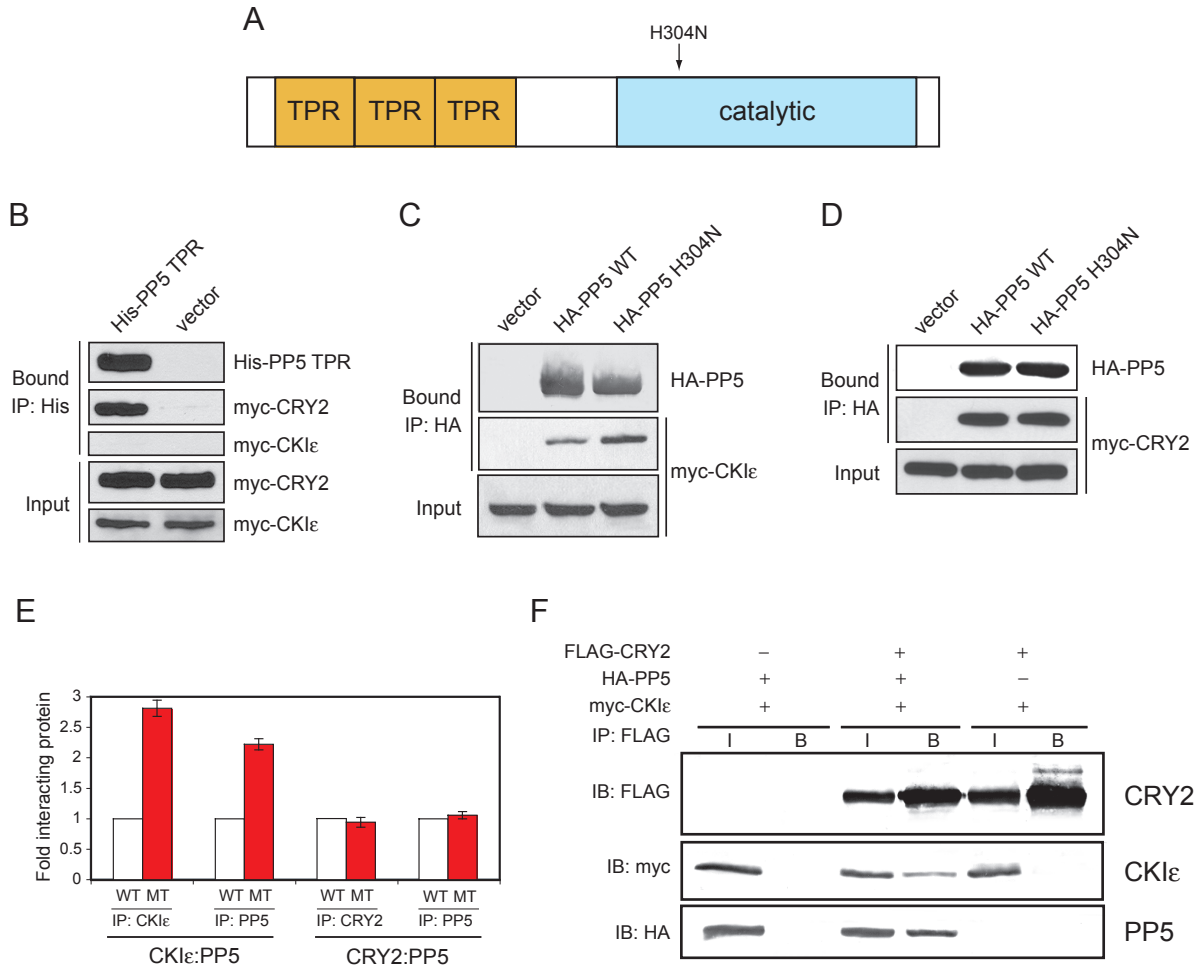

Figure 4.3 Effect of PP5 catalytic activity on interaction with CRY2 and CKIε
A. Schematic of PP5 protein domains. PP5 N-terminal autoregulatory domain has 3 tetratricopeptide repeats (TPR) and a catalytic serine/threonine phosphatase domain that is 44-46% conserved with PP1/PP2A. **B.** Interaction of TPR domains with CRY2. 293T cells were transfected with His-PP5-TPR or empty vector, and CRY2 or CKIε. PP5 was precipitated with anti-His agarose; TPR domains interact with CRY2 but not CKIε. **C.** Effect of PP5 catalytic activity on interaction with CKIε. Inactivation of PP5 catalytic domain stabilizes the CKIε:PP5 complex. **D.** Effect of PP5 catalytic activity on interaction with CRY2. Inactivation of PP5 catalytic domain has no effect on the CRY2:PP5 interaction. **E.** Quantitative analysis of reciprocal co-immunoprecipitation of CKIε or CRY2 with wild-type or H304N PP5. The amount of protein co-precipitated with PP5 H304N (red) was quantified by densitometry and normalized to the amount of protein interacting with WT PP5 (white). Average of data from 3 independent experiments (± SEM). **F.** PP5 forms a ternary complex with CRY2 and CKIε. Interaction of CRY2 and CKIε with distinct regions of PP5 allows formation of a stable ternary complex.

presence of PP5, indicating that both CRY2 and CKIε interact with PP5 at the same time to form a stable complex.

Activation of the CKIε kinase by PP5

The inability of CKIε to interact with microcystin-bound PP5 and stabilization of the CKIε:PP5 complex by inactivation of PP5 catalytic activity both suggest that CKIε may be a substrate of PP5. To determine if PP5 can dephosphorylate CKIε, I purified full-length, recombinant hCKIε from *E.coli* and incubated it with γ^{32}P-ATP in the presence or absence of PP5 (Figure 4.4A). PP5 significantly reduced CKIε autophosphorylation in this *in vitro* assay. To determine if dephosphorylation of CKIε by PP5 stimulates its kinase activity, I assayed the ability of autophosphorylated CKIε (CKIε-P) to phosphorylate casein in the presence or absence of PP5. As shown in Figure 4.4B and C, dephosphorylation of CKIε by PP5 resulted in a 2-fold increase in ^{32}P incorporation into casein, demonstrating that PP5 can activate CKIε kinase activity *in vitro*.

Cryptochrome inhibits PP5 activation of the CKIε kinase

Because our previous data indicated that cryptochromes inhibit PP5 phosphatase activity, I analyzed whether CRY2 could inhibit PP5 dephosphorylation of CKIε *in vitro*. I assayed the ability of PP5 alone, or PP5 that had been preincubated with either purified, active CRY2 or inactivated CRY, to dephosphorylate CKIε-P. The effect of CRY2 on PP5 activity was quantified by monitoring the level of autophosphorylated CKIε (Figure 4.5A). Under these conditions, CRY2 inhibited the ability PP5 of dephosphorylate CKIε by up to 5-fold (Figure 4.5B). In order to assess the concentration dependence of CRY2 inhibition, I preincubated PP5 with increasing concentrations of active CRY2 before addition of CKIε-P and monitored the degree of CKIε dephosphorylation that occurred in 15 minutes. While CRY2 alone had no effect on CKIε phosphorylation (data not shown), CRY2 inhibited PP5-mediated dephosphorylation of CKIε in a concentration-dependent manner with an IC_{50} of

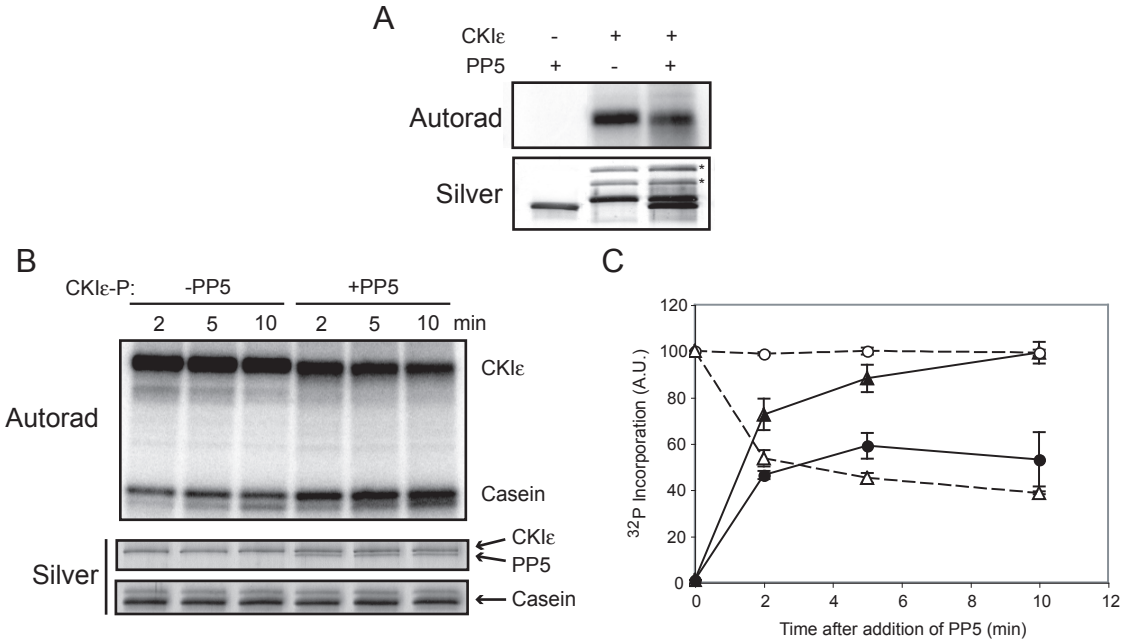

Figure 4.4 PP5 stimulates CKIε activity *in vitro*
A. PP5 dephosphorylates CKIε *in vitro*. CKIε was autophosphorylated with ^{32}P-ATP in the presence or absence of PP5. Reactions were resolved by SDS-PAGE, silver stained, and the phosphorylation status of CKIε was monitored by autoradiography. **B.** PP5 stimulates CKIε kinase activity *in vitro*. Autophosphorylated CKIε (CKIε–P) was incubated with casein in the absence or presence of PP5. Aliquots were taken at indicated times, resolved by SDS-PAGE, and monitored by autoradiography. **C.** Quantitative analysis of CKIε stimulation by PP5. ^{32}P-ATP incorporation in casein and CKIε was quantified from 3 independent experiments and normalized to peak phosphorylation (±SEM). Key: ^{32}P-casein, solid lines, ^{32}P-CKIε, dashed lines; - PP5 (circles), + PP5 (triangles). Addition of PP5 causes significant differences at each timepoint by paired t-test ($p<0.05$).

200 nM (Figure 4.5C-D). I then performed kinetic analyses using CKIε-P as a substrate and monitored dephosphorylation by PP5 in the presence or absence of 200 nM CRY2. Using a range of substrate concentrations (120-1200 nM), I obtained estimates of the Michaelis constant (K_m) and the maximal enzyme velocity (V_{max}) for PP5 alone or in the presence of CRY2; these data are graphically represented on a Lineweaver-Burk plot in Figure 4.5E. Including CRY2 in the reaction resulted in a 2.3-fold decrease in the V_{max} of PP5 without an apparent change in K_m, indicating that CRY2 is a non-competitive inhibitor of PP5. This is consistent with the finding that cryptochrome interacts with the N-terminal TPR domains of PP5 and not its C-terminal catalytic domain.

PP5 regulation of CKIε controls PER phosphorylation and clock cycling in vivo

Given that CKIε is a critical regulator of PER protein, I sought to determine if PP5 could affect PER phosphorylation by regulating CKIε kinase activity *in vivo*. I expressed PER1 in the presence or absence of CKIε and the H304N mutant of PP5 in 293T cells, and monitored the phosphorylation state of PER1 after cycloheximide treatment by western blotting. With the >2-fold increased stability of the CKIε:PP5 (H304N) complex over CKIε:wild-type PP5 (Figure 4.3E), the PP5 mutant should give rise to a dominant negative phenotype by inhibiting endogenous PP5 from activating CKIε. When expressed alone, PER1 exhibited a range of phosphorylated species due to phosphorylation by endogenous kinases (Figure 4.6A). Co-expression with CKIε resulted in hyperphosphorylation of PER1, as demonstrated by a significantly decreased electrophoretic mobility. Significantly, co-expression of CKIε with mutant PP5 resulted in decreased levels of hyperphosphorylated PER1, which were sustained for at least one hour after cycloheximide treatment. These data indicate that PP5 regulates CKIε activity and posttranslational modification of PER1 *in vivo*. It must be noted that overexpression of wild-type PP5 in 293T cells does result in dephosphorylation of PER1 and PER2; however, this is likely not physiologically relevant

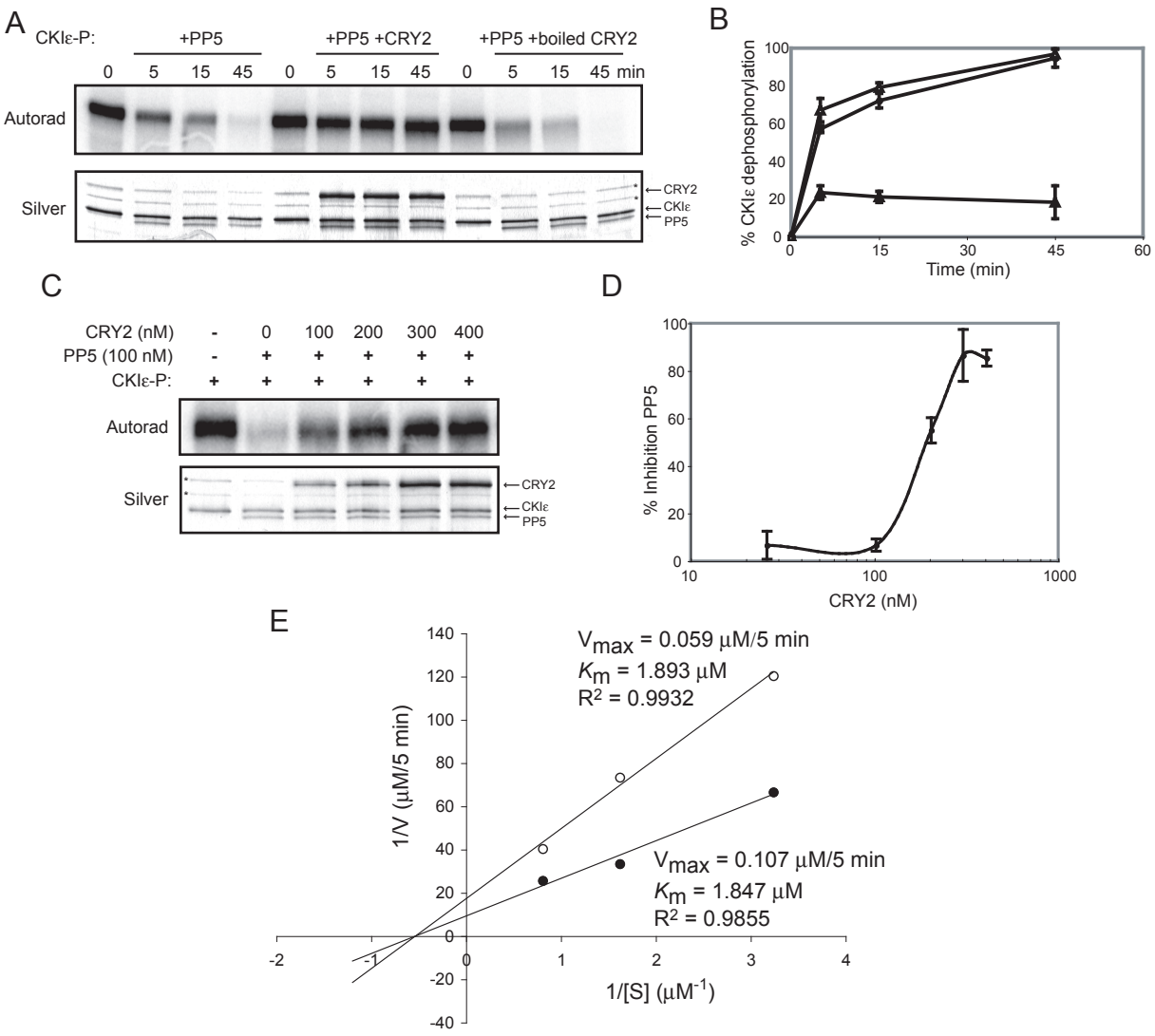

Figure 4.5 CRY2 inhibits PP5 and regulates CKIε phosphorylation *in vitro*.
A. CRY2 inhibits PP5 activity. PP5 was preincubated with active CRY2 or inactivated, boiled CRY2 as a buffer control and dephosphorylation reactions were initiated with CKIε-P. Aliquots were removed at indicated times and monitored by silver stain of SDS-PAGE and autoradiography. **B.** Quantitative analysis of CRY2 inhibition of PP5. Data from 4 independent experiments are plotted (± SEM). Key: no CRY2, circles; with active CRY2, filled triangles; with boiled CRY2, open triangles. **C.** Concentration dependence of CRY inhibition. PP5 was incubated with increasing concentrations of CRY2 before addition of CKIε-P; reactions were stopped at 15 min. **D.** Quantitative analysis of concentration dependence of CRY2 inhibition of PP5. Data from 3 independent experiments are plotted (± SEM). **E.** CRY2 is a non-competitive inhibitor of PP5. Kinetic analyses of CRY2 inhibition were performed by varying concentrations CKIε-P (120-1200 nM) and monitoring dephosphorylation by PP5 after 5 min in the presence or absence of CRY2. Apparent K_m and V_{max} values for PP5 (± CRY2) were determined by nonlinear least squares regression of the untransformed data, which are plotted on a double-reciprocal Lineweaver-Burk plot. Each point represents the mean value from 3 independent experiments. Key: without CRY2, filled circles; with CRY2, open circles.

since a moderate reduction in PP5 expression relative to PER eliminates this activity, and the H304N mutation does not stabilize an interaction between PP5 and either PER1 or PER2 (data not shown**)**.

To determine if PP5 regulation of CKIε activity affects circadian cycling *in vivo*, I examined the effect of PP5 downregulation on serum-induced circadian cycling in human diploid BJ fibroblasts. Two BJ cell lines were generated by stable transfection, either with an empty pSR retroviral vector or with pSR containing an shRNA sequence against hPP5 that resulted in >90% knockdown of endogenous PP5 expression without affecting expression of a related phosphatase (Figure 4.6B) (Zhang et al., 2005). I induced circadian cycling by serum shock in these two cell lines and analyzed clock protein expression at 6-hour intervals by western blotting. As shown in Figure 4.6B, serum shock induced comparable expression of PER proteins by 6 hours in both the wild type and PP5 knockdown BJ cell lines. However, induction of PER proteins in the WT cell line was followed by pronounced hyperphosphorylation, degradation, and robust resynthesis of PER on a circadian timescale, while downregulation of PP5 resulted in a dramatic reduction of fully phosphorylated PER1 and PER2, and a significant decrease in clock-dependent induction of PER proteins at 24-30 hours. As CKIε is the predominant PER kinase *in vivo* (Miyazaki et al., 2004), these data demonstrate that downregulation of PP5 severely compromises CKIε activity, resulting in hypophosphorylated PER and a disruption of the molecular clock.

I then monitored cycling of the BJ cell lines for 54 hours after serum shock, which should be sufficient to observe two cycles of clock-induced protein expression. BJ cells with normal levels of PP5 cycle efficiently in culture with a period of approximately 24 hours, and cells with downregulated PP5 have greatly compromised circadian oscillations (Figure 4.6C). The period of the molecular oscillator was determined in WT and PP5-deficient cells by quantifying expression of PER1 and PER2 after serum shock (Figure 4.6D-E).

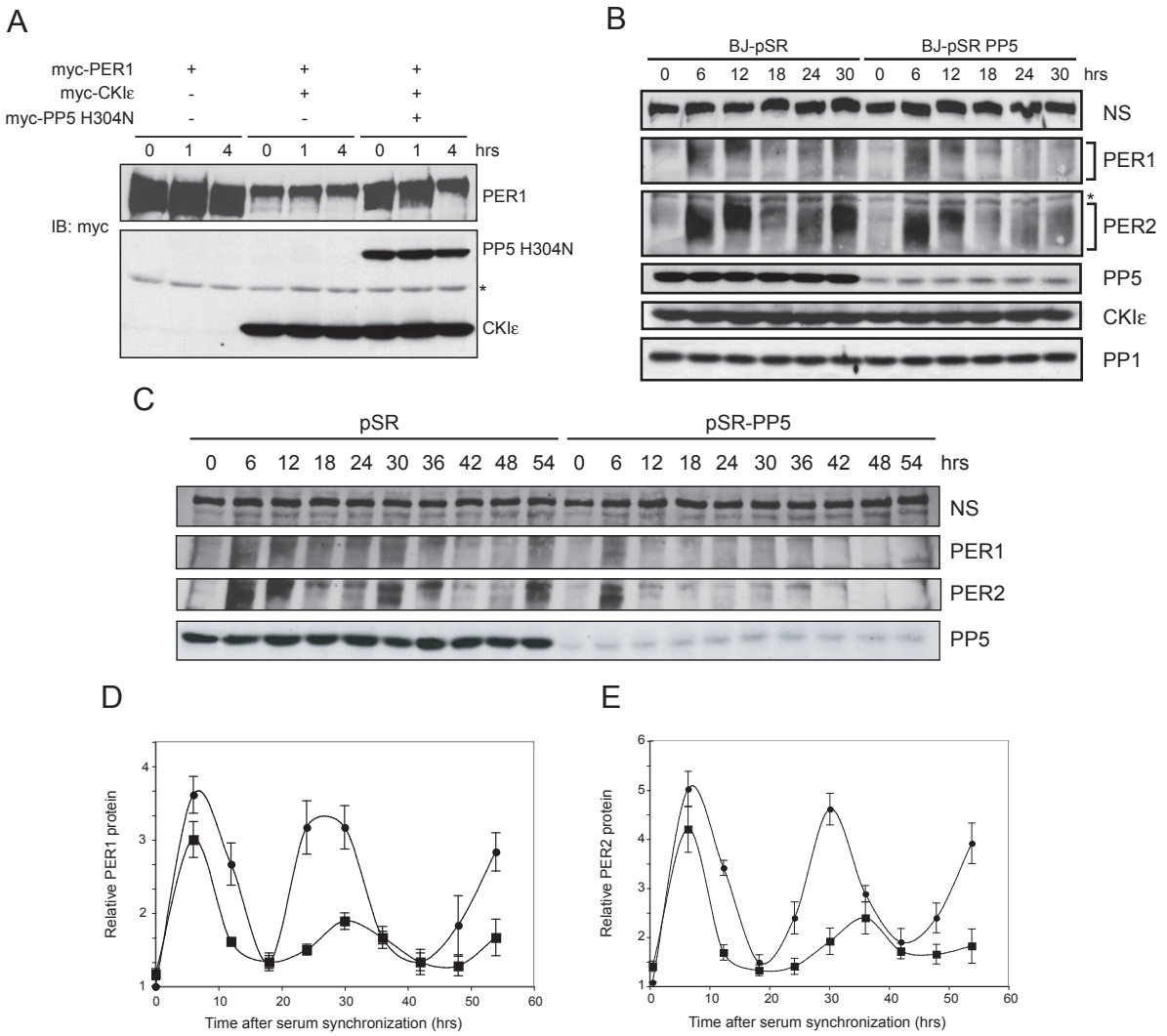

Figure 4.6 Loss of PP5 inhibits CKIε activity and disrupts circadian cycling
A. PP5 regulates phosphorylation of PER1 by CKIε *in vivo*. 293T cells transfected with myc-tagged PER1, CKIε and/or H304N PP5 were harvested after treatment with 100 μg/ml cycloheximide. Protein levels were monitored by western blot with anti-myc antibody. Asterisk indicates non-specific band. **B.** Knockdown of endogenous PP5 decreases PER phosphorylation. Circadian cycling was induced in confluent BJ fibroblast cultures (wild-type control, pSR; PP5 knockdown, pSR-PP5) by serum shock, and samples were harvested at the indicated times (hours after initiation of serum shock). Protein levels were monitored by western blot with antibodies to the native proteins. Brackets show phosphorylated species of PER. NS, non-specific band from PER1 western demonstrates equal loading and transfer of high MW region. Asterisk indicates non-specific band. **C.** Loss of PP5 disrupts circadian cycling. Serum-synchronized cultures were followed for two cycles and analyzed by western blot. **D.** Quantitative analysis of PER1 expression in cycling BJ fibroblast lines (n=4, ± SEM). **E.** Quantitative analysis of PER2 protein in cycling BJ fibroblasts (n=4, ± SEM). Key: pSR cells, circles; pSR-PP5 cells, squares.

Downregulation of PP5 results in a 6-hour increase in the intrinsic period of the clock and a severe dampening of the amplitude of clock protein expression, indicating that PP5 is required for normal cycling *in vivo*. The inability of PP5-deficient cells to efficiently cycle is most likely a result of the dramatic reduction in active, hyperphosphorylated PER proteins, as evidenced by both increased overall electrophoretic mobility and decreased abundance of the slower migrating forms of PER throughout the timecourse in PP5 knockdown cells. The decrease in PER phosphorylation cannot be explained by minimal differences in CKIε protein levels in the WT and PP5 knockdown cell lines, but may instead reflect decreased CKIε activity in the absence of its physiological activator, PP5.

Interaction of PP5 with the functional CLOCK/BMAL1 heterodimer

Because loss of PP5 resulted in severe circadian disruption, I wanted to further examine other possible roles of PP5 in the molecular clock. PP5 does not interact with CLOCK or BMAL1 monomers in mammalian cells, as shown by cotransfection/coimmunoprecipitation assays (Figure 4.2A); however, both CLOCK and BMAL1 are rapidly phosphorylated upon heterodimer formation (Kondratov et al., 2003), and these events could be required for interaction with PP5. Co-expression of FLAG-tagged CLOCK and BMAL1 in 293T cells resulted in the appearance of a distinct, slower migrating band of CLOCK, corresponding to the phosphorylated species (treatment with λ phosphatase collapsed the slower migrating band, data not shown), while I did not observe distinct changes in BMAL1 electrophoretic mobility under our conditions (Figure 4.7A). Significantly, PP5 was precipitated by the CLOCK/BMAL1 heterodimer, suggesting that heterodimer-induced phosphorylation may be required for interaction. I found that the CLOCK/BMAL1:PP5 complex was significantly stabilized with the inactive mutant, and PP5 reduced the phosphorylated species of CLOCK relative to co-expression with the H304N mutant (Figure 4.7B). Furthermore, I was unable to detect either CLOCK or BMAL1 with microcystin-precipitated PP5 (data not shown). These data suggest that the CLOCK/BMAL1

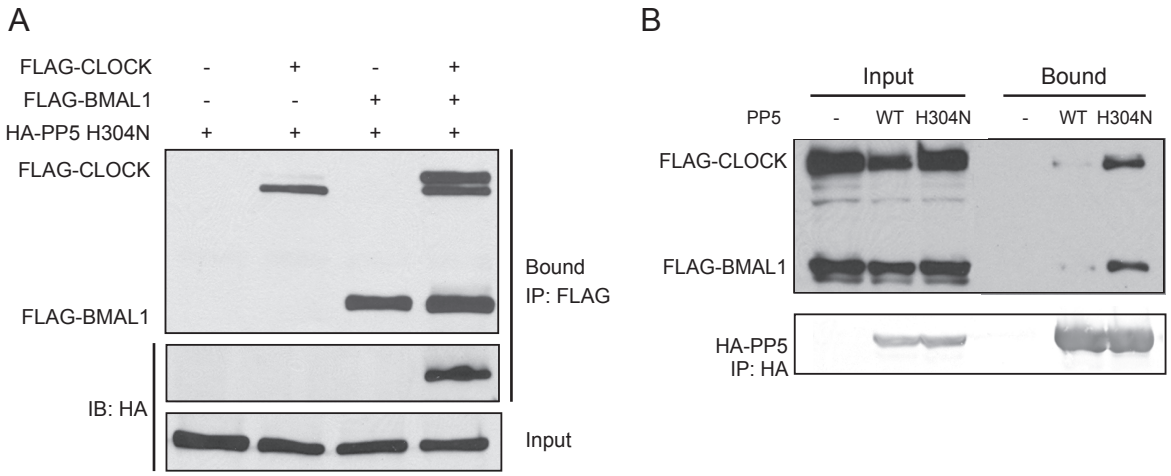

Figure 4.7 PP5 interacts with the functional CLOCK/BMAL1 heterodimer
A. Heterodimerization of CLOCK/BMAL1 is required for PP5 interaction. 293T cells were transfected with HA-PP5 and FLAG-CLOCK or BMAL1, or in combination, and complexes were precipitated with FLAG resin. **B.** Effect of PP5 catalytic activity on interaction with CLOCK/BMAL1. 293T cells were transfected with FLAG-CLOCK and BMAL1 and empty vector, HA-PP5, or HA-PP5 H304N, and precipitated with HA resin. Loss of PP5 catalytic activity stabilizes the PP5:CLOCK/BMAL1 complex.

heterodimer, like CKIε, may be a substrate for PP5. However, PP5 appears to precipitate the intact heterodimer, since equimolar amounts of CLOCK and BMAL1 are seen in PP5 precipitates (Figure 4.7B). The decrease in CLOCK/BMAL1 protein levels upon co-expression with WT PP5 does not explain the reduction in heterodimer precipitated by WT PP5 relative to PP5 H304N; in the reciprocal coimmunoprecipitation, only the inactive mutant was precipitated when limiting, equivalent concentrations of FLAG-CLOCK/BMAL1 were used with WT and H304N PP5 (data not shown).

Inhibition of CLOCK/BMAL1 transactivation activity by PP5

Phosphorylation of the CLOCK/BMAL1 heterodimer is positively correlated with transactivation of clock gene expression, although the mechanism by which phosphorylation stimulates or regulates CLOCK/BMAL1 activity is unknown. If PP5 dephosphorylates CLOCK/BMAL1, it should inhibit CLOCK/BMAL1-mediated transactivation of clock genes *in vivo*. I used luciferase reporter assays driven by the *mPer1* promoter in 293T cells to investigate regulation of CLOCK/BMAL1 by PP5. Expression of the heterodimer resulted in 30-fold stimulation of *mPer1*-driven luciferase expression (Figure 4.8A) over basal conditions, which was inhibited by PP5 in a concentration-dependent manner, while mutant PP5 had minimal effect on CLOCK/BMAL1 activity. I examined the phosphorylation state of CLOCK/BMAL1 from these extracts by western blotting and found that decreased transactivation of the *mPer1* promoter upon co-expression with PP5 correlated with a loss of phosphorylated CLOCK (Figure 4.8B). I did not observe a significant effect of PP5 on BMAL1 under my conditions, although the lack of detectable changes in electrophoretic mobility of BMAL1 under these conditions would preclude this. At their highest concentration, both WT and mutant PP5 appeared to stabilize dephosphorylated CLOCK, which may explain the minor reduction in heterodimer activity with mutant PP5. However, only WT PP5 reduced the amount of phospho-CLOCK and significantly inhibited

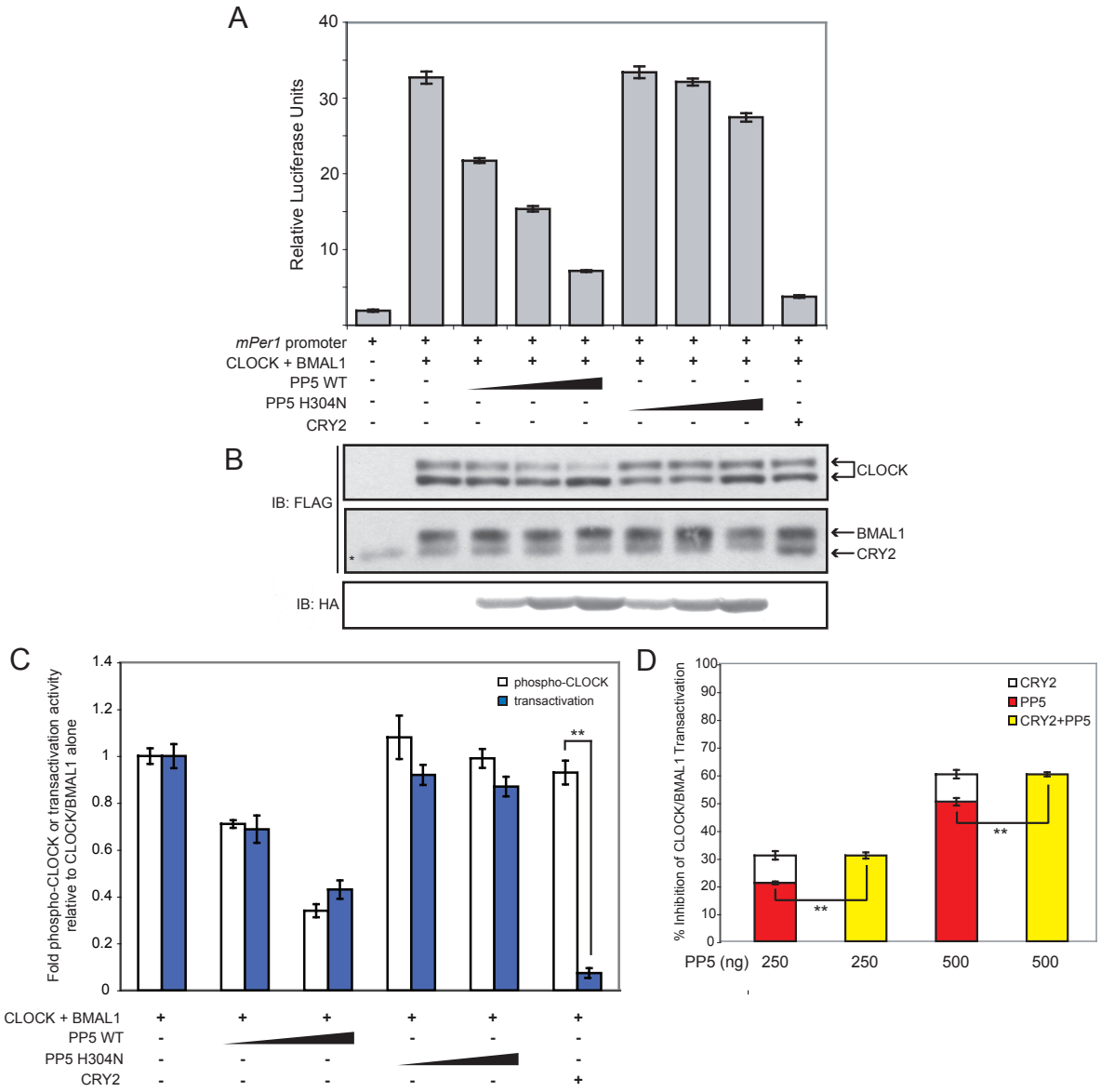

Figure 4.8 PP5 regulates CLOCK/BMAL1 activity and phosphorylation state
A. PP5 inhibits CLOCK/BMAL1-mediated transactivation of the *mPer1* promoter. Luciferase assays were performed in 293T cells using the *mPer1* promoter as a reporter for CLOCK/BMAL1 activity. Firefly luciferase activity from *mPer1* promoter was normalized to a *Renilla* transfection control. Data represent 3 independent experiments of duplicate samples (± SEM). **B.** Phosphorylation state of CLOCK and BMAL1 in luciferase assay samples. Total protein extracts were analyzed by western blot. Asterisk indicates non-specific band. **C.** Inhibition of CLOCK/BMAL1 by PP5 correlates with dephosphorylation of CLOCK. Quantitative analysis of correlation between phospho-CLOCK and luciferase activity in the presence of PP5 or CRY2. **D.** PP5 and CRY2 inhibit CLOCK/BMAL1 transactivation independently. Inhibition by PP5 or CRY2 alone is additive and equal to inhibition achieved by co-transfection of PP5 and CRY2. ** indicates significant difference ($p<0.001$).

heterodimer activity, suggesting that CLOCK phosphorylation is required for transactivation activity.

PP5 inhibits CLOCK/BMAL1 transactivation independently of CRY

Cryptochromes also act as potent inhibitors of CLOCK/BMAL1 transactivation (Figure 4.8A) (Griffin et al., 1999; Kume et al., 1999). Recent data suggest that CRYs may inhibit the CLOCK/BMAL1 complex by recruiting chromatin remodeling factors to target promoters (Naruse et al., 2004). In line with this, near complete inhibition of CLOCK/BMAL1 by CRY2 does not appreciably change the phosphorylation status of CLOCK or BMAL1 (Figure 4.8B), indicating that PP5 and CRY2 inhibit transactivation by the heterodimer using different mechanisms. I examined the role of CLOCK phosphorylation in inhibition of the heterodimer by PP5 or CRY2 by comparing the levels of phospho-CLOCK determined by western blotting to the activity of the CLOCK/BMAL1 heterodimer measured by luciferase assay. While inhibition by PP5 correlated well with loss of CLOCK phosphorylation, inhibition by CRY2 did not correlate with a change in CLOCK phosphorylation status (Figure 4.8C). Finally, I assayed the ability of sub-saturating amounts of PP5 or CRY2 alone, or in combination, to inhibit CLOCK/BMAL1 transactivation and confirmed that they act additively, and therefore, independently (Figure 4.8D). The inability of cryptochrome to inhibit PP5 regulation of the heterodimer is consistent with a model where posttranslational regulation of the heterodimer by PP5 occurs in a spatiotemporally distinct manner from inhibition by cryptochrome.

Discussion

Posttranslational regulation of circadian clock proteins is critical for establishing the near 24-hour period of nearly all molecular clocks identified to date, from cyanobacteria to *Neurospora* to humans. Phosphorylation, sumoylation, and ubiquitination of clock proteins provide mechanisms to regulate subcellular distribution, activity, and stability of both activators and inhibitors of the feedback loops, giving the molecular oscillator its stable 24-

hour periodicity and allowing phase adjustment by diverse external stimuli. In particular. phosphorylation plays a key role in modulating clock protein function in mammals: it is required for function of PER (Miyazaki et al., 2004), and precedes other posttranslational modifications, such as ubiquitination of PER and sumoylation of BMAL1 (Cardone et al., 2005; Eide et al., 2005), therefore serving as a critical point of regulation for clock protein function. Although the role of kinases in the clock has been fairly well studied, there are currently no data on the role of specific phosphatases. I have demonstrated here that PP5 regulates the activity of several clock proteins, and that regulation of PP5 activity by cryptochromes allows further crosstalk between clock proteins. These results demonstrate, both *in vitro* and *in vivo*, that PP5 is an important component of the mammalian circadian clock.

Identification of a physiological activator of CKIε

Regulation of protein kinase activity by inhibitory phosphorylation is a common theme that allows tight regulation of kinase activities involved in growth and developmental pathways (Knippschild et al., 2005; Roskoski, 2005). Inhibition of CKIε by autophosphorylation of its C-terminal domain is rapid, occurring within 5 minutes *in vivo* (Rivers et al., 1998). Furthermore, two recent studies have shown that CKIε is maintained in an inactive, autophosphorylated state *in vivo*, and is activated by unidentified phosphatases in a stimulus-dependent manner (Liu et al., 2002; Rivers et al., 1998; Swiatek et al., 2004). It is therefore likely that the activity of CKIε/δ in the molecular clock may require regulation by phosphatases. Although numerous *in vitro* studies have shown that both kinases can be activated by PP1, PP2A, and PP2B, this is the first study to demonstrate *in vivo* regulation of CKIε activity by any phosphatase. Loss of PP5 activity, either by dominant negative inhibition or siRNA-mediated depletion, results in hypophosphorylation of PER proteins, indicating that PP5 contributes significantly to the *in vivo* activation of CKIε.

The profiles of expression and circadian-regulated subcellular distribution of PP5 and CKIε coincide, supporting a role for PP5 as a *bona fide* regulator of CKIε function. While expression of most integral clock genes oscillates with 24-hour periodicity, there are notable exceptions that are expressed constitutively (Young and Kay, 2001). In particular, expression of clock kinases and phosphatase catalytic subunits in *Neurospora* (Yang et al., 2002; Yang et al., 2004), *Drosophila* (Kloss et al., 1998; Sathyanarayanan et al., 2004) and mammals (Ishida et al., 2001) is constant, indicating that clock protein levels oscillate but enzymes that modulate their activity and stability do not. The inability to detect a stable interaction between endogenous PP5 and its substrates (either CKIε or CLOCK/BMAL1) may result from obstruction of the active site by microcystin in our precipitation or the transient nature of the enzyme:substrate complexes. Stabilization of these complexes upon loss of PP5 catalytic activity, and lack of an effect of the inactivating mutation on the PP5:CRY interaction, support a role for PP5 in the physiological regulation of CKIε and CLOCK/BMAL1.

Phosphorylation of PER is required for mammalian clock function

Studies of the mammalian molecular oscillator demonstrate that PER phosphorylation is required for proper functioning of the major feedback loop. Phosphorylation of PER1 by CKIε is required for nuclear entry; PER1 lacking CKIε phosphoacceptor sites is retained in the cytoplasm, even in the presence of cryptochromes (Takano et al., 2004), indicating that phosphorylation of PER is a critical step in the execution the negative arm of the major feedback loop. Inhibition of CKIε/δ with chemical inhibitors interferes with normal cycling (Miyazaki et al., 2004) and loss of even a single phosphoacceptor site on PER2 causes a change in clock period that is manifested as a significant advance in onset of sleep in humans (Toh et al., 2001). One recent study has even suggested that PER3 cannot support molecular oscillations in the absence of PER1 or

PER2 due to its inability to effectively recruit CKIε for phosphorylation in the absence of heterodimerization with PER1 (Lee et al., 2004).

Bimodal regulation of PER function by phosphorylation

Mutations affecting CKIε kinase activity and phosphorylation of PER lead to multiple and opposing phenotypes in *Drosophila* and mammals. Mutations in DBT, the CKIε homolog in *Drosophila*, lead to both short and long period phenotypes (Kloss et al., 1998; Price et al., 1998), although the kinase activity of both mutants is decreased (Preuss et al., 2004). Similarly, inactivating mutations in CKIε/δ or loss of phosphoacceptor sites in PER2 and PER3 lead to both shortened and lengthened circadian periods in humans (Ebisawa et al., 2001; Toh et al., 2001; Xu et al., 2005). These opposing phenotypes are likely due to bimodal regulation of PER by phosphorylation, in which phosphorylation is first required for nuclear entry/retention to repress transcription, but which subsequently leads to loss of function due to degradation. Differential phosphorylation of sites responsible for nuclear entry or protein turnover of PER could produce opposing effects on period length. Alternatively, mutations in CKIε giving rise to different period length mutants could affect its intrinsic kinase activity or ability to regulate by autophosphorylation. The mechanisms behind bimodal regulation of PER function by phosphorylation are not known in any detail, although the collective activities of CKIε/δ and GSK-3β might contribute to this dynamic process (Dey et al., 2005; Iitaka et al., 2005).

Regulation of PP5 by cryptochromes may contribute to the bimodal regulation of PER by phosphorylation. Several studies suggest that PER phosphorylation is de-regulated in the absence of cryptochromes; notably, both PER1 and PER2 exhibit phenotypes of constitutive hyperphosphorylation (Shearman et al., 2000; Yagita et al., 2000), indicating that cryptochromes may normally inhibit or prevent PER phosphorylation. Regulation of PP5, and therefore CKIε activity, by cryptochrome may explain these *in vivo* observations.

Peak expression of CRY lags 2-4 hours behind that of both PER1 and PER2 in the mouse liver (Figure 4.1D and (Lee et al., 2001b), which would allow some degree of PP5-stimulated phosphorylation of PER by CKIε to occur, sufficient to allow nuclear entry of the complex. The addition of CRY to this complex promotes nuclear entry or retention of the repressive complex (Figure 4.9). Subsequent phosphorylation triggering ubiquitination and degradation of nuclear PER would decrease in the presence of CRY, which could be reversed as the multimeric nuclear clock complex disassembles. I therefore propose that regulation of PP5 activity by CRY could function as a molecular rheostat to control PER phosphorylation and ultimately, timing of the molecular clock.

A CRY-independent function for PP5 in the clock

In our reporter assay system, CRY2 and PP5 appear to inhibit CLOCK/BMAL1 transactivation by mechanistically distinct means. This is supported by two lines of evidence: first, inhibition by CRY2 does not correlate with altered phosphorylation levels of either CLOCK or BMAL1, while inhibition by PP5 does; and secondly, co-expression of sub-saturating amounts of CRY and PP5 results in additive inhibition of CLOCK/BMAL1, indicating that they work independently of one another. It is possible that CRY might inhibit PP5 regulation of CLOCK/BMAL1 with increased expression, since the *in vitro* data presented here suggest that efficient inhibition of PP5 by CRY requires a moderately high local concentration. However, since CRY is extremely effective at inhibiting CLOCK/BMAL1 by phosphorylation-independent mechanism, such an increase in CRY expression would mask any inhibition of PP5 activity in this assay. The final determination of the mechanisms of CLOCK/BMAL1 inhibition by CRY and PP5 may require uncoupling of direct heterodimer inhibition by CRY.

In any event, these data collectively highlight the importance of the spatiotemporal regulation of posttranslational modification of clock proteins. Activation of CKIε and inhibition of CLOCK/BMAL1 by PP5 may occur at distinct times throughout the circadian period and in

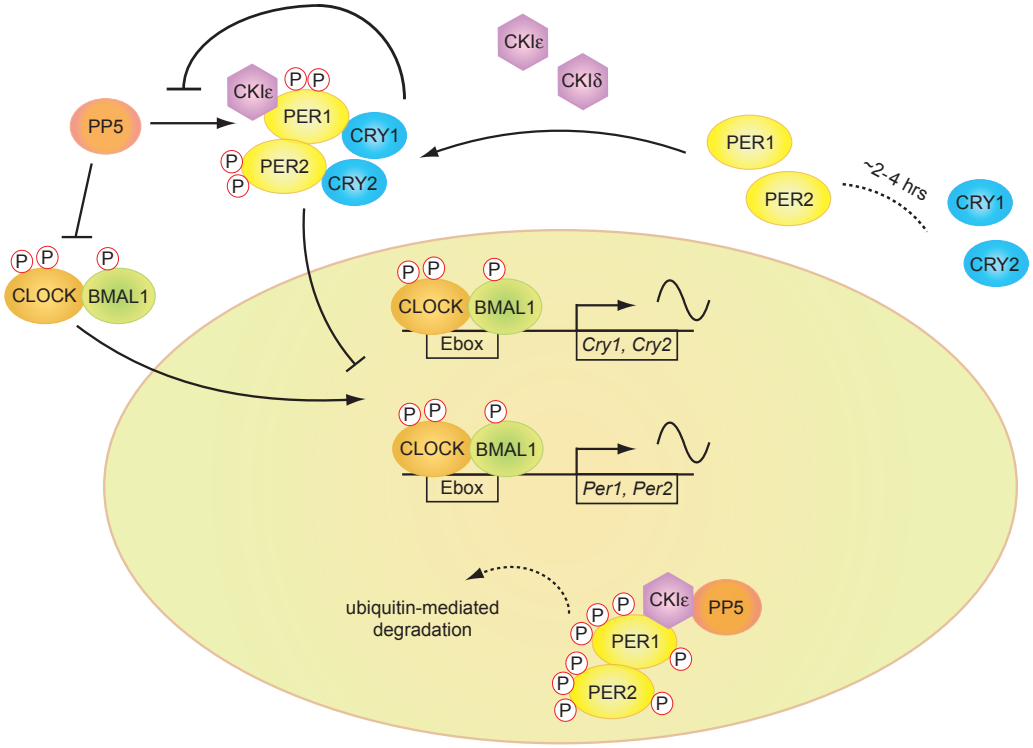

Figure 4.9 Dynamic regulation of the mammalian circadian clock by PP5 and cryptochrome

PP5 regulates both the positive (CLOCK/BMAL1-mediated transactivation of genes) and negative (PER/CRY inhibition of CLOCK/BMAL1) arms of the major feedback loop that constitute the molecular circadian clock. Inhibition of CLOCK/BMAL1 and stimulation of CKIε activity by PP5 cooperate to close the negative arm of the feedback loop. Differential regulation of PP5 activity by CRY could promote this common goal by optimizing nuclear entry of the repressive complex and permitting inhibition of CLOCK/BMAL1 by PP5. The spatiotemporal regulation of clock complex formation may play a role in the ability of CRY regulation of PP5.

different subcellular compartments. Although I present data that a stable CKIε:PP5:CRY2 complex can be purified from cells, efficient inhibition of PP5 by CRY *in vivo* may depend on their stable co-localization on a PP5 substrate; for example, PER proteins act as scaffolds for CKIε and CRY (Akashi et al., 2002). The exact timing and function of heterodimerization-induced phosphorylation of CLOCK and BMAL1 is not known; it may occur in the cytoplasm and act as a signal for nuclear entry or retention, or it may regulate transactivation by regulating protein-protein interactions or stability of the heterodimer (Kondratov et al., 2003). It has been proposed that a large, multimeric complex containing most, if not all clock proteins, forms on chromatin-bound CLOCK in the subjective night (Lee et al., 2001b). Future studies examining the timing and localization of posttranslational modification in relation to formation of this multimeric clock complex will be important for understanding the complex regulation of the molecular oscillator.

Requirement of PP5 for normal clock function in mammals

The functions of PP5 and CRY in the clock ultimately appear to serve a similar purpose: to promote execution of the negative arm of the major feedback loop. Reduction of PP5 activity compromises circadian cycling in cells, characterized by hypophosphorylated PER and an increase in period length with dampened amplitudes. This is reminiscent of phenotypes in *Neurospora* and *Drosophila* in which decreases in kinase activity result in hypophosphorylation of core oscillators and long periods with low amplitude (Price et al., 1998; Yang et al., 2003). Loss of kinase activity in these clocks results in arrhythmia in constant darkness, demonstrating the phosphorylation of core proteins is required to close the negative arm of the feedback loop (Price et al., 1998; Yang et al., 2004). Accordingly, if PP5 is shown to be the predominant phosphatase regulating CKIε function in the clock, I predict that loss of PP5 will disrupt clock function. The participation of phosphatases in the mammalian clock will almost certainly expand beyond PP5, since PER proteins are also

likely to be regulated by phosphatases that directly oppose the activity of CKIε/δ, such as PP2A in *Drosophila* (Sathyanarayanan et al., 2004) and an unidentified calyculin A-sensitive phosphatase in mammals (Eide et al., 2005).

Both PP5 and CKIε/δ have functions outside of the molecular clock, and have been implicated in cell cycle regulation and DNA damage responses, the Wnt/β-catenin pathway, and apoptotic signaling (Ali et al., 2004; Knippschild et al., 2005; Morita et al., 2001; Urban et al., 2003). Since molecular circadian rhythms are intrinsic to every cell, it is considerable interest to determine if circadian regulation of the activity and/or localization contributes to the ability of these proteins to function in other pathways, providing molecular links between the circadian cycle and its regulation of physiological processes.

Acknowledgements

This study benefited from collaboration with several members of the A. Sancar lab. I am particularly grateful for the work done by K. Shields, who worked with me to perform the *in vitro* assays shown in Figure 4.4 and begin work on the inhibition of PP5 by CRY. In addition, C. Thompson performed and analyzed *in situ* hybridization for *PP5* and *Per2*, shown in Figure 4.1A, and subcloned three constructs; C. Selby purified PP5, subcloned several constructs, and generated the mice used in the study. Figures 4.1B-C, 4.2, 4.3, and 4.5-4.9 are the direct products of my efforts. I thank S. Özgür for supplying insect cell-purified hCRY2 used in the *in vitro* assays and K. Ünsal-Kaçmaz for insightful discussions that helped to guide my research on this project.

I am also grateful for reagents provided to our lab from many researchers in the clock field that were used for the first time in this study: D. Virshup (University of Utah, Salt Lake City, UT) for providing the CKIε bacterial expression construct, S. Rossie (Purdue University, West Lafayette, IN) for the PP5 bacterial expression construct, J. Takahashi (Northwestern University) for the CLOCK and BMAL1 bacterial expression constructs, L. Ptácek (University of California at San Francisco, San Francisco, CA) for the PER2 mammalian expression construct, C. Weitz (Harvard University) for the pGL3::*mPer1* construct, N. Agarwal (University of North Texas Health Science Center, Fort Worth, TX) for the RGC-5 cell line, X.-F. Wang (Duke University) for providing the BJ cell lines, and C. Lee (Florida State University, Tallahassee, FL) for the PER1, PER2 and BMAL1 antibodies.

CHAPTER 5

SIGNALING IN FOUR DIMENSIONS: HOW CRYPTOCHROME EVOLVED TO COMMUNICATE LIGHT AND TIME INFORMATION

From the beginning of life on Earth, biopolymers have been waging a daily battle with ultraviolet solar radiation. In the absence of a protective ozone layer on primordial Earth, the first prokaryotes relied on photolyase as the only direct mechanism to protect the integrity of their genetic material from mutagenic ultraviolet light. Eventually, the deleterious effects of UV prompted organisms to avoid sunlight or adapt protective mechanisms. One of the founding fathers of chronobiology, C.S. Pittendrigh, hypothesized that this "escape from light" was the major driving force in the evolution of circadian rhythms (Pittendrigh, 1993). These molecular clocks, set by the solar cycle, allowed organisms to coordinate timing of physiological processes with respect to light to minimize UV damage (Nikaido and Johnson, 2000) and provided an internal timing mechanism to segregate incompatible physiological processes (Berman-Frank et al., 2001; Berman-Frank et al., 2003). As the complexity of organisms grew with the emergence of eukaryotes, so emerged the need for a multifunctional blue-light photoreceptor. Photolyase, with its flavin and folate chromophores, absorbs most strongly in the near-UV/blue-light region, overlapping with the UV components of sunlight that penetrate the ozone layer (Figure 5.1) (Bird et al., 1983; Gehring and Rosbash, 2003; Sancar, 2000). This spectral overlap, in combination with its existing function as a UV-induced DNA repair enzyme and wide distribution in prokaryotic organisms, therefore primed photolyase as a target for UV-directed adaptive evolution.

Cryptochromes evolved from photolyases to mediate non-repair functions such as growth and development in photosynthetic eukaryotes, and regulation of circadian rhythms in nearly all eukaryotes (Partch and Sancar, 2005). Perhaps the most distinguishing feature of cryptochrome is its change in substrate from a DNA photoproduct to the protein-protein interactions involved in intracellular signaling. Since structural studies of cryptochrome photolyase homology regions (Brautigam et al., 2004; Brudler et al., 2003) have not yielded an indication of the features of cryptochrome that contribute to this switch in function, I analyzed the photolyase/cryptochrome family from an evolutionary approach in order to

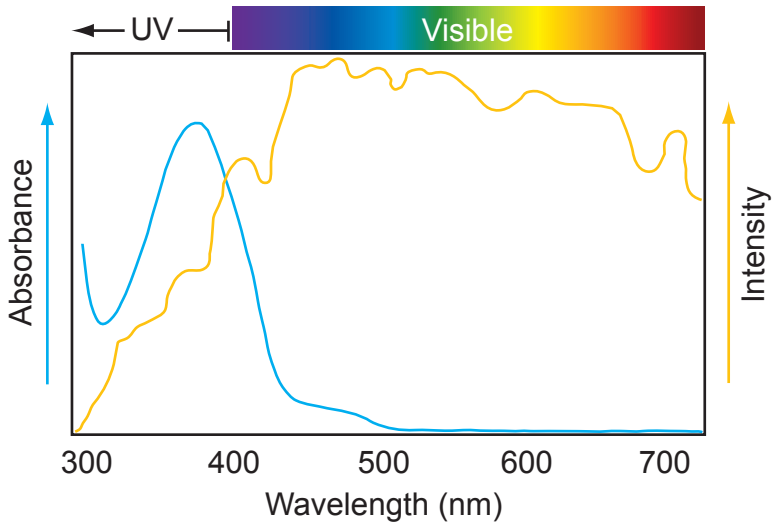

Figure 5.1 Photolyase preferentially absorbs the UV component of sunlight
The absorbance spectrum of purified VcPhr (blue) and intensity of AM1.5 solar radiation (yellow) on Earth demonstrate that cryptochrome absorbs in the near-UV and blue-light region, with peak absorbance in the UV.

identify functionally important, surface exposed residues that are unique to photolyases or cryptochromes. Evolutionary trace analysis suggests that loss of repair may have resulted from a change in location of highly conserved residues from the active site of photolyase to the opposite face of the protein in cryptochromes. Conserved residues on cryptochromes constitute a much larger solvent accessible surface area as opposed to photolyases, and may be involved in mediating the protein-protein interactions required for cryptochrome signaling, such as CRY:CRY dimerization and interaction with effectors.

Nearly all eukaryotic cryptochromes have also acquired C-terminal domains that regulate their light-dependent interaction and regulation of effector proteins (Partch and Sancar, 2005). I studied the structural properties of these unique C-terminal domains and found that they lack ordered tertiary structure, a feature that is common to domains involved in signal transduction. Structural plasticity could contribute to the ability of cryptochrome C-terminal domains to interact with multiple, structurally distinct proteins, from the photolyase homology region of cryptochrome to varied effector and modulatory proteins.

These studies also demonstrated a light-dependent conformational rearrangement in cryptochrome, characterized by release of the C-terminus from the photolyase homology region in response to light. Shown for the first time here, and recently supported independently by FTIR studies (Kottke et al., 2006), these data satisfy a supposition of the photolyase model of cryptochrome function: that a cryptochrome substrate must be bound in the dark, since the excitation energy generated by absorption of a photon by flavin will decay within 1-2 nanoseconds (Sancar, 2003). In the case of cryptochrome, the substrate may be the cryptochrome protein itself, undergoing a transient modification by photoexcited flavin that results in conformational rearrangement and release of the C-terminal domain. Now that we have a testable, light-dependent assay for cryptochrome function, it is possible to devise experiments that will identify this photoexcited state. The interaction of the CT and PHR domains can be studied in more detail, particularly to identify residues on the PHR that

contribute to CT domain binding, as these may be targets for modification by the photoexcited flavin. Once these residues have been identified, mutagenesis and photochemical studies may finally provide evidence of the elusive cryptochrome photocycle.

Photoinduced domain movement is a signal transduction mechanism shared by most, if not all, photosensory receptors. Rhodopsin (Okada et al., 2001), phytochrome (Park et al., 2000), phototropin (Harper et al., 2003), and photoactive yellow protein (Lee et al., 2001a) all undergo some form of conformational rearrangement after light exposure that contributes to generation of a signaling state, although our degree of understanding of their individual signaling mechanisms varies widely. In cases where downstream signaling events are known, however, it has been demonstrated that photoinduced domain movement usually involves de-repression of the effector-signaling domain. It is important to note that conformational change has been demonstrated in photosensory receptors utilizing chromophores that undergo cis-trans isomerization, such as rhodopsin, and in receptors that utilize flavin-based chromophores that do not undergo isomerization, such as phototropin, indicating that light-dependent chromophore isomerization is not a prerequisite to transduce conformational change in the protein. Collectively, these data suggest that cryptochrome uses its C-terminal domain to act as a light-dependent molecular switch to convey photic information to the cell.

This hypothesis was first introduced in 2000, when it was shown that overexpression of the C-terminal domains of plant cryptochromes signaled constitutive ‘light’ to its effector protein, COP1, in the absence of the photoreceptive domain of cryptochrome, suggesting that the C-termini are effector-signaling domains that are somehow repressed by the photolyase homology domain of cryptochrome in darkness (Wang et al., 2001; Yang et al., 2001; Yang et al., 2000). The identification of COP1-binding motifs in the light-dependent switch region of plant cryptochromes supports this model. Release of this switch region theoretically allows cryptochrome to compete for COP1 binding with its targets, such as HY5

and STO, allowing their accumulation and subsequent initiation of photomorphogenesis. It is presumed that cryptochrome would revert back to its native conformational state in the absence of light, allowing the switch to re-associate with the photolyase homology domain, making the CT domain a reversible, light-dependent switch. Studies of *Drosophila* cryptochrome also indicated an analogous role for its C-terminal domain in modulation of cryptochrome activity (Busza et al., 2004; Dissel et al., 2004; Rosato et al., 2001). However, dCRY appears to utilize its CT domain to regulate binding of effector proteins to the photolyase homology domain. Therefore, although the ultimate signaling endpoints are different in plant and animal cryptochromes, both depend on the light-dependent release of their CT domains from the photolyase homology domain.

In my studies, I identified several other structural and functional similarities in plant and animal cryptochromes, which evolved from divergent and functionally distinct progenitors: structural conservation of coiled-coil domains and residues putatively important for function, intrinsic disorder of their unrelated C-terminal domains and stabilization of the CT domain by interaction with the photolyase homology domain, homo- and heterodimerization of cryptochromes, and perhaps most interestingly, the conserved interaction of plant and animal cryptochromes with the ubiquitin E3 ligase COP1. The function of COP1 is highly conserved in both taxa, regulating cellular growth through the degradation of transcriptional activators (Yi and Deng, 2005). In plants, COP1 mediates light-induced changes in growth and development, and in animals, COP1 regulates cell cycle progression. Significantly, the pathways that COP1 regulates have been conserved throughout evolution as well; in plants, COP1 degrades the bZIP transcription factor HY5, and in animals, COP1 degrades its homolog, the proto-oncogene c-jun, in addition to the proto-oncogene p53.

The interaction of plant cryptochrome with COP1 occurs independently of light, and inhibition occurs after exposure to light. In animals, the CRY:COP1 interaction also occurs

independently of light, and at the current time, we do not know the functional consequences of this interaction and if it will be regulated by light. If animal cryptochromes modulate COP1 activity, it may be influenced by circadian changes in the abundance of cryptochrome protein, thereby conferring circadian regulation on COP1 activity, possibly influencing cell cycle/DNA damage checkpoint regulation. It is important to point out an obvious distinction: plants do not get cancer and mammals do not grow in response to light; however, the regulation of COP1 activity by plant and animal cryptochromes may indicate an overarching functional convergence of eukaryotic cryptochromes, where plant and animal cryptochromes both translate temporal information from the solar cycle to regulate growth.

The dual functionality of animal cryptochromes, possessing both light-dependent and light-independent functions, appears to be unique to the metazoan lineage. The light-independent function of animal cryptochromes may have arisen with the origin of the metazoan circadian clock. The structure of the molecular oscillator that engenders the metazoan circadian clock predates the split between bilateral animals, since the overall mechanism and clock proteins exhibit considerable similarity in *Drosophila* and mammals. However, the *Drosophila* cryptochrome acts both as a light-labile photoreceptor to reset circadian clocks within pacemaker cells and as a transcriptional repressor in peripheral cells (Ashmore and Sehgal, 2003; Collins et al., 2006), while mammalian cryptochromes contribute to non-visual photoreception in the retina and act as light-independent transcriptional repressors in the molecular clock mechanism. Therefore, one major goal of the chronobiology field has been to understand how or why such differences in cryptochrome function evolved in higher animals.

Since vertebrate-like cryptochromes were not previously detected in model invertebrates such as *C.elegans* and *D.melanogaster*, and the model chordate *Ciona intestinalis*, it is commonly believed that vertebrate cryptochromes evolved from (6-4) photolyases rather late in evolution. Based on the genome of *C.intestinalis*, as many as

one-sixth of all human genes were thought to be vertebrate innovations (Dehal et al., 2002). However, a study of expressed sequence tags in the cnidarian, *Acropora millepora*, an outgroup to bilateral animals, demonstrated that many genes in this coral are significantly conserved with humans, but not *D.melanogaster* or *C.elegans* (Kortschak et al., 2003). In fact, numerous studies have demonstrated asymmetry in gene loss and modification in bilaterean lineages, largely a consequence of the relative pace of change in model invertebrate genomes (Raible and Arendt, 2004; Thornton et al., 2003). The human genome, and therefore those of all vertebrates have diverged much less from the genome of our Urbilaterian ancestor than *D.melanogaster* (Krylov et al., 2003; Raible et al., 2005). Although beyond the scope of my studies, phylogenetic analyses of cryptochrome evolution indicate that *Drosophila* cryptochrome evolved from either a bilateral cryptochrome or a (6-4) photolyase progenitor. The alignment of *Drosophila*- and bilateral-specific motifs in primary sequence suggests that Drosophiloid cryptochromes evolved from bilateral cryptochromes, although this requires further study.

The identification of cryptochromes that are >95% identical to human cryptochromes in the other two branches of the Bilateria, the Ecdysozoans and the Lophotrochozoans, indicates that this gene, but not the *Drosophila*-like cryptochrome, was present in the last common ancestor (Figure 5.2). The monophyletic radiation of bilateral cryptochromes is also supported by a conservation of function. Another group recently published that vertebrate-like cryptochromes in honeybee and mosquito retain the ability to inhibit transactivation of clock genes by arthropod homologs of CLOCK/BMAL1 (Zhu et al., 2005). Collectively, these discoveries highlight many new model organisms that could potentially be used to study the function of bilateral cryptochromes.

I studied the light-independent function of cryptochromes in the molecular clock of mammals. Although cryptochrome was known to act as a transcriptional repressor (Griffin et al., 1999; Kume et al., 1999), phenotypic data from cryptochrome knockout mice

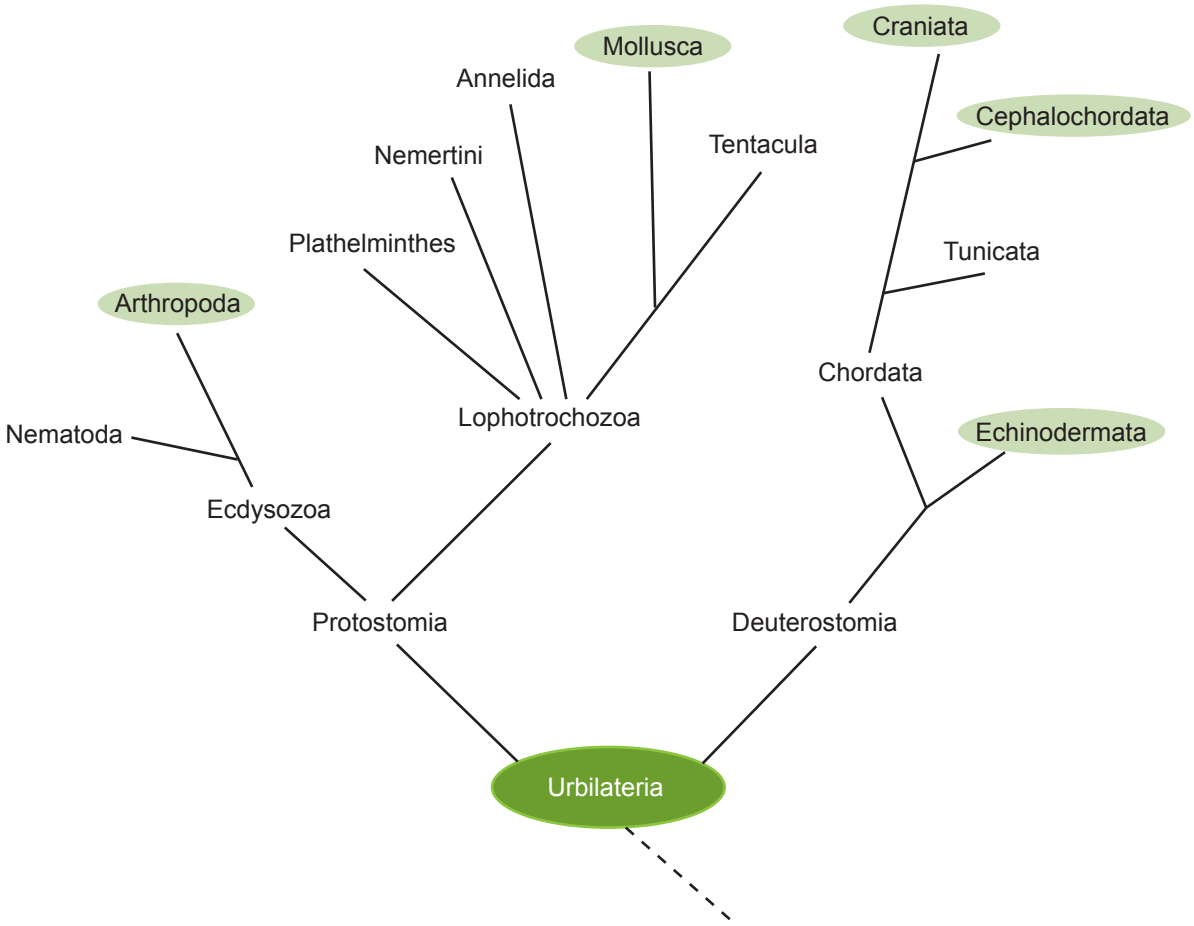

Figure 5.2 Monophyletic radiation of bilateral cryptochromes from Urbilateria
The phylogenetic tree of Bilateria has three main branches based on 18S rRNA and *Hox* genes: Ecdysozoa, Lophotrochozoa, and Deuterostomia. Using available sequence data, the presence of bilateral cryptochromes (green) was detected in all three branches evolving from their last common ancestor, the bilaterally symmetrical Urbilateria.

suggested that they might also play a role in the posttranslational modification of clock proteins (Shearman et al., 2000; Yagita et al., 2000). Building on previous work in the lab, demonstrating that both mammalian cryptochromes interact with, and inhibit the activity of, the serine/threonine phosphatase PP5 (Zhao and Sancar, 1997), I determined that PP5 has an important role in the core molecular clock mechanism of mammals. This study demonstrates that cryptochrome, through its regulation of PP5 activity, has the potential to modulate the activity of the major clock kinase, CKIε. This function is likely to be conserved in species that possess bilateral cryptochromes, since PP5 is also highly conserved in bilateral animals. Further characterization of the role of PP5 in the clock needs to be done, with particular emphasis on the circadian regulation of PP5 activity by cryptochrome. One interesting consequence of the modulation of PP5 activity by cryptochrome is the potential for another molecular interface between the circadian and cell cycles since PP5 regulates activation of the DNA damage checkpoints by ATM and ATR (Ali et al., 2004; Ünsal-Kaçmaz et al., 2005; Zhang et al., 2005). Investigation of the molecular interface between these two global regulatory systems has important consequences for human health.

Sunlight has many effects on living organisms: although it is inherently damaging to the molecules that define life on Earth, it provides a vital energy source and synchronizes the molecular clocks of living organisms to the rhythm of the Earth. In both plants and animals, cryptochrome communicates changes in light and time through a variety of mechanisms with a common goal, to provide living organisms with a basis for understanding their environment.

APPENDIX 1: Comprehensive phylogeny of the photolyase/cryptochrome family

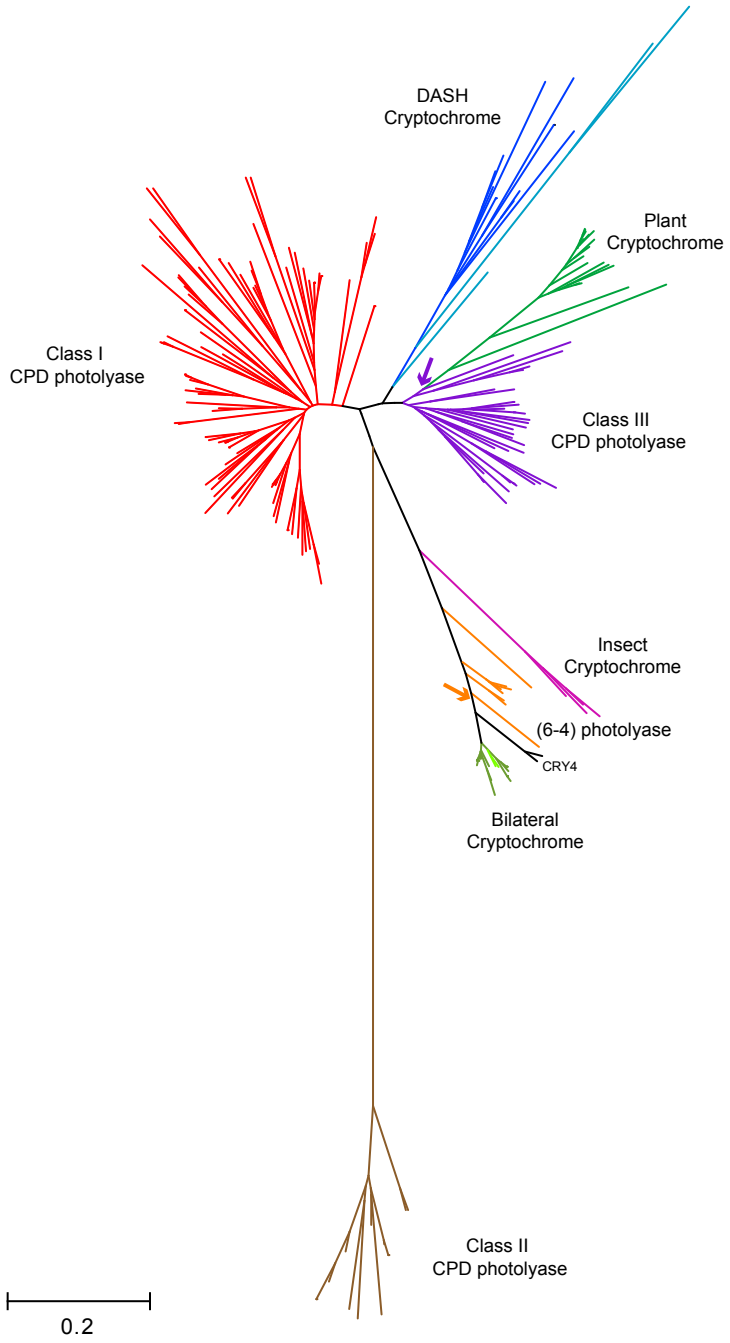

Phylogenetic analysis of more than 200 photolyases and cryptochromes
Classes are colored as in Figure 2.1. Purple arrow indicates ancestral node of plant cryptochromes, shared with Class III photolyases. Orange arrow indicates ancestral node of bilateral cryptochromes, shared with (6-4) photolyases.

APPENDIX 2: Photolyase/cryptochrome sequence information

Class I CPD Phr			
Gene/Organism Name	**Accession #**	**Gene/Organism Name**	**Accession #**
A.fumigatus	EAL87872	*P.atlantica*	ZP_00773583
A.nidulans	YP_399131	*P.cryohaloentis*	ZP_00654598
A.vinelandii	ZP_00416105	*P.fluorescens*	ABA76473
Acinetobacter sp.ADP1	CAG68060	*P.haloplanktis*	CAI89490
B.aphidicola	BAB13009	*P.marinus*	Q7V310
B.firmus	2017201A	*P.putida*	Q88PV9
B.fungorum	ZP_00280927	*P.syringae*	NP_790955
B.oryzae	BAD18969	*P.syringae* B728a	YP_234055
C.atlanticus HTCC2559	ZP_00951397	*R.eutropha*	AAZ60085
C.aurantiacus	EAO60601	*R.ferrireducens*	ZP_00692359
C.pelagibacter	AAZ22122	*R.gelatinosus*	ZP_00244738
C.psychrerythrea	AAZ26268	*R.metallidurans*	ZP_00593470
C.salexigens	ZP_00473478	*Roseobacter* sp. MED193	EAQ47411
C.violaceum	NP_903151	*S. enterica*	CAD05171
C.watsonii	ZP_00514659	*S.amazonesis*	ZP_00586280
D.hansenii	CAG84307	*S.baltica*	ZP_00581799
E.carotovora	CAG74259	*S.cerevisiae*	NP_015031
E.coli Phr	BAA35367	*S.coelicolor*	NP_625142
E.faecalis	AAO81383	*S.denitrificans*	EAN69010
F.oxysporum	AAP30741	*S.flexneri*	Q83L75
G.violaceus	Q7NMI2	*S.frigidimarina*	ZP_00637310
G.zeae	XP_380973	*S.griseus*	CAA33161
H.lixii (T.harzianum)	CAA08916	*S.oleracea*	AAP31407
H.marismortui	YP_135520	*S.oneidensis*	NP_718938
H.salinarum	AAG19671	*S.putrefaciens*	ZP_00814119
Jannaschia	ZP_00555485	*S.pyogenes*	AAZ51854
K.lactis	XP_453092	*S.solfatarius*	AAK42609
K.radiotolerans	EAM74689	*S.sonnei*	YP_309650
L.innocua	CAC95829	*S.tokodaii*	BAB65903
L.major	CAJ06003	*S.typhi*	Q828E2
L.mesenteroides	ZP_00064128	*Siicibacter* sp.TM1040	ZP_00619910
L.monocytogenes	NP_464116	*Sulfitobacter* sp. NAS-14	ZP_00962411
M.acetivorans	AAM07414	*Synechococcus* sp.WH8102	CAE06734
M.aquaeolei	ZP_00819133	*T.elongatus*	BAC07977
M.avium	NP_962015	*T.erythaeum*	ZP_00674183
M.burtonii	ZP_00563669	*U.maydis*	XP_762226
M.degradans	ZP_00314936	*V.cholerae*	AAF95971
M.flagellatus	ZP_00566430	*V.fischeri*	AAW87823
M.smegmatis	AAF04135	*V.parahaemolyticus*	BAC62814
N.aromaticivorans	ABD26199	*V.vulnificus*	BAC96383
N.crassa	CAA41549	*W.succinogenes*	CAE10587
N.pharaonis	YP_330750	*Wigglesworthia*	BAC24328
P.aeruginosa	Q9HVD2	*Y.pestis*	Q82D93
P.arcticus	AAZ18293	*Y.pseudotubercolosis*	CAH22151

Class II CPD Phr		Class III CPD Phr cont'd	
Gene/Organism Name	**Accession #**	**Gene/Organism Name**	**Accession #**
A.gambiae	EAA10141	*R.rubrum*	ABC23700
A.thaliana	NP_849651	*R.sphaeroides*	ABA78296
C.auratus	P34205	*S.pomeroyi*	AAV95194
C.sativus	BAB91322	*X.axonopodis*	AAM36348
C.reinhardtii	AAD39433	*X.campestris*	AAM40732
D.melanogaster	BAA05042	*X.oryzae*	BAE68170
F.virus	NP_039121	**(6-4) Phr**	
M.domestica	NP_001028149	**Gene/Organism Name**	**Accession #**
O.latipes	BAA05043	*A.clavatus* NRRL1	AAKD02000020
P.tridactylus	Q28811	*A.gambiae*	Ensemble 13343
S.oleracea	AAP31407	*A.thaliana*	NP_566520
M.thermautotrophicus	BAA06411	A.vastus	CAD24679
M.xanthus	AAC43723	*C.merolae*	CMJ130
Class III CPD Phr		*D.melanogaster*	NP_724274
Gene/Organism Name	**Accession #**	*D.pseudoobscura*	GA15376
A.tumefaciens	AAL42229	*D.rerio*	NP_571863
Arthrobacter	ZP_00412147	*D.salina*	AAX56342
B.ambifaria	ZP_00688329	*G.moniliformis* 7600	AAIM01000635
B.anthracis Ames	ZP_00393396	*G.violaceus*	Q7NJT3
B.cenocepacia	ZP_00461961	*G.zeae*	XP_386941
B.cepacia	ABB09082	*M.grisea*	XP_365369
B.cerus	AAP10079	*O.sativa*	XP_464551
B.flavum	AAK64295	*O.tauri*	AAU14280
B.japonicum	BAC50575	*P.nodorum* SN15	AAGI01000239
B.linens	ZP_00378974	*S.purpuratus*	XP_788938
B.mallei	AAU49686	*U.maydis*	XP_758291
B.pseudomallei	CAH36352	**DASH CRY**	
B.vietnamiensis	ZP_00420939	**Gene/Organism Name**	**Accession #**
C.burnetii	AAO90685	*A.thaliana* Cry3	NP_568461
C.crescentus	AAK23409	*C.hutchinsonii*	ZP_00308901
C.diphtheriae	CAE48617	*C.merolae*	CMA044
C.efficiens	BAC17457	*D.rerio* CryDASH	NP_991249
C.glutamicum	BAB98023	*F.tularensis*	YP_169849
D.acetoxidans	ZP_00549900	*G.violaceus*	Q7NMD1
E.litoralis	ABC63501	*L.esculentum* CryDASH	ABB01166
G.oxydans	AAW60748	*N.crassa* CryDASH	CAE76612
L.pneomophila	AAU26319	*R.baltica*	CAD77347
L.xyli sp. xyli	AAT88832	*Synechococcus* sp.WH8102	CAE08272
M.loti	BAB53733	*Synechocystis* sp.PCC6803	1NP7_B
Magnetococcus sp.MC-1	EAN29992	Uncultured marine bacterium	AAR38165
N.punctiforme	ZP_00106383	*V.cholerae* Cry1	AAF94962
P.aestuarii	ZP_00592239	*V.cholerae* Cry2	AAF94550
Parachlamydia sp.UWE25	CAF23396	*X.laevis* CryDASH	BAD08601
R.palustris	CAE28620	*Z.mobilis*	AAV90074

Bilateral CRY		Plant CRY	
Gene/Organism Name	**Accession #**	**Gene/Organism Name**	**Accession #**
A.gambiae Cry2	EAA44753	*A.capillus-veneris* Cry1	BAA32810
A.mellifera Cry2	XP_393680	*A.capillus-veneris* Cry2	BAA32811
B.mori (Silkbase clone)	brP-1009	*A.capillus-veneris* Cry3	BAA32812
B.mori (Silkbase clone)	NRPG1215	*A.capillus-veneris* Cry4	BAA88425
B.taurus Cry1	XP_616063	*A.capillus-veneris* Cry5	BAA88426
B.taurus Cry2	XP_585942	*A.rusticana* Cry2	BAC67177
C.familiaris Cry2	XP_540761	*A.thaliana* Cry1	AAB28724
D.plexippus Cry2	DQ184682	*A.thaliana* Cry2	AAL16379
D.rerio Cry1a	NP_571864	*Chlamydomonas* Cry	AAC37438
D.rerio Cry1b	BAA96847	*L.esculentum* Cry1	AAF72557
D.rerio Cry2a	NP_571866	*L.esculentum* Cry2	AAF72555
D.rerio Cry2b	NP_571867	*M.palacea*	BAE54524
D.rerio Cry3	BAA96850	*N.sylvestris* Cry1	ABB36796
G.gallus Cry1	NP_989576	*N.sylvestris* Cry2	ABB36797
G.gallus Cry2	NP_989575	*O.minor* Cry1	AAR08429
H.sapiens Cry1	NP_004066	*O.sativa* Cry1a	XP_466372
H.sapiens Cry2	NP_066940	*O.sativa* Cry2	CAD35495
M.fascicularis Cry1	BAB72089	*P.patens* Cry	BAB70665
M.musculus Cry1	AAH85499	*P.sativum* Cry1	AAS79663
M.musculus Cry2	Q9R194	*P.sativum* Cry2b	AAO23972
P.troglodytes Cry1	XP_509339	*S.alba* Cry	CAA50898
R.catesbeiana Cry	AAP13561	*S.bicolor* Cry2	AAN37909
R.norvegicus Cry1	AAQ11980	**Insect CRY**	
R.norvegicus Cry2	NP_596896	**Gene/Organism Name**	**Accession #**
S.borin Cry1	CAG14931	*A.gambiae* Cry1	EAA01270
S.purpuratus Cry1a	XP_785873	*A.pernyi* Cry	AAK11644
T.castaneum (Trace Archive)	589867845	*B.tryoni*	AAU14170
T.nigroviridis	CAF92156	*D.melanogaster* Cry	AAK92938
T.nigroviridis Cry1	CAF93038	*D.plexippus* Cry1	AAX58599
X.laevis Cry1	AAK94665	*S.crassipalpis* Cry	BAB85473
X.laevis Cry2b	AAK94667		
Other vertebrate CRYs			
D.rerio Cry4	NP_571862		
G.gallus Cry4	XP_419231		

APPENDIX 3: Sequence analysis of photolyase and cryptochromes

Sequences used to analyze motif conservation in cryptochrome vs. progenitor (Figure 2.7B)

Bilateral CRY	(6-4) Photolyase	Plant CRY	Class III
A.gambiae CRY2	*A.gambiae*	*A.thaliana* CRY1	*A.tumefaciens*
A.mellifera CRY	*A.thaliana*	*A.thaliana* CRY2	*B.cereus*
D.rerio CRY1a	*D.melanogaster*	*L.esculentum* CRY1	*B.japonicum*
D.rerio CRY2a	*D.rerio*	*L.esculentum* CRY2	*B.linens*
G.gallus CRY1	*D.salina*	*M.palacea* CRY	*B.mallei*
G.gallus CRY2	*G.zeae*	*N.sylvestris* CRY2	*C.crescentus*
H.sapiens CRY1	*M.grisea*	*O.minor* CRY	*D.acetoxidans*
H.sapiens CRY2	*O.sativa*	*O.sativa* CRY1a	*G.oxydans*
X.laevis CRY1	*O.tauri*	*P.patens* CRY	*L.pneumophila*
X.laevis CRY2b	*U.maydis*	*S.bicolor* CRY2	*X.campestris*

Sequences used to analyze mean class coiled-coil propensity (Figure 2.9C)

Class I/III Photolyase	DASH	Plant CRY	(6-4) Photolyase	Bilateral CRY	Insect CRY
A.nidulans	*D.rerio* CRY DASH	*A.thaliana* CRY1	*A.gambiae*	*A.gambiae* CRY2	*D.melanogaster*
A.tumefaciens	*Synechocystis* CRY DASH	*A.thaliana* CRY2	*A.thaliana*	*A.mellifera* CRY	*A.pernyi*
B.anthracis	*V.cholera* CRY1	*L.esculentum* CRY2	*D.melangaster*	*D.rerio* CRY1a	*B.tryoni*
B.cenocepacia	*X.laevis* CRY DASH	*L.esculentum* CRY1	*D.rerio*	*D.rerio* CRY1b	*A.gambiae* CRY1
B.firmus		*N.sylvestris* CRY1	*D.salina*	*D.rerio* CRY2a	
C.crescentus		*N.sylvestris* CRY2	*G.violaceum*	*D.rerio* CRY2b	
E.coli		*O.sativa* CRY1a	*G.zeae*	*H.sapiens* CRY1	
G.violaceus		*O.sativa* CRY2	*O.sativa*	*H.sapiens* CRY2	
R.baltica		*P.patens* CRY	*O.tauri*	*M.musculus* CRY1	
M.loti		*P.sativum* CRY1b	*S.purpuratus*	*M.musculus* CRY2	
R.palustris		*P.sativum* CRY2b	*U.maydis*	*X.laevis* CRY1	
S.alba		*S.bicolor* CRY2	*X.laevis*	*X.laevis* CRY2b	

APPENDIX 4: Retrieval of ancient photolyase and cryptochrome sequences

GenBank Trace Archive
Searching database with AtCry1

Record number	Organism	Common name	Seq similar to:	Protein sequences retrieved from tblastx alignments
1	963712406	*Selaginella moellendorffii*	spikemoss	plant	ESMNMFLRALGLREYSRYLSFNFPFTHKRSLLANLKHFPWRADEGYFKSWRQGRTGYPLVDAGMRQLWATGWLHGKIRVVV
					SSFLVKFLQVPWTWGMKYFWETLLDADVENDVLGWQYISGGLPDGHELDRWDNPQEEGYKLDPKGEYVRKWLPELSRVPID
					WIHHPWDAPSTILRAAGVELGSNYPRPIVEVAAAYYR

Also: sequences for pinus taeda (loblolly pine), aquilegia formosa (red columbine), glycine max (soybean), medicago trunculata (a legume), various orzyae (rice) species (nivara, australiensis, minuta, coarctata, alta, granulata, zea mays (corn), ricinus communis (caster bean) that are similar to plant Crys

Searching database with hCry1 or (6-4) photolyases

Record number	Organism	Common name	Seq similar to:	Protein sequences retrieved from tblastx alignments
1	273129842	*Thalassiosira pseudonana*	diatom	(6-4)	RMQDNPYCRNVPWSSDPKLLKAWKDGKTGFPWIDACMAQLRTEGWIHHLGRHAVACFLTRGDLWQSWEWGADHFEGEL
					LDADYALNNFNWLWLSCSGFFYQYFRCYSPVAFQKKNDVNGNYIRKWVPELAGLPAKYIYEPWKAPSSVLNAAGIKLGDNYPN
2	589650117	*Tribolium castaneum*	red flour beetle	bilateral	GQTGFPWIDAIMTQLREEGWIHHLARHAVACFLTRGDLWLSWEEGMKV
					KKAFPPLSLHGQLLWREFFYCAATKNPNFDKMIGNPICVQIPWDKNAEALAKWA
					VFEELLLDADWSVNAGMWMWLSCSSFFQQFFHCYCPIKFGRKAD
3	571192638	*Aedes aegypti*	yellow fever mosquito	bilateral	RFGCLSTRLFLLPTHRPVQEKSRKPAPPLSLHGQLLWREFFYCAATKNPNFDKMAGNPICVQIPWDRNAEALAKWASGQTGFP
					WIDIAMTQLREEGWIHHLARHAVACFLTRGDLWISWEEGMKVFEELLLDADWSVNAGMWMWLSCSSFFQQFFHCYCPVKFG
4	496489253	*Phaeodactylum tricornutum*	diatom	(6-4)	STPNFDKMIDNPIARQIPWDDDPDLLLAWKMSKTGYPYIDIAMTQLRETGWIHHLARHSVACFLTRGDLWQSWEDGATVFEE
					YLIDADWSINNFNWQWLSCTAHFYQ
	496045414				DGDYIRKWLPQFKDMPAKYIYEPWEAPIELQKKVGVIVGENYPHPIVDHKLVSKNNMSRMKEAYDAQKNRE
	496495713				AIHWFRNGLRFHDNPCLLDACQKSESLLPIYVVDPEFPFAQTAG
5	654177517	*Stagonospora nodorum*	fungus	bilateral/(6-4)	FPWIDALMRQLAREGWIHHLGRHAVACFLTRGGCYIDWERGAEVFEEFLIDHESACNIGNWQWLSCTAFFAQFFRCYSPVAF
					PAKWDKNGDFVRRYVPELAHFDKKFIYEPWKAPIADQKKWGC
6	814809451	*Daphnia pulex*	water flea	bilateral	KGQTGFPWIDAMTQLREEGWIHHLARHAVACFLTRGDLWISWEEGMKVF
					FNLFVLLLPQIKKAQPPLSLHGQVLWREFFYCAATNNPNFDKMIGNPICQIPWDSNAEALAKWA
					VFEELLLDADWSVNAGTWMWLSCSSFFHQFFHCYCPVRFGRKVDPTG
					SQTGLSPYLRFGCLSVRVF
7	454935760	*Phakospora pachyrhizi*	pathogenic fungus	bilateral-1	FPLRYIHEPWSAPEDVQLRAKCIIGQDYPLPIVNHNRASRIMDRMRQAYQQLSKFR
					LSLGDLWISWEEGMKVFDELLLDADWSVNAGQWMWLSCSSFFQQIFHCYCPVRFGRKADPNGDYIRKYLPCLK
8	455600694			bilateral-2	VFEELLLDADWSVNAGMWMWLSCSSFFQQFFHCYCPVRFGRKADPNGDYIRRYLPILKNFPTRYIHETWSAPENVQRAAKC
					GQTGFPWIDAIMTQLREEGWIHHLARHAVACFLTRGDLWISWEEGMKV
					KKAVPPSLLHGQLLWREFFYCAATRNPNFDKMQGNPVCVQIPWDHNLEAIAKWA
9	683172545	*Volvox carteri*	green algae	(6-4)	GFPWIDAIMTQLRQWGWMHHLARHGVACFLTRGDLYVSWERMQVSEELLID
	643083993				VGAHTPNFHRMIDGNPLCKQIPWDDDEELLAAWREARTG
	639669692				SILWFRKGLRLHDNPALLEACRGAAHVYPVFIL
10	560354999	*Nematostella vectensis*	sea anemone	bilateral/(6-4)	EKKSIPPATLFTGLVRRELFLHVASHNADLDKMVDNPLSVQFPWEENREGLERWKKGKTGFPWIDAMMRQLREEGWIHHLA
					RQAVGCFLTRGCLWVSWEEGFKAFDELQLDAEWSLNASNWLWLSCSSDVH
	557663472				FEERGWTIDEMFSNDAHLSPYMRFGCLSPRYYQQLALTY
					STELDPHWTGGELPEALRRLSAALKKVSF
					SKPPETLYTNLLWREFFFATASTNPDHHRMMGNPLALQIPWEQHPEALSLWKQ
					LKRGNWWLSCSSYVHGAVLWYCPGKSGKQVGPDG
11	274079115	*Phytophthera sojae*	oomycetes	(6-4)	WKEGRTGFPWIDAIMQLEEEGWMHHLARHSVACFLTRGDLYISWVRGLEVFKERLIDHDWSLNAGWLWLNSSYFFHCYFRV
					TILSPHLFYGCLSPRTFYHQLRDILQRHKNPSKPPVSLEGQLLWREFYHCHGHANPYFDKMEESPTCLQVDW
					GGEKKALSALKEYFADEERVAKFEKPNTSPAQTPPSP
12	324544936	*Phytophthera ramorum*	oomycetes	(6-4)	GFPWIDAIMTQLKEEGWMHHLARHSVACFLTRGDLYISWVRGLEVFQEYLIDHDWSLNAGSWLWLSSSYFFTAYFRVYSPISF
					GKKSDPEGHFIRKYIPALKKMPAKYIYEPWKAPMTLQHATGCIIGKDYPCPIVDHKESMSRCVAGMKMSY
13	602208862	*Branchiostoma floridae*	amphioxus	bilateral	QGQTGFPWIDAMAQLQQEGWIHHLARHAVACFLTRGDLWISWEEGMKV
	632469380				EVFEELLLDADQSVNAGSWMWLSCSSFFQQFFHYYCPVNFGRRTDPNGDFIR
14	106077780	*Nasonia vitripennis*	wasp	bilateral	QTGFPWIDAIMTQLREEGWIHQLARHAVACFLTRGDLWISWEEGMKVFDELLLDADWSINAGMWMWLSCSSFFQQFFHCYC
	105194248	(merged with above seq)			PVRFGRKADPNGDYIRRYLPVLKNFPTRYIHEPWNAPLSVQRAAKCIIGQEYALPMVNHSKSSRINVERMKRVYQQLSKYRAN
	105215690				HTVHWFRKGLRLHDNPSLREGLAGASTFRCVFVLDPWFAGSANVSINKWRFLLQCLEDLDRSLHQLNSRLFVIRGQPADALPKL
15	946666747	*Lottia gigantea*	owl limpet	bilateral	KYFQGMTGYPWIDAIMTQLKKDGWIHHLARHAVACFLTRGDLWLSWEEGMKV
	835444336				VFEEYLLDADWSLNAGNWMWLSASSFFYQYFRVYSPVAFGKKTDPNGLYIK
	946537407				QLNRGEEPSLAMYGQLLWREFFYLVARDNMKFDQMQGNPICCQIPWDKNSTALAKW
	986939203				FRFLLECLDLDSSLRKLNSRLYVVLGQPVAVFPSLFK
16	576530228	*Emiliana huxleyi*	phytoplankton	(6-4)	PWIDAAMTQLRREGWIHHLARHAVACFLTRGDLWQSETGAAVFEEYLLDADEAINFGNWMWLSCSSFFYQYFRCYSPVAFPQ
					KYDKQAGYVRHWLPQLARLPAKYIYEPWKAPIAVQKEAGCIIGVDYPKPIVDHQ
	577668965				RHSQPPVSLHGQLLWREFYVCCMHATPNYRRMVGNPICRQISWGEDAALVAAWREGRTGY
					HAIPSLEELGLEPMGDASVIARGGEGAALRAMEAHLRRRDWIASFEKPKTSPTEMLASTTVLSPYLTFGCLSSRLLYERVAAVYAE
17	201488075	*Gibberella zeae*	pathogenic fungus	(6-4)	GFPWIDALMRQLKDEGWIHHLGRHAVACFLTRGGCYIDWERGCEVFEEWLIDHEPACNVGNWQWLSCSAFFSQYFRCYSPV
		(aka *Fgraminium*)			AFGQKWDKKGEFIRRYVPELKNMDAKYIYEPWKAPLTDQKKA
					TLLSPHLHFGSLSVREFYWRVKDVVDSYKGASSPPESLIGQLLFRDMTFAAQAALGYVFSQTANNPYCRFIPW
	204740827				YPKPMFDFAKRRDVCISSMKVAYQ
	202761595				VEVIIVSGRTLGTADQIVEKHGGQPMSITQLQPAGSKL

18	288892792	*Euprymna scolopes*	bobtail squid	bilateral	FPWIDAIMKQLRKEGWIHHLARHAVACFLTRGDLWISWEDGMKVFEELLLDADWSVNAGMWMWLSCSSFFQQFFHCYCPV
					GFGKRIDPNGDFIRHYLPILKRFAAKYIYEPWNAPESVQKTAKCIIGKDYPVPMVNHSEVSRINMERMRQVYHRLT
19	1035881135	*Aspergillus clavatus*	fungus	bilateral/(6-4)	RWKEGRTGFPWIDALMRQLKLEGWIHHLGRHSVACFLTRGGCYVSWERGAEVFEDWLVD
					GGETAALRVLAGYIQDGEYVGTFEKPK
	1035771714				LRQDTDAYARDRDEAVLRMARDAGVEVIVQMGRTLFDPDELVRKNGGKPTMSIAQVQKAAEKI
20	965446289	*Botryotinia fuckeliana*	pathogenic fungus	bilateral/(6-4)	GFPWIDALMRQLKDEGWIHHLGRHAVACFLTRGGCYIDWERGCEVFEEWLIDHEPACNAGNWQWLSCTAFFSQYFRCYSPI
					AFGQKWDKEGNFIRRYVPELKNMDSKYIYEPWKAPLPDQKKA
		(aka *B.cinerea*)			TGLSPYLHFGALSVRLFYWRVREIVDSYGNGASTP

Also: many records for bilateral cryptochromes from various vertebrate organisms (not saved since they are >95% identical to known vertebrate cryptochrome sequences)

Swiss-Prot/TrEMBL
Searching database with hCry1 or (6-4) photolyases

	Record number	Organism	Common name	Seq similar to:	
1	Q4PCL9	*U.maydis*	fungus	bilateral/(6-4)	full-length sequence retrieved
2	Q4I7P3	*G.zeae*	fungus	bilateral/(6-4)	full-length sequence retrieved

Cyanidioschyzon merolae **Genome Project**
Searching database with AtCry1

	Record number	Organism	Common name	Seq similar to:	
1	CMM076C	*C.merolae*	red algae	plant	full-length sequence retrieved

TIGR Gene Indices
Searching database with hCry1

	Record number	Organism	Common name	Seq similar to:	
1	TC7521	*Spisula solidisissima*	clam	bilateral	full-length sequence retrieved

APPENDIX 5: Mean PONDR VL-XT values for photolyase and cryptochrome PLD and CT domains

Protein	Accession #	PLD (aa)	PLD Disorder	CT (aa)	CT Disorder
hCry1	NP_004066	479	0.1899	107	0.6879
hCry2	NP_0066940	498	0.2487	96	0.6768
mCry1	AAH22174	479	0.1866	128	0.8124
mCry2	NP_034093	497	0.2482	95	0.7276
rCry1	NP_942045	479	0.1865	109	0.8549
rCry2	NP_596896	497	0.2507	97	0.7035
chCry1	NP_989576	479	0.2120	142	0.7160
chCry2	NP_989575	488	0.2216	94	0.6497
xCry1	AAK94665	479	0.1927	137	0.7787
xCry2a	AAK94666	407*	0.2315	94	0.6483
xCry2b	AAK94667	483	0.2152	87	0.6497
zCry1a	NP_571864	479	0.2119	77	0.5938
zCry1b	NP_571865	479	0.2088	127	0.5949
zCry2a	NP_571866	479	0.1930	176	0.6866
zCry2b	NP_571867	481	0.2267	157	0.6743
zCry3	NP_571861	479	0.2219	119	0.8222
zCry4	NP_571862	476	0.1649	82	0.6422
zCry5	NP_571863	478	0.2508	40	0.8032
AtCry1	NP_567341	479	0.1649	202	0.7320
AtCry2	NP_849588	476	0.2031	136	0.6512
AtCry3	NP_568461	482	0.2600	43	0.7387
OsCry1a	BAB70686	488	0.2418	222	0.6384
OsCry1b	BAB70688	488	0.2554	212	0.5606
OsCry2	CAP35495	476	0.1992	175	0.5560
PsCry1	AAO23970	472	0.2066	210	0.6501
PsCry2b	AAO23972	472	0.1668	125	0.6136
ArmCry2	BAC67179	416	0.1883	141	0.6695
LeCry1b	AAL02094	472	0.2003	207	0.5658
LeCry2	AAF72556	473	0.1719	162	0.6137
xCryD	BAD08601	479	0.2735	44	0.6133
zCryD	NP_991249	478	0.2017	42	0.6352
RcCry2	AAP13561	484	0.2128	59	0.7075
MfCry1	BAB72089	479	0.1886	107	0.6864
SbCry2	AAN37909	485	0.2480	206	0.5544
PpCry	BAB70665	475	0.2302	252	0.6049
AcCry2	BAA32808	477	0.2061	202	0.5771
AcCry3	BAA32809	474	0.2185	244	0.5237
VcCry2	NP_231036	458	0.1697	46	0.6817
d(6-4)	NP_724274	497	0.2160	43	0.8797
z(6-4)	BAA96852	475	0.2479	44	0.7895
AnthpCry	AAK11644	484	0.1749	41	0.4058
AnopCry	21288977	507	0.1823	46	0.5106
SarcoCry	BAB85473	173*	0.1421	43	0.5941
dCry	NP_732407	502	0.1403	40	0.4916
AcCry1	BAA32807	471	0.2380	166	0.4720
SynCryD	1NP7_A	489	0.1225	0	---
VcCry1	NP_231448	461	0.1377	4	---
GvCry	NP_923781	484	0.2348	16	---
MesoCry	NP_108272	477	0.2408	5	---
BradyCry	AP005954†	442*	0.3430	3	---
RhodoCry	ZP_00012696	483	0.2360	5	---
AgroCry	AAK87020	479	0.2864	6	---
BurkCry	ZP_00031703	529	0.2134	4	---
RalstCry	ZP_0025079	513	0.2661	8	---
VcPhr	NP_232458	469	0.1715	0	---
EcPhr	P00914	471	0.2495	0	---
dPhr	NP_724613	640	0.2155	0	---
AtPhr	NP_849651	488	0.2657	8	---

* N-terminal truncated sequence in GenBank

† Genome sequence; gene # blr5310

REFERENCES

Adams, M. D., Kerlavage, A. R., Fleischmann, R. D., Fuldner, R. A., Bult, C. J., Lee, N. H., Kirkness, E. F., Weinstock, K. G., Gocayne, J. D., White, O., and et al. (1995). Initial assessment of human gene diversity and expression patterns based upon 83 million nucleotides of cDNA sequence. Nature *377*, 3-174.

Ahmad, M., and Cashmore, A. R. (1993). HY4 gene of *A. thaliana* encodes a protein with characteristics of a blue-light photoreceptor. Nature *366*, 162-166.

Ahmad, M., Jarillo, J. A., and Cashmore, A. R. (1998a). Chimeric proteins between cry1 and cry2 *Arabidopsis* blue light photoreceptors indicate overlapping functions and varying protein stability. Plant Cell *10*, 197-207.

Ahmad, M., Jarillo, J. A., Smirnova, O., and Cashmore, A. R. (1998b). The CRY1 blue light photoreceptor of *Arabidopsis* interacts with phytochrome A in vitro. Mol Cell *1*, 939-948.

Akashi, M., Tsuchiya, Y., Yoshino, T., and Nishida, E. (2002). Control of intracellular dynamics of mammalian period proteins by casein kinase I epsilon (CKI epsilon) and CKI delta in cultured cells. Mol Cell Biol *22*, 1693-1703.

Ali, A., Zhang, J., Bao, S., Liu, I., Otterness, D., Dean, N. M., Abraham, R. T., and Wang, X. F. (2004). Requirement of protein phosphatase 5 in DNA-damage-induced ATM activation. Genes Dev *18*, 249-254.

Ang, L. H., Chattopadhyay, S., Wei, N., Oyama, T., Okada, K., Batschauer, A., and Deng, X. W. (1998). Molecular interaction between COP1 and HY5 defines a regulatory switch for light control of *Arabidopsis* development. Mol Cell *1*, 213-222.

Aronin, N., Sagar, S. M., Sharp, F. R., and Schwartz, W. J. (1990). Light regulates expression of a Fos-related protein in rat suprachiasmatic nuclei. Proc Natl Acad Sci USA *87*, 5959-5962.

Ashmore, L. J., and Sehgal, A. (2003). A fly's eye view of circadian entrainment. J Biol Rhythms *18*, 206-216.

Bahl, R., Bradley, K. C., Thompson, K. J., Swain, R. A., Rossie, S., and Meisel, R. L. (2001). Localization of protein Ser/Thr phosphatase 5 in rat brain. Brain Res Mol Brain Res *90*, 101-109.

Balsalobre, A., Damiola, F., and Schibler, U. (1998). A serum shock induces circadian gene expression in mammalian tissue culture cells. Cell *93*, 929-937.

Batschauer, A. (2005). Plant Cryptochromes: Their Genes, Biochemistry, and Physiological Roles, in Handbook of Photosensory Receptors, W. R. Briggs, and Spudich, J.L., ed. (Wiley-VCH), pp. 211-246.

Beason, R., Dussourd, N., and Deutschlander, M. (1995). Behavioural evidence for the use of magnetic material in magentoreception by a migratory bird. J Exp Biol *198*, 141-146.

Bell, S., Klein, C., Muller, L., Hansen, S., and Buchner, J. (2002). p53 contains large

unstructured regions in its native state. J Mol Biol *322*, 917-927.

Bender, R. A. (1984). Ultraviolet mutagenesis and inducible DNA repair in *Caulobacter crescentus*. Mol Gen Genet *197*, 399-402.

Berman-Frank, I., Lundgren, P., Chen, Y. B., Kupper, H., Kolber, Z., Bergman, B., and Falkowski, P. (2001). Segregation of nitrogen fixation and oxygenic photosynthesis in the marine cyanobacterium *Trichodesmium*. Science *294*, 1534-1537.

Berman-Frank, I., Lundgren, P., and Falkowski, P. (2003). Nitrogen fixation and photosynthetic oxygen evolution in cyanobacteria. Res Microbiol *154*, 157-164.

Berson, D. M., Dunn, F. A., and Takao, M. (2002). Phototransduction by retinal ganglion cells that set the circadian clock. Science *295*, 1070-1073.

Bird, R. E., Hulstrom, R. L., and Lewis, L. J. (1983). Terrestrial solar spectral data sets. Solar Energy *30*.

Borthwick, E. B., Zeke, T., Prescott, A. R., and Cohen, P. T. (2001). Nuclear localization of protein phosphatase 5 is dependent on the carboxy-terminal region. FEBS Lett *491*, 279-284.

Bouly, J. P., Giovani, B., Djamei, A., Mueller, M., Zeugner, A., Dudkin, E. A., Batschauer, A., and Ahmad, M. (2003). Novel ATP-binding and autophosphorylation activity associated with *Arabidopsis* and human cryptochrome-1. Eur J Biochem *270*, 2921-2928.

Brautigam, C. A., Smith, B. S., Ma, Z., Palnitkar, M., Tomchick, D. R., Machius, M., and Deisenhofer, J. (2004). Structure of the photolyase-like domain of cryptochrome 1 from *Arabidopsis thaliana*. Proc Natl Acad Sci USA *101*, 12142-12147.

Briggs, W. R., Christie, J. M., and Salomon, M. (2001). Phototropins: a new family of flavin binding blue light receptors in plants. Antioxid Redox Signal *3*, 775-788.

Brudler, R., Hitomi, K., Daiyasu, H., Toh, H., Kucho, K., Ishiura, M., Kanehisa, M., Roberts, V. A., Todo, T., Tainer, J. A., and Getzoff, E. D. (2003). Identification of a new cryptochrome class. Structure, function, and evolution. Mol Cell *11*, 59-67.

Bunger, M. K., Wilsbacher, L. D., Moran, S. M., Clendenin, C., Radcliffe, L. A., Hogenesch, J. B., Simon, M. C., Takahashi, J. S., and Bradfield, C. A. (2000). Mop3 is an essential component of the master circadian pacemaker in mammals. Cell *103*, 1009-1017.

Busza, A., Emery-Le, M., Rosbash, M., and Emery, P. (2004). Roles of the two *Drosophila* CRYPTOCHROME structural domains in circadian photoreception. Science *304*, 1503-1506.

Cardone, L., Hirayama, J., Giordano, F., Tamaru, T., Palvimo, J. J., and Sassone-Corsi, P. (2005). Circadian clock control by SUMOylation of BMAL1. Science *309*, 1390-1394.

Cashmore, A. R. (2003). Cryptochromes: enabling plants and animals to determine circadian time. Cell *114*, 537-543.

Cashmore, A. R., Jarillo, J. A., Wu, Y. J., and Liu, D. (1999). Cryptochromes: blue light receptors for plants and animals. Science *284*, 760-765.

Cegielska, A., Gietzen, K. F., Rivers, A., and Virshup, D. M. (1998). Autoinhibition of casein kinase I epsilon (CKI epsilon) is relieved by protein phosphatases and limited proteolysis. J Biol Chem *273*, 1357-1364.

Ceriani, M. F., Darlington, T. K., Staknis, D., Mas, P., Petti, A. A., Weitz, C. J., and Kay, S. A. (1999). Light-dependent sequestration of TIMELESS by CRYPTOCHROME. Science *285*, 553-556.

Cermakian, N., Pando, M. P., Thompson, C. L., Pinchak, A. B., Selby, C. P., Gutierrez, L., Wells, D. E., Cahill, G. M., Sancar, A., and Sassone-Corsi, P. (2002). Light induction of a vertebrate clock gene involves signaling through blue-light receptors and MAP kinases. Curr Biol *12*, 844-848.

Chaves, I., Yagita, K., Barnhoorn, S., Okamura, H., van der Horst, G. T., and Tamanini, F. (2006). Functional evolution of the photolyase/cryptochrome protein family: importance of the C terminus of mammalian CRY1 for circadian core oscillator performance. Mol Cell Biol *26*, 1743-1753.

Cho, H. S., Liu, C. W., Damberger, F. F., Pelton, J. G., Nelson, H. C., and Wemmer, D. E. (1996). Yeast heat shock transcription factor N-terminal activation domains are unstructured as probed by heteronuclear NMR spectroscopy. Protein Sci *5*, 262-269.

Collins, B., Mazzoni, E. O., Stanewsky, R., and Blau, J. (2006). *Drosophila* CRYPTOCHROME Is a Circadian Transcriptional Repressor. Curr Biol *16*, 441-449.

Daiyasu, H., Ishikawa, T., Kuma, K., Iwai, S., Todo, T., and Toh, H. (2004). Identification of cryptochrome DASH from vertebrates. Genes Cells *9*, 479-495.

Davis-Searles, P. R., Saunders, A. J., Erie, D. A., Winzor, D. J., and Pielak, G. J. (2001). Interpreting the effects of small uncharged solutes on protein-folding equilibria. Annu Rev Biophys Biomol Struct *30*, 271-306.

De Robertis, E. M., and Sasai, Y. (1996). A common plan for dorsoventral patterning in Bilateria. Nature *380*, 37-40.

DeCoursey, P. J., and Krulas, J. R. (1998). Behavior of SCN-lesioned chipmunks in natural habitat: a pilot study. J Biol Rhythms *13*, 229-244.

DeCoursey, P. J., Krulas, J. R., Mele, G., and Holley, D. C. (1997). Circadian performance of suprachiasmatic nuclei (SCN)-lesioned antelope ground squirrels in a desert enclosure. Physiol Behav *62*, 1099-1108.

Dedmon, M. M., Patel, C. N., Young, G. B., and Pielak, G. J. (2002). FlgM gains structure in living cells. Proc Natl Acad Sci USA *99*, 12681-12684.

Dehal, P., Satou, Y., Campbell, R. K., Chapman, J., Degnan, B., De Tomaso, A., Davidson, B., Di Gregorio, A., Gelpke, M., Goodstein, D. M.*, et al.* (2002). The draft genome of *Ciona intestinalis*: insights into chordate and vertebrate origins. Science *298*, 2157-2167.

Delaglio, F., Grzesiek, S., Vuister, G. W., Zhu, G., Pfeifer, J., and Bax, A. (1995). NMRPipe: a multidimensional spectral processing system based on UNIX pipes. J Biomol NMR *6*, 277-293.

Dey, J., Carr, A. J., Cagampang, F. R., Semikhodskii, A. S., Loudon, A. S., Hastings, M. H., and Maywood, E. S. (2005). The tau mutation in the Syrian hamster differentially reprograms the circadian clock in the SCN and peripheral tissues. J Biol Rhythms *20*, 99-110.

DiGiammarino, E. L., Filippov, I., Weber, J. D., Bothner, B., and Kriwacki, R. W. (2001). Solution structure of the p53 regulatory domain of the p19Arf tumor suppressor protein. Biochemistry *40*, 2379-2386.

Dissel, S., Codd, V., Fedic, R., Garner, K. J., Costa, R., Kyriacou, C. P., and Rosato, E. (2004). A constitutively active cryptochrome in *Drosophila melanogaster*. Nat Neurosci *7*, 834-840.

Donne, D. G., Viles, J. H., Groth, D., Mehlhorn, I., James, T. L., Cohen, F. E., Prusiner, S. B., Wright, P. E., and Dyson, H. J. (1997). Structure of the recombinant full-length hamster prion protein PrP(29-231): the N terminus is highly flexible. Proc Natl Acad Sci USA *94*, 13452-13457.

Doolittle, R. F. (1994). Convergent evolution: the need to be explicit. Trends Biochem Sci *19*, 15-18.

Duek, P. D., Elmer, M. V., van Oosten, V. R., and Fankhauser, C. (2004). The degradation of HFR1, a putative bHLH class transcription factor involved in light signaling, is regulated by phosphorylation and requires COP1. Curr Biol *14*, 2296-2301.

Dunker, A. K., Obradovic, Z., Romero, P., Garner, E. C., and Brown, C. J. (2000). Intrinsic protein disorder in complete genomes. Genome Inform Ser Workshop Genome Inform *11*, 161-171.

Dvornyk, V., and Knudsen, B. (2005). Functional divergence of the circadian clock proteins in prokaryotes. Genetica *124*, 247-254.

Dyson, H. J., and Wright, P. E. (2002). Coupling of folding and binding for unstructured proteins. Curr Opin Struct Biol *12*, 54-60.

Ebihara, S., and Tsuji, K. (1980). Entrainment of the circadian activity rhythm to the light cycle: effective light intensity for a Zeitgeber in the retinal degenerate C3H mouse and the normal C57BL mouse. Physiol Behav *24*, 523-527.

Ebisawa, T., Uchiyama, M., Kajimura, N., Mishima, K., Kamei, Y., Katoh, M., Watanabe, T., Sekimoto, M., Shibui, K., Kim, K.*, et al.* (2001). Association of structural polymorphisms in the human period3 gene with delayed sleep phase syndrome. Embo Rep *2*, 342-346.

Edmonds, D. (1996). A sensitive optically detected magnetic compass for animals. Proc R Soc B *263*, 295-298.

Eide, E. J., Vielhaber, E. L., Hinz, W. A., and Virshup, D. M. (2002). The circadian regulatory

proteins BMAL1 and cryptochromes are substrates of casein kinase Iepsilon. J Biol Chem *277*, 17248-17254.

Eide, E. J., Woolf, M. F., Kang, H., Woolf, P., Hurst, W., Camacho, F., Vielhaber, E. L., Giovanni, A., and Virshup, D. M. (2005). Control of mammalian circadian rhythm by CKIepsilon-regulated proteasome-mediated PER2 degradation. Mol Cell Biol *25*, 2795-2807.

Emery, P., Stanewsky, R., Hall, J. C., and Rosbash, M. (2000a). A unique circadian-rhythm photoreceptor. Nature *404*, 456-457.

Emery, P., Stanewsky, R., Helfrich-Forster, C., Emery-Le, M., Hall, J. C., and Rosbash, M. (2000b). *Drosophila* CRY is a deep brain circadian photoreceptor. Neuron *26*, 493-504.

Esteve, V., Canela, N., Rodriguez-Vilarrupla, A., Aligue, R., Agell, N., Mingarro, I., Bachs, O., and Perez-Paya, E. (2003). The structural plasticity of the C terminus of p21Cip1 is a determinant for target protein recognition. Chembiochem *4*, 863-869.

Farrow, N. A., Muhandiram, R., Singer, A. U., Pascal, S. M., Kay, C. M., Gish, G., Shoelson, S. E., Pawson, T., Forman-Kay, J. D., and Kay, L. E. (1994). Backbone dynamics of a free and phosphopeptide-complexed Src homology 2 domain studied by ^{15}N NMR relaxation. Biochemistry *33*, 5984-6003.

Farrow, N. A., Zhang, O., Forman-Kay, J. D., and Kay, L. E. (1997). Characterization of the backbone dynamics of folded and denatured states of an SH3 domain. Biochemistry *36*, 2390-2402.

Folta, K. M., Pontin, M. A., Karlin-Neumann, G., Bottini, R., and Spalding, E. P. (2003). Genomic and physiological studies of early cryptochrome 1 action demonstrate roles for auxin and gibberellin in the control of hypocotyl growth by blue light. Plant J *36*, 203-214.

Fontana, A., De Laureto, P. P., Spolaore, B., Frare, E., Picotti, P., and Zambonin, M. (2004). Probing protein structure by limited proteolysis. Acta Biochim Pol *51*, 299-321.

Frank, K. D., and Zimmerman, W. F. (1969). Action spectra for phase shifts of a circadian rhythm in *Drosophila*. Science *163*, 688-689.

Froy, O., Chang, D. C., and Reppert, S. M. (2002). Redox potential: differential roles in dCRY and mCRY1 functions. Curr Biol *12*, 147-152.

Fuxreiter, M., Simon, I., Friedrich, P., and Tompa, P. (2004). Preformed structural elements feature in partner recognition by intrinsically unstructured proteins. J Mol Biol *338*, 1015-1026.

Gehring, W., and Rosbash, M. (2003). The coevolution of blue-light photoreception and circadian rhythms. J Mol Evol *57 Suppl 1*, S286-289.

Gekakis, N., Staknis, D., Nguyen, H. B., Davis, F. C., Wilsbacher, L. D., King, D. P., Takahashi, J. S., and Weitz, C. J. (1998). Role of the CLOCK protein in the mammalian circadian mechanism. Science *280*, 1564-1569.

Giebultowicz, J. M., Stanewsky, R., Hall, J. C., and Hege, D. M. (2000). Transplanted *Drosophila* excretory tubules maintain circadian clock cycling out of phase with the host. Curr Biol *10*, 107-110.

Gietzen, K. F., and Virshup, D. M. (1999). Identification of inhibitory autophosphorylation sites in casein kinase I epsilon. J Biol Chem *274*, 32063-32070.

Giovani, B., Byrdin, M., Ahmad, M., and Brettel, K. (2003). Light-induced electron transfer in a cryptochrome blue-light photoreceptor. Nat Struct Biol *10*, 489-490.

Goehring, L., and Oberhauser, K. S. (2002). Effects of photoperiod, temperature, and host plant age on induction of reproductive diapause and development time in *Danaus plexippus*. Ecol Entomol *27*, 674-685.

Green, R. M., Tingay, S., Wang, Z. Y., and Tobin, E. M. (2002). Circadian rhythms confer a higher level of fitness to *Arabidopsis* plants. Plant Physiol *129*, 576-584.

Griffin, E. A., Jr., Staknis, D., and Weitz, C. J. (1999). Light-independent role of CRY1 and CRY2 in the mammalian circadian clock. Science *286*, 768-771.

Guido, M. E., Goguen, D., De Guido, L., Robertson, H. A., and Rusak, B. (1999). Circadian and photic regulation of immediate-early gene expression in the hamster suprachiasmatic nucleus. Neuroscience *90*, 555-571.

Harper, S. M., Neil, L. C., and Gardner, K. H. (2003). Structural basis of a phototropin light switch. Science *301*, 1541-1544.

Hattar, S., Liao, H. W., Takao, M., Berson, D. M., and Yau, K. W. (2002). Melanopsin containing retinal ganglion cells: architecture, projections, and intrinsic photosensitivity. Science *295*, 1065-1070.

Hattar, S., Lucas, R. J., Mrosovsky, N., Thompson, S., Douglas, R. H., Hankins, M. W., Lem, J., Biel, M., Hofmann, F., Foster, R. G., and Yau, K. W. (2003). Melanopsin and rod-cone photoreceptive systems account for all major accessory visual functions in mice. Nature *424*, 76-81.

Hedges, S. B., Blair, J. E., Venturi, M. L., and Shoe, J. L. (2004). A molecular timescale of eukaryote evolution and the rise of complex multicellular life. BMC Evol Biol *4*, 2.

Heelis, P. F., and Sancar, A. (1986). Photochemical properties of *Escherichia coli* DNA photolyase: a flash photolysis study. Biochemistry *25*, 8163-8166.

Helfrich-Forster, C., Winter, C., Hofbauer, A., Hall, J. C., and Stanewsky, R. (2001). The circadian clock of fruit flies is blind after elimination of all known photoreceptors. Neuron *30*, 249-261.

Herzog, E. D., and Huckfeldt, R. M. (2003). Circadian entrainment to temperature, but not light, in the isolated suprachiasmatic nucleus. J Neurophysiol *90*, 763-770.

Hirayama, J., Nakamura, H., Ishikawa, T., Kobayashi, Y., and Todo, T. (2003). Functional and structural analyses of cryptochrome. Vertebrate CRY regions responsible for interaction

with the CLOCK:BMAL1 heterodimer and its nuclear localization. J Biol Chem *278*, 35620-35628.

Hitomi, K., Okamoto, K., Daiyasu, H., Miyashita, H., Iwai, S., Toh, H., Ishiura, M., and Todo, T. (2000). Bacterial cryptochrome and photolyase: characterization of two photolyase-like genes of *Synechocystis* sp. PCC6803. Nucleic Acids Res *28*, 2353-2362.

Hoffman, P. D., Batschauer, A., and Hays, J. B. (1996). PHH1, a novel gene from *Arabidopsis thaliana* that encodes a protein similar to plant blue-light photoreceptors and microbial photolyases. Mol Gen Genet *253*, 259-265.

Holm, M., Hardtke, C. S., Gaudet, R., and Deng, X. W. (2001). Identification of a structural motif that confers specific interaction with the WD40 repeat domain of *Arabidopsis* COP1. Embo J *20*, 118-127.

Hsu, D. S., Zhao, X., Zhao, S., Kazantsev, A., Wang, R. P., Todo, T., Wei, Y. F., and Sancar, A. (1996). Putative human blue-light photoreceptors hCRY1 and hCRY2 are flavoproteins. Biochemistry *35*, 13871-13877.

Hunter-Ensor, M., Ousley, A., and Sehgal, A. (1996). Regulation of the *Drosophila* protein timeless suggests a mechanism for resetting the circadian clock by light. Cell *84*, 677-685.

Husain, I., and Sancar, A. (1987). Photoreactivation in phr mutants of *Escherichia coli* K-12. J Bacteriol *169*, 2367-2372.

Husain, I., Sancar, G. B., Holbrook, S. R., and Sancar, A. (1987). Mechanism of damage recognition by *Escherichia coli* DNA photolyase. J Biol Chem *262*, 13188-13197.

Iakoucheva, L. M., Brown, C. J., Lawson, J. D., Obradovic, Z., and Dunker, A. K. (2002). Intrinsic disorder in cell-signaling and cancer-associated proteins. J Mol Biol *323*, 573-584.

Iakoucheva, L. M., Radivojac, P., Brown, C. J., O'Connor, T. R., Sikes, J. G., Obradovic, Z., and Dunker, A. K. (2004). The importance of intrinsic disorder for protein phosphorylation. Nucleic Acids Res *32*, 1037-1049.

Iitaka, C., Miyazaki, K., Akaike, T., and Ishida, N. (2005). A role for glycogen synthase kinase-3 beta in the mammalian circadian clock. J Biol Chem *280*, 29397-29402.

Irwin, W. P., and Lohmann, K. J. (2005). Disruption of magnetic orientation in hatchling loggerhead sea turtles by pulsed magnetic fields. J Comp Physiol A Neuroethol Sens Neural Behav Physiol *191*, 475-480.

Ishida, Y., Yagita, K., Fukuyama, T., Nishimura, M., Nagano, M., Shigeyoshi, Y., Yamaguchi, S., Komori, T., and Okamura, H. (2001). Constitutive expression and delayed light response of casein kinase I epsilon and I delta mRNAs in the mouse suprachiasmatic nucleus. J Neurosci Res *64*, 612-616.

Ivanchenko, M., Stanewsky, R., and Giebultowicz, J. M. (2001). Circadian photoreception in *Drosophila*: functions of cryptochrome in peripheral and central clocks. J Biol Rhythms *16*, 205-215.

Johnson, B. A. (1994). NMRView: A computer program for the visualization and analysis of NMR data. J Biomol NMR *4*, 603-614.

Johnson, J. L., Hamm-Alvarez, S., Payne, G., Sancar, G. B., Rajagopalan, K. V., and Sancar, A. (1988a). Identification of the second chromophore of *Escherichia coli* and yeast DNA photolyases as 5,10-methenyltetrahydrofolate. Proc Natl Acad Sci USA *85*, 2046-2050.

Johnson, R. F., Moore, R. Y., and Morin, L. P. (1988b). Loss of entrainment and anatomical plasticity after lesions of the hamster retinohypothalamic tract. Brain Res *460*, 297-313.

Kanai, S., Kikuno, R., Toh, H., Ryo, H., and Todo, T. (1997). Molecular evolution of the photolyase-blue-light photoreceptor family. J Mol Evol *45*, 535-548.

Kavakli, I. H. and Sancar, A. (2004). Analysis of the role of intraprotein electron transfer in photoreduction by DNA photolyase in vivo. Biochemistry, *43*, 15103-15110.

Kihara, J., Moriwaki, A., Matsuo, N., Arase, S., and Honda, Y. (2004). Cloning, functional characterization, and near-ultraviolet radiation-enhanced expression of a photolyase gene (PHR1) from the phytopathogenic fungus *Bipolaris oryzae*. Curr Genet *46*, 37-46.

Kim, J. I., Shen, Y., Han, Y. J., Park, J. E., Kirchenbauer, D., Soh, M. S., Nagy, F., Schafer, E., and Song, P. S. (2004). Phytochrome phosphorylation modulates light signaling by influencing the protein-protein interaction. Plant Cell *16*, 2629-2640.

Kirschvink, J. L., and Gould, J. L. (1981). Biogenic magnetite as a basis for magnetic field detection in animals. Biosystems *13*, 181-201.

Kirschvink, J. L., Walker, M., Chang, S., Dizon, A., and Peterson, K. (1985). Chains of single-domain magnetite particles in chinook salmon. J Comp Physiol *157*, 375-381.

Kleine, T., Lockhart, P., and Batschauer, A. (2003). An *Arabidopsis* protein closely related to *Synechocystis* cryptochrome is targeted to organelles. Plant J *35*, 93-103.

Klemm, E., and Ninneman, H. (1976). Detailed action spectrum for the delay shift in pupae emergence of *Drosophila pseudoobscura*. Photochem Photobiol *24*, 369-371.

Kloss, B., Price, J. L., Saez, L., Blau, J., Rothenfluh, A., Wesley, C. S., and Young, M. W. (1998). The *Drosophila* clock gene double-time encodes a protein closely related to human casein kinase I epsilon. Cell *94*, 97-107.

Knippschild, U., Wolff, S., Giamas, G., Brockschmidt, C., Wittau, M., Wurl, P. U., Eismann, T., and Stoter, M. (2005). The Role of the Casein Kinase 1 (CK1) Family in Different Signaling Pathways Linked to Cancer Development. Onkologie *28*, 508-514.

Knudson, G. B. (1985). Photoreactivation of UV-irradiated *Legionella pneumophila* and other *Legionella species*. Appl Environ Microbiol *49*, 975-980.

Knudson, G. B. (1986). Photoreactivation of ultraviolet-irradiated, plasmid-bearing, and plasmid-free strains of *Bacillus anthracis*. Appl Environ Microbiol *52*, 444-449.

Kobayashi, Y., Ishikawa, T., Hirayama, J., Daiyasu, H., Kanai, S., Toh, H., Fukuda, I., Tsujimura, T., Terada, N., Kamei, Y.*, et al.* (2000). Molecular analysis of zebrafish photolyase/cryptochrome family: two types of cryptochromes present in zebrafish. Genes Cells *5*, 725-738.

Kohn, W. D., Mant, C. T., and Hodges, R. S. (1997). Alpha-helical protein assembly motifs. J Biol Chem *272*, 2583-2586.

Komori, H., Masui, R., Kuramitsu, S., Yokoyama, S., Shibata, T., Inoue, Y., and Miki, K. (2001). Crystal structure of thermostable DNA photolyase: pyrimidine-dimer recognition mechanism. Proc Natl Acad Sci USA *98*, 13560-13565.

Kondratov, R. V., Chernov, M. V., Kondratova, A. A., Gorbacheva, V. Y., Gudkov, A. V., and Antoch, M. P. (2003). BMAL1-dependent circadian oscillation of nuclear CLOCK: posttranslational events induced by dimerization of transcriptional activators of the mammalian clock system. Genes Dev *17*, 1921-1932.

Koornneef, M., Rolf, E., and Spruit, C. J. P. (1980). Genetic control of light-inhibited hypocotyl elongation in *Arabidopsis thaliana*. Z Pflanzenphysiology *100*, 147-160.

Kornhauser, J. M., Nelson, D. E., Mayo, K. E., and Takahashi, J. S. (1990). Photic and circadian regulation of c-fos gene expression in the hamster suprachiasmatic nucleus. Neuron *5*, 127-134.

Kortschak, R. D., Samuel, G., Saint, R., and Miller, D. J. (2003). EST analysis of the cnidarian *Acropora millepora* reveals extensive gene loss and rapid sequence divergence in the model invertebrates. Curr Biol *13*, 2190-2195.

Kottke, T., Batschauer, A., Ahmad, M., and Heberle, J. (2006). Blue-Light-Induced Changes in *Arabidopsis* Cryptochrome 1 Probed by FTIR Difference Spectroscopy. Biochemistry *45*, 2472-2479.

Krylov, D. M., Wolf, Y. I., Rogozin, I. B., and Koonin, E. V. (2003). Gene loss, protein sequence divergence, gene dispensability, expression level, and interactivity are correlated in eukaryotic evolution. Genome Res *13*, 2229-2235.

Kume, K., Zylka, M. J., Sriram, S., Shearman, L. P., Weaver, D. R., Jin, X., Maywood, E. S., Hastings, M. H., and Reppert, S. M. (1999). mCRY1 and mCRY2 are essential components of the negative limb of the circadian clock feedback loop. Cell *98*, 193-205.

Lee, B. C., Croonquist, P. A., Sosnick, T. R., and Hoff, W. D. (2001a). PAS domain receptor photoactive yellow protein is converted to a molten globule state upon activation. J Biol Chem *276*, 20821-20823.

Lee, C., Bae, K., and Edery, I. (1999). PER and TIM inhibit the DNA binding activity of a *Drosophila* CLOCK-CYC/dBMAL1 heterodimer without disrupting formation of the heterodimer: a basis for circadian transcription. Mol Cell Biol *19*, 5316-5325.

Lee, C., Etchegaray, J. P., Cagampang, F. R., Loudon, A. S., and Reppert, S. M. (2001b). Posttranslational mechanisms regulate the mammalian circadian clock. Cell *107*, 855-867.

Lee, C., Weaver, D. R., and Reppert, S. M. (2004). Direct association between mouse PERIOD and CKI epsilon is critical for a functioning circadian clock. Mol Cell Biol *24*, 584-594.

Li, Y. F., Heelis, P. F., and Sancar, A. (1991). Active site of DNA photolyase: tryptophan-306 is the intrinsic hydrogen atom donor essential for flavin radical photoreduction and DNA repair in vitro. Biochemistry *30*, 6322-6329.

Li, Y. F., Kim, S. T., and Sancar, A. (1993). Evidence for lack of DNA photoreactivating enzyme in humans. Proc Natl Acad Sci USA *90*, 4389-4393.

Lichtarge, O., Bourne, H. R., and Cohen, F. E. (1996). An evolutionary trace method defines binding surfaces common to protein families. J Mol Biol *257*, 342-358.

Lin, C., Robertson, D. E., Ahmad, M., Raibekas, A. A., Jorns, M. S., Dutton, P. L., and Cashmore, A. R. (1995). Association of flavin adenine dinucleotide with the *Arabidopsis* blue light receptor CRY1. Science *269*, 968-970.

Lin, C., and Shalitin, D. (2003). Cryptochrome structure and signal transduction. Annu Rev Plant Biol *54*, 469-496.

Lin, C., and Todo, T. (2005). The cryptochromes. Genome Biology *6*, 220.

Lin, C., Yang, H., Guo, H., Mockler, T., Chen, J., and Cashmore, A. R. (1998). Enhancement of blue-light sensitivity of *Arabidopsis* seedlings by a blue light receptor cryptochrome 2. Proc Natl Acad Sci USA *95*, 2686-2690.

Lin, F. J., Song, W., Meyer-Bernstein, E., Naidoo, N., and Sehgal, A. (2001). Photic signaling by cryptochrome in the *Drosophila* circadian system. Mol Cell Biol *21*, 7287-7294.

Linding, R., Jensen, L. J., Diella, F., Bork, P., Gibson, T. J., and Russell, R. B. (2003). Protein disorder prediction: implications for structural proteomics. Structure (Camb) *11*, 1453-1459.

Litts, J. C., Kelly, J. M., and Lagarias, J. C. (1983). Structure-function studies on phytochrome. Preliminary characterization of highly purified phytochrome from *Avena sativa* enriched in the 124-kilodalton species. J Biol Chem *258*, 11025-11031.

Liu, F., Virshup, D. M., Nairn, A. C., and Greengard, P. (2002). Mechanism of regulation of casein kinase I activity by group I metabotropic glutamate receptors. J Biol Chem *277*, 45393-45399.

Lohmann, K. J., and Johnsen, S. (2000). The neurobiology of magnetoreception in vertebrate animals. Trends Neurosci *23*, 153-159.

Lowrey, P. L., Shimomura, K., Antoch, M. P., Yamazaki, S., Zemenides, P. D., Ralph, M. R., Menaker, M., and Takahashi, J. S. (2000). Positional syntenic cloning and functional characterization of the mammalian circadian mutation tau. Science *288*, 483-492.

Lucas, R. J., Hattar, S., Takao, M., Berson, D. M., Foster, R. G., and Yau, K. W. (2003). Diminished pupillary light reflex at high irradiances in melanopsin-knockout mice. Science

299, 245-247.

Lupas, A. (1996). Prediction and analysis of coiled-coil structures. Methods Enzymol *266*, 513-525.

Lupas, A., Van Dyke, M., and Stock, J. (1991). Predicting coiled coils from protein sequences. Science *252*, 1162-1164.

Ma, B., Tromp, J., and Li, M. (2002). PatternHunter: faster and more sensitive homology search. Bioinformatics *18*, 440-445.

Ma, L., Li, J., Qu, L., Hager, J., Chen, Z., Zhao, H., and Deng, X. W. (2001). Light control of *Arabidopsis* development entails coordinated regulation of genome expression and cellular pathways. Plant Cell *13*, 2589-2607.

Maeda, T., Imanishi, Y., and Palczewski, K. (2003). Rhodopsin phosphorylation: 30 years later. Prog Retin Eye Res *22*, 417-434.

Malhotra, K., Kim, S. T., Batschauer, A., Dawut, L., and Sancar, A. (1995). Putative blue light photoreceptors from *Arabidopsis thaliana* and *Sinapis alba* with a high degree of sequence homology to DNA photolyase contain the two photolyase cofactors but lack DNA repair activity. Biochemistry *34*, 6892-6899.

Matsushita, N., Mochizuki, N., and Nagatani, A. (2003). Dimers of the N-terminal domain of phytochrome B are functional in the nucleus. Nature *424*, 571-574.

Matsuzaki, M., Misumi, O., Shin, I. T., Maruyama, S., Takahara, M., Miyagishima, S. Y., Mori, T., Nishida, K., Yagisawa, F., Nishida, K.*, et al.* (2004). Genome sequence of the ultrasmall unicellular red alga *Cyanidioschyzon merolae* 10D. Nature *428*, 653-657.

Matthews, J. R., Nicholson, J., Jaffray, E., Kelly, S. M., Price, N. C., and Hay, R. T. (1995). Conformational changes induced by DNA binding of NF-kappa B. Nucleic Acids Res *23*, 3393-3402.

McDowell-Buchanan, C. M. (2006) RNA Photolyase Activity of *Vibrio cholerae* Cryptochrome 1, Ph.D. Thesis, University of Washington, Seattle.

Meador, W. E., Means, A. R., and Quiocho, F. A. (1992). Target enzyme recognition by calmodulin: 2.4 A structure of a calmodulin-peptide complex. Science *257*, 1251-1255.

Meek, S., Morrice, N., and MacKintosh, C. (1999). Microcystin affinity purification of plant protein phosphatases: PP1C, PP5 and a regulatory A-subunit of PP2A. FEBS Lett *457*, 494-498.

Mees, A., Klar, T., Gnau, P., Hennecke, U., Eker, A. P., Carell, T., and Essen, L. O. (2004). Crystal structure of a photolyase bound to a CPD-like DNA lesion after in situ repair. Science *306*, 1789-1793.

Melyan, Z., Tarttelin, E. E., Bellingham, J., Lucas, R. J., and Hankins, M. W. (2005). Addition of human melanopsin renders mammalian cells photoresponsive. Nature *433*, 741-745.

Michael, T. P., Salome, P. A., Yu, H. J., Spencer, T. R., Sharp, E. L., McPeek, M. A., Alonso, J. M., Ecker, J. R., and McClung, C. R. (2003). Enhanced fitness conferred by naturally occurring variation in the circadian clock. Science *302*, 1049-1053.

Miyamoto, Y., and Sancar, A. (1998). Vitamin B2-based blue-light photoreceptors in the retinohypothalamic tract as the photoactive pigments for setting the circadian clock in mammals. Proc Natl Acad Sci USA *95*, 6097-6102.

Miyamoto, Y., and Sancar, A. (1999). Circadian regulation of cryptochrome genes in the mouse. Brain Res Mol Brain Res *71*, 238-243.

Miyazaki, K., Nagase, T., Mesaki, M., Narukawa, J., Ohara, O., and Ishida, N. (2004). Phosphorylation of clock protein PER1 regulates its circadian degradation in normal human fibroblasts. Biochem J *380*, 95-103.

Mockler, T., Yang, H., Yu, X., Parikh, D., Cheng, Y. C., Dolan, S., and Lin, C. (2003). Regulation of photoperiodic flowering by *Arabidopsis* photoreceptors. Proc Natl Acad Sci USA *100*, 2140-2145.

Moller, A., Sagasser, S., Wiltschko, W., and Schierwater, B. (2004). Retinal cryptochrome in a migratory passerine bird: a possible transducer for the avian magnetic compass. Naturwissenschaften *91*, 585-588.

Morita, K., Saitoh, M., Tobiume, K., Matsuura, H., Enomoto, S., Nishitoh, H., and Ichijo, H. (2001). Negative feedback regulation of ASK1 by protein phosphatase 5 (PP5) in response to oxidative stress. Embo J *20*, 6028-6036.

Mouritsen, H., Janssen-Bienhold, U., Liedvogel, M., Feenders, G., Stalleicken, J., Dirks, P., and Weiler, R. (2004). Cryptochromes and neuronal-activity markers colocalize in the retina of migratory birds during magnetic orientation. Proc Natl Acad Sci USA *101*, 14294-14299.

Mrosovsky, N. (1999). Masking: history, definitions, and measurement. Chronobiol Int *16*, 415-429.

Mulkidjanian, A. Y., Cherepanov, D. A., and Galperin, M. Y. (2003). Survival of the fittest before the beginning of life: selection of the first oligonucleotide-like polymers by UV light. BMC Evol Biol *3*, 12.

Nagoshi, E., Saini, C., Bauer, C., Laroche, T., Naef, F., and Schibler, U. (2004). Circadian gene expression in individual fibroblasts: cell-autonomous and self-sustained oscillators pass time to daughter cells. Cell *119*, 693-705.

Naidoo, N., Song, W., Hunter-Ensor, M., and Sehgal, A. (1999). A role for the proteasome in the light response of the timeless clock protein. Science *285*, 1737-1741.

Nakamura, Y., Kaneko, T., Sato, S., Mimuro, M., Miyashita, H., Tsuchiya, T., Sasamoto, S., Watanabe, A., Kawashima, K., Kishida, Y*., et al.* (2003). Complete genome structure of *Gloeobacter violaceus* PCC 7421, a cyanobacterium that lacks thylakoids. DNA Res *10*, 137-145.

Naruse, Y., Oh-hashi, K., Iijima, N., Naruse, M., Yoshioka, H., and Tanaka, M. (2004).

Circadian and light-induced transcription of clock gene Per1 depends on histone acetylation and deacetylation. Mol Cell Biol *24*, 6278-6287.

Neduva, V., and Russell, R. B. (2005). Linear motifs: evolutionary interaction switches. FEBS Lett *579*, 3342-3345.

Ng, W. O., and Pakrasi, H. B. (2001). DNA photolyase homologs are the major UV resistance factors in the cyanobacterium *Synechocystis* sp. PCC 6803. Mol Gen Genet *264*, 924-930.

Nikaido, S. S., and Johnson, C. H. (2000). Daily and circadian variation in survival from ultraviolet radiation in *Chlamydomonas reinhardtii*. Photochem Photobiol *71*, 758-765.

Ohata, K., Nishiyama, H., and Tsukahara, Y. (1998). Action spectrum of the circadian clock photoreceptor in *Drosophila melanogaster*, in Biological Clocks: Mechanisms and Applications, Y. Touitou, ed. (Amsterdam: Elsevier).

Okada, T., Ernst, O. P., Palczewski, K., and Hofmann, K. P. (2001). Activation of rhodopsin: new insights from structural and biochemical studies. Trends Biochem Sci *26*, 318-324.

Oro, J., Miller, S. L., and Lazcano, A. (1990). The origin and early evolution of life on Earth. Annu Rev Earth Planet Sci *18*, 317-356.

Osterlund, M. T., and Deng, X. W. (1998). Multiple photoreceptors mediate the light-induced reduction of GUS-COP1 from *Arabidopsis* hypocotyl nuclei. Plant J *16*, 201-208.

Osterlund, M. T., Hardtke, C. S., Wei, N., and Deng, X. W. (2000). Targeted destabilization of HY5 during light-regulated development of *Arabidopsis*. Nature *405*, 462-466.

Ouyang, Y., Andersson, C. R., Kondo, T., Golden, S. S., and Johnson, C. H. (1998). Resonating circadian clocks enhance fitness in cyanobacteria. Proc Natl Acad Sci USA *95*, 8660-8664.

Özgür, S. (2005) Purification and properties of human cryptochrome 2, PhD Thesis, University of North Carolina, Chapel Hill.

Özgür, S., and Sancar, A. (2003). Purification and properties of human blue-light photoreceptor cryptochrome 2. Biochemistry *42*, 2926-2932.

Panda, S., Nayak, S. K., Campo, B., Walker, J. R., Hogenesch, J. B., and Jegla, T. (2005). Illumination of the melanopsin signaling pathway. Science *307*, 600-604.

Panda, S., Provencio, I., Tu, D. C., Pires, S. S., Rollag, M. D., Castrucci, A. M., Pletcher, M. T., Sato, T. K., Wiltshire, T., Andahazy, M.*, et al.* (2003). Melanopsin is required for non image-forming photic responses in blind mice. Science *301*, 525-527.

Pando, M. P., Pinchak, A. B., Cermakian, N., and Sassone-Corsi, P. (2001). A cell-based system that recapitulates the dynamic light-dependent regulation of the vertebrate clock. Proc Natl Acad Sci USA *98*, 10178-10183.

Park, C. M., Bhoo, S. H., and Song, P. S. (2000). Inter-domain crosstalk in the phytochrome

molecules. Semin Cell Dev Biol *11*, 449-456.

Park, H. W., Kim, S. T., Sancar, A., and Deisenhofer, J. (1995). Crystal structure of DNA photolyase from *Escherichia coli*. Science *268*, 1866-1872.

Partch, C. L., Clarkson, M. W., Özgür, S., Lee, A. L., and Sancar, A. (2005). Role of structural plasticity in signal transduction by the cryptochrome blue-light photoreceptor. Biochemistry *44*, 3795-3805.

Partch, C. L., and Sancar, A. (2005). Photochemistry and photobiology of cryptochrome blue-light photopigments: the search for a photocycle. Photochem Photobiol *81*, 1291-1304.

Patterson, M., and Chu, G. (1989). Evidence that xeroderma pigmentosum cells from complementation group E are deficient in a homolog of yeast photolyase. Mol Cell Biol *9*, 5105-5112.

Payne, G., Heelis, P. F., Rohrs, B. R., and Sancar, A. (1987). The active form of *Escherichia coli* DNA photolyase contains a fully reduced flavin and not a flavin radical, both in vivo and in vitro. Biochemistry *26*, 7121-7127.

Pittendrigh, C. S. (1993). Temporal organization: reflections of a Darwinian clock-watcher. Annu Rev Physiol *55*, 16-54.

Prakash, S., Tian, L., Ratliff, K. S., Lehotzky, R. E., and Matouschek, A. (2004). An unstructured initiation site is required for efficient proteasome-mediated degradation. Nat Struct Mol Biol *11*, 830-837.

Preuss, F., Fan, J. Y., Kalive, M., Bao, S., Schuenemann, E., Bjes, E. S., and Price, J. L. (2004). *Drosophila* doubletime mutations which either shorten or lengthen the period of circadian rhythms decrease the protein kinase activity of casein kinase I. Mol Cell Biol *24*, 886-898.

Price, J. L., Blau, J., Rothenfluh, A., Abodeely, M., Kloss, B., and Young, M. W. (1998). double-time is a novel *Drosophila* clock gene that regulates PERIOD protein accumulation. Cell *94*, 83-95.

Provencio, I., Rodriguez, I. R., Jiang, G., Hayes, W. P., Moreira, E. F., and Rollag, M. D. (2000). A novel human opsin in the inner retina. J Neurosci *20*, 600-605.

Qiu, X., Kumbalasiri, T., Carlson, S. M., Wong, K. Y., Krishna, V., Provencio, I., and Berson, D. M. (2005). Induction of photosensitivity by heterologous expression of melanopsin. Nature *433*, 745-749.

Qu, Y., Bolen, C. L., and Bolen, D. W. (1998). Osmolyte-driven contraction of a random coil protein. Proc Natl Acad Sci USA *95*, 9268-9273.

Quadro, L., Blaner, W. S., Salchow, D. J., Vogel, S., Piantedosi, R., Gouras, P., Freeman, S., Cosma, M. P., Colantuoni, V., and Gottesman, M. E. (1999). Impaired retinal function and vitamin A availability in mice lacking retinol-binding protein. Embo J *18*, 4633-4644.

Ragni, M. (2004). Light as an information carrier underwater. Journal of Plankton Research

26, 433-443.

Raible, F., and Arendt, D. (2004). Metazoan evolution: some animals are more equal than others. Curr Biol *14*, R106-108.

Raible, F., Tessmar-Raible, K., Osoegawa, K., Wincker, P., Jubin, C., Balavoine, G., Ferrier, D., Benes, V., de Jong, P., Weissenbach, J.*, et al.* (2005). Vertebrate-type intron-rich genes in the marine annelid *Platynereis dumerilii*. Science *310*, 1325-1326.

Ramsey, A. J., and Chinkers, M. (2002). Identification of potential physiological activators of protein phosphatase 5. Biochemistry *41*, 5625-5632.

Reppert, S. M., and Weaver, D. R. (2002). Coordination of circadian timing in mammals. Nature *418*, 935-941.

Ritz, T., Adem, S., and Schulten, K. (2000). A model for photoreceptor-based magnetoreception in birds. Biophys J *78*, 707-718.

Ritz, T., Thalau, P., Phillips, J. B., Wiltschko, R., and Wiltschko, W. (2004). Resonance effects indicate a radical-pair mechanism for avian magnetic compass. Nature *429*, 177-180.

Rivers, A., Gietzen, K. F., Vielhaber, E., and Virshup, D. M. (1998). Regulation of casein kinase I epsilon and casein kinase I delta by an in vivo futile phosphorylation cycle. J Biol Chem *273*, 15980-15984.

Romero, P., Obradovic, Z., and Dunker, A. K. (1999). Folding minimal sequences: the lower bound for sequence complexity of globular proteins. FEBS Lett *462*, 363-367.

Romero, P., Obradovic, Z., Li, X., Garner, E. C., Brown, C. J., and Dunker, A. K. (2001). Sequence complexity of disordered protein. Proteins *42*, 38-48.

Rosato, E., Codd, V., Mazzotta, G., Piccin, A., Zordan, M., Costa, R., and Kyriacou, C. P. (2001). Light-dependent interaction between *Drosophila* CRY and the clock protein PER mediated by the carboxy terminus of CRY. Curr Biol *11*, 909-917.

Rosenfeld, R., Vajda, S., and DeLisi, C. (1995). Flexible docking and design. Annu Rev Biophys Biomol Struct *24*, 677-700.

Roskoski, R., Jr. (2005). Src kinase regulation by phosphorylation and dephosphorylation. Biochem Biophys Res Commun *331*, 1-14.

Ruby, N. F., Brennan, T. J., Xie, X., Cao, V., Franken, P., Heller, H. C., and O'Hara, B. F. (2002). Role of melanopsin in circadian responses to light. Science *298*, 2211-2213.

Salghetti, S. E., Caudy, A. A., Chenoweth, J. G., and Tansey, W. P. (2001). Regulation of transcriptional activation domain function by ubiquitin. Science *293*, 1651-1653.

Sancar, A. (2000). Cryptochrome: the second photoactive pigment in the eye and its role in circadian photoreception. Annu Rev Biochem *69*, 31-67.

Sancar, A. (2003). Structure and function of DNA photolyase and cryptochrome blue-light

photoreceptors. Chem Rev *103*, 2203-2237.

Sancar, A. (2004). Regulation of the mammalian circadian clock by cryptochrome. J Biol Chem *279*, 34079-34082.

Sancar, G. B., Jorns, M. S., Payne, G., Fluke, D. J., Rupert, C. S., and Sancar, A. (1987). Action mechanism of *Escherichia coli* DNA photolyase. III. Photolysis of the enzyme substrate complex and the absolute action spectrum. J Biol Chem *262*, 492-498.

Sancar, G. B., Smith, F. W., Lorence, M. C., Rupert, C. S., and Sancar, A. (1984). Sequences of the *Escherichia coli* photolyase gene and protein. J Biol Chem *259*, 6033-6038.

Sang, Y., Li, Q. H., Rubio, V., Zhang, Y. C., Mao, J., Deng, X. W., and Yang, H. Q. (2005). N-Terminal Domain-Mediated Homodimerization Is Required for Photoreceptor Activity of *Arabidopsis* CRYPTOCHROME 1. Plant Cell *17*, 1569-1584.

Sathyanarayanan, S., Zheng, X., Xiao, R., and Sehgal, A. (2004). Posttranslational regulation of *Drosophila* PERIOD protein by protein phosphatase 2A. Cell *116*, 603-615.

Sato, T. K., Panda, S., Miraglia, L. J., Reyes, T. M., Rudic, R. D., McNamara, P., Naik, K. A., FitzGerald, G. A., Kay, S. A., and Hogenesch, J. B. (2004). A functional genomics strategy reveals Rora as a component of the mammalian circadian clock. Neuron *43*, 527-537.

Sauman, I., Briscoe, A. D., Zhu, H., Shi, D., Froy, O., Stalleicken, J., Yuan, Q., Casselman, A., and Reppert, S. M. (2005). Connecting the navigational clock to sun compass input in monarch butterfly brain. Neuron *46*, 457-467.

Saxena, C., Sancar, A., and Zhong, D. (2004). Femtosecond dynamics of DNA photolyase: energy transfer of antenna initiation and electron transfer of cofactor reduction. J Phys Chem B *108*, 18025-18033.

Saxena, C., Wang, H., Kavakli, I. H., Sancar, A., and Zhong, D. (2005). Ultrafast dynamics of resonance energy transfer in cryptochrome. J Am Chem Soc, *127*, 7984.

Schulten, K. (1982). Magnetic field effects in chemistry and biology, in Festkorperprobleme, J. Treusch, ed. (Vieweg), pp. 61-83.

Schulz, G. E. (1979). Molecular mechanism of biological recognition, in Nucleotide binding proteins, M. Balaban, ed. (New York: Elsevier/North-Holland Biomedical Press), pp. 79-94.

Selby, C. P., Thompson, C., Schmitz, T. M., Van Gelder, R. N., and Sancar, A. (2000). Functional redundancy of cryptochromes and classical photoreceptors for nonvisual ocular photoreception in mice. Proc Natl Acad Sci USA *97*, 14697-14702.

Semm, P., and Demaine, C. (1986). Neurophysiological properties of magnetic cells in the pigeon's visual system. J Comp Physiol [A] *159*, 619-625.

Shalitin, D., Yang, H., Mockler, T. C., Maymon, M., Guo, H., Whitelam, G. C., and Lin, C. (2002). Regulation of *Arabidopsis* cryptochrome 2 by blue-light-dependent phosphorylation. Nature *417*, 763-767.

Shalitin, D., Yu, X., Maymon, M., Mockler, T., and Lin, C. (2003). Blue light-dependent in vivo and in vitro phosphorylation of *Arabidopsis* cryptochrome 1. Plant Cell *15*, 2421-2429.

Shearman, L. P., Sriram, S., Weaver, D. R., Maywood, E. S., Chaves, I., Zheng, B., Kume, K., Lee, C. C., van der Horst, G. T., Hastings, M. H., and Reppert, S. M. (2000). Interacting molecular loops in the mammalian circadian clock. Science *288*, 1013-1019.

Shearman, L. P., Zylka, M. J., Weaver, D. R., Kolakowski, L. F., Jr., and Reppert, S. M. (1997). Two period homologs: circadian expression and photic regulation in the suprachiasmatic nuclei. Neuron *19*, 1261-1269.

Shenoy, S. K., Drake, M. T., Nelson, C. D., Houtz, D. A., Xiao, K., Madabushi, S., Reiter, E., Premont, R. T., Lichtarge, O., and Lefkowitz, R. J. (2006). beta-arrestin-dependent, G protein-independent ERK1/2 activation by the beta2 adrenergic receptor. J Biol Chem *281*, 1261-1273.

Shoemaker, B. A., Portman, J. J., and Wolynes, P. G. (2000). Speeding molecular recognition by using the folding funnel: the fly-casting mechanism. Proc Natl Acad Sci USA *97*, 8868-8873.

Sinclair, C., Borchers, C., Parker, C., Tomer, K., Charbonneau, H., and Rossie, S. (1999). The tetratricopeptide repeat domain and a C-terminal region control the activity of Ser/Thr protein phosphatase 5. J Biol Chem *274*, 23666-23672.

Sowa, M. E., He, W., Slep, K. C., Kercher, M. A., Lichtarge, O., and Wensel, T. G. (2001). Prediction and confirmation of a site critical for effector regulation of RGS domain activity. Nat Struct Biol *8*, 234-237.

Sowa, M. E., He, W., Wensel, T. G., and Lichtarge, O. (2000). A regulator of G protein signaling interaction surface linked to effector specificity. Proc Natl Acad Sci USA *97*, 1483-1488.

Spolar, R. S., and Record, M. T., Jr. (1994). Coupling of local folding to site-specific binding of proteins to DNA. Science *263*, 777-784.

Stanewsky, R., Kaneko, M., Emery, P., Beretta, B., Wager-Smith, K., Kay, S. A., Rosbash, M., and Hall, J. C. (1998). The *cry*^{b} mutation identifies cryptochrome as a circadian photoreceptor in *Drosophila*. Cell *95*, 681-692.

Subramanian, C., Kim, B. H., Lyssenko, N. N., Xu, X., Johnson, C. H., and von Arnim, A. G. (2004). The *Arabidopsis* repressor of light signaling, COP1, is regulated by nuclear exclusion: mutational analysis by bioluminescence resonance energy transfer. Proc Natl Acad Sci USA *101*, 6798-6802.

Swiatek, W., Tsai, I. C., Klimowski, L., Pepler, A., Barnette, J., Yost, H. J., and Virshup, D. M. (2004). Regulation of casein kinase I epsilon activity by Wnt signaling. J Biol Chem *279*, 13011-13017.

Takano, A., Isojima, Y., and Nagai, K. (2004). Identification of mPer1 phosphorylation sites responsible for the nuclear entry. J Biol Chem *279*, 32578-32585.

Tamada, T., Kitadokoro, K., Higuchi, Y., Inaka, K., Yasui, A., de Ruiter, P. E., Eker, A. P., and Miki, K. (1997). Crystal structure of DNA photolyase from *Anacystis nidulans*. Nat Struct Biol *4*, 887-891.

Tamaru, T., Isojima, Y., van der Horst, G. T., Takei, K., Nagai, K., and Takamatsu, K. (2003). Nucleocytoplasmic shuttling and phosphorylation of BMAL1 are regulated by circadian clock in cultured fibroblasts. Genes Cells *8*, 973-983.

Thompson, C. L., Blaner, W. S., Van Gelder, R. N., Lai, K., Quadro, L., Colantuoni, V., Gottesman, M. E., and Sancar, A. (2001). Preservation of light signaling to the suprachiasmatic nucleus in vitamin A-deficient mice. Proc Natl Acad Sci USA *98*, 11708-11713.

Thompson, C. L., Rickman, C. B., Shaw, S. J., Ebright, J. N., Kelly, U., Sancar, A., and Rickman, D. W. (2003). Expression of the blue-light receptor cryptochrome in the human retina. Invest Ophthalmol Vis Sci *44*, 4515-4521.

Thompson, C. L., Selby, C. P., Partch, C. L., Plante, D. T., Thresher, R. J., Araujo, F., and Sancar, A. (2004a). Further evidence for the role of cryptochromes in retinohypothalamic photoreception/phototransduction. Brain Res Mol Brain Res *122*, 158-166.

Thompson, C. L., Selby, C. P., Van Gelder, R. N., Blaner, W. S., Lee, J., Quadro, L., Lai, K., Gottesman, M. E., and Sancar, A. (2004b). Effect of vitamin A depletion on nonvisual phototransduction pathways in cryptochromeless mice. J Biol Rhythms *19*, 504-517.

Thornton, J. W., Need, E., and Crews, D. (2003). Resurrecting the ancestral steroid receptor: ancient origin of estrogen signaling. Science *301*, 1714-1717.

Thresher, R. J., Vitaterna, M. H., Miyamoto, Y., Kazantsev, A., Hsu, D. S., Petit, C., Selby, C. P., Dawut, L., Smithies, O., Takahashi, J. S., and Sancar, A. (1998). Role of mouse cryptochrome blue-light photoreceptor in circadian photoresponses. Science *282*, 1490-1494.

Todo, T. (1999). Functional diversity of the DNA photolyase/blue light receptor family. Mutat Res *434*, 89-97.

Todo, T., Ryo, H., Yamamoto, K., Toh, H., Inui, T., Ayaki, H., Nomura, T., and Ikenaga, M. (1996). Similarity among the *Drosophila* (6-4) photoyase, human photolyase homolog, and the DNA photolyase-bllue-light photoreceptor family. Science *272*, 109-112.

Toh, K. L., Jones, C. R., He, Y., Eide, E. J., Hinz, W. A., Virshup, D. M., Ptacek, L. J., and Fu, Y. H. (2001). An hPer2 phosphorylation site mutation in familial advanced sleep phase syndrome. Science *291*, 1040-1043.

Torii, K. U., McNellis, T. W., and Deng, X. W. (1998). Functional dissection of *Arabidopsis* COP1 reveals specific roles of its three structural modules in light control of seedling development. Embo J *17*, 5577-5587.

Tu, D. C., Batten, M. L., Palczewski, K., and Van Gelder, R. N. (2004). Nonvisual photoreception in the chick iris. Science *306*, 129-131.

Ünsal-Kaçmaz, K., Mullen, T. E., Kaufmann, W. K., and Sancar, A. (2005). Coupling of human circadian and cell cycles by the timeless protein. Mol Cell Biol *25*, 3109-3116.

Urban, G., Golden, T., Aragon, I. V., Cowsert, L., Cooper, S. R., Dean, N. M., and Honkanen, R. E. (2003). Identification of a functional link for the p53 tumor suppressor protein in dexamethasone-induced growth suppression. J Biol Chem *278*, 9747-9753.

van der Horst, G. T., Muijtjens, M., Kobayashi, K., Takano, R., Kanno, S., Takao, M., de Wit, J., Verkerk, A., Eker, A. P., van Leenen, D.*, et al.* (1999). Mammalian Cry1 and Cry2 are essential for maintenance of circadian rhythms. Nature *398*, 627-630.

van der Horst, M. A., and Hellingwerf, K. J. (2004). Photoreceptor proteins, "star actors of modern times": a review of the functional dynamics in the structure of representative members of six different photoreceptor families. Acc Chem Res *37*, 13-20.

Van Gelder, R. N., and Sancar, A. (2003). Cryptochromes and inner retinal non-visual irradiance detection. Novartis Found Symp *253*, 31-42; discussion 42-55, 102-109, 281-104.

Van Gelder, R. N., Wee, R., Lee, J. A., and Tu, D. C. (2003). Reduced pupillary light responses in mice lacking cryptochromes. Science *299*, 222.

Vihinen, M., Torkkila, E., and Riikonen, P. (1994). Accuracy of protein flexibility predictions. Proteins *19*, 141-149.

Vitaterna, M. H., Selby, C. P., Todo, T., Niwa, H., Thompson, C., Fruechte, E. M., Hitomi, K., Thresher, R. J., Ishikawa, T., Miyazaki, J.*, et al.* (1999). Differential regulation of mammalian period genes and circadian rhythmicity by cryptochromes 1 and 2. Proc Natl Acad Sci USA *96*, 12114-12119.

von Arnim, A. G., Osterlund, M. T., Kwok, S. F., and Deng, X. W. (1997). Genetic and developmental control of nuclear accumulation of COP1, a repressor of photomorphogenesis in *Arabidopsis*. Plant Physiol *114*, 779-788.

Wang, H., Kang, D., Deng, X. W., and Wei, N. (1999). Evidence for functional conservation of a mammalian homologue of the light-responsive plant protein COP1. Curr Biol *9*, 711-714.

Wang, H., Ma, L. G., Li, J. M., Zhao, H. Y., and Deng, X. W. (2001). Direct interaction of *Arabidopsis* cryptochromes with COP1 in light control development. Science *294*, 154-158.

Weber, S. (2005). Light-driven enzymatic catalysis of DNA repair: a review of recent biophysical studies on photolyase. Biochim Biophys Acta *1707*, 1-23.

Wheeler, D. A., Hamblen-Coyle, M. J., Dushay, M. S., and Hall, J. C. (1993). Behavior in light-dark cycles of *Drosophila* mutants that are arrhythmic, blind, or both. J Biol Rhythms *8*, 67-94.

Whitmore, D., Foulkes, N. S., and Sassone-Corsi, P. (2000). Light acts directly on organs and cells in culture to set the vertebrate circadian clock. Nature *404*, 87-91.

Wiltschko, W., Gesson, M., Stapput, K., and Wiltschko, R. (2004). Light-dependent magnetoreception in birds: interaction of at least two different receptors. Naturwissenschaften *91*, 130-134.

Wiltschko, W., and Wiltschko, R. (1995). Magnetic orientation of european robins is afffected by the wavelength of light as well as by a magnetic pulse. J Comp Physiol *177*, 363-369.

Wishart, D. S., and Sykes, B. D. (1994). Chemical shifts as a tool for structure determination. Methods Enzymol *239*, 363-392.

Woelfle, M. A., Ouyang, Y., Phanvijhitsiri, K., and Johnson, C. H. (2004). The adaptive value of circadian clocks: an experimental assessment in cyanobacteria. Curr Biol *14*, 1481-1486.

Wollnik, F., Brysch, W., Uhlmann, E., Gillardon, F., Bravo, R., Zimmermann, M., Schlingensiepen, K. H., and Herdegen, T. (1995). Block of c-Fos and JunB expression by antisense oligonucleotides inhibits light-induced phase shifts of the mammalian circadian clock. Eur J Neurosci *7*, 388-393.

Worthington, E. N., Kavakli, I. H., Berrocal-Tito, G., Bondo, B. E., and Sancar, A. (2003). Purification and characterization of three members of the photolyase/cryptochrome family blue-light photoreceptors from *Vibrio cholerae*. J Biol Chem *278*, 39143-39154.

Wu, G., Xu, G., Schulman, B. A., Jeffrey, P. D., Harper, J. W., and Pavletich, N. P. (2003). Structure of a beta-TrCP1-Skp1-beta-catenin complex: destruction motif binding and lysine specificity of the SCF(beta-TrCP1) ubiquitin ligase. Mol Cell *11*, 1445-1456.

Wylie, D. R., Bischof, W. F., and Frost, B. J. (1998). Common reference frame for neural coding of translational and rotational optic flow. Nature *392*, 278-282.

Xu, X., Lagercrantz, J., Zickert, P., Bajalica-Lagercrantz, S., and Zetterberg, A. (1996). Chromosomal localization and 5' sequence of the human protein serine/threonine phosphatase 5' gene. Biochem Biophys Res Commun *218*, 514-517.

Xu, Y., Padiath, Q. S., Shapiro, R. E., Jones, C. R., Wu, S. C., Saigoh, N., Saigoh, K., Ptacek, L. J., and Fu, Y. H. (2005). Functional consequences of a CKI delta mutation causing familial advanced sleep phase syndrome. Nature *434*, 640-644.

Yagita, K., Yamaguchi, S., Tamanini, F., van Der Horst, G. T., Hoeijmakers, J. H., Yasui, A., Loros, J. J., Dunlap, J. C., and Okamura, H. (2000). Dimerization and nuclear entry of mPER proteins in mammalian cells. Genes Dev *14*, 1353-1363.

Yamaguchi, Y., Katoh, H., Mori, K., and Negishi, M. (2002). Galpha(12) and Galpha(13) interact with Ser/Thr protein phosphatase type 5 and stimulate its phosphatase activity. Curr Biol *12*, 1353-1358.

Yang, H. Q., Tang, R. H., and Cashmore, A. R. (2001). The signaling mechanism of *Arabidopsis* CRY1 involves direct interaction with COP1. Plant Cell *13*, 2573-2587.

Yang, H. Q., Wu, Y. J., Tang, R. H., Liu, D., Liu, Y., and Cashmore, A. R. (2000). The C termini of *Arabidopsis* cryptochromes mediate a constitutive light response. Cell *103*, 815-827.

Yang, Y., Cheng, P., He, Q., Wang, L., and Liu, Y. (2003). Phosphorylation of FREQUENCY protein by casein kinase II is necessary for the function of the *Neurospora* circadian clock. Mol Cell Biol *23*, 6221-6228.

Yang, Y., Cheng, P., and Liu, Y. (2002). Regulation of the *Neurospora* circadian clock by casein kinase II. Genes Dev *16*, 994-1006.

Yang, Y., He, Q., Cheng, P., Wrage, P., Yarden, O., and Liu, Y. (2004). Distinct roles for PP1 and PP2A in the *Neurospora* circadian clock. Genes Dev *18*, 255-260.

Yang, Z., Emerson, M., Su, H. S., and Sehgal, A. (1998). Response of the timeless protein to light correlates with behavioral entrainment and suggests a nonvisual pathway for circadian photoreception. Neuron *21*, 215-223.

Yao, H., Kristensen, D. M., Mihalek, I., Sowa, M. E., Shaw, C., Kimmel, M., Kavraki, L., and Lichtarge, O. (2003). An accurate, sensitive, and scalable method to identify functional sites in protein structures. J Mol Biol *326*, 255-261.

Yasui, A., Eker, A. P., Yasuhira, S., Yajima, H., Kobayashi, T., Takao, M., and Oikawa, A. (1994). A new class of DNA photolyases present in various organisms including aplacental mammals. Embo J *13*, 6143-6151.

Yi, C., and Deng, X. W. (2005). COP1 - from plant photomorphogenesis to mammalian tumorigenesis. Trends Cell Biol *15*, 618-625.

Young, M. W., and Kay, S. A. (2001). Time zones: a comparative genetics of circadian clocks. Nat Rev Genet *2*, 702-715.

Zeugner, A., Byrdin, M., Bouly, J. P., Bakrim, N., Giovani, B., Brettel, K., and Ahmad, M. (2005). Light-induced electron transfer in *Arabidopsis* cryptochrome 1 correlates with in vivo function. J Biol Chem *280*, 19437-19440.

Zhang, J., Bao, S., Furumai, R., Kucera, K. S., Ali, A., Dean, N. M., and Wang, X. F. (2005). Protein phosphatase 5 is required for ATR-mediated checkpoint activation. Mol Cell Biol *25*, 9910-9919.

Zhao, S., and Sancar, A. (1997). Human blue-light photoreceptor hCRY2 specifically interacts with protein serine/threonine phosphatase 5 and modulates its activity. Photochem Photobiol *66*, 727-731.

Zhao, X., Liu, J., Hsu, D. S., Zhao, S., Taylor, J. S., and Sancar, A. (1997). Reaction mechanism of (6-4) photolyase. J Biol Chem *272*, 32580-32590.

Zhong, D., and Zewail, A. H. (1999). Femtosecond dynamics of dative bonding: Concepts of reversible and dissociative electron transfer reactions. Proc Natl Acad Sci USA *96*, 2602-2607.

Zhu, H., Conte, F., and Green, C. B. (2003). Nuclear localization and transcriptional repression are confined to separable domains in the circadian protein CRYPTOCHROME. Curr Biol *13*, 1653-1658.

Zhu, H., and Green, C. B. (2001). A putative flavin electron transport pathway is differentially utilized in Xenopus CRY1 and CRY2. Curr Biol *11*, 1945-1949.

Zhu, H., Yuan, Q., Froy, O., Casselman, A., and Reppert, S. M. (2005). The two CRYs of the butterfly. Curr Biol *15*, R953-954.

Zimmerman, W. F., and Goldsmith, T. H. (1971). Photosensitivity of the circadian rhythm and of visual receptors in carotenoid-depleted *Drosophila*. Science *171*, 1167-1169.

Zuker, C. S. (1996). The biology of vision of Drosophila. Proc Natl Acad Sci USA *93*, 571-576